19th World Congress of Soil Science

Symposium 2.1.2
The physics of soil pore structure dynamics

Soil Solutions for a Changing World,

Brisbane, Australia

1 – 6 August 2010

Table of Contents

Table of Contents (Cont.)

3-D pore geometry as a function of rock weathering: a CT-analysis

Ranjith P. Udawatta[A], Clark J. Gantzer[B], Stephen H. Anderson[B], Ann M. Rossi[C], Robert C. Graham[C] and Richard A. Ketcham[D]

[A]Center for Agroforestry and Department of Soil, Environmental and Atmospheric Sciences, School of Natural Resources, University of Missouri, MO 65211, USA, Email UdawattaR@missouri.edu
[B]Department of Soil, Environmental and Atmospheric Sciences, University of Missouri, MO 65211, USA.
[C]Department of Environmental Sciences, University of California, Riverside, CA 92521-0424, USA.
[D]Jackson School of Geosciences, University of Texas, Austin, TX 78712-1100, USA.

Abstract
An evaluation of geometrical pore parameters as influenced by rock weathering is helpful in understanding the development of soil. The objective of this study was to investigate three-dimensional (3-D) geometrical pore characteristics in rocks as affected by the degree of weathering. Rock fragments (clasts) from several moraines, ranging in age from 15-ky to 160-ky, were scanned using high-resolution X-ray computed tomography (CT) at 39–42 µm resolution. From each sample a 480×480×580 data block were extracted for analysis with 3-Dimensional Medial Axis Rock (3DMA-Rock) computer software. As weathering increased, samples developed more pores, and these pores were more extensively connected to other pores. Highly weathered samples had pores with the highest coordination numbers and characteristic coordination number constants. These parameters were significantly different from the un-weathered or partially weathered samples. More weathering also resulted in longer path lengths (PLs) and larger path length constants. PLs were < 2 mm for the un-weathered samples while partial and more fully weathered samples had values ranging up to 6 mm. The average tortuosity values decreased from 2.34 to 1.30 with weathering. Results indicated that 3-dimensional analysis of pore geometry can be used to discriminate rock weathering as well as to better understand the spatial variations in pore parameters.

Key Words
Moraine, pore connectivity, pore coordination number, pore path length, pore tortuosity, thresholding

Introduction
Soil formation from rock weathering is an on-going process which can be evaluated over time (Buol *et al*., 2003). Until recent years, weathering was extensively and intensively studied by examining physical and chemical changes in materials. These properties include changes in bulk density, porosity, texture, shape, form, surface features and chemistry. Although geometrical pore features affect the above properties, pore features are seldom examined at a high level of detail. Additionally, traditional procedures of pore evaluation are time consuming and provided no information on internal changes in the pore structure in 3-D as well as spatial differentiations within the structure.

In contrast, higher-resolution imaging techniques at µm- or sub-µm-scale can provide information on spatial variation of pores and geometrical differences in pore structure during rock weathering. Tomographic image slices can be acquired with X-ray, γ-radiation, or nuclear magnetic resonance energy techniques. By assembling contiguous cross-sectional images into data volumes, the three-dimensional distribution and nature of porosity can be visualized using a process called volume rendering, and additional 3D analysis tools can be used to quantify porosity information and geometrical pore parameters for rock, soil, and porous materials.

Quantitative information of rock weathering is required to improve our understanding of water and contaminant movement through materials, and to develop model parameters associated with fluid and gas transport. For example, Udawatta *et al*. (2008a) and Udawatta and Anderson (2008) compared medical X-ray CT-measured (190- by 190- by 500-µm) pore characteristics of various soils as influenced by soil management. These studies elucidated that number of pores, number of macropores, porosity, macroporosity, circularity, and fractal dimension of macropores correlated well with measured saturated hydraulic conductivity. In another study with images acquired at 85-µm resolution, pore tortuosity, connectivity, and other geometrical parameters correlated with management (Udawatta *et al*., 2008b). Comparing differences in throat size, tortuosity, and path characteristics between micro aggregates at 3.2 to 5.4 µm resolution, Peth *et al*. (2008) differentiated conventional tilled and grass soils. Using rock samples, Lindquist *et al*. (2000) compared tortuosity, pore connectivity, pore-channel length, and throat and nodal parameters of Fontainebleau sandstone ranging from 7.5% to 22% porosity.

1 – 6 August 2010, Brisbane, Australia. Published on DVD.

The 5.7-µm resolution images distinguished sandstone material based on coordination numbers of nodal pores, and channel, pore, and throat parameters. However, the literature lacks 3-D evaluation of geometrical pore structure at µm resolution on rock weathering.

According to Birkeland (1999), moraines are well suited for studying rock weathering chronosequences since soil forming factors such as parent material, topography, biota, and climate are approximately constant. Thus, transformations with time can be examined. Evaluation of geometrical pore parameters at µm resolution will improve our understanding of rock weathering and help predict water transport and storage during rock weathering. The objective of the study was to test the hypothesis that internal 3-D geometrical pore parameters change during rock weathering. Analysis compared pore connectivity, pore paths, and tortuosity on weathered clasts from moraines with 3DMA-Rock computer software.

Materials and Methods

The clasts analyzed in this study were collected from moraines in the eastern Sierra Nevada, California, USA. Cosmogenic ^{36}Cl surface exposure dating has estimated that these materials were deposited between 15 ka and 170 ka (Phillips *et al*. in press).

Eight clasts were scanned at the High Resolution X-Ray CT facility at the University of Texas, Austin, USA. The X-ray scanner settings were 210 kV, 0.128 mA, with the intensity control set on, and with the high power mode using no filter. Slice spacing was 42 µm, and data for 25 slices were acquired in each turntable rotation. The raw data were corrected for X-ray fluctuations and ring artifacts prior to image reconstruction. Data were reconstructed as 1024×1024 16-bit TIFF images with a field of view of 40 µm, resulting in a pixel spacing of 39 µm. Contiguous scans were stacked to render 3-D volumes. To reduce edge effects, all samples were trimmed to 580 images, and then 480 by 480 pixel volumes were used for image analysis.

The 3DMA-Rock software was used for 3-D quantification of pore characteristics (Lindquist and Venkatarangan 1999). A number of algorithms are implemented in the image analysis software to accomplish the six main steps: segmentation of image, extraction and modification of the medial axis of pore paths, throat construction using the medial axis, pore surface construction, assembly of pore throat network, and geometrical characterization of pore throat network. Analysis followed information outlined in Lindquist *et al*. (2005) and generated information for: number of branch clusters and associated number of paths; as well as corresponding probabilities for coordination numbers, path lengths, path tortuosity, pore volume, effective radii, throat area, and throat radii. Only pore connectivity, pore path lengths, and path tortuosity and probability densities associated with these three parameters are presented to differentiate pore characteristics as affected by the degree of rock weathering.

Results

The coordination number (CN) characterizes pore topology, the number of paths meeting at one node. Figure 1 shows that the 15 ky sample had no pores with higher coordination-numbers while the 160 ky sample had the largest number of pores with higher CNs. The probabilities associated with these pores were higher than the partially weathered samples. In support of these scanning results, Rossi and Graham (in press) used the same rock material and observed 0.06 to 0.01% porosity formation per 1000 yrs using the bulk density method. Although the scanning method underestimates porosity, which depends on scanner resolution and thresholding, the bulk density and scanning methods both depicted the same trend, i.e., porosity increased with age. Results show that as rocks weather, they develop pores with higher CNs, i.e., more connected pores. The exponential distribution between CN and probability density had r^2 values between 0.62 and 0.92. Although the characteristic coordination number constant (Co) increases with more connected pores, the youngest sample with only a few pores resulted in a higher Co as compared to the two intermediate samples. This could be due to isolation of a smaller number of connected pores rather than sparsely distributed pores in the partially weathered samples.

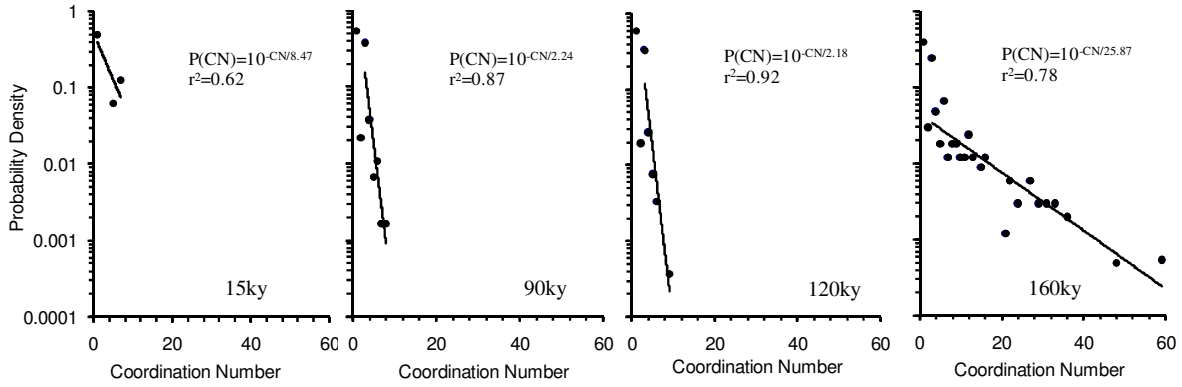

Figure 1. Probability density distribution vs. coordination numbers for 15-, 90-, 120-, and 160-ky age moraine samples from Sierra Nevada, California, USA.

Pore path lengths (PLs) ranged from 0.07 mm in the 15 ky sample to 6 mm in the other three samples (Figure 2). The 15 ky sample did not have PLs longer than 2 mm and they were significantly smaller than those of the other samples. Data also show that the 15 ky sample with smaller PLs had a narrower probability distribution range. Exponential relationships between the PLs and probability density resulted in the smallest path length constant (PLo) for the 15 ky sample (1.20) and the largest for the 160 ky sample (1.80). PLo values were in between for the moderately weathered samples (1.41 and 1.45). The exponential distribution resulted in r^2 values ranging from 0.62 and 0.93. Similar to these results, Udawatta *et al.* (2008b) observed increasing PLo for more porous soils as compared to less porous row crop soils in a CT study comparing agroforestry buffer and row crop soils. The results of this study also show that highly weathered samples possess pores with longer PLs and the probability for those pores is larger than the un-weathered or partially weathered samples.

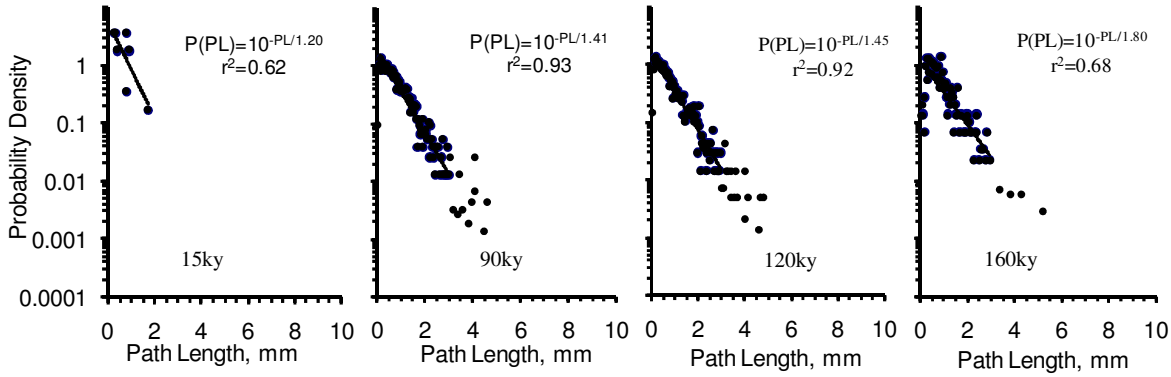

Figure 2. Probability density distribution vs. pore path length for 15-, 90-, 120-, and 160-ky age moraine samples from Sierra Nevada, California, USA.

Average path tortuosity decreased with rock weathering (Figure 3). Among the ten evaluated samples, the 15 ky sample had the highest average tortuosity (2.34) while the weathered samples had lower average values. The number of paths also varied among treatments with values being seven for the 15 ky sample to 34 for the 160 ky sample. The probability for pore path tortuosity decreased with increasing path tortuosity. However, the 15 ky sample had higher probabilities for higher tortuosities while the 160 ky sample had lower probabilities for higher tortuosities. The cumulative probability distributions of path tortuosity showed distinct differences among the treatments.

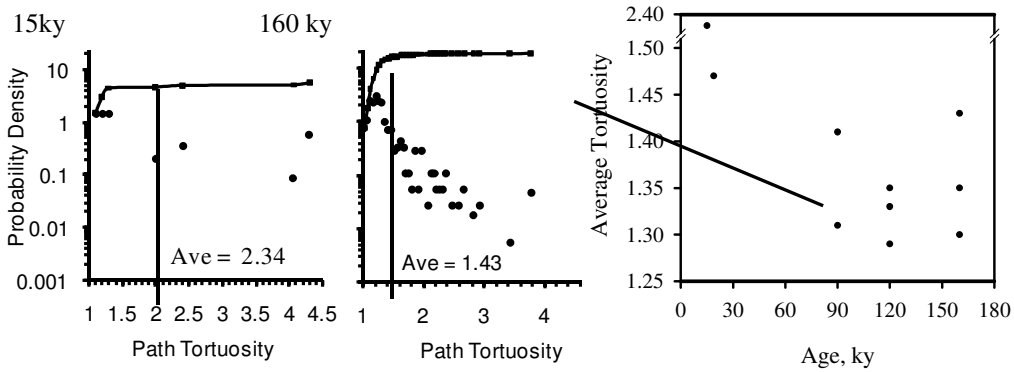

Figure 3. Probability density vs. path tortuosity (solid points) and cumulative probability density (solid line) for 15- and 160-ky samples. Average path tortuosity values for the ten examined samples with sample age.

Conclusions

Characteristic distributions of geometrical pore parameters were compared as influenced by rock weathering. Pore coordination numbers, path lengths, and path tortuosity changed during rock weathering. As pore structure develops and evolves, pores become connected with more pores, path lengths increase, and pore tortuosity decreases. Probabilities associated with these parameters increased as weathering proceeds. Results elucidate that analysis of high resolution images and 3-D visualization may assist in distinguishing geometrical pore parameters for better understanding of rock weathering. These results may help in predicting movement of liquids and gases within rocks as well as use of rock formations for storage of hazardous compounds. Future studies may be directed towards identifying a minimum set of parameters to discriminate gas and liquid transport through the material and understanding storage of hazardous materials for extended periods.

References

Birkeland PW (1999) 'Soil and Geomorphology'. 3rd Ed. (Oxford University Press: New York, NY, USA).

Buol SW, Southard RJ, Graham RC, McDaniel PA (2003) 'Soil Genesis and Classification'. (Iowa University Press: Ames, IA, USA).

Lindquist WB, Venkatarangan AB (1999) Investigating 3D geometry of porous media from high resolution images. *Physics and Chemistry of the Earth* (A) **25**, 593-599.

Lindquist WB, Venkatarangan AB, Dunsmuir JH, Wong TF (2000) Pore and throat size distributions measured from synchrotron X-ray tomographic images of Fontainebleau sandstones. *Journal of Geophysical Research* 105B, 21509-21528.

Lindquist WB, Lee SM, Oh W, Venkatarangan AB, Shin H, Prodanovic M (2005) 3DMA-Rock A Software Package for Automated Analysis of Rock Pore Structure in 3-D Computed Microtomography Images. [Online]. Available at http://www.ams.sunysb.edu/~lindquis/3dma/3dma_rock/3dma_rock.html (verified 18 September, 2009). Department of Applied Mathematics and Statistics, SUNY at Stony Brook, Stony Brook, NY, USA.

Peth S, Horn R, Beckmann F, Donath T, Fisher J, Smucker AJM (2008) Three-dimensional quantification of intra-aggregate porespace features using synchrotron-radiation-based microtomography. *Soil Science Society of America Journal* **72**, 897-907.

Phillips FM, Zreda M, Plummer MA, Elmore D, Clark DH (in press) Glacial geology and chronosequence of Bishop Creek and vicinity, eastern Sierra Nevada, California. *Geological Society of America Bulletin*.

Rossi AM, Graham RC (in press) Weathering and porosity formation in sub-soil granitic clasts, Bishop Creek Moraines, California. *Soil Science Society of America Journal* **74**, 172-185.

Udawatta RP, Anderson SH (2008) CT-measured pore characteristics of surface and subsurface soils influenced by agroforestry and grass buffers. *Geoderma* 145, 381-389.

Udawatta RP, Anderson SH, Gantzer CJ, Garrett HE (2008a) Influence of prairie restoration on CT-measured soil pore characteristics. *Journal of Environmental Quality* **37**, 219-228.

Udawatta RP, Gantzer CJ, Anderson SH, Garrett HE (2008b) Agroforestry and grass buffer effects on high resolution X-ray CT-measured pore characteristics. *Soil Science Society of America Journal* **72**, 295-304.

Aggregation and morphological properties of a degraded Oxisol receiving organic amendments

Marlene Cristina Alves[A], Joann K. Whalen[B], Ricardo Antonio Ferreira Rodrigues[A] and Débora de Cássia Marchini[A]

[A]Faculdade de Engenharia, Universidade Estadual Paulista, UNESP, Ilha Solteira, São Paulo, Brasil, Email mcalves@agr.feis.unesp.br
[B]Department of Natural Resource Sciences, McGill University, Montreal, Canada. E-mail: joann.whalen@mcgill.ca

Abstract
Continuous soil use and inadequate conditions in urban or rural zones cause soil degradation. This study aimed to investigate the recovery of a degraded Oxisol. The research was installed in 2004 in a degraded area by the removal of a 8.60 m layer soil for civil construction. The site is located in Selvíria, Mato Grosso do Sul, Brazil. The experimental design was a randomized blocks with three treatments, two depths and three replicates. The treatments were: degraded soil; native vegetation and *Astronium fraxinifolium*+*Brachiaria decumbens*+sewage sludge. Undisturbed soil samples were collected in soil layers: 0-5 and 5-10 cm. The aggregate soil morphology, physical and chemical properties analyzed were: images of the aggregates, aggregate stability, projected area, carbon, nitrogen, iron and aluminum. The conclusions were: aggregate morphology showed that sewage sludge associated the tree savannah species and grass contribute to soil re-structuring; the aggregate morphology analysis image was a indicative of structure quality.

Key Words
Organic matter, aggregate stability, structuring, soil degradation, carbon, sewage sludge

Introduction
Many tropical soils are degraded or at risk for degradation due to human activities, which diminishes their capacity to produce food, fiber and fuel. Natural rangelands and savannahs are particularly vulnerable for soil degradation because they may be perceived as having low value, compared to cultivated agricultural lands. The construction of a hydroelectric power station, led to the removal of a big layer of topsoil for building earthworks and foundations. Topsoil removal exposed subsoil with low fertility and poor physical structure, which poses a major constraint to natural revegetation of plants from the surrounding native savannah. Organic amendments such as sewage sludge could be used to rehabilitate this degraded site. Indeed, the application of 60 t ha^{-1} of sewage sludge, improved the growth of trees and leguminous crops planted on this degraded Oxisol (Alves *et al*., 2007; Campos and Alves, 2008). Sewage sludge can enhance plant productivity as it contains a considerable amount of N, P and traced elements. Organic matter from the sewage sludge, plant roots and microbial cells (e.g., extracellular polysaccharides, fungal hyphae) is essential for binding and forming soil aggregates, fundamental for the eventual development of soil structure and physical properties that resemble the natural soil conditions. The purpose of this study was to evaluate the aggregation of a degraded Oxisol that was restored with organic amendments or left in the degraded state, compared to natural soil conditions, using an approach based on micromorphology imaging and soil chemical analysis. This study was development in Selviria, Mato Grosso do Sul, Brazil.

Methods
The experiment was conducted at the Teaching and Research Farm of the Faculty of Engineering, Ilha Solteira Campus, Universidade Estadual Paulista (UNESP), located in Selvíria, Mato Grosso do Sul, Brazil (51° 22'W, 20° 22' S) at an elevation of 327 m above sea level. The annual average temperature is 23.5°C and the Köppen type climate is Aw (humid tropical climate, with rainy season in summer and dry in winter). Annual rainfall is 1370 mm, relative humidity is between 70 and 80% year-round. The soil under native savannah is a Typic Haplortox or an Orthic Ferralsol according to the FAO classification (FAO, 1998), and a clayey-loam texture (200-350 g kg^{-1} of clay). Clay mineralogy is dominated by gibbsite and kaolinite.
The soils selected for this study came from experimental plots established on degraded soils in 2004 (two treatments selected) or from an adjacent area under native savannah that was not impacted by soil excavation in the 1960s. The experimental plots were laid out in a completely randomized block design with five soil restoration treatments and untreated, degraded soil as a control. Each plot was 150 m^2 (15 m x 10 m) and the experimental treatments were replicated in five blocks in a total of 30 plots. One restoration treatment was used in this study, namely the *Astronium fraxinifolium- Brachiaria decumbens*-sewage sludge treatment. Briefly, plots were prepared by clearing the surface, subsoiling, plowing, harrowing and leveling, applying lime (2 t ha^{-1})

and sewage sludge (60 t ha^{-1}, from a city treatment station handling mostly domestic waste in Araçatuba, São Paulo State, Brazil) in February, 2004. The perennial grass *B.decumbens* was planted to promote soil restoration and eventually serve as forage for grazing animals. Samples collected for this study came from three replicate plots of the following treatments: (1) the *A. fraxinifolium- B. decumbens*-sewage sludge restoration treatment, and (2) untreated, degraded soil. Three representative samples were also collected from (3) adjacent native savannah.

Soils were collected in February 2008, four years after the establishment of the restoration treatment. Soil blocks (15 cm by x 15 cm) were removed from two layers: 0-5 and 5-10 cm. The initial size aggregates were passed in the 6 mm mesh and withheld the 4 mm. About 40 g of field-moist soil will be spread evenly on the largest sieve of a stack of sieves with openings of 4.0, 2.0, 1.0, and 0.25 mm. The soil properties were analyzed: total organic carbon and nitrogen (Skjemstad and Baldock, 2008) using the equipament NC Soil Analyzer – Flash 1112 Series EA; and analyzing surfaces aggregate image with scanning electron microscope-SEM (Goldstein *et al*., 2003).

Data were analyzed by one-way analysis of variance, followed by a post-hoc Tukey test ($P<0.05$) for mean comparisons, using SAS software (1999). Aggregate analysis data were transformed from % aggregate data before statistical analysis.

Results

The organic C content was greater in the natural soil than the degraded Oxisols, with no difference between restored and degraded treatments (Table 1). The total N content was similar in all treatments at the 0-5 cm depth, but the total N content followed the pattern natural > restored> degraded soils in the 5-10 cm depth (Table 1). It is hypothesized that C accumulation in organo-mineral complexes begins when N-rich, hydrophobic proteins bind to soil mineral surfaces (Klebber *et al*., 2007). If this is occurring in the 5-10 cm depth, then it suggests that the first steps leading to aggregate formation are underway in the restored soils. However although they are not visible in these black and white photos, the colour was slightly darker in aggregate fractions from restored and natural soils, suggesting more organic matter (Figure 1). Closer examination of the 6-4 mm aggregate size fraction revealed morphological differences under low magnification (10 x). Aggregates from the natural and restored soils appeared to have rough, uneven surfaces, compared to the smooth, flat surface of aggregates from the degraded soil (Figure 1, a, b, c). The mean surface area of this fraction was 10.11 to 11.10 cm^2 in the 0-5 cm depth and 10.27 to 11.5 cm^2 in the 5-10 cm depth. Although the size was similar, there were qualitative differences in surface morphology visible under higher magnification. The smooth surface of the 6-4 mm aggregate size fraction from degraded soils was particularly evident at high magnification (250 x), compared to the rough, bumpy surfaces of aggregates from restored and natural soils (Figure 1, d, e, f).

Restoration of these soils with organic amendments is expected to eventually increase the aggregation and soil organic C content. The visual observation of aggregate morphology coupled with soil organic-mineral analysis seems to indicate that changes are occurring in the restored soils. Further study is required to determine the length of time necessary to achieve a significant improvement in soil physical characteristics such as aggregation and soil structure, and if it is possible to return the soil to the same conditions as the natural site. In Figure 1, a, b, c one can observe the morphology aggregate characteristics for soil condition studied. The aggregate natural condition surface and the soil restoration (images with 25 and 50 magnifications) are more rough and one can that observe the micro-aggregates presence is better defined and intact. While the macro-aggregates in degraded soil surface are more smooth and with lower visual perception of the micro-aggregates, principally in the image with 50 magnification. Perception is better in the image with 250 magnification. In this case one can see different colors that probably indicate the organic matter present for the natural and restored conditions. A similar comportment can be observed to depth 5-10 cm, including the degraded soil which practically does not display roots or fungal hyphae. There is evidence in the images results scanning electron microscopy (SEM) of the differences between the aggregate morphology soil conditions for two depths. The observed comportment in analyzed images from SEM was also detected by other authors. Based on micro-morphological examination, the topsoil and subsoil, also SEM images, Kapur *et al*. (2007) concluded that SEM images showed considerable variation among the samples with topsoil samples of each rotation being different visually, and appearing more aggregated than subsoil samples. Mueller *et al*. (2008) concluded that method of visual soil structure evaluation was a feasible tool to provide fast semi-quantitative information on the status of physical soil quality.

Table 1. Organic carbon and total nitrogen in the 0-5 cm and 5-10 cm depths of an Oxisol under native savannah (natural soil) and from a degraded Oxisol that received sewage sludge and were revegetated (restored soil) or left untreated (degraded soil).

Mean

Treatment	Total Carbon	Total Nitrogen
	g kg^{-1}	
	Depth – 0 - 5 cm	
Natural soil	9.13 A	0.78
Restored soil	5.44 B	0.54
Degraded soil	5.63 B	0.52
F – Test	13.9335*	3.7764ns
V. C. - %	18.486	27.424
MSD – 5 %	3.14	0.30
	Depth – 5 - 10 cm	
Natural soil	7.61 A	0.66 A
Restored soil	4.00 B	0.41 B
Degraded soil	2.49 B	0.21 C
F – Test	33.7318*	56.1852*
V. C. - %	21.543	15.741
MSD – 5 %	2.55	0.17

values followed by the same symbol in a column are not significantly different (5% level) according Tukey test. *= 5% significance, ns= no significance. MSD= minimum significant difference. V.C.= Coefficient of variation.

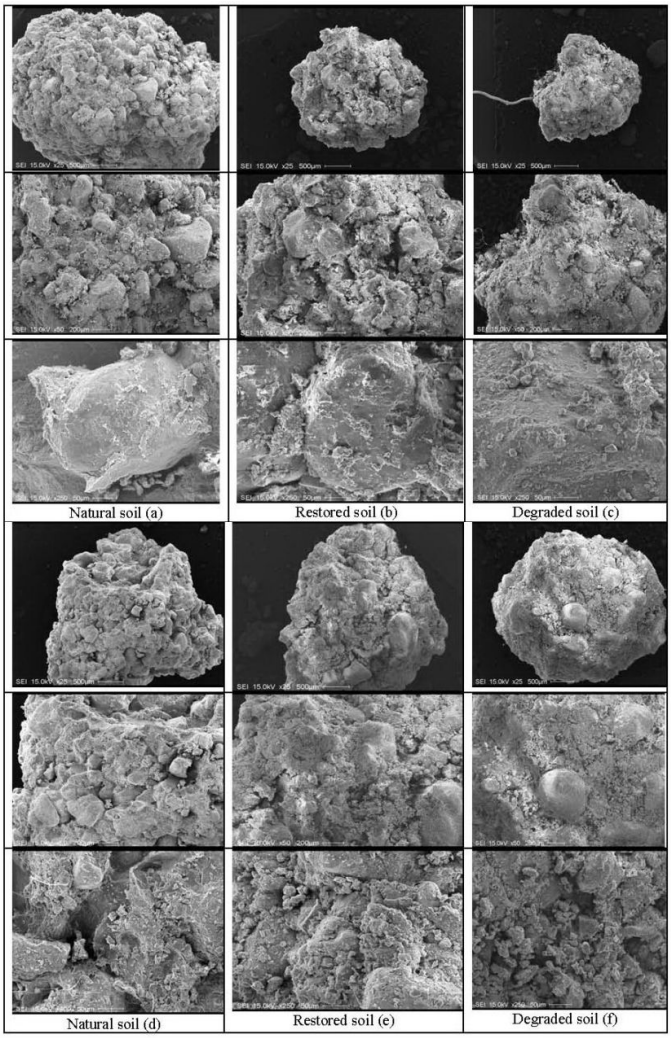

Figure 1. Scanning electron microscopy of soil aggregates (size between 6-4 mm) from the 0-5 cm depth (a, b, c) and 5-1- cm (d, e, f) of an Oxisol under native savannah (natural soil) and from a degraded Oxisol that received sewage sludge and was revegetated (restored soil) or left untreated (degraded soil). The magnification increases from top to bottom: 25 ×, 50 × and 250 ×.

Conclusion

After four years the visual evaluate restoration, by aggregates morphology of the degraded Oxisol, detected that sewage sludge associate the tree savannah species and grass are contributing to soil re-structuring. The aggregate morphology analysis image was more sensitive than the content of organic C and aggregate stability and is indicative of the structure quality evolution over a short time in the degraded Oxisol. Aggregate morphology can better express the restoration of this tropical soil.

References

Alves MC, Suzuki LGAS, Suzuki LEAS (2007) Densidade do solo e infiltração de água como indicadores da qualidade física de um Latossolo Vermelho Distrófico em recuperação. *Revista Brasileira de Ciência do Solo* **31**, 617-625.

Campos FS, Alves MC (2008) Uso de lodo de esgoto na reestruturação de solo degradado. *Revista Brasileira de Ciência do Solo* **32**, 1389-1397.

FAO (1998) World reference base for soil resources. World soil resources reports. Nº 84. FAO. Roma pp.88

Goldstein J, Newbury DE, Echlin P, Ryman CE, Joy, DC, Lifshin, E, Sawyer, LC, Michael JR (2003) Scanning Electron Microscopy and x-Ray Microanalysis. (2nd. Edition. Springer) pp. 689.

Kapur S, Ryan J, Akça E, Çelik I, Pagliai M, Tülün Y (2007) Influence of mediterranean cereal-based rotations on soil micromorphological characteristics. *Geoderma* **142**, 318-324.

Keller T, Arvidsson J, Dexter A (2007) Soil structures produced by tillage as affected by soil water content and the physical quality of soil. *Soil Tillage Research* **92**, 45-52.

Mueller L, Kay BD, Deen B, Hud C, Zhan, Y, Wolff M, Eulenstein F, Schindler U (2008) Visual assessment of soil structure: Part II. Implications of tillage, rotation and traffic on sites in Canada, China and Germany. *Soil & Tillage Research*. In press. 312 pp.

Skjemstad JO, Baldock JA (2008) Total and Organic Carbon. In ´Soil Sampling and Methods of Analysis´. (Second Edition. Canadian Society of Soil Science). pp.225-237.

Statistical Analysis System Institute (1999) SAS/STAT Procedure guide for personal Computers (5.Ed. Cary: SAS Institute Inc) pp. 334.

Can micromorphological characteristics predict infiltration and sediment generation properties of degraded rangeland soils of north-eastern Queensland?

Christian H Roth[A] and Louis-Marie Bresson[B]

[A]CSIRO Sustainable Ecosystems, 306 Carmody Rd, St Lucia, QLD 4067, Australia, Email christian.roth@csiro.au
[B]Formerly INAPG-INRA, UMR Environnement et Grandes Cultures, 78850 Thiverval-Grignon, France, Email lmbresson@orange.fr

Abstract
Micromorphological analyses were conducted on samples from two sites representing a range of surface conditions with different crust morphologies typically observed in degraded, grazed rangelands of northern Australia. Crust typologies of the samples studied were consistent with typologies previously reported by Valentin and Bresson (1992). Crust morphology only partially explained the infiltration response, while there was a closer relationship between crust typology and concentration of fine sediments in runoff. Most samples showed a high degree of bioturbation beneath the surface layer, with many macropores in-filled with smaller pellets. It is possible that the signs of bioturbation are relic, given the degraded state of the sites investigated, but these results do point to the potential role biological activity can play in rehabilitating degraded grazed soils, corroborating earlier work by Roth (2004).

Key Words
Micromorphology, crust typology, rangeland soils, infiltration, sediment generation

Introduction

Soil surface crusts in rangelands and their role in runoff and erosion have long been recognized in tropical Australia. However, these crusts are much less documented than the crusts developed in southern and central arid and semi-arid Australia. The aim of this study was (i) to gain more information about the morphology, genesis and behaviour of soil surface crusts in north-eastern Australian rangelands, (ii) to test the relevance of the crust typology suggested by Valentin and Bresson (1992), (iii) to investigate the possible relationships between crust type and plot infiltration rate and sediment concentration and (iv) to discuss the relevance of integrating crust typology within a soil surface assessment framework suggested by Roth (2004).

Methods

Two degraded rangeland sites were selected for the micromorphological studies, about 80 km west of Townsville. Soil types at both sites were Red Chromosols, derived from metamorphic rocks and sedimentary rocks (Devonian), respectively. Vegetation at site 1 was dominated by Reid River Box (*Eucalyptus brownie*) and Desert Bluegrass (*Bothriochloa ewartiana*), in contrast to Narrow-Leafed Ironbark (*Eucalyptus crebra*) and Desert Bluegrass (*B. ewartiana*) at site 2. Rainfall simulation was used to simultaneously determine rainfall infiltration and sediment detachment for 26 small runoff plots (0.24 m^2, surrounded by a 0.3 m buffer zone) while at the same time providing rainfall impacted plots for micromorphological sampling. Plot selection was carried out on the basis of soil surface condition classes as proposed by Roth (2004). An infiltration index (I_{30}, the infiltration rate in mm/h after 30 mm of simulated rainfall) and a sediment concentration index (Sed_{30}, the concentration of fine silt + clay in runoff in g/L after 30 mm of applied rainfall) were used to compare the infiltration and sediment detachment response of plots with different surface conditions. Details on rainfall experimentation, sampling protocols and site properties are provided by Roth *et al.* (2003).

Undisturbed samples of the top 15 cm of the soil were taken from each plot after rainfall simulation. These undisturbed samples were dried prior to impregnation with epoxy resin in which an ultraviolet fluorescent dye was incorporated. One vertical cross section cut from each impregnated block was photographed under UV light using a digital camera. One 6x13 cm vertical thin section was prepared from each impregnated block and observed using a polarizing stereomicroscope. The samples were classified after the typology suggested by Valentin and Bresson (1992) and Bresson and Moran (2004).

Results and discussion

Crust morphology

Selected images covering the major crust types observed at site 1 are presented in Figure 1. The soil material below the crust (0-5 cm) was characterized by a 70/30 coarse versus fine (C/f) distribution ratio, the C-f limit being 20 µm. The textural fabric was chitonic (packing of clay-coated sand grains) to close porphyric (grains embedded in a continuous fine mass), with 50-100 µm packing voids. The soil matrix was quite heterogeneous, rather dense areas contrasting with loosely packed areas that looked like channels filled in by biological or 'faecal' pellets (Figure 1). Most pellets were irregular microaggregates, 100-300 µm in diameter, only some of them incorporating decayed organic fragments. There were also a few round to oval pellets, 0.5-1 mm in diameter. There were many roots 100-300 µm in diameter. Channels 1-2 mm in diameter were rather common. The surface overlying this material was classified as follows:

No crusts (Figure 1a) were characterized by a litter of leaves and grasses with many organic and organomineral biological pellets, 1-6 mm thick, overlaying a microaggregated layer with many pellets mixed up with microaggregates and with many compound packing voids. There were many channels 1-8 mm in diameter, sometimes filled in with pellets/microaggregates. However, the orientation and continuity of channels could not be reliably assessed from one vertical section and therefore data on orientation was not generated.

In *packing crusts* (Figure 1b), the surface was sealed by a very thin, 250-500 µm thick, structural crust with closely packed microaggregates, overlying moderately packed microaggregated material with compound packing voids. There were channels 1-5 mm in diameter sometimes filled in with pellets/microaggregates.

Pavement crusts (Figure 1c) were characterized by a gravel lag at the soil surface. Most of these gravels were not incorporated within the underlying sandy layer that exhibited many 0.3-3 mm vesicles, especially at the bottom of this layer. Cappings made of fine (silt-sized) particles occurred at the top of some gravels and vesicles. Underneath, a typical thin plasmic layer, 1-3 mm thick, was observed, that included many small vesicles 100-300 µm in diameter.

A thin plasmic layer right at the soil surface characterized *erosion crusts* (Figure 1d). The surface was rather smooth, with a few protruding sand grains. This plasmic layer, 100-500 µm thick, also sealed surface cracks. In the sample shown in Figure 1d there was no cryptogam cover. However, in other plots not shown here, the erosion crust was colonized by filamentous cryptogams that formed a discontinuous, felt-like cover. Crust typologies observed at site 2 were similar to those observed at site 1, despite a slightly lighter texture. In addition, one sample showed a *sieving crust*. The soil material below the crust (0-5 cm) was sandier and more microporous than the soil at site 1, with a 80/20 C/f distribution ratio and a chitonic textural fabric with many 100-200 µm compound packing voids. However, macropores, especially channels 1-2 mm in diameter, were less abundant. Like in site 1 plots, the site 2 soil matrix was strongly affected by biological activity, as evidenced by the occurrence of many channels that was usually filled in by biological pellets.

Relationship of crust morphology with infiltration

At site 1, crust types generally clearly differentiated between I_{30} > 20 mm/hr (*packing* and *no crusts)* and I_{30} < 15 mm/hr (*erosion* and *pavement crusts*). At site 2 the differentiation was less clear: some *packing crusts* had a higher I_{30} than some *no crusts*. Also, some *erosion crusts* had a rather high I_{30} (16.1 and 18.5 mm/hr, respectively), which is consistent with the weak development of these crusts. On the other hand, the *sieving crust* had an unexpectedly low I_{30} (7.9 mm/hr). The statistical analysis of the relationships between crust types and infiltration rates (Student's T-test) shows that there are only two significant differences between crust types, i.e. *no crust* versus *erosion crust* and *no crust* versus *pavement crust* (Table 1). This suggests that parameters other than crust type controlled infiltration rates. It is suggested that the denser matrix underlying uncrusted surfaces that is presumed to result from hoof compaction (Greene *et al.*, 1994) is likely to contribute to the reduction in hydraulic conductivity.

Table 1. Crust types and infiltration rate. Probability level of significance P(T <= 1) from unpaired, two tailed Student's T-test run after comparison of variances using a F-test.

	No crust	Packing	Pavement	Erosion
No crust	-	0.299	0.025	0.010
Packing	-	-	0.094	0.158
Pavement	-	-	-	0.464
Erosion	-	-	-	-

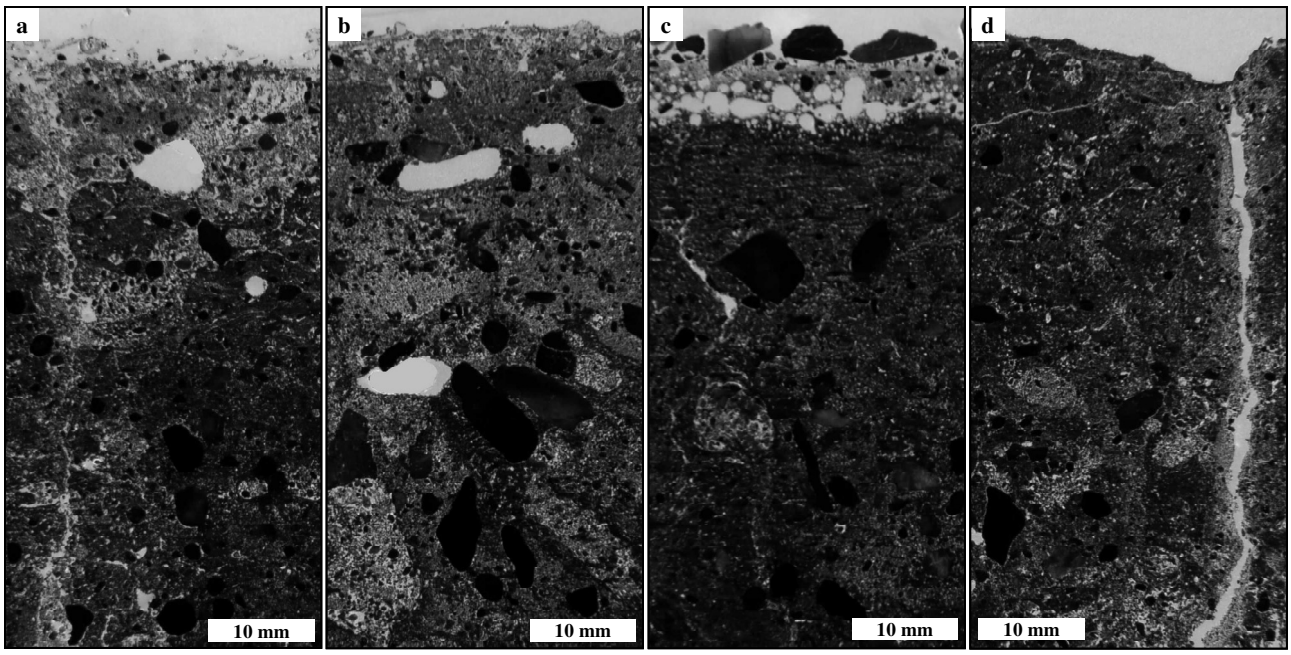

Figure 1. Crust types at site 1: (a) no crust , (b) packing crust, (c) pavement crust and (d) erosion crust. Images of polished blocks, UV.

Relationship of crust morphology with fine sediment generation

At site 1, crust types clearly discriminated between $Sed_{30} > 0.7$ g/L (*erosion crusts*) and $Sed_{30} < 0.7$ g/L (*no crust, packing crusts and pavement crusts*). At site 2, *erosion crusts* were also > 0.7 g/L, with the exception of one plot, where the cryptogam cover present might account for the lower sediment concentration. The statistical analysis of the relationships between crust types and sediment concentration (Student's T-test) shows that *erosion crusts* are significantly different from every other crust type (Table 2).

Table 2. Crust types and sediment concentration. Probability level of significance P(T <= 1) from unpaired, two tailed Student's T-test run after comparison of variances using a F-test.

	No crust	Packing	Pavement	Erosion
No crust	-	0.537	0.124	0.003
Packing	-	-	0.133	0.003
Pavement	-	-	-	0.005
Erosion	-	-	-	-

Conclusion

Overall, the micromorphology of the soil surface crusts from grazed soils in north-eastern Australia studied here is in good agreement with the typology suggested by Valentin and Bresson (1992). Structural crusts developed on these soils through compaction by raindrop impact (*packing crusts*) as well as through vertical sorting of soil particles by winnowing and sieving (*sieving crusts* and also *pavement crusts*). Most *erosion crusts* formed through erosion of the top sandy layer of *sieving crusts*, but some *erosion crusts* were transitional with *packing crusts*, as evidenced by a very thin surface plasmic layer without any vesicles. The crust micromorphology is also in good agreement with the soil surface conditions suggested by Roth (2004).

Below the crusted layers, the soil matrix showed signs of an intense bioturbation, as evidenced by the abundance of channels, either empty or filled in with pellets and/or microaggregates. However, there appears to be no clear relationship between bioturbation intensity and crust type. Even though there is no clear evidence of the relict or active character of the empty and filled in channels, the high degree of bioturbation points to ability of degraded grazed surfaces to recover and regain hydrological function.

There was no clear differentiation of crust types by infiltration rate. Several reasons might be invoked. First, at site 2, crusts were sampled 6 months after the rainfall simulation instead of 1 day at site 1. Second, it appears that the infiltration rates of many of the well covered plots were controlled by the underlying soil, i.e. a dense matrix (site 1) or a buried plasmic layer (site 2), rather than by the surface crust. Therefore, some form of matrix characterization might be required for relating surface condition assessment and soil hydrological properties. Sediment concentration appears to be more related to crust types than infiltration rate, especially when the

ground cover was low. In such conditions, *erosion crusts* generated a sediment concentration much higher than *sieving crusts* and *pavement crusts* did.

References

Bresson LM, Moran CJ (2004) Micromorphological study of slumping in a hardsetting seedbed under various wetting conditions. *Geoderma* **118**, 277-288.

Greene RSB, Kinnell PIA, Wood JT (1994) Role of plant cover and stock trampling on runoff and soil erosion from semi-arid wooded rangeland. *Aust. J. Soil Res*. **32**, 953-973.

Roth CH (2004) A framework relating soil surface condition to infiltration and sediment and nutrient mobilization in grazed rangelands of north-eastern Queensland, Australia. *Earth Surf. Processes Landforms* **29**, 1093-1104.

Roth CH, Prosser IP, Post D, Gross J, Webb M (2003) Reducing sediment and nutrient export from grazed land in the Burdekin catchment for sustainable beef production. Volume II. Appendices. Final report submitted to MLA (Project 3.224). (CSIRO Land and Water: Townsville). www.clw.csiro.au/publications/consultancy/2003/Sed_export_from_Burdekin_catch_Vol-2_Appendices.pdf

Valentin C, Bresson LM (1992) Morphology, genesis and classification of surface crusts in loamy and sandy soils. *Geoderma* **55**, 225-245.

CT-measured macropore parameters for estimating saturated hydraulic conductivity at four study sites

Stephen H. Anderson[A], Ranjith P. Udawatta[AB], Sandeep Kumar[A], Clark J. Gantzer[A], and Achmad Rachman[C]

[A]Dept. of Soil, Environmental & Atmospheric Sciences, Univ. of Missouri, Columbia, MO, USA, Email andersons@missouri.edu
[B]Center for Agroforestry, University of Missouri, Columbia, MO, USA
[C]Indonesian Soil Research Institute, Jl. Ir. H. Juanda 98, Bogor, West Java, Indonesia

Abstract
Saturated hydraulic conductivity is a critical physical parameter essential for predicting infiltration in soils as well as runoff. X-ray computed tomography (CT) has been used as a measurement tool for assessment of soil pore parameters important for water transport. The objective of this study was to use CT-measured soil pore data to predict saturated hydraulic conductivity from four study sites with multiple treatments and soil depths. Soil cores were removed from four study sites in Iowa and Missouri. Study sites included soils developed on deep loess as well as loess and glacial till. Treatments evaluated at the four sites include: row crop, stiff-stemmed grass hedges, agroforestry buffers, grass buffers, conservation reserve program (CRP) management, restored prairie and native prairie. All samples (76 mm diam. by 76 mm long) were scanned using a Siemens Somatom with a 0.19 by 0.19 by 0.5 mm resolution. Pore parameters estimated by CT included macroporosity (> 1000 μm diam.), coarse mesoporosity (200 to 1000 μm diam.), number of pores, circularity of pores, and fractal dimension of macroporosity. The best regression model for estimating the log-transformed saturated hydraulic conductivity was the logarithm of number of pores ($r^2 = 0.69$). This study illustrates the application of CT methods as a characterization tool of soil pores for prediction of hydraulic conductivity.

Key Words
Circularity, coarse mesoporosity, fractal dimension, macroporosity, saturated hydraulic conductivity, x-ray computed tomography

Introduction
Saturated hydraulic conductivity is an important soil parameter which is highly influenced by soil management (Udawatta et al. 2008). Perennial vegetative buffers have been shown to maintain or improve soil hydraulic properties (Rachman et al. 2005). These buffers include stiff-stemmed warm season grasses (Rachman et al. 2005), trees and grasses (Udawatta and Anderson 2008), and cool season grasses (Udawatta and Anderson 2008). The purpose of these buffer systems is to control surface runoff and sediment loss from land under row crop and grazing management practices. Since vegetation is perennial, soil under buffers may develop biologically produced macropores as a result of active growth of grass roots and associated fauna.

An important soil pore parameter for infiltrating water is the degree of macroporosity (Allaire-Leung et al. 2000). Macropores (relatively large soil pores > 1000 μm diameter) allow water to penetrate into the soil and, under ponded conditions at the soil surface, water flow in soils will be dominated by the macropore system. Water transport follows the path of least resistance through these macropores, while in contrast, water movement in soil without macropores occurs through smaller pores or voids between the grains or aggregates (Warner et al. 1989). For both macropore flow and matrix flow, the shape, size, orientation and distribution of soil pores influence the rate of water flow and retention in the soil (Rasiah and Aylmore 1998).

Porosity is often characterized using analysis of soil water characteristic curves, tension infiltrometer data, and soil bulk density data (Everts and Kanwar 1992). These are an indirect measure of porosity or pore size distribution, and do not include any detailed information on the nature of the pores or their spatial distribution (Gantzer and Anderson 2002). A recent measurement tool used by soil scientists to assess soil pores is X-ray computed tomography (CT; Perret et al. 2000; Gantzer and Anderson 2002) which can be used for *in situ*, nondestructive, and repetitive measurements at sub-millimeter scales. Detection of macropore features and their relative frequency has been done using CT methods to quantify macropore diameters as small as 0.15 mm (Gantzer and Anderson 2002). The objectives of this study were to characterize macropores of intact soil samples using CT methods from four study sites with selected land management treatments, and correlate saturated hydraulic conductivity with CT-measured macropore parameters.

1 – 6 August 2010, Brisbane, Australia. Published on DVD.

Methods

Study sites and core samples

Data used for the current study were obtained from four study sites which compared CT-measured macropore parameters for selected soil management treatments (Kumar et al. 2010; Rachman et al. 2005; Udawatta and Anderson 2008; Udawatta et al. 2008). Rachman et al. (2005) compared CT-measured macropore properties within the 0 to 20 cm soil depth for stiff-stemmed grass hedge, row crop and deposition zone treatments (30 cores) on Monona silt loam (fine-silty, mixed, superactive, mesic Typic Hapludolls). CT-measured macropore properties were assessed within the 0 to 40 cm depth of Mexico silt loam (fine, smectitic, mesic Vertic Epiaqualfs) for four treatments (96 cores): row crop, native-undisturbed prairie, restored prairie, and conservation reserve program (CRP) treatments (Udawatta et al. 2008). Udawatta and Anderson (2008) evaluated macropores for agroforestry buffer, grass buffer and row crop treatments (90 cores) within the 0 to 50 cm depth of Putnam silt loam (fine, smectitic, mesic Vertic Albaqualf). Macropore properties were measured for continuously grazed pasture, rotationally grazed pasture, agroforestry buffer and grass buffer treatments (120 cores) within the upper 50 cm of Menfro silt loam (fine-silty, mixed, superactive, mesic Typic Hapludalf; Kumar et al. 2010). A total of 336 core samples were used for this study. The Monona and Menfro soils formed on deep loess while the Mexico and Putnam soils (claypan soils) formed on loess and glacial till.

Intact soil cores (76.2 mm diameter by 76.2 mm long) housed in Plexiglas cylinders with 4 mm wall thickness were collected from each site. A plastic cap was placed on each end of the soil core secured with masking tape. Cores were then placed in sealed plastic bags, transported to the laboratory, and stored in a refrigerator at 4° C.

The lower end of each core was covered with 2 layers of fine nylon mesh to contain soil within cylinders. Cores were slowly saturated from the bottom with water (6.24 g L^{-1} $CaCl_2$ and 1.49 g L^{-1} $MgCl_2$) using a Mariotte system. Samples were drained and equilibrated to –3.5 kPa using a glass-bead tension table. Samples were weighed and transported to the CT scanner for measurement. Two phantoms, distilled water in an aluminum tube and a solid copper wire, were attached to each core before scans were taken. Phantoms were to assure that data were comparable between scans for different treatments.

Scanning and image analysis

The CT scanner used for all studies was a Siemens Somatom Plus 4 Volume Zoom. The scan system parameters were set to 125 kV, 400 mA and 1.5-s scan time to provide detailed and low noise projections. The field of view, i.e. the cross sectional dimension, was 100 mm with 512 by 512 picture elements (pixels) giving a pixel size of 0.19 by 0.19 mm. The x-ray beam width or slice thickness was 0.5 mm, producing a volume element (voxel) size of 0.018 mm^3. Five scan slices were taken in each core with a 10 mm distance between each scan. The first scan slice was taken at a 15 mm distance from the top of the soil core. After scanning, saturated hydraulic conductivity was measured using either the constant head method or falling head method. The soil cores were then dried to determine bulk density.

The scanned images were analyzed for macropore (>1000-µm diam.) and mesopore (200- to 1000-µm diam.) characteristics using the *ImageJ* version 1.27 computer software package (Rasband 2002). The macropore and mesopore characteristics analyzed included the number of pores, macroporosity, coarse mesoporosity, pore area, perimeter of pores, and macropore fractal dimension (fractal D). Pore circularity was estimated using pore area and perimeter of pores. Macroporosity and mesoporosity at each depth were calculated from the total area of all macropores and mesopores isolated in the image at a given depth divided by the cross sectional area of the selected region on the soil core image.

The *Region of Interest* (ROI) tool was used to select a circular region of 73-mm diam. in each image. This region was selected to exclude voids near the core walls and minimize the effects of beam hardening due to the Plexiglas cylinder. The *Clear Outside* tool was used to clear areas outside the selected region. The *Threshold* tool was used to partition pores from solids after converting the image into an 8-bit grayscale image. The threshold values selected to analyze all images were from zero to 40 grayscale (range is 0 to 255). These grayscale values are the relative attenuation values (RAV) that are related to porosity (Gantzer and Anderson 2002). The *Analyze Particles* tool was used to measure statistics of individual pores.

Fractal dimension values were analyzed within a 50-mm by 50-mm square image in the center of the core. The threshold values for estimating the fractal dimension of the macropores were from zero to 100 RAV or grayscale. The higher RAV (100) for fractal dimension analyses as compared to pore characteristic analyses (40) was used to increase data density.

Pearson correlation coefficients were estimated between saturated hydraulic conductivity and the CT-measured pore parameters. Regression analyses were performed between saturated hydraulic conductivity and CT-measured pore parameters. Log_{10}-transformations were conducted on K_{sat} and CT-measured number of pores, since these distributions were positively skewed. These transformations normalized the data.

Results

Correlation among CT-measured parameters and K_{sat}

Linear correlation coefficients among bulk core properties (bulk density and saturated hydraulic conductivity, K_{sat}) and CT-measured pore parameters are shown in Table 1. The parameter with the highest correlation with $\log(K_{sat})$ was CT-measured number of pores ($r = 0.830$, $P < 0.001$). Fractal dimension of macroporosity was the parameter with the next highest correlation ($r = 0.704$, $P < 0.001$). These two CT-measured parameters (number of pores and fractal dimension) were also highly correlated ($r = 0.781$, $P < 0.001$).

Regression relationships for K_{sat}

Regression parameters for estimating $\log(K_{sat})$ using log(CT-measured number of pores) for the four study sites are included in Table 2. Coefficients of determination ranged from 0.50 to 0.76. The lowest intercept value was found for the Rachman et al. (2005) study site while the highest value occurred with the Kumar et al. (2010) study. The Rachman et al. (2005) study site had the highest slope (1.84) while the Kumar et al. (2010) study site had the lowest slope value (1.28).

Table 1. Correlation matrix of CT-measured macropore pararameters and log(saturated hydraulic conductivity, K_{sat}).

	Macro-f† ($cm^3\ cm^{-3}$)	Coarse Meso-f† ($cm^3\ cm^{-3}$)	Log (Number of Pores)	Pore Circularity	Fractal Dimension of Macro-f	Bulk Density ($g\ cm^{-3}$)	$Log(K_{sat})$ [$log(mm\ hr^{-1})$]
Macro-f	1.000	0.458‡	0.618	-0.088	0.768	-0.514	0.572
Coarse Meso-f		1.000	0.435	-0.052	0.480	-0.280	0.380
Log(Number of Pores)			1.000	0.301	0.781	-0.144	0.830
Pore Circularity				1.000	-0.033	0.324	0.180
Fractal D of Macro-f					1.000	-0.509	0.704
Bulk Density						1.000	-0.173
$Log(K_{sat})$							1.000

†Macro-f = macroporosity, Meso-f=mesoporosity.

‡Correlation values higher than 0.175 or lower than -0.175 correspond to $P < 0.001$.

Table 2. Regression parameters and coefficients of determination for predicting log(Ksat) from log(number of pores) at four study sites.

Study Site	Intercept	Slope	r^2	n
Rachman et al. (2005)	-1.74	1.84	0.62	30
Udawatta et al. (2008)	-1.12	1.44	0.69	96
Udawatta/Anderson (2008)	-1.50	1.77	0.76	90
Kumar et al. (2010)	-0.76	1.28	0.50	120

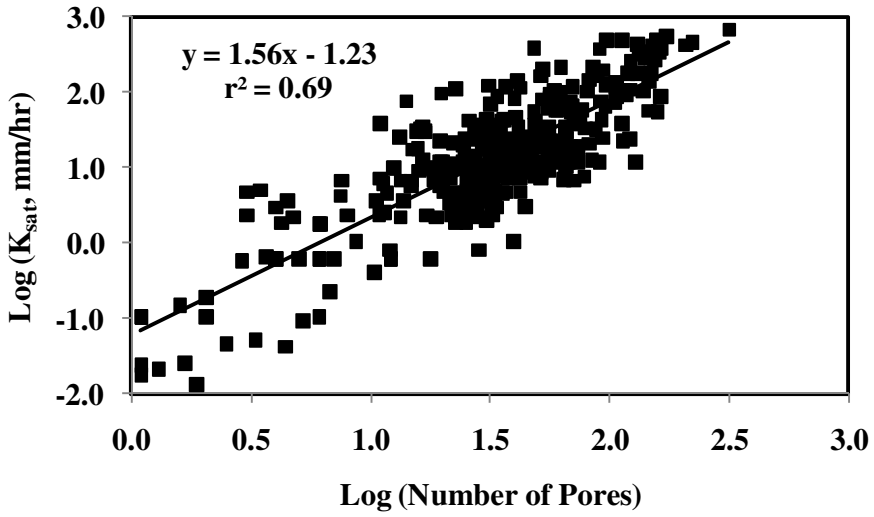

Figure 1. Regression relationship between saturated hydraulic conductivity [log(K_{sat})] and CT-measured number of pores [log(number of pores)].

The overall regression relationship between log(K_{sat}) and log(CT-measured number of pores) is shown in Figure 1. Adding the fractal dimension of macroporosity into the regression relationship increased the r^2 value from 0.69 to 0.70. Including additional parameters did not improve the coefficient of determination.

Conclusion

A study was conducted to compare how well CT-measured pore parameters performed in estimating saturated hydraulic conductivity from four study sites in Iowa and Missouri. CT-measured pore parameters included number of pores, macroporosity, coarse mesoporosity, pore circularity, and fractal dimension of macroporosity. The best regression model for estimating log(saturated hydraulic conductivity) was log(number of pores) with a coefficient of determination of 0.69. Results of the study indicate that CT methods may be very useful for characterizing pores from multiple sites with several land management treatments and can potentially estimate saturated hydraulic conductivity.

References

Allaire-Leung SE, Gupta SC, Moncreif JF (2000) Water and solute movement in soil as influenced by macropore characteristics: I. Macropore continuity. *Journal of Contaminant Hydrology* **41**, 283-301.

Everts CJ, Kanwar RS (1992) Interpreting tension-infiltrometer data for quantifying soil macrpores: Some practical considerations. *Transactions of ASAE* **36**, 423-428.

Gantzer CJ, Anderson SH (2002) Computed tomographic measurement of macroporosity in chisel-disk and no-tillage seedbeds. *Soil and Tillage Research* **64**, 101-111.

Perret J, Prasher SO, Kantzas A, Langford C (2000) A two-domain approach using CAT scanning to model solute transport in soil. *Journal of Environmental Quality* **29**, 995–1010.

Kumar S, Anderson SH, Udawatta RJ (2010) Agroforestry and grass buffer influences on macropores measured by computed tomography under grazed pasture systems. *Soil Science Society of America Journal* **74,** 203-212.

Rachman A, Anderson SH, Gantzer CJ (2005) Computed-tomographic measurement of soil macroporosity parameters as affected by stiff-stemmed grass hedges. *Soil Science Society of America Journal* **69,** 1609-1616.

Rasiah V, Aylmore LAG (1998) Characterizing the changes in soil porosity by computed tomography and fractal dimension. *Soil Science* **163**, 203-211.

Rasband W (2002) NIH Image J. Research Service Branch, National Institute of Mental Health, National Institute of Health. Bethesda, MD, USA. (http://rsb.info.nih.gov/ij/docs/intro.html).

Udawatta RP, Anderson SH (2008) CT-measured pore characteristics of surface and subsurface soils influenced by agroforestry and grass buffers. *Geoderma* **145,** 381-389.

Udawatta RP, Anderson SH, Gantzer CJ, Garrett HE (2008) Influence of prairie restoration on CT-measured soil pore characteristics. *Journal of Environmental Quality* **37,** 219-228.

Warner GS, Nieber JL, Moore ID, Geise RA (1989) Characterizing macropores in soil by computed tomography. *Soil Science Society of America Journal* **53**, 653-660.

Dynamics of soil pore space structure investigated by X-ray microtomography

Stephan Peth[A], Jens Nellesen[B], Gottfried Fischer[C], Felix Beckmann[D] and Rainer Horn[A]

[A]Institute of Plant Nutrition and Soil Science, Christian-Albrechts-University zu Kiel, Germany
[B]Lehrstuhl für Qualitätswesen, Department of Mechanical Engineering, Technische Universität Dortmund, Germany
[C]Dortmunder Initiative zur rechnerintegrierten Fertigung (RIF) e.V., Joseph-von-Fraunhofer-Str. 20, D-44227 Dortmund, Germany
[D]GKSS Research Centre, Hamburger Synchrotron-Strahlungslabor, Deutsches Elektronensynchrotron, Hamburg, Germany

Abstract
Transport and transformation processes of solid, liquid and gaseous compounds/components in soils are intimately connected and strongly dependent on the state of soil structure and pore space geometries. Soil structure in turn is inherently dynamic due to changes in pore water pressure resulting in shrinking and swelling and/or soil compaction and shear deformation by applying external loads and last but not least also continuously modified by biological factors (root growth and soil faunal activities). Studying the dynamic properties of soils and functions requires observing the evolution of soil structure with changing boundary conditions without disturbing the processes of structure formation. Non-invasive techniques such as X-ray microtomography are able to resolve soil structure and associated pore architectures on various scales and at the same time allow for non-destructive observations of structural dynamics upon changes in boundary conditions. We used synchrotron- and X-ray microfocus tube-based microtomography (SR-µCT and MF-µCT resp.) systems to investigate soil structural dynamics of soil aggregates and typical core-size soil samples. The effects of shrinking/swelling and compaction on pore space architectures were studied under controlled boundary conditions (matric potential, mechanical loads). Three-dimensional reconstructions of the pore space were analyzed with 3D image analysis tools to quantify changes in morphological characteristics of soil structure and related pore networks upon changes in boundary conditions, respectively. The potential of such quantitative data to further develop modeling approaches of transport and deformation processes in soils will be discussed. Further improvements in µCT imaging approaches and 3D image analysis of soil structure dynamics coupled with physical measurements of transport functions are essential to achieve a more comprehensive understanding of soil-ecosystem fluxes and interactions.

Key Words
X-ray microtomography, image analysis, 3D correlation analysis, soil mechanics, soil deformation, soil structure

Introduction

Non-invasive three dimensional imaging microscopy using microtomography techniques provide a useful method to directly observe and quantify soil structure formation and deformation with changes in hydraulic and mechanical stress state. The advantage over other imaging techniques applied in soil morphology analysis (e.g. thin sectioning) is that tomography measurements account for the 3D nature of the specimen and that samples remain intact after CT image acquisition measurement allowing for repeated imaging and thus monitoring soil structure dynamics. The latter is a prerequisite to observe spatial modifications of the soil pore microenvironment caused by dynamic processes continuously re-arranging pore networks hence feeding back on soil functions. On the other hand, indirect assessments of soil structural attributes such as the pore size distribution (PSD) derived from water retention curves (WRC) render inaccurately in a sense that with changes in hydraulic stress during the measurement pore geometries may change resulting in a continuously modified pore size distribution during the course of the measurement. The same is true for the derivation of hydraulic model parameters from such indirect measurement methods since the non-rigidity of pore systems caused by shrinking–swelling processes is not considered. Non-invasive imaging techniques could overcome some of the limitations of routinely applied methods for assessing soil structure and associated soil functions.

Methods

We used two sets of samples for this study:
Firstly, a soil aggregate sample (~5 mm across) was collected from an *Alfisol* (Rotthalmünster, Germany) from the topsoil layer. The soil aggregate sample was scanned in air dry condition at the synchrotron microtomography facility operated by the GKSS Research Center at HASYLAB (Hamburger Synchrotron Strahlungslabor) of DESY (Deutsches Elektronen Synchrotron) in Hamburg/Germany. The microtomography was completed at beamline BW2. The sample was mounted on a rotary stage and scanned at a photon energy of 24 keV and a voxel resolution (voxel edge length) of 4.38 µm. During the microtomographical scan the sample

was rotated at different projection angles between 0 and π, at 0.5° degree intervals. The absorption radiographs for the different viewing angles were projected onto a $CdWO_4$ fluorescent screen and recorded by a 1536×1024 pixel CCD camera. Image reconstruction was accomplished using a filtered back-projection algorithm in IDL™ (Research Systems Inc.). Attenuation coefficients are expressed as grayscale values ranging from [255] for the highest attenuation coefficient to [0] for the lowest attenuation coefficient reached. After the initial scan the sample was wetted via a glass fibre wick from below at a suction of -7 hPa with a 1M KI-doped solution to increase the attenuation contrast of the fluid phase. After imbibition the same aggregate was scanned a second time.

In a second series bulk soil samples have been prepared in the laboratory. Remoulded loess soil material has been filled into 5 cm diameter *Plexiglas® cylinders* at three different initial bulk densities (1.00, 1.20 and 1.33 g/cm^3, respectively). Samples were scanned at three different conditions: 1) initial homogeneous condition, 2) after saturation and 3) after subsequent air drying. Following the investigation of shrinking/swelling effects on soil structure development we studied the response of the structured soil to mechanical stresses. To do this we applied stepwise increasing mechanical loads of up to 400 kPa to the dried sample with the intermediate packing density (1.20 g/cm^3) in air dry condition. For the loading steps of 0, 20, 50, 100, 200, and 400 kPa we tomographed the sample immediately after loading.

The above mentioned remoulded soil samples were scanned in a lab by a *phoenix v|tome|x | 240* (GE Sensing & Inspection Technologies GmbH, Wunstorf, Germany). Scanning procedure is similar to the procedure done at the HASYLAB except that a polychromatic and cone shaped X-ray beam is used instead of a monochromatic parallelized beam as it is generated at synchrotron facilities. X-ray parameters used were 200 keV scanning energy with 1440 projections per sample with a voxel resolution between 38.4 and 41.0 µm. The basic setup of the scanning system and image processing is shown in Figure 1.

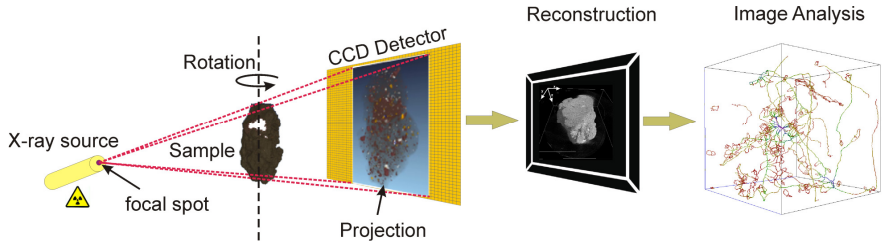

Figure 1. Setup of the X-ray microfocus tube tomography system and subsequent image reconstruction and analysis.

Volume rendering of the image reconstructions has been carried out with VG-Studio Max 2.0 (Volume Graphics GmbH, Heidelberg, Germany). Morphological image analysis of the grayscale images has been performed with a suite of algorithms assembled in the software package *3dma-Rock* (Lindquist *et al.* 2005) and in VG-Studio Max 2.0. A full 3D image analysis consists of a succession of image transformations and ends with the quantification of pore network characteristics (Figure 2). Basic image transformations are *segmentation*, *disconnected cluster clean up*, *medial axis construction* and *throat and pore size computation*. An analysis of strain localisation was performed by digital 3D tomogram correlation after Crostack *et al.* (2008). A reference tomogram was divided into cuboid regions which are regularly distributed on a regular grid. Each cuboid represents the local microstructure in the reference state (before shrinking or loading) at its grid point. The cuboids in the reference tomogram are iteratively mapped onto the corresponding more or less deformed microstructural parallelepiped-shaped region in the comparison tomogram (after shrinking or loading). By coordinate transformations a mean deformation gradient F and the Lagrangian strain tensor γ are derived and from this scalar deformation quantities like volume change dV/V and equivalent strain ε_{equ} can be calculated. Further details on the method and its application for the determination of localized soil deformation using microtomography images are provided in Peth *et al.* (2010).

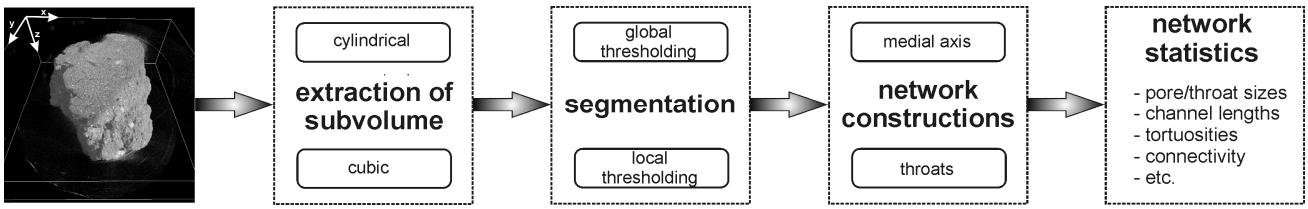

Figure 2. Basic image transformation steps in *3dma-Rock*.

Results

The effect of a change in hydraulic stress on pore geometry is demonstrated in Figure 3 where the tomograms of a soil aggregate scanned in air dry condition and after imbibition of a 1M KI-solution at -7hPa are compared. After imbibition a rearrangement of particles accompanied by a restructuring of the pore space was observed. This is apparent from closing coarse, soil structure related pores (e.g. cracks) and interestingly also from the formation of new coarse pores that remain gas filled. Swelling is a common process in clay rich soils and well known to partially close previously generated cracks. In contrast the formation of new coarse pores during wetting is a phenomenon that has to the best of our knowledge not yet been observed directly. An explanation could be microscale gas flow processes leading to a local entrapment of air within the aggregate and subsequent deformation of the soil matrix as air pressure exceeds local soil strength (Peth *et al.* 2008b). Another reason could be contractile forces during capillary wetting of the previously air dry sample leading to the generation of new or a widening of pre-existing cracks. These observations underline the complexity of interactive transport and deformation mechanisms resulting in dynamic soil pore spaces pointing out that the investigation of pore scale processes requires non-invasive techniques.

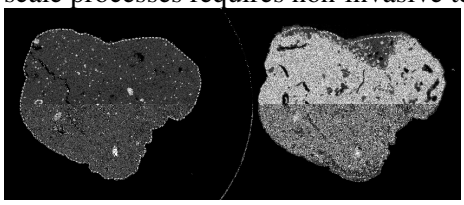

Figure 3. Tomograms before (left) and after (right) imbibition with 1M KI-solution at a matric potential of -7 hPa. The dashed line indicates the rim of the air dry sample before the sample was wetted. (taken from Peth 2010)

Development of soil structure in bulk soil samples is shown in Figure 4 exemplarily for the loose packing (1.00 g/cm^3) for the three conditions (initially dry homogenous, after saturation and after subsequent air drying). We observed almost no macropores in the initially homogeneous dry condition as it is shown more clearly in the binarized images in the bottom part of Figure 4. After saturation a substantial number of new macropores pores (> resolution limit which was approximately 40 µm) were generated indicated by the white areas in the binarized image. After drying the sample, again large cracks developed in the middle of the sample separating the bulk soil into five newly formed aggregates.

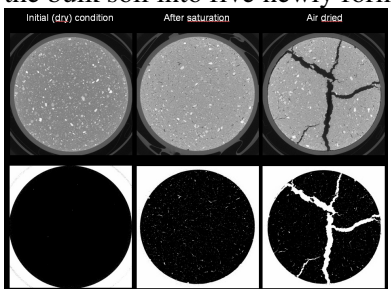

Figure 4. Tomograms (top) before (left) after saturation (middle) and after air drying (right). The binarized images (bottom) indicate the generation of new macropores by changes in hydraulic stresses (saturation and subsequent air drying).

Frequency distributions of pore size classes derived from morphological image analysis show that saturating the sample generated numerous macropores (Figure 5). Note that since close to the resolution limit (in this case ~ 40 µm) the detection of pores is associated with uncertainty due to binarization of the grayscale images only pores > 8 voxels (2 voxels wide in each spatial direction ➔ $2^3 = 8$) were counted to ensure that only real pores are included in the statistics. Interestingly subsequent shrinkage created a large crack, counted as one interconnected pore with a volume of 5.790 mm^3 (plotted at class < 10.000 mm^3 in Figure 5), but left the remainder pore size frequency distribution with pore volumes between > 0.0001 and < 1.000 mm^3 almost unchanged. Consequently, the pore volume gain within the newly formed crack must have been accommodated by pore volume reduction in pores smaller than 8 voxels in size corresponding to a volume equivalent diameter of spherical pores of < 50 µm.

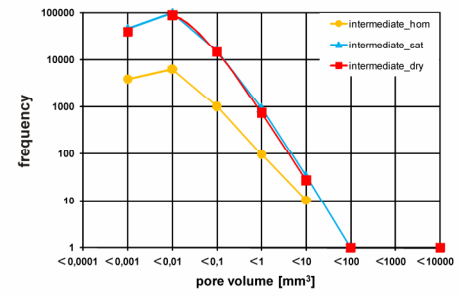

Figure 5. Frequency distribution of different pore size classes for the sample with intermediate packing density (1.20 g/cm^3; shown in Figure 4.) at three different conditions: initially homogenized = hom, saturated = sat, after shrinkage = dry).

Figure 6 presents the local soil deformation resulting from hydraulic (shrinkage, Figure 6A) and mechanical stresses (external loading, Figure 6B). The orientation of the major axis of the tensor ellipsoids (in this case represented as cuboids) in Figure 6A reveals a change in the orientation of the strain field from predominantly horizontal deformation at the outer rim of the sample to predominantly vertical deformation in the vicinity of the cracks in the centre of the sample during shrinkage. External mechanical loading of the sample in air dry condition resulted in spatially heterogeneous soil deformation (Figure 6B). We observed a strain concentration in the vicinity of larger cracks where plastic flow indicates a closure of the large cracks while within the interior of aggregates deformation is lower. A decreasing crack volume with mechanical loading was also determined by morphological image analysis (data not shown).

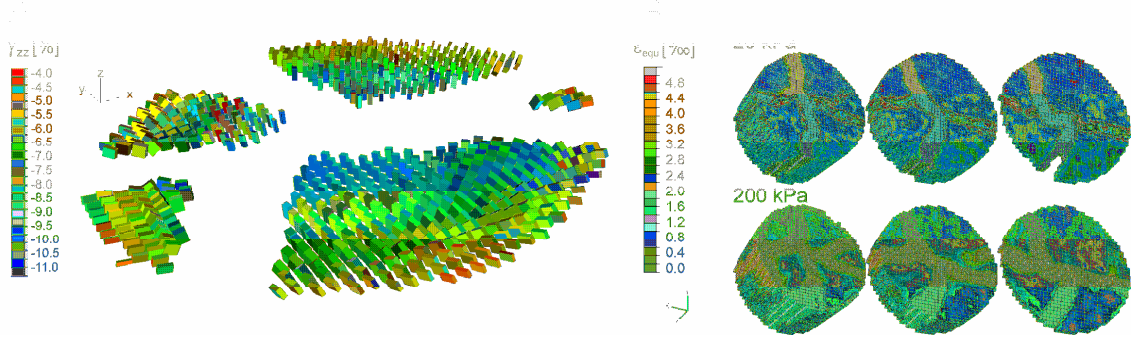

Figure 6. (A) Spatial orientation of the Lagrangrian strain tensor □ represented as cuboids for a tomogram correlation of the state before and after shrinkage showing the local magnitude of strain and the orientation of the maximum strain gradient. The slice represents a horizontal section near the top through the sample shown in B before mechanical loading. (B) Spatial distribution of the equivalent strain $\square_{equ}$ for two different external mechanical loads. The color scale is adjusted to lower strain values to indicate the deformation within the aggregates. The corresponding reference tomogram for the grayscale correlation analysis was in each case the unloaded state. Gray color coded areas indicate values of equivalent strain $\square_{equ}$ exceeding a specified threshold value (> 4.8 ‰) corresponding to a larger deformation in the vicinity of cracks.

Conclusion

Soil structure and associated pore space geometries are to be considered highly dynamic. Even in structurally mature units such as aggregates we observe modifications in the pore space by changing hydraulic stresses (imbibition). X-ray microtomography in conjunction with 3D image analysis techniques is capable to quantify the dynamic pore space in relation to changes of hydraulic and mechanical stress boundary conditions. The results presented here strongly suggest that soils are non-rigid systems where both hydraulic and mechanical stresses locally modify pore space geometries. These modifications are associated with a simultaneous destruction/reduction of pores/pore sizes and the generation of new pores. This fact has to be considered in modelling transport, deformation and exchange processes in soils and between the pedosphere and the atmosphere.

References

Crostack H-A, Nellesen J, Fischer G, Weber U, Schmauder S, Beckmann F (2008) 3D Analysis of MMC microstructures and deformation by µCT and FE simulations. In 'Developments in X-ray Tomography'. (Ed SR Stock). pp. 70781I1-12., VI, Vol. 7078 (SPIE, San Diego, CA).

Lindquist WB, Lee S-M, Oh W, Venkatarangan AB, Shin H, Prodanovic M (2005) 3DMA-Rock: A Software Package for Automated Analysis of Rock Pore Structure in 3-D Computed Microtomography Images. http://www.ams.sunysb.edu/~lindquis/3dma/3dma_rock/3dma_rock.html.

Peth S, Horn R, Beckmann F, Donath T, Fischer J, Smucker AJM (2008a) Three-Dimensional Quantification of Intra-Aggregate Pore-Space Features using Synchrotron-Radiation-Based Microtomography. *Soil Science Society of America Journal* **72,** 897-907.

Peth S, Horn R, Beckmann F, Donath T, Smucker AJM (2008b) The Interior of Soil Aggregates investigated by Synchrotron-Radiation-based Microtomography. In 'Developments in X-ray Tomography VI' (Ed SR Stock) pp. 70781H-12. (SPIE: San Diego, CA).

Peth S (2010) Applications of Microtomography in Soils and Sediments. In 'Synchrotron-Based Techniques in Soils and Sediments'. (Eds B Singh, M Gräfe) pp. 73-101.,Vol. 34. (Elsevier, Heidelberg).

Peth S, Nellesen J, Fischer G, Horn R (2010) Non-invasive 3D analysis of local soil deformation under mechanical and hydraulic stresses by µCT and digital image correlation. *Soil and Tillage Research*. (In press).

Dynamics of Soil Structure as a Function of Hydraulic and Mechanical Stresses

X. Peng[A], J. Dörner[B], R. Horn[C]

[A]State Key Laboratory of Soil and Sustainable Agriculture, Institute of Soil Science, CAS, Nanjing, 210008, P. R. China, Email xhpeng@issas.ac.cn
[B]Instituto de Ingenierı´a Agraria y Suelos, Universidad Austral, Casilla 567, Valdivia, Chile
[C]Institute of Plant Nutrition and Soil Science, Christian-Albrechts-Universität, 24118 Kiel, Germany

Abstract
The dynamics of soil structure is driven by hydraulic and mechanical stresses. Hydraulic stress causes soil swelling and shrinkage during natural wetting and drying. Mechanical load results in soil compaction. In this paper we combined the hydraulic and mechanical stresses by considering shrinkage, moisture release and compaction concurrently. The volume of rigid pores compacted by mechanical stress do not alter soil pore shrinkage capacity. Their shrinkage curves are parallel to each other with an identical coefficient of linear extensibility (COLE) and shrinkage slope, although their structural shrinkage phases narrow with an increase in compaction stress. With different shrinkage properties of rigid and non-rigid pores, we proposed numerical methods to illustrate the bundle of the e-ϑ-σ relationship as affected by mechanical stress stemming from tillage management, and to model the loaded soil shrinkage behavior. The similarity of soil shrinkage behavior before and after tillage management can be easily assessed regarding the dynamics of soil structure during natural wetting and drying cycles.

Key Words
Soil shrinkage, soil compaction, water retention curve, soil tillage

Introduction
For a nonrigid soil, soil porosity (e.g. void ratio, e) changes not only with mechanical stress (σ) but also soil moisture (e.g. moisture ratio, ϑ). The relationship between e and ϑ is well defined as soil shrinkage behavior, which has in general been studied under load-free conditions. The relationship between e and σ is often cited as the soil strain-stress, commonly used in both agricultural and geotechnical engineering to derive soil mechanics parameters. Baumgartl and Köck (2004) summarized the three relationships of e-ϑ, e-σ and ϑ-ψ, and addressed a similar behavior between soil deformation and soil moisture release due to hydraulic stress ψ or mechanical stress σ. However, knowledge of soil shrinkage as affected by soil loading conditions, which involves a bundle of shrinkage curves under mechanical stress, is still unclear. The mechanical stress from tractors occurs rapidly and is removed as soon as the tillage operation is complete. Thus, the soil becomes load-free again after the removal of the stress. Soil pores can be intensively compacted by a heavy agricultural machine in which structural pores or macropores are most susceptible but textural pores remain unaffected. Soil shrinkage is principally induced by the textural pores derived from active clay, rather than by the structural pores. Thus, we hypothesize that this tractor load does not modify soil shrinkage behavior.

Theory
Soil volume change by hydraulic stress
The soil volume (e.g., void ratio, e) can vary either with hydraulic stress or moisture ratio (ϑ) or with mechanical stress (σ). The relationship between the change of soil volume and hydraulic stress is defined as soil shrinkage and swelling, generally presenting a sigmoidal curve. In this study, we used a modified van Genuchten equation to fit the relationship between void ratio (e) and moisture ratio (ϑ):

$$e(\vartheta) = e_r + \frac{e_s - e_r}{\left[1 + (\chi\vartheta)^{-p}\right]^q} \qquad 0 \le \vartheta \le \vartheta_s, \qquad (1)$$

where χ, p and q are dimensionless fitting parameters. Parameter p in Equation 1 is always a positive value. e_s and e_r are the saturated and residual void ratios, respectively, which can be obtained either by measurements or by fitting. In this paper, we used the measured data. ϑ_s is the saturated moisture ratio.
If combining χ, p and q parameters, Equation 1 can be simplified as:

$$e(\vartheta) = e_r + (e_s - e_r)k(\vartheta), \qquad (2)$$

where

$$k(\vartheta) = \frac{1}{[1 + (\chi\vartheta)^{-p}]^q}. \qquad (3)$$

As discussed in Peng and Horn (2005), $k(\vartheta)$ describes a basic shape of soil shrinkage, depending on the type and the amount of active clay.

Soil volume change by mechanical stress

The change of soil volume (e) with the mechanical stress (σ) is termed as soil strain-stress relation or soil compaction in soil science and engineering. The relationship between them is in general a negative exponential as follows:

$$e(\sigma) = e_0 \exp(-b\sigma), \quad (4)$$

where e_0 is the initial void ratio prior to loading. Parameter b is the fitting dimensionless parameter.

Rigid and nonrigid pores of the soil

In this paper, we separated total pores ($V_{t.p}$) of a nonrigid soil into rigid ($V_{r.p}$) and nonrigid pores ($V_{nr.p}$) according their shrinkage and swelling capacity.

$$V_{t.p} = V_{r.p} + V_{nr.p}. \quad (5)$$

Hereby it needs to be pointed out that the 'rigid' of soil pores is not relative to the mechanical stress, but to the hydraulic stress or soil moisture.

Soil shrinkage under the mechanical stress

After loading by a mechanical stress, some rigid pores are lost, with macropores being the most susceptible. However, nonrigid pores are less affected, either by regaining structure immediately after stress removal or in the case of a large stress after subsequent wetting under load-free conditions. Therefore, the mechanical stress (σ_i) from tractor tillage only reduces rigid pores.

$$\Delta V_{t.pi} = \Delta V_{r.pi}. \quad (6)$$

Then, at a given moisture ratio (ϑ), the loaded void ratio ($e_i(\vartheta)$) is

$$e_i(\vartheta) = \frac{V_{t.p0}(\vartheta) - \Delta V_{r.pi}}{V_s}, \quad (7)$$

where V_s is the solid volume, independent of stress, $V_{t.p0}$ is the total pore volume of the soil prior to loading. In Equation (7), the subtract component $\Delta V_{r.pi}$ is constant during the entire shrinkage process, because the change of rigid pores is independent of soil moisture. Therefore, the difference of void ratios between the loaded soils before ($e_0(\vartheta)$) and after stress application ($e_i(\vartheta)$) is constant over the whole range of soil moisture.

$$e_0(\vartheta) - e_i(\vartheta) = \frac{\Delta V_{r.pi}}{V_s}. \quad (8)$$

Owing to no alteration of nonrigid pores, the pore shrinkage capacity (ζ), defined as the first derivative of soil shrinkage, remains identical after loading:

$$\frac{\partial e_i}{\partial \vartheta_i} = \frac{\partial e_0}{\partial \vartheta_0}. \quad (9)$$

Hereby we introduce the load-shrinkage factor (ϖ), defined as the ratio of the loaded to unloaded pore shrinkage capacity at a given moisture ratio. For the tractor-loaded soil, $\varpi(\vartheta, \sigma_i)$ is always 1 over the range of soil moistures.

$$\omega(\vartheta, \sigma_i) = \frac{\zeta_i(\vartheta, \sigma_i)}{\zeta_0(\vartheta, \sigma_0)} = 1. \quad (10)$$

In Equation (10), the unity ϖ is independent of the mechanical stress and soil moisture. If taking Equation (1) to fit soil shrinkage, an identical shrinkage slope can be defined before and after loaded as follows:

$$(e_{si} - e_{ri})k_i'(\vartheta) = (e_{s0} - e_{r0})k_0'(\vartheta). \quad (11)$$

In Equation (10), it must be

$$k_i'(\vartheta) = k_0'(\vartheta). \quad (12)$$

The $k(\vartheta)$, or three parameters of χ, p and q, describing the basic shape of soil shrinkage, are independent of the stress. The difference between e_s and e_r is a factor for the magnitude of the pore shrinkage capacity. Their soil shrinkage curves derived from various transient stresses are thus parallel to each other. The only difference between them is a shift of void ratio with a magnitude of $\Delta V_{r.pi}/V_s$. The maximum shift should take place when all rigid pores ($V_{r.p}$) are compacted. Therefore, the loaded soil shrinkage curve can be derived from the load-free soil shrinkage as follows:

$$e_i(\vartheta_i) = e_{r0} - (e_{s0} - e_{si}) + \frac{e_{s0} - e_{r0}}{[1 + (\chi\vartheta_i)^{-p}]^q} \quad 0 \le \vartheta_i \le \vartheta_{si}. \quad (13)$$

If the residual void ratio of the loaded soil (e_{ri}) is available, Equation (13) can be simplified as:

$$e_i(\vartheta_i) = e_{ri} + \frac{e_{s0} - e_{r0}}{[1+(\chi\vartheta_i)^{-p}]^q} \quad 0 \le \vartheta_i \le \vartheta_{si}. \qquad (14)$$

In Equation (14), e_{si} is an exponential decay with the applied stress (σ) (see Equation 4). If combining Equations (4) and (14), the loaded soil shrinkage can be rewritten as:

$$e_i(\vartheta_i, \sigma_i) = e_{r0} - e_{s0}[1-\exp(-b_i\sigma_i)] + \frac{e_{s0} - e_{r0}}{[1+(\chi\vartheta_i)^{-p}]^q} \qquad 0 \le \vartheta_i \le \vartheta_{s0} - \frac{\Delta V_{r.pi}}{V_s}. \qquad (15)$$

Equation (15) formulates the relation between soil volume (e), soil moisture (ϑ) and stress (σ_i).

Table 1. Saturated void ratio (e_s) of different textural soils after loaded by the mechanical stress.

Treatments	Added sand /g kg^{-1}	Clay /g kg^{-1}	Silt + sand /g kg^{-1}	150 kPa (1.208)[a]	400 kPa (0.893)	1400 kPa (0.656)
S 0	0	649	351	1.600 ± 0.024[b]	1.293 ± 0.028	1.082 ±0.011
S 1	100	590	410	1.522 ± 0.008	1.192 ± 0.030	0.942 ± 0.017
S 2	200	541	459	1.476 ± 0.017	1.184 ± 0.022	0.930 ± 0.016
S 3	300	499	501	1.453 ± 0.009	1.144 ± 0.025	0.913 ± 0.009

[a] Stress followed by the corresponding initial void ratio in parentheses.
[b] Mean saturated void ratio ± standard deviation.

Materials and methods

Sieved <2 mm soil samples were added with 0%, 10%, 20%, and 30% clean sand (0.2-0.63 mm) in mass. The four soil-sand admixtures of adding 0%, 10%, 20%, and 30% were defined as treatments of S0, S1, S2, and S3, respectively, in this paper. The soil-sand admixtures were then wetted with distilled water up to a defined water content at the plastic limit. The admixtures were homogeneously repacked by uniaxial compressive loads of 150, 400, or 1400 kPa (Model 5569 series, Instron, UK). It took about 30 sec to reach the desired stress at the speed of 60 mm min^{-1}. The stress was released immediately after compacting. Three initial void ratios of 1.208, 0.893, and 0.656 were obtained corresponding to the three stresses (Table 1). Each treatment was in triplicate. During the wetting process, soils swelled to some extent, depending on soil texture and initial void ratio. The addition of sand increased void ratio and decreased swelling (Table 1). The part of swelling soils above the cylinder was cut. The saturated soil samples were then dehydrated successively on ceramic plates at water potential of -3, -6, -15, -30, -50, -100, and -500 kPa. At the water potential more negative than -500 kPa, samples were shifted to air-dry at a room temperature of 20 ± 2°C continuously for 7 d. Measurements were taken on the second day (airdry02), fourth day (airdry04), and seventh day (airdry07). They were then stepwise ovendried at 30, 60, and 105°C. At each step, soil moisture ratios were recorded from mass measurement, and the vertical deformations were measured at 9-points on the soil surface using a caliper gauge. Due to homogeneous samples, the soil-volume changes in this study were assumed to result from isotropic shrinkage. For more details please see Peng *et al.* (2009).

Results and discussion

All measured soil shrinkage curves are sigmoidal for the four different soil-sand mixtures, although their starting points of the saturated void ratios are different (Figure 1). The stronger the applied stress, the more the saturated void ratio and the total pore volume were reduced. At a given soil texture, the three soil shrinkage curves, derived from three different transient stresses, were parallel to each other. The only difference was that soils loaded by the stronger stress presented a narrower structural shrinkage phase on the moisture ratio aspect. The coefficient of linear extensibility (COLE), which is defined as the one-dimensional variation of soils between wet and dry states, was not significantly different between the three loaded soils (Figure 2). Figure 2 also shows that their slopes at the inflection point of their shrinkage curves fitted by Equation (1) were identical. This similarity demonstrates that the mechanical stress simulating the tractor load does not alter soil shrinkage behavior.

Effect of stress on soil moisture release

The rigid pores reduced by the stress were in general macropores, while the micropores were far less susceptible. Therefore, moisture ratios were smaller at less negative water potentials for the soils loaded by higher stress, but they finally tended to converge together with those of the lightly-loaded soils when the water potential reached more negative than -30 kPa (Figure 3). Consequently, hydraulic properties were different at near saturation as affected by the stress, but they were assumed to be same for the pores which were finer than the pore size equivalent to -30 kPa water potential.

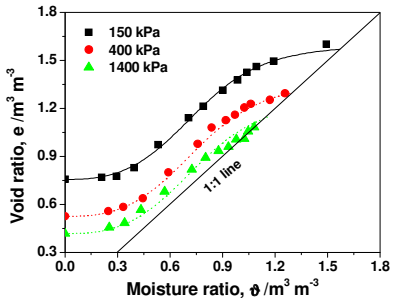

Figure 1. Example of parallel shrinkage curves loaded by different mechanical stresses (S 0)

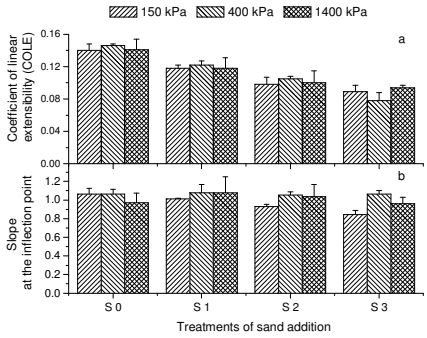

Figure 2. Effects of mechanical stress on the COLE (a) and the slope at the inflection point (b) of soil shrinkage curves fitted by Equation (1) for the four soil-sand mixtures.

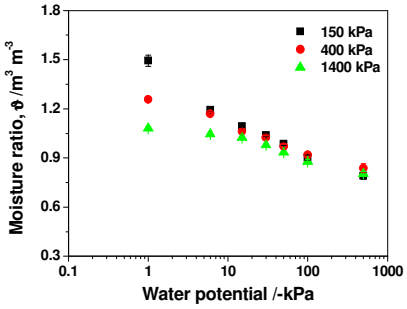

Figure 3. Example of soil water release curves loaded by different mechanical stresses (S 0)

Conclusions

The mechanical stress stemming from tractor tillage management cannot change nonrigid pores but it can compact rigid pores, especially macropores. The change of rigid pores does not modify pore shrinkage capacity, so that the loaded soil shrinkage curves are parallel to each other with identical shrinkage slope and COLE values. Based on these, we developed a numerical model to explain the relationship between soil volume (e), soil moisture (ϑ) and mechanical stress (σ). The soil shrinkage behavior after loading can be predicted. This study improves our understanding of the dynamic of nonrigid soil structure with hydraulic and mechanical stress.

References

Baumgartl T, Köck B (2004) Modeling volume change and mechanical properties with hydraulic models. *Soil Science Society of America Journal* **68**, 57-65.

Peng X, Horn R (2005) Modeling soil shrinkage curve across a wide range of soil types. *Soil Science Society of America Journal* **69**, 584-592.

Peng X, Dörner J, Zhao Y, Horn R (2009) Shrinkage behaviour of transiently- and constantly-loaded soils and its consequences for soil moisture release. *European Journal of Soil Science* **60**, 681-694.

Richard G, Cousin I, Sillon JF, Bruand A, Guérif J (2001) Effect of compaction on the porosity of a silty soil: influence on unsaturated hydraulic properties. *European Journal of Soil Science* **52**, 49-58.

Effect of land use changes on the dynamic behaviour of structure dependent properties of an Andisol in southern Chile

José Dörner[A], Dorota Dec[A], Rainer Horn[B] and Xinhua Peng[C]

[A]Faculty of Agricultural Sciences, Austral University of Chile, Valdivia, Chile, Email josedorner@uach.cl
[B]Faculty of Agricultural and Nutritional Sciences, University of Kiel, Kiel, Germany, Email rhorn@soisl.uni-kiel.de
[C]State Key Laboratory of Soil and Sustainable Agriculture, Chinese Academy of Sciences, Nanjing, China Email xhpeng@issas.ac.cn

Abstract
In order to describe the effect of land use changes on the dynamic behaviour of structure dependent properties of an Andisol in southern Chile, disturbed and undisturbed soil samples were collected in a native forest (NF), cropland (C) and 30 year old pasture (P). The soil cores were subject to mechanical (n: 4) and hydraulic stresses (n: 7) to evaluate their i) soil deformation (COLE: coefficient of linear extensibility calculated for mechanical and hydraulic stresses), ii) pore functions and iii) resilience. The hydraulic deformation was less ($COLE_{hd}$: 0.04-0.08) when compared to the effect of mechanical stresses ($COLE_{ml}$: 0.3-0.5). On the other hand, the volume recovered after the hydraulic (52% and 33% in 5 and 20 cm depth) stress was greater than after the mechanical stress (28% and 19% in 5 and 20 cm depth). The land use change affected the volumetric resilience of the soil, particularly after soil compression. The latter is related to the amount of soil organic carbon. Both mechanical and hydraulic stresses altered the bulk density of the soil. However, while the loading cycle induced a decrease of air conductivity as a consequence of a reduction of macro pores, the drying cycle caused an increase in air conductivity due to the formation of continuous macro pores between aggregates.

Key Words
Soil structure, consolidation, shrinkage, resilience, pore functions, volcanic soils

Introduction
It is well known that Andisols (Soil Survey Staff, 2006) exhibit very special natural properties like variable charge, high phosphate retention (Shoji *et al.,* 1993), low bulk density, large air and water holding capacity (Ellies, 1988; Dorel *et al.,* 2000), high hydraulic conductivity (Ellies *et al.,* 1997), stable soil aggregates (Hoyos and Comerford, 2005) and great shrinkage capacity (Dörner *et al.,* 2009). The volcanic soils in southern Chile cover a wide range of land uses (e.g. native forest, grasslands and croplands) allowing us to evaluate the effect of an intensification of land use on structure dependent properties and their resilience after different kinds of stresses. The structural changes are not only due to external forces like e.g. soil compaction (Ellies, 1988; Ellies *et al.,* 2000), but also to internal processes as a consequence of water menisci forces during wetting and drying cycles (Seguel and Horn, 2006; Dörner *et al.,* 2009). This study's objective was to describe the effect of land use changes on the dynamic behaviour of structure dependent properties of an Andisol depending on external and internal forces and their consequences on soil deformation, function and resilience.

Methods
Soil and land uses
An Andisol (Serie Los Lagos) was used to determine the effect of three land use systems (NF: native forest, C: crop, P: 30 years old pasture) on the dynamic behaviour of structure dependent properties (bulk density and air conductivity) as a function of load/unload (l/u) and drying/wetting (d/w) cycles.

Soil sampling and measurements
The sampling took place at the beginning of October 2008. Disturbed and undisturbed soil samples were collected at 5 and 20 cm depths at the three land uses of NF, C and P. In order to define the soil response to mechanical and hydraulic stresses, the undisturbed soils were sampled in metallic cylinders of 220 and 110 cm^3, respectively.

Laboratory determinations
General properties of the soil such as soil texture, organic carbon, and allophane among others, were measured as presented in Dörner *et al.* (2009).
In order to determine the soil shrinkage curve, the samples (n: 7) were first carefully saturated from beneath and then drained at matric potential values of -1, -2, -3, -6, -15, -33, -50 kPa. To characterize the shrinkage behaviour at matric potentials lower than -50 kPa, samples were shifted to dry air conditions (20 and 30ºC for

10 and 14 days, respectively). Thereafter, the samples were rewetted again and then dried at the same matric potential values as in the first drying cycle and shifted to dry air conditions (20 ± 2°C) for 14 d and then stepwise oven dried at 30, 60, and 105°C. From saturation and throughout the different matric potentials, dehydration temperatures and rewetting, the water content and vertical deformation (measured in 7 points for each soil sample) were recorded with an electronic balance and caliper gauge (0.05 mm accuracy). The air conductivity of each sample was recorded with an air permeameter at a matric potential of -60 hPa.

To define the soil response to mechanical stresses, soil samples (n: 4) equilibrated at matric potential values of -60 hPa were placed in an odometer to define the consolidation curve. The samples were stressed uniaxially at 6, 12, 25, 50, 100, 200 and 400 kPa by static loading for 6 minutes. Thereafter, the loads (σ_n) were removed until 200, 100, 50, 6, 1 kPa were reached. The soil deformation was measured during the experiment (0.05 mm accuracy).

Calculations

The coefficient of linear extensibility (COLE) was used to evaluate the effect of the land use change on the dynamic behaviour of the soil volume as a consequence of a load/unload and drying/rewetting cycle. This index, which defines the one-dimensional variation of soils from wet to dry conditions (Grossman *et al.* 1968) has been used by many authors (Gray and Allbrook, 2002; Peng *et al.,* 2007) to quantify the shrinkage magnitude. The hydraulic COLE during rewetting (hr) after air drying at 30ºC and after complete drying (hd) was calculated as follows:

$$COLE_{hr} = \frac{L_{30°C} - L_0}{L_{30°C}} \qquad (1) \qquad\qquad COLE_{hd} = \frac{L_0 - L_{105°C}}{L_{105°C}} \qquad (2)$$

where L_0, $L_{30ºC}$ and $L_{105ºC}$ are the length of the sample at saturation and after air and oven drying at 30 and 105 ºC, respectively. We modified the index for the load ($COLE_{ml}$) and unload cycle ($COLE_{mu}$):

$$COLE_{ml} = \frac{L_0 - L_{\sigma_n}}{L_{400kPa}} \qquad (3) \qquad\qquad COLE_{mu} = \frac{L_{400kPa} - L_{\sigma_n}}{L_{400kPa}} \qquad (4)$$

where L_0, $L_{\sigma n}$ and L_{400kPa} are the length of the sample at the beginning, after different normal stresses and 400 kPa.

Results

General properties of the soils

The high SOC concentration, large TP and the presence of allophane are typical characteristics of volcanic soils (Table 1). SOC and allophane are depth-dependent properties. While allophane and particle density both increase, SOC decreases with soil depth in NF and P. SOC in C slightly increase as a consequence of soil ploughing. Among the three land uses the grain size distribution and the amount of allophane did not present large differences at the same depth. However, the shift from NF to cropland causes a decrease of SOC by 20% in C and 22% in P for the top 5 cm layer. On the other hand, the total porosity (TP) decreased by 5 and <1% when land use changed from NF to C and to P.

Table 1: General properties of the soils studied.

Land Use	Depth	Sand	Silt	Clay	Allophane	SOC	ρ_s	TP
[-]	[cm]	----------[g/kg]----------					[g/cm^3]	[%]
NF	5	354	531	115	70	93.9	2.05	66.9
	20	546	350	105	118	47.6	2.36	71.5
C	5	366	512	123	80	75.4	2.24	62.9
	20	480	407	113	105	80.0	2.30	64.7
P	5	377	493	130	94	73.1	2.24	66.5
	20	410	470	120	110	68.4	2.36	74.9

Sand: 2000 – 630 µm, Silt: 630 – 2 µm, Clay: <2 µm; SOC: soil organic carbon, ρ_s: particle density, TP: total porosity,

Effect of land use on soil deformation and resilience as a consequence of mechanical and hydraulic stresses

Both mechanical and hydraulic stresses induced soil deformation as expressed by COLE (Figure 1A). The hydraulic deformation was smaller as compared to the effect of mechanical stresses. The change in land use affected the mechanical COLE, i.e. as the soil was disturbed/ploughed and then compacted (soil under crop and pasture) the COLE decreased from NF to C 23% and NF to P 38% at the 5 cm depth. Similar tendencies were observed at the 20 cm depth and were also true when the drying intensity of the soil in the field increased as a

consequence of the land use change (exception NF to P at the 5 cm depth).

The soil resilience was also evaluated with COLE (Figure 1B). All depths were able to recuperate partly as compared to the initial conditions. The volume recuperation after the hydraulic (π: 52% and 33% at 5 and 20 cm depths) stress was greater than the mechanical (π: 28% and 19% at 5 and 20 cm depths) indicating that the applied load largely exceeded the precompression stress while the preshrinkage stress probably did not. The land use change affected the volumetric resilience of the soil, particularly, after soil compression. The latter, which was not so clear after hydraulic stress, is related to SOC as also assessed by Ellies (1988).

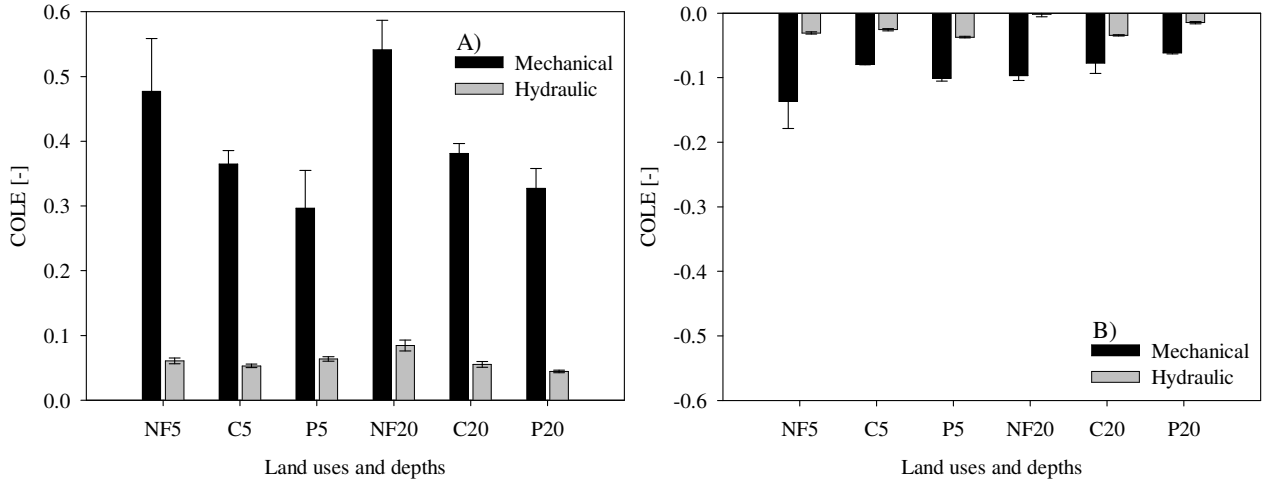

Figure 1. Effect of mechanical and hydraulic stresses on the coefficient of linear extensibility (COLE) after (A) load (0 – 400 kPa)/drying (0 hPa – 105ºC) and (B) unload (400 – 0 kPa)/rewetting (30ºC – 0hPa) for different land uses (NF: native forest, C: crop, P: 30 years old pasture) and depths (5 and 20 cm). Bars indicate ± 1 standard error.

Soil structure and its functional resilience after mechanical and hydraulic stresses
Both kinds of stress induced an increase in the bulk density (Figure 2). The mechanical stress induced the largest differences in bulk density before and after the compression cycle (NF: 34%, C: 29% and P: 19%).

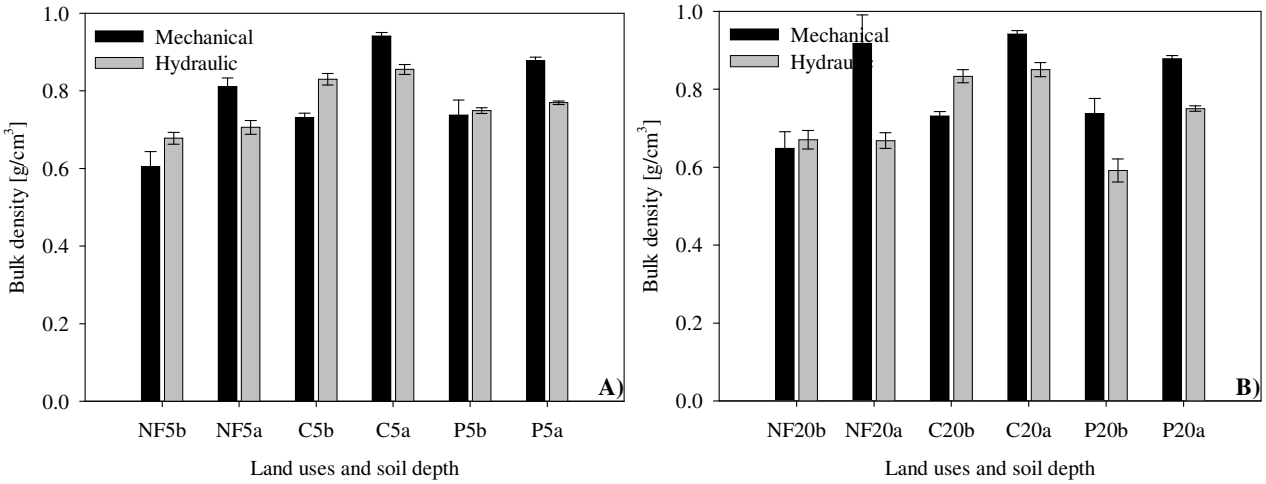

Figure 2. Effect of mechanical and hydraulic stresses (b and a: before and after compression or drying cycle, respectively) on the bulk density for different land uses and depths (A: 5cm and B: 20 cm depth). Bars indicate ± 1 standard error.

The soil deformation altered the soil structure (Figure 2) and consequently the pore functions as expressed by the air conductivity (Figure 3). However, the effect of both kinds of stress differed, i.e. while the air conductivity decreased as a consequence of soil compaction, the same property increased when, due to water menisci formation, soil shrinkage and crack formation took place.

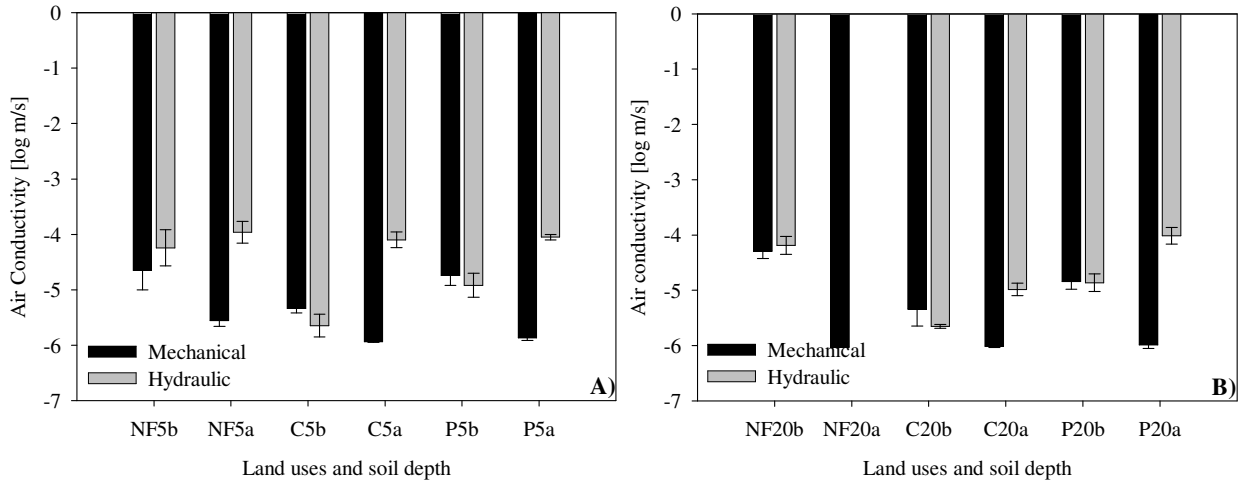

Figure 3. Effect of mechanical and hydraulic stresses (b and a: before and after compression or drying cycle, respectively) on air conductivity for different land uses and depths (A: 5cm and B: 20 cm depth). Bars indicate ± 1 standard error.

Conclusion

The soil structure (e.g. bulk density) of the studied Andisol presented a dynamic behaviour and changed as a consequence of drying/rewetting and load/unload cycles. An intensification of the land use induced greater mechanical and hydraulic stresses in the soil. The latter meant improved structure stability (e.g. lower COLE) but lower resilience. Both mechanical and hydraulic stresses altered the bulk density of the soil. However, while the loading cycle induced a decrease of air conductivity as a consequence of a reduction of macro pores, the drying cycle caused an increase in air conductivity due to the formation of continuous macro pores between aggregates.

Acknowledgements

This study was sponsored by FONDECYT 11060130. The authors also thank the international cooperation programs FONDECYT 7070332 and CONICYT - DFG.

References

Dörner J, Dec D, Peng, X, Horn R (2009) Change of shrinkage behavior of an Andisol in southern Chile: Effects of land use and wetting/drying cycles. *Soil and Tillage Research* **106**, 45-56.

Ellies A (1988) Mechanical consolidation in volcanic ash soils. In 'Impact of Water and External Forces on Soil Structure'. (Eds J Drescher, R Horn, M De Boodt). Catena, Suppl. **11**, pp. 87-92.

Ellies A, Grez R, Ramírez C (1997) La conductividad hidráulica en fase saturada como herramienta para el diagnóstico de la estructura del suelo. *Agro. Sur.* **25**(1), 51-56.

Gray CW, Allbrook R (2002) Relationships between shrinkage indices and soil properties in some New Zealand soils. *Geoderma* **108**, 287-299.

Grossman RH, Brasher BR, Franzmeier DP, Walker JL (1968) Linear extensibility as calculated from natural-clod bulk density measurements. *Soil Science Society of America Proceedings* **32**, 570-573.

Hoyos N, Comerford N (2005) Land use and landscape effects on aggregate stability and total carbon of Andisols from Colombian Andes. *Geoderma* **129**, 268-278.

Peng X, Horn R, Smucker A (2007) Pore shrinkage dependency of inorganic and organic soils on wetting and drying cycles. *Soil Science Society of America Journal* **71**, 1095-1104.

Seguel O, Horn R (2006) Structure properties and pore dynamics in aggregate beds due to wetting-drying cycles. *Journal of Plant Nutrition and Soil Science* **169**, 221-232.

Shoji S, Nanzyo M, Dahlgren RA (1993) 'Volcanic Ash Soils – Genesis, Properties and Utilization'. (Elsevier: Amsterdam). 288pp.

Soil Survey Staff (2006) 'Keys to Soil Taxonomy'. 10th ed. (NRCS: Washington DC).

Effects of soil slaking and sealing on infiltration – experiments and model approach

Jürgen Schmidt[A]

[A]Faculty of Geosciences, Technical University Freiberg, Saxony, Germany, Email jschmidt@tu-freiberg.de

Abstract
The use of soils for agriculture replaces natural vegetation cover with an intermittent coverage by crops. Thus, the protection of soils from direct raindrop impact is temporarily suspended. Soil slaking and sealing are the inevitable consequences. Although these processes affect only the uppermost soil layer of some millimetres in depth, soil slaking and sealing impede substantially the infiltration of rainwater into the soil. The paper presents a theoretical approach which allows one to estimate the change of hydraulic permeability at the soil surface as a function of time after tillage and tillage practice. Based on laboratory and field experiments the method is tested exemplarily.

Key Words
Soil structure, rain water infiltration, soil erosion

Introduction

Soil slaking and sealing are frequent features of many cultivated soils. The terms ‘slaking’ and ‘sealing’ refer to the breakdown of soil aggregates and the formation of a sealing skin that makes the soil surface less permeable (Mualem *et al* 1990; Assouline 2004). The physical processes of soil slaking and sealing are the result of the kinetic impact of raindrops on the soil surface and the translocation of soil particles by flowing water. When the drop impact forces exceed the internal cohesion of the impacted soil aggregates they break down into primary mineral particles. These particles are transported by surface runoff or washed into the soil surface layer (Figure 1). When deposited the translocated particles could clog soil pores and form superficial layers characterised by higher bulk density and lower saturated hydraulic conductivity than the soil beneath (Betzalel *et al* 1995). Due to the loss of soil water storage and infiltration capacities soil erosion and the risk of flooding are substantially increased. Based on laboratory and field experiments this study aims to estimate the change of hydraulic permeability at the soil surface as a function of time after tillage and tillage practice.

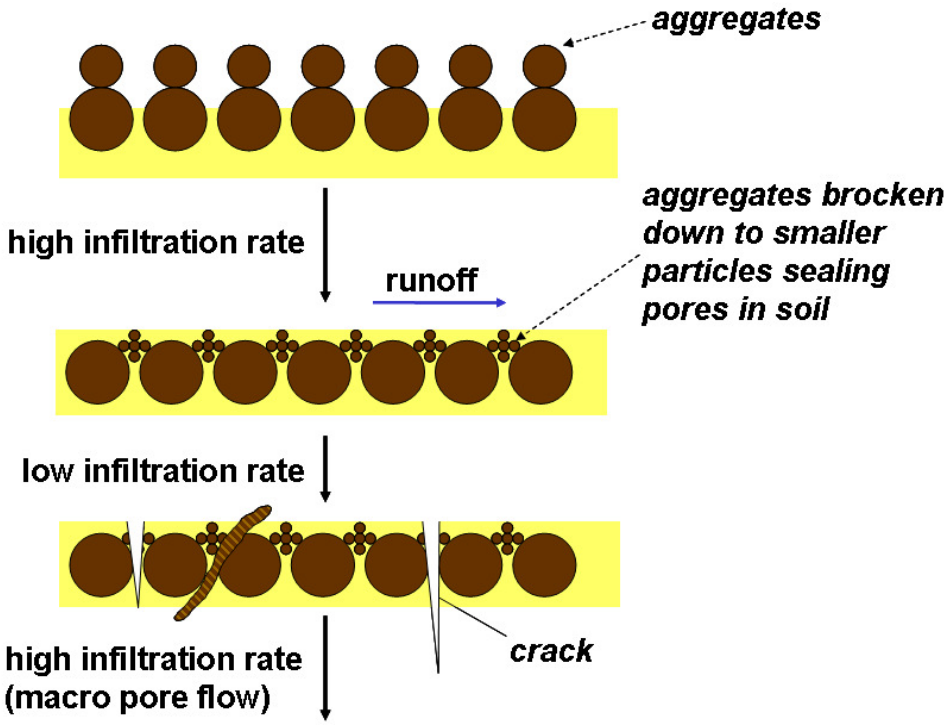

Figure 1. Scheme of soil slaking and sealing processes (adapted from Greener (2001)).

Methods

This paper refers to the EROSION 2D/3D computer model which simulates soil erosion by water on single slopes and small catchments (Schmidt 1996). The runoff subroutine of EROSION 2D/3D uses a modified Green and Ampt infiltration equation in order to calculate rainfall excess:

$$i = k_s \cdot g + k_s \cdot \frac{\Psi_{m0}}{\sqrt{\frac{2k_s \cdot \Psi_{m0} \cdot t}{\rho_f \cdot (\Theta_s - \Theta_0)}}}$$

where i ... infiltration rate [kg/(m^2 s)], k_s ... saturated hydraulic conductivity [(kg s)/m^3], g ... gravity [m/s^2], Ψ_{mo} ... matric potential related to the initial water content Θ_0 [N m/kg], t ... time [s], ρ_f ... fluid density [kg/m^3], Θ_s ... saturated water content [m^3/m^3], Θ_0 ... initial water content [m^3/m^3].

According to Campbell 1985 the saturated hydraulic conductivity can be estimated by applying the following empirical function:

$$k_s = 4 \cdot 10^{-3} \cdot \left(1{,}3 \cdot 10^{-3} / \rho_b\right)^{1{,}3 \cdot b} \cdot \exp\left(-0{,}069 \cdot T - 0{,}037 \cdot U\right)$$

with

$$b = \left(10^{-3} \cdot D\right)^{-0{,}5} + 0{,}2 \cdot \delta_p$$

where k_s ... saturated hydraulic conductivity [(kg s)/m^3], ρ_b ... bulk density [kg/m^3], T ... clay content [kg/kg], U ... silt content [kg/kg], b ... parameter [-], D ... mean diameter of soil particles [m], σ_P ... standard derivation of the mean diameter of soil particles [-].

Because Campbell's equation presupposes a rigid soil matrix the temporal variability of soil structure due to tillage, slaking and sealing, shrinking and swelling, biological activities etc. have to be considered by an additional empirical parameter which allows one to calibrate the saturated hydraulic conductivity k_s on the basis of measured data. In the EROSION 2D/3D model this parameter is called skin-factor Sk_f. Values of Sk_f <1 reduce the infiltration rate, in order to take the effects of soil slaking and sealing as well as anthropogenic compaction into account. Values of Sk_f >1 causes a positive correction of infiltration rate, e.g. for the consideration of an increased infiltration in macropores due to soil shrinking, biological activity or tillage impact. If Skf =1 infiltration rate is obviously not affected by either slaking and sealing or macropores. Figure 2 shows the effect of altering the skin-factor in order to fit simulated infiltration rates to measured data from plot experiments.

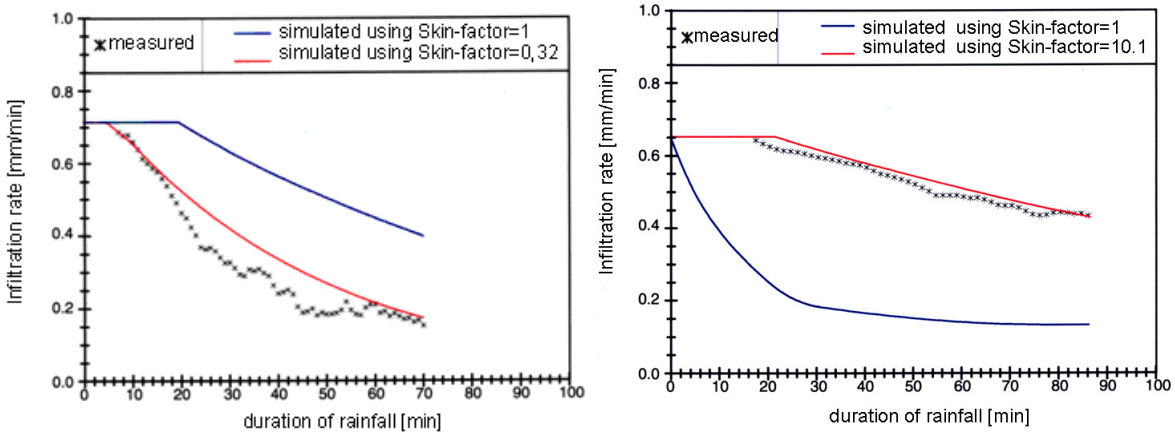

Figure 2. Measured and simulated infiltration rates as a function of time with skin-factor used as fitting parameter.

Results

Using experimental data from two soil erosion plots the temporal variability of skin-factors was estimated as a function of time after tillage. Experiments were conducted on silty soils because these are susceptible to soil slaking and sealing in particular. Data refer to 6 natural rainfall events over a period of approx. 100 days. Generally the results show that just after ploughing the hydraulic conductivity of the top soil is artificially increased and Skin-factors are characterized by values >1. However, because of the weak stability of the loosened top soils they change back to their original bulk density after a certain period of time. Linked to this process generally a compacted and less permeable skin is formed at the soil surface. Accordingly Skinfactors decrease to values <1.

Figure 4 refers to results of laboratory experiments using three different rainfall intensities produced by a capillary rainfall simulator. The skin-factor is plotted as a function of cumulative rainfall instead of time as depicted in Figure 3. The loosened soil at the beginning of the experiment results in rather high skin-factors. As expected, skin-factors decrease with cumulative rainfall and approach a constant value of approximately 1 indicating a stable soil structure. Surprisingly, rainfall intensity does not affect the skin-factor reaction. Consequently kinetic energy of raindrop impact can not be the main trigger for seal formation in contrary to the results of Betzalel *et al* (1995).

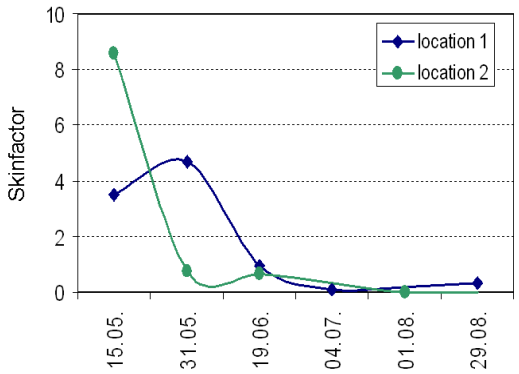

Figure 3. Change of skin-factors over time after tillage (based on experimental results of Botschek 1998).

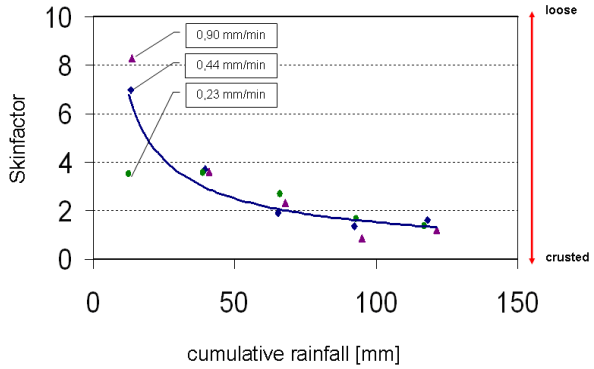

Figure 4. Skin-factor as a function cumulative rainfall

Figure 5 shows skin-factors of 32 fields in the loess region of southeast Germany classified according to different tillage practices. Data are results from plot experiments using a nozzle-type rainfall simulator.

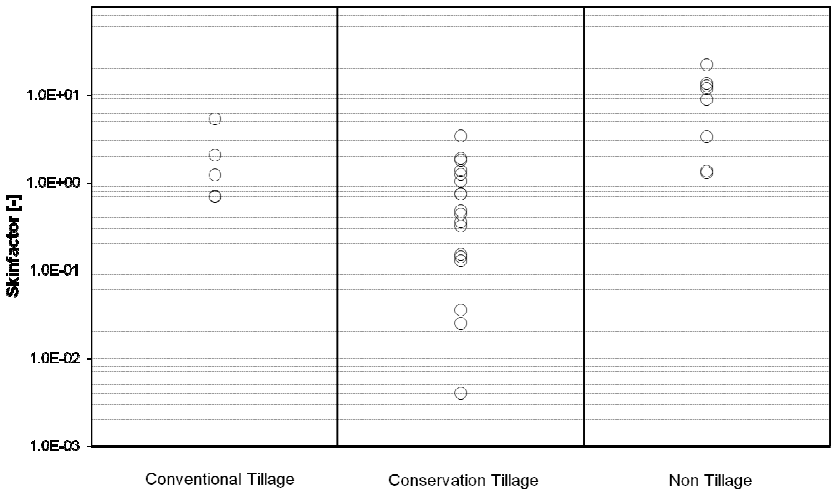

Figure 5. Variation of skin-factors depending on tillage practice (Schindewolf and Schmidt 2009).

Conservation tillage aims to reduce the impact of tillage operation on soil structure by using shallow working cultivators instead of more invasive plows. However, conservation tillage techniques are not defined very well, which might be the reason for the great variation of the resulting skin-factors compared to conventional tillage. Non-tillage practices result in significantly higher skin-factors indicating a higher amount of macropores open to the soil surface compared to conventional and conservation tillage.

Conclusion

The hydrologic effects of soil slaking and sealing can be estimated adequately by using the skin-factor approach. Skin-factors decrease with time after tillage respectively cumulative rainfall due to gradual structural disintegration of the soil surface. The decrease is not affected by rainfall intensity. Non-tillage practices tend to increase skin-factors suggesting a higher share of macropore-flow to infiltration compared to conventional and conservation tillage.

References

Assouline S (2004) Rainfall-Induced Soil Surface Sealing. *Vadose Zone Journal* **3,** 570-591.

Betzalel I, Morin J, Benyamini Y, Agassi M, Shainberg I (1995) Water drop energy and soil seal properties. *Soil Science* **159,** S. 13-22.

Botschek J (1998) Kennzeichnung des Bodenerosionspotentials von Oberflächen- und Zwischenabfluß - dargestellt an zwei kleinen Wassereinzugsgebieten. Habilitations-thesis University of Bonn.

Campbell GS (1985) 'Soil Physics with Basic: Transport models for soil-plant systems'. (Elsevier*:* Amsterdam, Oxford, New York, Tokyo).

Greener M (2001) Incorporating sediment transport competence into existing soil erosion models. PhD thesis, University of Leicester.

Mualem Y, Assouline S, Rohdenburg RH (1990) Rainfall induced soil seal (A) A critical review of observations and models. *Catena* **17,** S. 185-203.

Schindewolf M, Schmidt J (2009) Parameterization of a soil erosion model using a small scale rainfall simulator and upstream runoff simulation. *Catena* (submitted).

Schmidt J (1996) Entwicklung und Anwendung eines physikalisch begründeten Simulationsmodells für die Erosion geneigter landwirtschaftlicher Nutzflächen. Berliner Geographische Abhandlungen 61.

Hydrodynamic behaviour of Segura River basin soils: Effects of texture and moisture contents

Antonio Sánchez Navarro[A] , Purificación Marin Sanleandro[A], Mª José Delgado Iniesta,[A] Maria García González[A], Arantzazu Blanco Bernardeau[A], Juana María Gil Vázquez and **Roque Ortiz Silla[A]**

Agricultural Chemistry, and Pedology Dept, Faculty of Chemistry, University of Murcia, Murcia, Spain. Email rortiz@um.es

Abstract
Soil physical and chemical properties determine the hydrological behaviour of soil. From this hypothesis, the objective of this study was to establish pedotransfer functions able to determine soil hydrodynamic characteristics from the analytical data available in the current soil maps of Segura River watershed. The range of values and the average of every soil parameter were estimated for every soil type. In this work, granulometric characterization was carried out in addition to water retention capacity at 1/3 and 15 atm pressure to 685 arable soil layer samples corresponding to surface A horizons from the soil profiles. It was proven that these parameters did not show important changes on most predominant soil types of the area, being only different in Arenosols, Cambisols, Vertisols and Fluvisols. Therefore, hydrodynamic behaviour of these soil types must be influenced by those parameters.

Key Words
Hydrodynamic properties, FAO soil units, texture, water retention capacity, semiarid soil

Introduction

Water flow and availability of the soils-plant-atmosphere system is controlled by its hydric and hydrodynamic properties. The soil water behaviour is conditioned by physical properties and the chemical properties affecting to soil physical characteristics. Soil surface characteristics regulate water distribution in the hydrological cycle. In this way, soil water has a dynamic behaviour whose understanding achieves a key importance, mainly in areas with serious water stress as it occurs in the Segura River catchment.

A very important soil function, as a component of the ecosystem, is the collecting, storage and control of water dynamic within soil profile. This soil function is fundamental for biomass productivity and suitable environmental conditions. An appropriate soil infiltration increases the soil capacity for the storage of available water for plants and aquifers recharge with the decrease as a consequence of runoff and soil erosion. Soil water movement and storage are controlled by the structure of surface soil horizons. Crust formation and soil compaction could lead to soil sealing. (Duley 1939; Morin *et al*. 1989).

In this study the soil granulometric characterization and soil moisture retention at 1/3 and 15 atm from the A horizons of 685 soil profiles were accomplished. From these data base an estimation of the effects of above mentioned parameters on hydrodynamic soil properties of the Segura River Basin was carried out.

Methods

Study area and previous data
The study was carried out in the Segura River Basin (Murcia, Spain) from the data base constituted by soil parameters of surface horizons (A) of soil profiles studied in the LUCDEME Project (Fight against the desertification in the Mediterranean, 1983-2006).

Statistical methods.
The data were statistically treated using the R software. When conditions of normality and homoscedasticity could be assumed, an ANOVA test was carried out to compare means; otherwise a non-parametric test of comparison of ranges was applied (Wilcoxon Test)

Laboratory methods
Soils were classified following the "World Reference Base for Soil Resources 2006" (FAO-ISRIC-IUSS, 2006). Surface soil samples (0-30 cm) for laboratory analysis were sieved through 2 mm mesh. The following parameters were analysed: Water retention capacity was determined by membrane method (Richards 1941) at 1/3 atm (field capacity) and 15 atm (wilting point). Available Water (AW) was considered the difference

between water retained at pF 1/3 and 15 atm. Granulometric analysis was determined after total dispersion of soil samples by shaking with sodium hexametaphosphate at 5%. Sand, silt and clay fractions were isolated from the dispersed samples through decantation and extraction with a Robinson pipette.

Results

More than 40% of the total soil units in the FAO-ISRIC-UISS (2006) classification were differentiated in the Segura Basin (Figure 1) The most spreaded soil was Calcisols, covering 51% of the Basin area. The following in extension order were Regosols, Leptosols and Fluvisols covering 14,86, 14,24 and 10,93 of the surface area respectively. The other nine units constitute all together, only the 8% of the Basin area. There was evidence, out of this soil units distribution, of the predominance of soils with ochric epipedon, while the mollic epipedon was only evident in Kastanozems, Phaeozems and some Leptosol.

With regard to granulometric composition, in general the balanced textures prevail, with sand and silt averages ranging between 30 and 40% and clay about 20%. However, a more detailed analysis of the data showed clear differences among some of the main soil units. In this way, the highest differences occur in Arenosols, which, as can be expected, have a very coarse texture, being the sand average near 95% of the total mineral fractions in the soil. The same occurs with Cambisols, where the sand fraction was the 67.83%, while clay and silt fraction only reach 14%.

Totally opposite to those mentioned above are Vertisols, in which the prevailing fractions are clay (56.52%) and silt (42.80%), with sand averages lower than 1%.

The rest of the main units showed apparently similar granulometric compositions, with clay aggregates close to 20% except for the Fluvisols where this percentage has an increase up to a bit more of 25%, may be as a consequence of their fluventic origin and their physiographic location, predominantly valley bottoms and alluvial plains.

The pF values at 1/3 and 15 atm and, therefore, the water availability, showed that the most main units have levels ranging between 12 and 13%, so that, as it happened with the granulometric composition, we can assume that their hydrodynamic behaviour is very similar. Arenosols and Cambisols have statistically lower water availability values ($p<0,01$), in concordance with their sandy texture, while in Gleysoles and Fluvisols, values were 14.80 and 19.64% respectively, so higher than the media, although this diference has no statistical signification.

Table 1. Average values of water content (%) and principal granulometric fractions of surface horizons by RSG.

Soil Group	pF 1/3 atm	pF 15 atm	AW*	Sand (%)	Silt (%)	Clay (%)	Area (%)
Arenosols	3,85	1,66	2,19^{a}	94,23^{a}	2,37^{a}	3,40^{a}	0,24
Calcisols	23,59	12,16	11,43^{b}	39,82^{b}	35,49^{b}	19,98^{b}	51,97
Cambisols	15,34	7,78	7,56^{a}	67,82^{a}	14,85^{a}	14,28^{a}	0,24
Fluvisols	34,43	14,79	19,64^{b}	26,65^{b}	42,13^{c}	25,47^{b}	10,93
Gipsisols	26,21	14,38	11,83^{b}	35,35^{b}	41,94^{c}	13,51^{a}	3,26
Gleysols	25,90	11,10	14,80^{b}	44,00^{b}	29,21^{b}	23,5^{b}	0,05
Kastanozems	25,79	12,73	13,06^{b}	34,60^{b}	39,89^{b}	22,11^{b}	0,05
Leptosols	29,78	16,75	13,03^{b}	40,38^{b}	34,10^{b}	19,14^{b}	14,24
Luvisols	26,25	12,63	13,62^{b}	38,01^{b}	34,81^{b}	19,38^{b}	0,38
Phaeozems	28,16	14,53	13,62^{b}	45,04^{b}	33,40^{b}	19,95^{b}	0,48
Regosols	25,15	12,72	12,44^{b}	36,97^{b}	37,52^{b}	20,20^{b}	14,86
Solonchaks	27,20	14,58	12,63^{b}	32,87^{b}	44,26^{c}	18,94^{a}	2,59
Vertisols	33,00	20,90	12,10^{b}	0,68^{c}	42,80^{c}	56,52^{c}	0,05

Therefore, we can say that Calcisols, Leptosols and Regosols represent more than 80% of the soils of the area we are studying and according to their texture and water retention capacity they must have a very similar hydrodynamic behaviour, regarding the A horizon level. Fluvisols are on the fourth place with almost 11% of total surface. These soils showed a statistically higher clay percentage (99%, $p<0,01$) than Arenosols,

Cambisols, Gypsisols, Solonchaks and as a consequence their hydrodynamic behaviour is expected to be different. The nine main units of remaining soils are scarcely represented, since they together do not reach the 8% of the surface, and their hydrodynamic behaviour, in accordance with the variables considered, must be similar to the three first soils. In the case of Arenosols and Cambisols, with higher sand percentages than other units ($p<0,001$), different hydrodynamic properties can be expected .

Eventually, Pearson correlation index has been obtained (Table 2) for the variables studied, and we can say that the pF both at 1/3 and 15 atm are well correlated with the granulometric components, particularly with the sand. Likewise, as for the water availability (AW) the best correlation occurs with lime.

Table2. Correlation (Pearson index) between soil water content and granulometric analysis.

	pF 1/3 atm	pF 15 atm	AW	Sand	Silt	Clay
pF 1/3 atm	1	0,930982365	0,909533383	-0,918501816	0,908744499	0,658574037
pF 15 atm		1	0,695027606	-0,942378689	0,872894029	0,767700954
AW			1	-0,736050239	0,795942793	0,423790508
Sand				1	-0,919147198	-0,824896878
Silt					1	0,546740641
Clay						1

After considering the results and, without regarding the main soils groups that show significant differences both in their texture and water retention capacity (AW) and which on the other side are those in percentage terms less represented in the area, we can state that these parameters do not determine the hydrodynamic soil properties, at least at the surface horizon.

In this sense, and bearing in mind that the water storage and movement are controlled by the texture and structure of horizons close to the surface (Duley 1939; Morin *et al.* 1989), we can expect that the structure development and stability in the soils studied will not be as homogeneous as the texture and therefore, the structure will be the main contributor to the soils hydrodynamic properties. Likewise , the soil use affect the infiltration capacity (Kutilek and Nielsen 1994) so that the different size pores distribution and continuity as well as the cracks present among the aggregates are deeply affected by it, what we can translate as a reduction of the water availability and the number of biopores (Francis and Knight 1993)

Conclusions

At the sight of the results we can conclude that:

1. In the area, 13 out of the 32 main soil groups are represented. These groups according to their relevance are: Calcisols, Regosols, Leptosols, Fluvisols, Gipsisols, Solonchaks, Phaeozems, Luvisols, Arenosols, Cambisols, Greysols, Kastanozems, and Vertisols.
2. According to the horizon surface texture (A), more than 80% of soils have a very similar composition and, therefore, their hydrodynamic behaviour in terms of this parameter must be similar.
3. Arenosols and Cambisols have textures whose predominant fraction is sand, with percentages of 94.23 and 67.83% respectively. Likewise, water retention capacity is very low (2.19 and 7.56, respectively). On the other hand, Vertisols have the highest percentage of clay and the lowest of sand and their water retention capacity is 12.10%. According to this, these variables can be used to differentiate the hydrodynamic behaviour of these soils..
4. The pF both at 1/3 and 15 atm is well correlated with the granulometric components and best of all with sand. Likewise, as for the water availability (AW) is best correlated with lime.

Acknowledgements

To the Instituto Euromediterráneo del Agua for making possible the development of the research project "Characterization of the Segura River Basin physical and hydrodynamic properties" inside which the studies of this paper are framed.

References

Aguilar J, y Ortiz R (1992) Metodología de capacidad de uso agrícola de suelos. *In* 'III Congreso Nacional de la Ciencia del Suelo. Conferencias plenarias y comunicaciones'. pp. 281-286 (Ed Eurograf SL Pamplona).

Bouma J, Van Lanen A (1987) Transfer functions and threshold values: from soil characteristics to land qualities. In'Proceedings of an International Workshop on Quantified Land Evaluation Studies' (Ed. KJ Ter Beek, PA Burrough, DE McCormack). pp. 106–110. (ITC, Enschede, the Netherlands).

Duley FL (1939) Surface factors affecting the rate of intake of water by soils. *Soil Sci. Soc. Am. Proc*. **4,** 60-64.

FAO (1977) Guidelines for soil description (Rome)

FAO-ISRIC-IUSS (2006) World reference base for soil resources 2006. In 'World Soil Resource Reports' Volº 103. FAO. Rome.

Kutilek M, Nielsen DR (1994) Soil hydrology. Catena-Verlag, Germany.

Morin J, Karen R, Benyamini Y, Ben-Hur M, Shainberg I (1989) Water infiltration as affected by soil crust and moisture profile. *Soil Science* **148**, 53-59.

Walkley A, Black IA (1934) An examination of the method for determining soil organic matter and a proposed modification of the cromic acid titration method. *Journal of Soil Science* **37**, 29-38.

Image analysis of differently managed clayey surface soils of Finland

Kimmo Rasa[A], Thilo Eickhorst[B], MarkkuYli-Halla[A] and Rolf Tippkötter[B]

[A]Department of Applied Chemistry and Microbiology, University of Helsinki, Helsinki, Finland, Email kimmo.rasa@helsinki.fi
[B]Institute of Soil Science, University of Bremen, Bremen, Germany

Abstract
The porosities and pore shapes of boreal clayey surface soils (5 cm) were studied using image analysis of soil thin sections. The three adjacent sites investigated were vegetated buffer zones (BZs), which were either grazed, harvested or not managed at all. The purpose of the study was to evaluate the impact of these management practices on the surface soil structure of BZs. Water infiltration is essential for functioning of the BZs, as it reduces overland flow and contributes to reduced load from agricultural areas to water bodies. The results revealed that macro porosity (> 50 µm) was high in all studied sites. The majority of the macro pores consisted of large (>1000 µm) elongated irregular pores, indicating a complex and well-interconnected pore system, which is conducive to water infiltration. The differences between the studied sites were smaller than expected. It was hypothesized, that biological activity and fluctuating soil moisture typical of the boreal climate zone, i.e. wetting-drying and freezing-thawing cycles, might have reduced off the differences in the surface soil structure in the studied sites.

Key Words
Image analysis, soil structure, porosity, clay soil, buffer zone, boreal climate

Introduction
Vegetated buffer zones (BZ) are established to mitigate erosion and nutrient load from agricultural areas to water bodies. For the proper functioning of BZ, the structure of the surface soil should allow adequate infiltration in order to reduce overland water flow. Regardless of management practice, the surface soil structure of BZ should not be damaged. In Finland, vegetation from BZ is commonly removed by grazing cattle, but this practice may have destructive effects on soil structure (Pietola, 2005).

For decades, soil micromorphology has been qualitatively used to study soil structure as it appears in nature (Kubiena, 1938). In the 1970s, technological development allowed quantitative detection of soil porosity with computer aided digital image analysis of soil thin sections (e.g. Murphy *et al*., 1977). Image analysis proved to be an efficient tool to study differences in soil structure under various management practices or treatments (Ringrose-Voase, 1991). For example, changes in pore number, pore size distribution and pore shape pattern have been used as indices of the effects of conventional and zero tillage on soil structure (Pagliai *et al*., 1984).

The aim of this study was to document the surface soil porosity, especially the complexity of the pore system, of three differently managed vegetated BZs using soil thin sections. Quantitative information of pore size, number, and shape was obtained using image analysis. This study contributes to increasing of structural properties of boreal clay soils in general. More specifically, these results help assess the effects of different management practices on the functioning of vegetated BZs.

Material and methods
Experimental area and soil sampling
Soil samples were taken from a Vertic Stagnic Cambisol (IUSS Working Group WRB 2006) at Jokioinen, in southwestern Finland (60° 48' N, 23° 28' E). The texture was silty clay (clay 51%, silt 42%, and sand 7%). Three replicates of undisturbed soil samples were collected from the surface soil of three adjacent experimental areas, differing in management practice and vegetation, to prepare soil thin sections. These sites were a) 14-year-old natural vegetation with grass species and scrubs at natural state (natural), b) 14-year-old vegetation with grass species, harvested once a year (harvested) and c) 3-year-old vegetation with grass species, grazed by cattle (grazed). The names in parentheses are used later on.

Preparation of soil thin sections
Water was removed from the soil by wet dehydration applying a graded series of acetone (Tippkötter et al., 1986). Unsaturated polyester resin (Palatal P50-01, Büfa) with acetone as a thinner was used for the embedding of these samples (Tippkötter and Ritz, 1996). Polymerization time was set by the concentrations of the hardener

CHP (1.7 ‰) and the cobalt-accelerator (0.85 ‰) and resulted in seven weeks at room temperature. Totally, nine vertical thin sections were produced.

Image acquisition and analysis
Thin sections were placed on a transilluminator and images for the analyses of porosity were taken with a digital camera (Canon EOS 350D; 8 megapixels). These images were transformed to binary images (Photoshop CS, Adobe) and the image analysis software AnalySIS 3.2 (Soft Imaging) was used to measure pore area (A), perimeter (Pe) and convex perimeter (Peco) for pores larger than 50 µm equivalent pore diameter (EPD). The form factor (F) was calculated by the equation $F = A\ Pe^{-2}$. Elongated pores have a form factor <0.015, for irregular pores this factor is 0.015–0.04 and for rounded pores >0.04 (Bouma *et al*., 1977). Elongated pores were further classified into four shape classes according to Pagliai *et al*. (1984): convex perimeter per perimeter ratio is <0.3 for very irregular pores, 0.3–0.5 for moderately irregular pores, 0.5–0.7 for moderately regular pores and >0.7 for regular pores.

Results

Soil porosity (equivalent pore diameter > 50 µm), expressed as a percentage of investigated area, was highest (17%) in the grazed site, whereas in the natural and harvested sites the porosity was 14% and 12%, respectively (SE 3.9, LSD 13.4). The number of pores per cm^2 varied between 97 and 118 (SE 7, LSD 23).

Soil porosities expressed as a percentage of investigated area in different shape classes according to shape factor are presented in Table 1. Elongated pores contributed major proportion of the porosity, with the minor variation between the sites. The number of pores per cm^{-2} decreased in the following order: elongated < irregular < rounded.

Table 1. Porosity in different pore shape classes in vertical thin sections expressed as a percentage of total porosity and the number of pores per cm^2. Results are averages of three thin sections. Standard errors (SE) and least significant difference (LSD) are with 6 degrees of freedom.

	% of total porosity			Number of pores per cm^2		
	Rounded	Irregular	Elongated	Rounded	Irregular	Elongated
Natural	1	4	95	46	33	18
Harvested	2	6	92	57	41	20
Grazed	1	4	95	48	38	21
SE	0.5	1.4	1.9	3.0	3.1	1.8
LSD	1.7	4.9	6.6	10.5	10.8	6.1

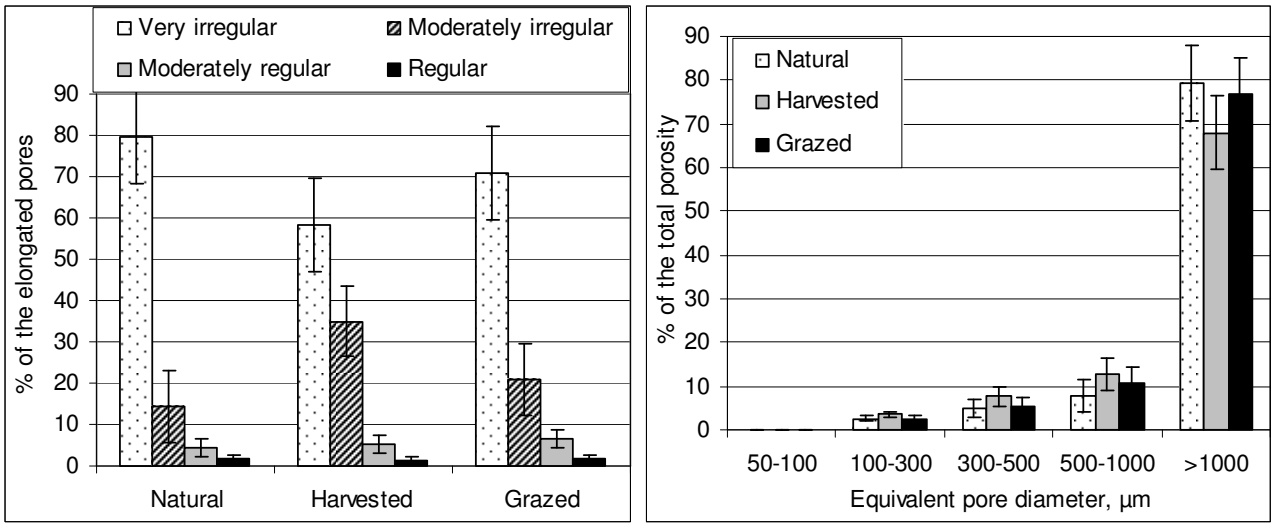

Figure 1. Pore shape distribution of elongated pores analyzed by image analysis in vertical thin sections (left). Pore size distribution (EPD) of elongated pores analyzed by image analysis in vertical thin sections (right). Error bars indicate standard errors of the means.

The shape distribution of elongated pores expressed as a percentage of porosity related to elongated pores (representing over 90% of the total porosity) is presented in Figure 1 (left). High irregularity was typical for

elongated pores, less than 10% of them were classified regular and moderately regular pores, irrespectively to management practice. A clear majority of the porosity consisted of pores larger than 1000 µm EPD (Figure 1, right). Differences between the studied sites were minor.

Discussion

Soil macro porosity (equivalent pore size > 50 µm) was large in the surface soil of all studied sites. Detected pores were divided into three shape classes: rounded, irregular and elongated, according to form factor. Less than 10% of the porosity consisted of rounded and irregular pores. All rounded pores belonged to the size classes smaller than 300 µm EPD, probably generated by small roots and soil fauna (VandenBygaart *et al*., 1998). Pores belonging to the elongated class were studied in more detail because of their high relevancy.

Classification of pores according to ratio between the convex perimeter to perimeter divides pores into classes ranging from regular (rectangular pores) to the very irregular (tortuous, curved, digitate, U-shaped pores). The majority of the elongated pores were characterized by irregularity, which expresses the complexity and interconnectivity of the pore system (VandenBygaart, 1999). Moreover, the pore size distribution of the elongated pores revealed that far over 65% of the detected soil macro porosity was composed of large elongated pores >1000 µm EPD.

Differences in soil porosity between studied vegetated buffer zones were less evident than expected. In the boreal climate periods of water saturation, dry spells and freeze-thaw cycles have an impact on soil structure. These factors, together with biological activity, level off differences in soil structure (Sveistrup *et al*., 2005).

Conclusions

The macro porosity was large in all studied sites. It was strongly dominated by large elongated and irregular pores. This indicates a complex and well-interconnected pore system, which favors water infiltration into the soil. Seasonal changes in soil moisture content and biological activity were suggested to level off differences between the studied sites managed differently. Image analysis provided valuable information about soil porosity, but did not lead to an unambiguous conclusion whether vegetated BZ can be grazed without detrimental influence on surface soil structure. Further studies, such as qualitative description of thin sections and additional image analysis of horizontal thin sections are still needed to verify these results.

References

Bouma J, Jongerius A, Boersma O, Jager A, Schoonderbeek D (1977) The function of different types of macropores during saturated flow through four swelling soil horizons. *Soil Science Society of America Journal* **41**, 945-950.

FAO (Food and Agriculture Organization of the United Nations) (2006) 'Guidelines for Soil Description.' 4th ed. (FAO: Rome).

IUSS Working Group WRB (2006) 'World reference base for soil resources 2006.' 2nd ed. World Soil Resources Reports No. 103. (FAO: Rome).

Kubiena WL (1938) 'Micropedology' (Collegiate Press: Ames, Iowa).

Murphy CP, Bullock P, Turner RH (1977) The measurement and characterization of voids in soil thin sections by image analysis. Part I. Principles and techniques. *Journal of Soil Science* **28**, 498-508.

Pagliai M, Marca LA, Lucamante G, Genovese L (1984) Effects of zero and conventional tillage on the length and irregularity of elongated pores in a clay loam soil under viticulture. *Soil & Tillage Research* **4**, 433-444.

Pietola L, Horn R, Yli-Halla M (2005) Effects of trampling by cattle on the hydraulic and mechanic properties of soil. *Soil & Tillage Research* **82**, 99-108.

Ringrose-Voase AJ (1991) Micromorphology of soil structure: description, quantification, application. *Australian Journal of Soil Research* **29**, 777-813.

Sveistrup TE, Haraldsen TK, Langohr R, Macelino V, Kvaerner J (2005) Impact of land use and seasonal freezing on morphological and physical properties of silty Norwegian soils. *Soil & Tillage Research* **81**, 39-56.

Tippkötter R, Ritz K, Darbyshire JF (1986) The preparation of soil thin-sections for biological studies. *The Journal of Soil Science* **37**, 681-690.

Tippkötter R, Ritz K (1996) Evaluation of polyester, epoxy and acrylic resins for suitability in preparation of soil thin sections for in situ biological studies. *Geoderma* **69**, 31-57.

Vandenbygaart AJ, Protz R, Tomlin AD (1999a) Changes in a no-till chronosequense of silt loam soils, Southern Ontario. *Canadian Journal of Soil Science* **79**, 149-160.

Vandenbygaart AJ, Protz R, Tomlin AD Miller JJ (1999b) Tillage system effects on near-surface soil morphology: observations from the landscape to micro-scale in silt loam soils of southwestern Ontario. *Soil & Tillage Research* **51**, 139-149.

Insights into the processes and effects of root-induced changes to soil hydraulic properties

Craig Scanlan[A, B] and Christoph Hinz[B]

[A]Department of Agriculture and Food WA, Northam, WA, Australia, Email craig.scanlan@agric.wa.gov.au
[B]School of Earth and Environment, University of Western Australia, Crawley, WA, Australia, Email christoph.hinz@uwa.edu.au

Abstract
Root-induced changes to soil hydraulic properties (SHP) are a vital component of the soil-vegetation hydrological feedback, and the change in water balance that occurs following a change in land use such as revegetation of mine earth covers. In this paper we review our recent work that attempts to quantify the processes by which soils modify SHP and the consequences of this for the water balance. We illustrate the dominant mechanism by which roots modify SHP is the modification of pore geometry. We developed models to predict the effect of roots on SHP, based upon the assumption that the geometry of roots within pore space can be represented by concentric cylinders. Model predictions agreed with observations: the greatest effect of roots on SHP is in near- to saturated hydraulic conductivity; however, the size of the effect depends upon soil texture, root decay, and the connectivity of root modified pores. Simulation modelling showed that the root modification of SHP caused the greatest change to the water balance in fine-textured soils, mainly because of an increase in infiltration rate and subsequent decrease in runoff. We identify a number of areas that require further investigation to improve our understanding of how roots modify SHP.

Key Words
Roots, soil, water, model, hydraulic conductivity, ecohydrology

Introduction

Root-induced changes to soil hydraulic properties (SHP) can have a significant effect on the hydrology of an ecosystem. In arid environments, these changes are an important component of the soil-vegetation hydrological feedback, where they contribute to increased water availability to plants by increasing the rate and /or depth of rainfall infiltration where vegetation is present. This feedback can lead to the development of spatial vegetation patterns that form an optimal run on – run off system. Also, when a land use change occurs such as from annual crops to forestry, or the revegetation of mine-site covers.

Until recently, the most common approach to modelling root-induced changes to SHP employed an empirical relationship between vegetation density and infiltration rate (HilleRisLambers *et al.,* 2001). This model has been used to investigate the effect of environment factors on the spatial organisation of vegetation in arid areas (e.g. Ursino, 2007). However, this relationship is not universally applicable to all ecosystems and it assumes an instantaneous increase in infiltration rate, whereas in reality there is a time lag between plant establishment and an increase in infiltration rate that is dependent upon the lifespan and rate of decay of the root system. The development of a model that was process based and applicable to a range of soils and plant types was a major motivation of the work we report here.

In this paper we review our recent work that attempts to bridge the gap between studies on root physiology and root-induced changes to SHP. First, we discuss the processes associated with root growth that lead to changes in SHP. We then present a modelling framework for quantifying the impact of roots on soil hydraulic conductivity and water retention, which has the advantage of being compatible with physically-based water flow models and we illustrate the impacts of root-induced changes on the water balance by combining the two. Finally, we discuss the research questions that our work has raised which need to be addressed to improve our capacity to predict the impact of root-induced changes on SHP at an ecosystem level.

Processes by which roots modify soil hydraulic properties

The evidence available suggests that changing pore space geometry is the dominant mechanism by which roots modify SHP (Scanlan, 2009). First, changes to pore geometry are more permanent, lasting for time periods of months to years (e.g. Petersson *et al.,* 1987), while changes to fluid properties and aggregation persist over much shorter time scales (e.g. Norton *et al.,* 1990). Second, the changes to pore geometry lead to changes in SHP of a greater magnitude. For example, changes in saturated hydraulic conductivity of -90% (Barley, 1953) to 650% (Li and Ghodrati, 1994) have been attributed to roots blocking pore space, and creating macro-pores

1 – 6 August 2010, Brisbane, Australia. Published on DVD.

when they decay respectively. In contrast, changes to fluid properties only changed water content by 7% where the whole soil solution was treated, whereas in reality only the solution in the vicinity of the root is affected. Based upon this, we developed a modeling framework that considered root-induced changes to pore geometry only.

Modeling Framework

The central assumption to our modelling framework is that the geometry of roots with pores can be simplified to concentric cylinders (Scanlan, 2009) (see Figure 1). To calculate capillary rise within concentric cylinders h_c we derived an expression based upon the same assumptions used to calculate capillary rise within a single cylinder h_s. Specifically, these assumptions are that capillary rise is due to a balance of upward and downward forces acting on the liquid, where the upward forces are a product of cylinder radius, surface tension and wetting angle, and the downward forces are a product of cylinder radius, liquid density and gravitational acceleration. Expressions for flux between concentric cylinders had been derived previously (Cutlip and Shacham, 1999; Wantanabe and Flury, 2008).

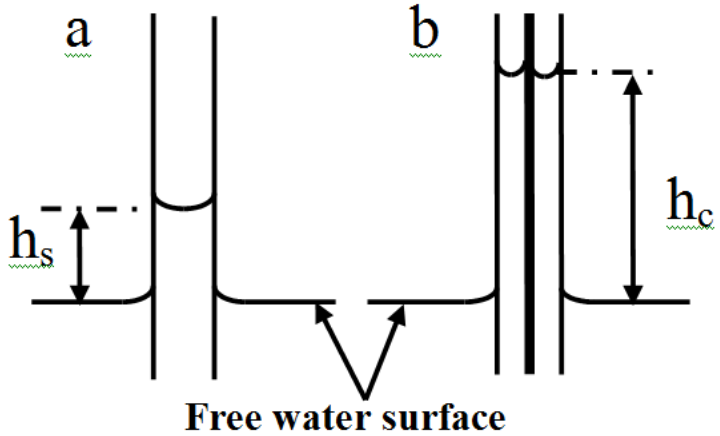

Figure 1. Cross-sectional illustration of capillary rise within a single cylinder (a) and within concentric cylinders (b). Note – drawing not to scale.

To quantify how capillary rise, flux and volume within a single cylinder will change when an inner cylinder is introduced we derived dimensionless expressions that are a function of the ratio of root radius to pore radius β only (Scanlan 2009). These ratios are presented graphically in Figure 2. We followed this approach because it allowed us to examine the effect of varying root radii on soil hydraulic properties.

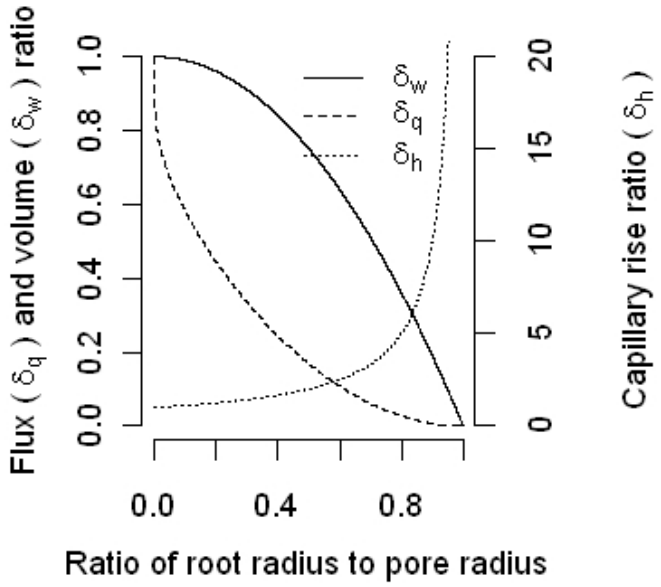

Figure 2. The effect of the ratio of root radius to pore radius on the change in flux, volume and capillary rise in pores with roots present (Scanlan, 2009).

Figure 2 illustrates the effect that the ratio of the radius of the inner cylinder to the radius of the outer cylinder has on flux, capillary rise and volume. The steepest increase in capillary rise occurs when β is greater than 0.8. The steepest decrease in flux occurs at values of β near to 0, which occurs because the inner cylinder is placed where velocity is highest in a single cylinder.

We modified existing models that predict the hydraulic conductivity and water retention functions of soil to include our scaling functions for flux, capillary rise and volume for root-occupied pores (Scanlanl 2009). We modified the capillary bundle model by conceptualising the pore volume as bundles of pores with and without roots present. We assumed that roots modified the radius of pores that they occupy according to their root radius frequency distribution. We then modified the van Genuchten-Mualem model (van Genuchtenl 1980) using the multi-domain approach (e.g. Ross and Smetteml 1993), conceptualising the soil as two domains: pore space with and without roots. While both of these models predict the same output, they are fundamentally different. The capillary bundle model is based upon physical principles with only one empirical parameter that describes the connectivity of the flow path, whereas the (van Genuchtenl 1980) effective saturation function requires empirical parameters that describe the shape of the hydraulic conductivity and water retention functions. The differing basis of these models provided a complementary approach in our attempt to quantify the most important factors leading to root-induced changes to SHP.

Comparison of predicted changes in SHP with observations

Overall, the changes in hydraulic conductivity and water retention predicted by our models are in agreement with observations. The greatest effects predicted and observed due to root-induced changes were in the near- to saturated range of hydraulic conductivity (K_s). Our models also predicted either an increase or a decrease in K_s depending upon β, soil texture and the connectivity of root-occupied pores. This is in agreement with observations, where a decrease in K_s due to roots typically occurs when the plant is young and the roots are fully intact (e.g. Barley, 1954), then an increase in K_s occurs when the roots decay and create macro-pores (e.g. Li and Ghodrati, 1994): analogous to high and low values of β respectively.

Simulation modelling showed that root profile and soil texture determined the amount of change to the water balance. We implemented the modified van Genuchten (1980) model in a one dimensional soil-water flow model and simulated infiltration under ponded conditions for a loam soil one metre deep with free drainage at the bottom of the profile (Scanlan, 2009). When comparing infiltration rate in the loam before and after root modification we found that it was only greater, by approximately 700%, when the connectivity of root-modified pores was high and where roots were evenly distributed throughout the profile. This is slightly greater than the range of 200% (Meek *et al.,* 1989) to 600% (Rachman *et al.,* 2004) increases in ponded infiltration rate in field conditions that have been attributed to root-modification of SHP. However, there are two important differences between the simulated and real conditions: the vertical distribution of roots in real soils is typically exponential (e.g. Jackson *et al.,* 1996), and under real ponded infiltration lateral divergence of water flow occurs. Comparison of the simulated and observed changes in ponded infiltration rate suggests that the increase in infiltration rate that has been observed is due to a small number of relatively straight root-induced macro-pores.

Year-long simulations using high resolution rainfall data showed that root-induced changes had a significant effect on the water balance on fine-textured soils. We compared runoff, storage, and uptake for perennial plants growing on a sand, loam and clay with and without root-induced changes to SHP. Storage and uptake were significantly greater on the root-modified clay compared to the clay in its original state, which was due to an increase in hydraulic conductivity near the soil surface and as a result, a greater amount of rainfall infiltrating into the soil. This work provided a valuable first step in assessing how root induced changes will affect the water balance, however, further work is required as the impact of these changes on the water balance is likely to be sensitive to the combination of soil texture, plant type and rainfall distribution (Fernandes-Illescas *et al.,* 2001).

Outlook

Our research has highlighted a number of areas of research that require further work to improve our capacity to predict how root-induced changes to SHP affect the water balance. Field and laboratory measurement of SHP before and after root modification is required to test the validity of our assumptions: the connectivity of root-modified pores in particular. Also, in our work the parameterisation of the domain with roots was based upon 'fine' roots only, which were usually excised from larger roots. The multi-domain structure of our modified van Genuchten model is ideally suited to incorporating large roots and warrants further work.

We anticipate that moving from one- to two-dimensional analysis will also help to improve our understanding of how root-induced changes affect the water balance.

References

Barley KP (1953) The root growth of irrigated perennial pastures and its effect on soil structure. *Australian Journal of Agricultural Research* **53**, 283-291.

Barley KP (1954) Effects of root growth and decay on the permeability of a synthetic sandy loam. *Soil Science* **78**, 205-210.

Cutlip MB, Shacham M (1999) Fluid mechanics. In 'Problem solving in chemical engineering with numerical methods' pp. 159-208. (Prentice-Hall Inc.: Sydney).

Fernandes-Illescas CP, Porporato A, Laio F, Rodriguez-Iturbe I (2001) The ecohydrological role of soil texture in a water-limited ecosystem. *Water Resources Research* **37**, 2863-2872.

HilleRisLambers R, Rietkerk M, Bosch Fvd, Prins HHT, Kroon Hd (2001) Vegetation Pattern Formation in Semi-Arid Grazing Systems. *Ecology* **82**, 50-61.

Jackson RB, Canadell J, Ehleringer JH, Mooney HA, Sala OE, Schulze ED (1996) A global analysis of root distributions for terrestrial biomes. *Oecologica* **108**, 389-411.

Li Y, Ghodrati M (1994) Preferential transport of nitrate through soil columns containing root channels. *Soil Science Society of America Journal* **58**, 653-659.

Meek BD, Rechel ER, Carter LM, Detar WR (1989) Changes in infiltration rate under alfalfa as influenced by time and wheel traffic. *Soil Science Society of America Journal* **53**, 238-241.

Norton JM, Smith JL, Firestone MK (1990) Carbon flow in the rhizosphere of Ponderosa pine seedlings. *Soil Biology and Biochemistry* **22**, 449-455.

Petersson H, Messing I, Steen E (1987) Influence of root mass on saturated hydraulic conductivity in arid soils of central Tunisia. *Arid Soil Research and Rehabilitation* **1**, 149-160.

Rachman A, Anderson SH, Gantzer CJ, Alberts EE (2004) Soil Hydraulic Properties Influenced by Stiff-Stemmed Grass Hedge Systems. *Soil Science Society of America Journal* **68**, 1386-1393.

Ross PJ, Smettem KRJ (1993) Describing soil hydraulic properties with sums of simple functions. *Soil Science Society of America Journal* **57**, 26-29.

Scanlan CA (2009) Processes and effects of root-induced changes to soil hydraulic properties. PhD Thesis, University of Western Australia.

Ursino N (2007) Modeling banded vegetation patterns in semiarid regions: Interdependence between biomass growth rate and relevant hydrological processes. *Water Resources Research* **43**, doi:10.1029/2006WR005292.

van Genuchten MT (1980) A closed-form equation for predicting the hydraulic conductivity of unsaturated soils. *Soil Science Society of America Journal* **44**, 892-898.

Wantanabe K, Flury M (2008) Capillary bundle model of hydraulic conductivity for frozen soil. *Water Resources Research* **44**, doi:10.1029/2008WR007012.

Least limiting water range and S index to evaluate some soil physical quality in the northeast Brazil

Virginia Pires Pereira[A], **Maria Eugenia Ortiz-Escobar**[B], Genelício Crusué Rocha[C] and Teogenes Senna de Oliveira[D]

[A]Universidade Federal do Ceara, Fortaleza, CE, Brazil, Email virpires@yahoo.com.br
[B]Soil Science, Universidade Federal do Ceará, Fortaleza, CE, Brazil, Email mariaeugenia@ufc.br
[C]Soil Physics, Universidade Federal de Viçosa, Viçosa, MG, Brazil, Email genelicio.rocha@ufv.br
[D]Soil Management, Universidade Federal do Ceará, Fortaleza, CE, Brazil, Email teo@ufc.br

Abstract
The concern with soil physical quality has grown in recent years, particularly due to serious problems caused by soil use. The objective of this research was to evaluate the soil physical quality of irrigated areas in the State of Ceará, Brazil, through the use of the Least limiting Water Range (LLWR) and the S index. Undisturbed soil samples were collected at 5-10cm depth in three areas, natural vegetation (NV), area under banana cultivation (B) and a pasture area (P), all located in Jaguaribe-Apodi Irrigated District, Limoeiro do Norte, Ceará, Brazil. The LLWR was determined using the water retention curve, the soil resistance to penetration and soil bulk density, parameters needed to obtain the upper and lower limit. The S index was obtained from the water retention curve. The S index was sensitive to soil structure alterations caused probably by tillage. The variation of the LLWR differed between the studied areas as a function of the soil bulk density. The LLWR and S index seem to be good indicators of soil physical quality, and it was noticed that soils under cultivation suffer an alteration of their structure compared to soils under natural vegetation.

Key Words
Soil water retention curve, soil resistance to penetration, inflection point, soil degradation, soil structure

Introduction
Soil physical quality is a concept of growing interest in recent years due to the knowledge that soil use may cause disturbance, and consequently, reduce its capacity for sustainable production (Silva *et al.,* 2007). The Least Limiting Water Range (LLWR) is an indicator of soil physical quality and soil structure that joins in only one parameter the effects of bulk density, aeration, soil resistance to penetration and soil water retention on the development of plants, being capable to indicate situations of stress (Tormena *et al.,* 1998; Leão, 2002). The S index was first proposed by Dexter (2004) as an indicator of soil physical and structural quality, based on the water retention curve (WRC), where the inflection point curvature is zero, corresponding to the S index. Being in a semi-arid region, the area of Jaguaribe-Apodi in the State of Ceará, Brazil, is dependent on irrigation practices to be productive, with soil degradation resulting from intensive use and inadequate soil practices. Thus, this study was conducted to evaluate the soil physical quality of irrigated cultivated areas compared to areas under natural vegetation, in the State of Ceará, Brazil, through the use of the LLWR and S index.

Methods
Site location and description of soils
The areas for the study are located in the Jaguaribe-Apodi Irrigated District, Limoeiro do Norte, Ceará State, Brazil, and classified as Haplic Cambisols (Embrapa, 2006). The climate of the region is BSw'h', characterized as hot and semi-arid. It has an annual maximum and minimum temperature of 36ºC and 22ºC, respectively, with annual mean temperature of 28.5°C. The area receives approximately 772 mm of annual mean precipitation, with an annual mean potential evapotranspiration of 3215 mm and annual relative humidity of 62%. The dominant relief of the region is regular, uniform, very soft declivity, varying between 0.5 – 1.5%, and situated 100 m above sea level (DNOCS, 2009). The selected areas were as follows: Banana (B) (5°9'15" S and 37°59'55" W), cultivated with banana cv. "Prata anã" irrigated daily during the dry season (June-December) with microsprinklers; the machines used in the area is tractor with subsoiling. Second, a Pasture area (P) (5°12'54" S and 38°01'52" W), cultivated for 10 years with "capim tifton" (*Cynodon niemfluesis*) and irrigated with center pivot irrigation systems. Also during the dry season, the machines used in the area during the haymaking are: line trimmer, hay bob, baling press and tractors, and, third, an area without agricultural management under natural vegetation (NV) located next the cultivated areas, considered as a reference area.

1 – 6 August 2010, Brisbane, Australia. Published on DVD.

Sampling and analysis

Undisturbed soil samples (5-cm diam. by 5-cm length on average) were collected at 5-10cm depth, saturated with water and split into twelve groups, each of which were equilibrated on pressure plates at twelve matric pressures: -10; -20; -40; -60; -80; -100; -300; -500; -800; -1000; -5000 and -15000 KPa (Klute, 1986). After equilibration, samples were weighed and soil resistance to penetration (PR) was measured on each sample with an electronic penetrometer, with a constant speed penetration of 1 cm min^{-1}. The samples were then oven dried at 105 ºC for 48h and the water content and bulk density determined (Blake and Hartge, 1986). The values of PR data were regressed against θ and *D*s using the model proposed by Busscher (1990), described as follows: $PR = a\ \theta^b\ Ds^c$ [1], where PR is the penetration resistance (MPa), Ds is the bulk density (Mg m^{-3}), θ is the volumetric humidity ($m^3\ m^{-3}$) and, *a, b* and *c* are constants.

The least limiting water range was determined following the methodology described by Silva *et al.* (1994) and Tormena *et al.* (1998). The critical values of humidity associated with the matric potential, penetration resistance and air-filled porosity were selected from the literature: field capacity (θ_{FC}) at -0.01 MPa (Reichardt, 1988); permanent wilting point (θ_{PWP}) at -1.5 MPa (Savage 1996); penetration resistance (θ_{PR}) at 2.0 MPa (Taylor, 1966) and air-filled porosity (θ_{PA}) at 0.10 $m^3\ m^{-3}$ (Grable and Siemer, 1968). At each Ds the LLWR is the difference between the upper limit and the lower limit. The upper limit is the drier θ of either θ_{FC} or θ_{PWP} whereas the lower limit is the wetter θ of either θ_{PWP} or θ_{PR} (Silva *et al.* 1994).

To the elaboration of the soil water retention curve (SWRC) were used three samples of each area for each pressure and adjusted according to the equation [2] proposed by van Genuchten (1980):

$$\theta = \theta r + \frac{(\theta s - \theta r)}{\left[1 + (\alpha\psi)^n\right]^m} \qquad [2]$$

where, θ is the water content ($m^3\ m^{-3}$); θs is the saturated water content ($m^3\ m^{-3}$); θr is the residual water content ($m^3\ m^{-3}$); ψ is the matric potential (MPa); *α* and *n* are constants; *m* was considered independent of *n*, being equivalent to 1-1/n. The van Genuchten model (1980) was used to calculate the inflection point values of the water retention curve; this is the S index value, using the equation [3]:

$$S = -n.(\theta s - \theta r).\left[1 + \frac{1}{m}\right]^{-(1+m)} \qquad [3]$$

The negative sign associated to the *n* parameter of equation [3] was corrected once the adjustment of the SWRC was done considering the matric potential, consequently, facilitating the discussion of the results. An S value of 0.035 was established as the limit between soils with good and poor soil structural quality (Dexter, 2004).

All samples were analyzed using orthogonal contrasts from the unfolding of the two degrees of freedom for each treatment. The contrasts were tested by the *F* test ($P< 0.01$) against the mean square of the residue gotten by the analysis of variance, in a completely randomized design with three replications. The natural vegetation area (NV) was compared against the Banana area resulting in the contrast C1. The contrast C2 compared the NV against the Pasture area, and, the contrast C3 compared the two cultivated areas.

Results

The estimated soil physical quality data using the S index are shown in Table 1, where van Genuchten parameters of the model were highly influenced by the soil management practices as observed by the coefficients. The θsat parameter was significant ($P<0.05$) for the contrast C1 and C2, being higher for the NV area, followed by Banana and Pasture areas. The θr and *m* parameters were significant ($P<0.01$) for contrast C2, *n* was significant ($P<0.05$) for contrast C1 and C2, and S was also significant for contrast C1 and C2 ($P<0.01$) and for contrast C3 ($P<0.1$). The S index varied in function of the soil management systems, revealing to be a good sensitive parameter to describe the soil structure alterations. The pasture area showed an index of 0.028, lower to the limit between a good and poor soil structural quality, probably having an inadequate pore distribution, consequently having unfavorable physical conditions for root development.

The four limiting water contents, i.e., θ_{FC}, θ_{PWP}, θ_{PR}, and θ_{PA}, as well as the LLWR for each observed *Ds* are shown in Figure 1. Shaded areas represent the LLWR, where the upper limit corresponds to θ_{PA} from Ds values

of 1.54, 1.59 and 1.57 Mg m^{-3}, for natural vegetation, banana and pasture areas, respectively. These high values of bulk density can be associated to an inadequate root development influenced by poor oxygen diffusion. The θ_{PR} defined the lower limit, but, the higher influence of the LLWR was also found in various soils with different soil textures, from clayed soils (Tormena *et al.,* 1998) to silt and sandy loam (Silva *et al.,* 1994).

The area under natural vegetation did not show LLWR null values for the Ds (Figure 1A), that combined with the high value of the S index, confirming the indications that soils under natural vegetation generally have better physical properties (Reynolds *et al.,* 2002). On the other hand, in the areas under cultivation, were observed either increases on the θ_{PR} and declines on the θ_{PA} as a consequence of the rise in the Ds, in agreement with the results showed by Silva *et al.* (1994). The LLWR narrowing observed in Figures 1B and 1C characterized the losses of physical soil quality as a result of the stress caused by the soil management under the cultivation areas, as stated by Silva and Kay (1996). Crops grown on soils that have a narrow LLWR are hypothesized (Kay, 1989) to be more vulnerable to both drought and excess wetness than soils having a wider LLWR.

The total variation extent of the LLWR was less for the area under pasture cultivation in comparison to the other two areas, varying from 0.27 to 0.31 m^3m^{-3} for θv and from 1.51 to 1.61 Mg m^{-3} for bulk density. This lower extent of the LLWR in conjunction with the lower S index value, characterize the loss of soil physical quality, where the soil humidity at the moment of soil tillage during the haymaking could contribute to the significant increase of soil degradation in the area.

Table 1. Water retention curve coefficients for the van Genuchten model (θsat, θres, α, m, n), coefficient of determination (R^2) and S index of the cultivated areas and under natural vegetation in the Jaguaribe-Apodi Irrigated District, Ceará State, Brazil.

	van Genuchten Parameters						
Area/	***θsat***	***θres***	***A***	***m***	***n***	***S***	**R^2**
Contrast	**m^3 m^{-3}**						
NV	0.465	0.179	0.106	0.163	10.95	0.062	1
B	0.387	0.199	0.217	0.266	1.915	0.041	1
P	0.375	0.169	0.219	0.167	1.598	0.028	1
	Orthogonal contrast						
C1	**	ns	ns	ns	**	***	
C2	**	*	ns	*	**	***	
C3	ns	ns	ns	ns	ns	*	

NV: Natural Vegetation; **B:** area under Banana cultivation; **P:** area under Pasture cultivation. ***θsat***: saturated water content; ***θres***: residual water content; ***α***, ***m*** e ***n***: van Genuchten parameters; **C1** = (B *vs* NV); **C2** = (P *vs* VN); **C3** = (B *vs* P). ***, **, * and ns = significant at 1%, 5%, 10% and not significant, respectively.

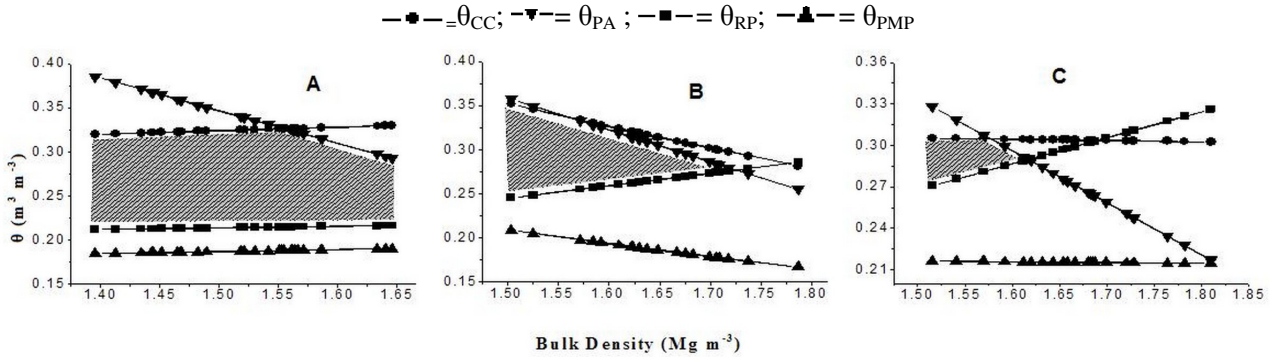

Figure 1. Variation of water content in function of the bulk density (Mg m^{-3}) under the critical levels of field capacity (ψ = -0.01 MPa), permanent wilting point (ψ = -1.5 MPa), air-filled porosity of 10% and penetration resistance of 2 MPa, at a 5-10 cm depth in areas under Natural Vegetation (A), under Banana cultivation (B) and under Pasture cultivation (C). Shaded areas represent the LLWR.

Conclusion

Both, the LLWR and S index showed to be good indicators of soil physical quality in irrigated areas in the State of Ceará, Brazil, where soils under intensive cultivation might lead to detrimental effects in some properties as structural degradation compared to areas under natural vegetation. It is time for these areas to turn into no-till management especially if they are predicted to be a long-term soil use.

References

Blake GR, Hartge KH (1986) Bulk density. In 'Methods of soil analysis. 2nd ed.' (Ed. A Klute) pp. 363-375. (American Society of Agronomy, Soil Science Society of America: Madison, USA).

Busscher WJ (1990) Adjustment of flat-tipped penetrometer resistence data to common water content. *Transactions of the American Society of Agricultural Engineering* **3**, 519-524.

Dexter AR (2004) Soil physical quality Part I. Theory, effects of soil texture, density and organic matter and effects on root growth. *Geoderma* **120**, 201-214

DNOCS (2009) Projetos: Perímetro irrigado Jaguaribe - Apodi. http://www.dnocs.gov.br/~dnocs/doc/canais/perimetros_irrigados/ce/jaguaribe_apodi.html].

EMBRAPA (2006) 'Sistema brasileiro de classificação de solos'. (Centro Nacional de Pesquisa de Solos: Rio de Janeiro). 306pp.

Grable AR, Siemer EG (1968) Effects of bulk density, aggregate size, and soil water suction on oxygen diffusion, redox potential and elongation of corn roots. *Soil Science Society of America Journal* **32**: 180-186.

Kay BD (1989) Assessing the suitability of different soils for new cropping systems in terms of rates of change in soil structure. In 'Mechanics and related processes in structural agricultural soils'. (Ed. WE Larson). (Kluwer Academic Publishers: Dordrecht, the Netherlands).

Klute A (1986) Water retention: laboratory methods. In 'Methods of Soil analysis. I. Physical and mineralogical methods. 2nd ed.'. pp. 635-662 (American Society of Agronomy, Soil Science Society of America: Madison, WI).

Leão TP (2002) Intervalo hídrico ótimo em diferentes sistemas de pastejo e manejo de pastagem. Dissertação de mestrado, Universidade de São Paulo, São Paulo.

Reichardt K (1988) Capacidade de campo. *Revista Brasileira de Ciencia do Solo* **12,** 211-216.

Reynolds WD, Bowman BT, Drury CF, Tan CS, Lu X (2002) Indicators of good soil physical quality: density and storage parameters. *Geoderma* **110,** 131-146.

Savage MJ, Ritchie JT, Bland WL, Dugas WA (1996) Lower limit of soil water availability. *Agronomy Journal* **88**, 844-851.

Silva AP, Kay BD (1996) The sensivity of shoot growth of corn to the least limiting water range of soils. *Plant and Soil* **184**, 323-329.

Silva AP, Kay B, Perfect E (1994) Characterization of the least limiting water range. *Soil Science Society of America Journal* **58**, 1775- 1778.

Silva LFS da, Weill MAM, Silva AP da, Javarez Júnior A (2007) Determinação do índice S de um Latossolo Vermelho Distroférrico típico cultivado sob diferentes sistemas de manejo. In "Reunião Brasileira de Manejo e Conservação do Solo e da Água, Aracaju, SE and XXXI Congresso Brasileiro de Ciência do Solo, Viçosa, MG " p. 1-1 (Sociedade Brasileira de Ciência do Solo).

Taylor HM, Roberson GM, Parker Jr. JJ (1966) Soil strength-root penetration relations to medium to coarsed-extured soil materials. *Soil Science* **102,** 18-22.

Tormena CA, Silva AP, Libardi PL (1998) Caracterização do intervalo hídrico ótimo de um Latossolo Roxo sob plantio direto. *Revista Brasileira de Ciencia do Solo* **22,** 573-581.

Van Genuchten MT (1980) A closed-form equation for predicting the hydraulic conductivity of unsaturated soil. *Soil Science Society of America Journal* **44,** 892-898.

Measurement of gas transport parameters for final cover soil at Maharagama landfill in Sri Lanka

Praneeth Wickramarachchi[A], Kaushalya Ranasinghe[B], Udeni P. Nawagamuwa[B], Ken Kawamoto[A], Shoichiro Hamamoto[A], Per Moldrup[C] and Toshiko Komatsu[A]

[A]Faculty of Civil and Environmental Engineering, Saitama University, Saitama, Japan, Email praneeth1977@yahoo.co.uk
[B]Dept. of Civil Engineering, University of Moratuwa, Katubedda, Sri Lanka, Email udeni@civil,.mrt.ac.lk
[C]Dept. of Biotechnology Chemistry and Environmental Engineering, Aalborg University, Aalborg, Denmark, Email pm@bio.aau.dk

Abstract
To make a proper evaluation and better understanding of gas component movement inside a landfill site, and investigation of the different parameters related to gas flow is important. In this study, air permeability (k_a) and gas diffusivity (D_p/D_o; where D_o is the gas diffusion coefficient in free air) were measured as a function of soil air content (ε) in final cover soil at Maharagama landfill in Sri Lanka. The k_a and D_p were measured at different gravimetric water content in some samples and another set of samples were treated under different pF conditions (pF= log (-φ) where φ is the soil water matric potential in cm H_2O). Results showed that greater variation of k_a with ε in both experimental conditions. The k_a rapidly increased with ε at relatively higher gravimetric water condition and then less variation near field water content and finally at drier condition the ka increased again with ε significantly. D_p/D_o exhibited exponential variation with ε. Based on measured data, predictive models for D_p and k_a were tested and pore connectivity parameter (α) and water blockage parameter (X) were calculated accordingly.

Key Words
Air permeability, gas diffusion coefficient, predictive models, pore connectivity, water blockage

Introduction

Gas generation and transport phenomenon are very important to understand in landfills to improve environmental aspects, landfill gas recovery or air supply for a better aeration inside the site. Moreover, when landfill gas is released into the atmosphere or migrates beyond landfill boundaries, it threatens the environment as well (Kallel *et al.,* 2004). In recent years, landfills have been identified in greenhouse warming scenarios as significant sources of atmospheric methane (CH_4). In addition, it is well known that toxic gases such as hydrogen sulphide (H_2S) and volatile organic chemicals (VOC) are emitted from the landfill sites (Song *et al.,* 2007). All these gases are emitted to the environment through the final cover soil layer, therefore better understanding of transport, fate and emission of gases through such a final cover layer plays vital role as mentioned in many studies (Moon *et al.,* 2008; Kallel *et al.,* 2004). Moreover, open dumpsites are being gradually replaced by sanitary landfills where negative impacts to the environment are less compared to open dump site in developing countries (Chiemchaisri *et al.,* 2007).

The gas exchange through the final cover soils is controlled by advective and diffusive gas transport. Air permeability governs the advective gas transport induced by soil-air pressure gradient, while gas diffusion coefficient is governed by soil-gas concentration gradient. Generally, landfill final cover soils are highly compacted to prevent precipitation infiltration. Weeks *et al.* (1992) have reported bulk density (ρ_b) ranging from 1.57- 1.74 (g cm^{-3}) for differently-textured landfill cover soils. Further in this study, the field investigation showed that the in situ bulk density reached 1.90 (g cm^{-3}). Soil compaction has a major impact on gas transport characteristics. Hamamoto *et al.* (2009) showed that soil compaction simultaneously caused reduced water blockage effects and reduction of larger-pore spaces. It is a widely accepted fact that the soil physical and chemical properties of soil and soil texture are also vital for gas transport phenomena. Therefore selection of construction material for final cover soils is needed to be considered in engineering applications.

In this study, the main objective was to measure the gas transport parameters and to test with some acceptable models in landfill final cover soil at Maharagama in Sri Lanka where municipal solid wastes were dumped and final soil cover was applied.

Methods

Materials and Method

A waste landfill site located at Maharagama in Sri Lanka was selected as a sampling site in this study. The final

cover soil at the sampling site is highly compacted, exhibiting dry bulk density (ρ_b) of around 1.90 (g cm^{-3}) and a total porosity (ϕ) of 0.35. Further, some data used in this study was from Saitama landfill. Undisturbed soil samples were taken from the final cover soil and the soil sample was sieved through 2 mm mesh to eliminate effects of gravel and coarse sand size fractions (75.0-2.0 mm) on gas transport and obtain homogeneous physical properties. The composition and physical properties of the soil samples are shown in Table 1.

Table 1. Composition and physical properties of Maharagama and Saitama landfill cover soils.

Landfill site	Particle size fraction (%)				Soil texture	Particle density	Bulk density	Total porosity	pH	EC
	Gravel (> 4.75 mm)	Sand (4.75-0.075 mm)	Silt (0.075-0.005m m)	Clay (<0.005m m)		ρ_s (g cm^{-3})	ρ_b (g cm^{-3})	ϕ		mS m^{-1}
Maharagama	10	40	35	15	Silty Sand	2.77	≈ 1.90	≈ 0.35	5.4	32
Saitama	36	42	13	9	Silty Sand	2.66	≈ 1.85	≈ 0.29	5.6	27

Compaction tests were performed for soil samples at different water content using (ASTM D 698-07). Water contents of soil samples were adjusted by adding water to air-dried soil samples. In the compaction tests, the soil samples were repacked into large soil cores (i.d. 15 cm, length 12 cm) at a compaction level (600 kN m^{-2}) (Figure 1). The falling height (H) and weight of rammer (M) for compaction levels was 30.5 cm, and 2.5 kg, respectively and 56 blows were applied per layer (3 layers). The results of the compaction tests are shown in Figure 1.

After compaction tests, two 100 cm^3 core samples (i.d. 5.1 cm, length 4.1 cm) were taken inside each repacked large core. After each 100 cm^3 core sample was water-saturated, the core samples were drained at different matric suctions and the gas diffusion coefficient (D_p) and air permeability (k_a) were measured. The D_p was measured on the repacked 100 cm^3 soil cores with a diffusion chamber method. Oxygen was used as tracer gas and measured as a function of time in the diffusion chamber. In this study, the gas diffusion coefficient of oxygen in free air (D_0) at 20 °C was used as 0.20 (cm^2 s^{-1}). The k_a was measured by flowing air through a repacked 100 cm^3 soil core. The k_a was calculated from the Darcy's equation based on the pressure difference across the core and the viscosity of the air (1.86×10^{-5} Pa s).

Models applied

Power-law type models for D_p/D_0 and k_a can be written in general form (Hamamoto *et al.,* 2009; Moldrup *et al.,* 1998) as,

$$\frac{D_p}{D_0} = \alpha_p \varepsilon^{X_P} \quad [1]$$

$$\frac{k_a}{k_{a,100}} = \left(\frac{\varepsilon}{\varepsilon_{100}} \right)^{\eta} \quad [2]$$

where α_p is pore connectivity parameters for D_p/D_0 , and X_p is water blockage parameters for D_p/D_0. The $k_{a,100}$ and ε_{100} are reference point values, where first term is for k_a at pF 2 and latter was ε at pF 2, while η represents the combined effects of tortuosity and connectivity of air-filled pores. Kawamoto *et al.* (2006) found that η= 1+3/b, where b is the slope of soil-water characteristic curve in log-log coordinate system.

Results

Compaction curve for the investigated landfill cover soil

The results of the compaction tests of standard method for investigated soil are shown in Figure 1. The bulk density (ρ_b) ranged from 1.88-1.93 (g cm^{-3}) for the soil. The optimum moisture content was around 0.14 % for soil and the correspondent maximum dry bulk density was 1.93 g cm^{-3}. The field water content was 10.50 %. From the Table 1, it is clear that the physical and chemical properties are different (mainly different clay, silt and gravel contents) in the both soils.

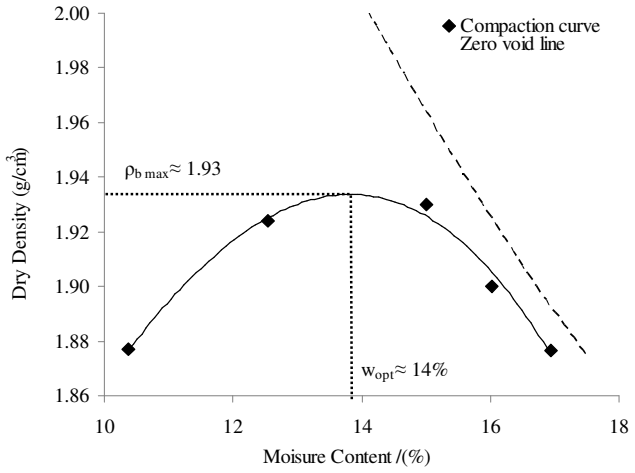

Figure 1. Compaction curve for the investigated Sri Lankan Soil.

Soil water retention curve and equivalent pore radius distribution function for soil

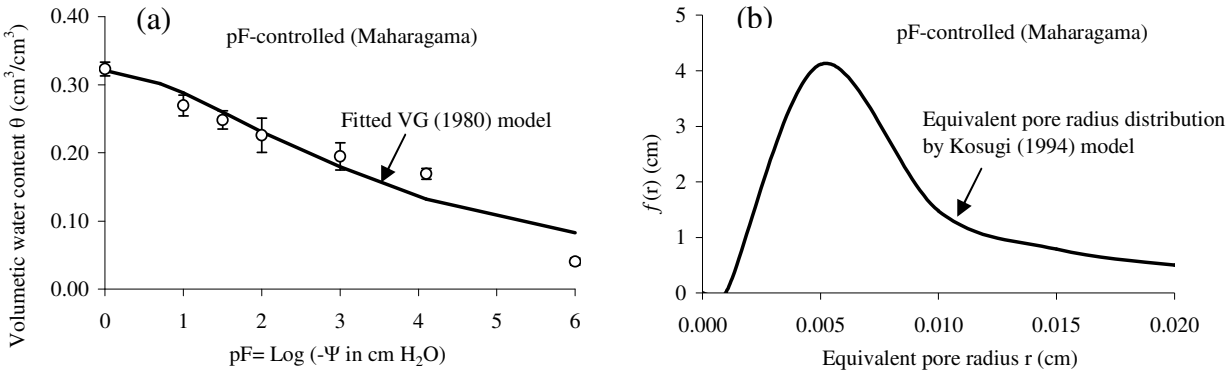

Figure 2. (a) Soil water retention curve; (b) equivalent pore radius distribution function

The soil-water retention curve and equivalent pore radius for soil are shown in Figures 2(a) and 2(b) respectively. In Figure 2(a) solid line shows the fitted van Genuchten (1980) model and open circles denote the experimental data in Maharagama landfill data with standard deviation. The next figure shows the equivalent pore radius distribution curve by Kosugi (1994) model.

Gas transport parameter variation and model fitting

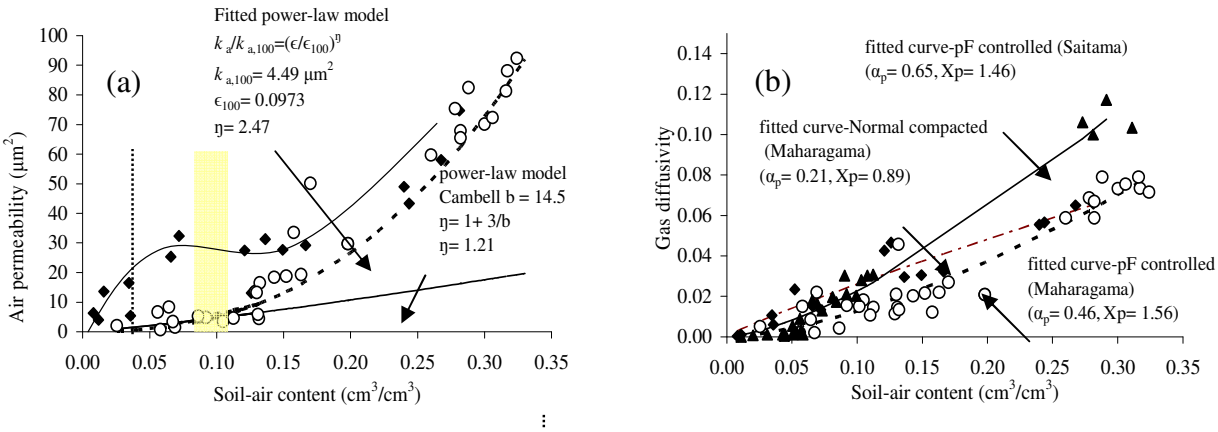

Figure 3. (a) air permeability and (b) gas diffusivity variation with soil air content.

Figure 3(a) shows the air permeability variation of soil. Solid line was drawn to show the tendency of k_a with ε over the gravimetric water content from 10.0 to 17.0%. The open circles denoted the pF controlled samples of

Maharagama soil while closed squares denote the normal compacted samples. The closed rectangles show the pF controlled Saitama samples. The shaded area is to illustrate the soil air content relevant to field water content and dotted line is the optimum water content respectively. For the pF controlled samples power law model (Moldrup *et al.*, 1998) fitted well. The relevant values and fitting parameters are shown in Figure 3(a). In addition to that power law model (Kawamoto *et al.,* 2006) was fitted but it underestimated the experimental values. In the case of normal compacted samples the air permeability variation was significant at wetter condition and drier condition and at around field water content it was not so significant. For this kind of variation one reason may be the changes of structure formation as suggested by Poulsen *et al.* (2008). Other possible reason could be the packing effects of two different procedures. Figure 3(b) shows the gas diffusivity with ε. Eq.1 was fitted with data and fitting parameters are shown in the figure. For the comparison Japanese soil with fitting curve is shown. In generally gas diffusion is increased with ϵ and power law model and is well fitted with measured data.

Conclusion

Air permeability and gas diffusivity were measured as a function of soil air content in different water content. In normal compaction sample k_a was initially increased with ε and then around ε correspondent to field water content, its variation was not so significant. Finally k_a was increased significantly with drier conditions. This scenarios may suggest the structure formation with water content. In the case of pF controlled samples, k_a was increased exponentially. Gas diffusivity was increased with ε and power law modal was fitted well. In comparison the two soils were nearly close in dry bulk densities and the fitting parameters were also approximately equal.

Acknowledgement

This work was partially supported by a grant from the Research Management Bureau, Saitama University and by the Takahashi Sangyo-Keizai Kenkyu Foundation. This work was also in part supported by the Research grant for promoting technological seeds, JST.

References

Chiemchaisri C, Junga JP, Visvanathan C (2007) Municipal solid waste management in Thailand and disposal emission inventory. *Environmental Monitoring and Assessment* **135**, 13-20.

Hamamoto S, Moldrup P, Kawamoto K, Komatsu T (2009) Effects of particle size and soil compaction on gas transport parameters in variably-saturated, sandy soils. *Vadose Zone Journal* **8**, 986-995

Kallel A, Tanka N, Matsuto T (2004) Gas permeability and tortuosity for packed layers of processed municipal soil wastes and incineration residue. *Waste Management and Research* **22**, 186-194.

Kawamoto K, Moldrup P, Schjonning P, Iversen VB, Komatsu T, Rolston DE (2006) Gas transport parameters in the vadose zone: Development and tests of power-law models for air permeability. *Vadose Zone Journal* **5**, 1205-1215.

Kosugi K (1994) Three-parameter lognormal distribution model for soil water retention. *Water Resources Research* **30**, 891-901.

Moldrup P, Poulsen TG, Schjonning P, Olesen T, Yamaguchi T (1998) Gas permeability in undisturbed soils: measurements and predictive models. *Soil Science* **163**, 180-189.

Poulsen TG, Blendstrup H, Schjonning P (2008) Air permeability in repacked porous media with variable structure-forming potential. *Vadose Zone Journal* **7**, 1139-1143.

Seheum M, Kyoungphile N, Jae YK, Shim KH, Moonkyung C (2008) Effectiveness of compacted soil liner as a gas barrier layer in the landfill final cover system. *Waste Management* **28**, 1909-1914.

Song SK, Shon ZH, Kim KH, Kim SC, Kim YK, Kim JK (2007) Monitoring of atmosphere reduced sulfer compounds and their oxidation in two coastal landfill areas. *Atmospheric Environment* **41**, 974-988.

Weeks OL, Mansell RS, McCallister ST (1992) Evaluation of soil-top cover system to minimize infiltration into a sanitary landfill: A case study. *Environmental Geology and Water Science* **20**, 139-151.

Van Genuchten MTH (1980) A closed-form equation for predicting the hydraulic conductivity of unsaturated soils. *Soil Science Society of America Journal* **44**, 892-898.

Mobilization and transport of natural and water dispersible colloids in repacked Okinawa red-yellow soil columns

Anu Sharma[A], Taiki Hirata[A], Ken Kawamoto[A,B], Chamindu Deepagoda T.K.K.[C], Per Moldrup[C], and Toshiko Komatsu[A,B]

[A]Graduate School of Science and Engineering, Saitama University, Japan, Email: anu.sharma192@gmail.com
[B]Institute for Environmental Science and Technology, Saitama University, Japan
[C]Environmental Engineering Section, Dept. of Biotechnology, Chemistry and Environmental Engineering, Aalborg University, Denmark.

Abstract
Mobilization, transport and deposition of soil colloids are the fundamental processes governing colloid-facilitated transport of contaminants. Although significant progress has been made in understanding the processes involving mobilization and transport of colloids in porous media, the leaching of natural colloids from soil parent material is not yet fully understood. This study investigates the leaching of natural red-yellow soil colloids and simultaneous transport of applied water dispersible colloids (RYS-WDC) in the saturated soil columns packed with red-yellow soil from Okinawa, Japan at two different flow rates (60mm/h and 300mm/h) at different pH conditions (natural and low pH). The effluent was measured for turbidity, pH, EC, particle size distribution and bromide tracer applied with RYS-WDC. The leaching of natural soil colloid showed similar trend but different magnitude of leached colloids concentration. The breakthrough curve showed the highest colloid leaching at initial pore volumes and gradual decrease with significant tailing effect. Transport of applied colloid was observed to follow a different kinetics without tailing effects. Thus, it suggested that the natural leaching of colloids from red-yellow soil and the transport of applied water dispersible colloid extracted from the same red-yellow soil followed different kinetics.

Key Words
Soil colloids, column experiment, leaching, breakthrough curves

Introduction
Colloid mobilization and transport in porous media is of great significance for colloid-facilitated transport of organic and inorganic contaminants that adsorb to the particles and travel to a greater distance and cause soil and groundwater contaminations. (Grolimund *et al*., 1996; Kersting *et al*., 1999). Among the different sources of mobile colloids, particles that originate from the parent materials through particle release and detachment is the most common process (Ryan and Elimelech, 1996). Such in situ release of colloidal particles is mainly due to physical perturbations or changes in chemical composition of the pore water (Ryan and Elimelech, 1996). The mobilized colloids are transported through the subsurface and result into deposition. Colloid attachment and straining (Bradford *et al*., 2002) are the two key processes for colloid deposition in the porous media. Despite the potential importance of the mobilization and transport processes, the release of colloid particles is poorly understood. Recently, a number of studies have been conducted focusing on different aspects of colloidal phenomena in porous media. However, most of the researches are focused on the transport of particles or model colloids, while release and mobilization of natural colloids from parent materials have received very little attention (Grolimund and Borkovec, 2001).

This study investigated leaching, transport and deposition of natural colloids and water dispersible colloids extracted from red-yellow soil in saturated repacked column under steady irrigation using artificial rain water. The characteristics of natural colloids leaching and breakthrough of applied soil colloids were investigated at different flow rates and pH conditions.

Methods
Kunigami mahji, a red-yellow soil (RYS), sampled at a depth of 0-5cm from hilly site of Nakijison, Okinawa, Japan was used as the porous medium in all soil columns. The physiocochemical properties of the soil are given in table 1.

1 – 6 August 2010, Brisbane, Australia. Published on DVD.

Table 1. Physicochemical properties of Okinawa red-yellow soil.

Soil Name	Depth cm	Soil texture	Clay %	Silt %	Sand %	Loss on ignition %	Particle density g cm^{-3}	pH	Electrical conductivity mS/m
Red-yellow soil	0-5	Clay loam	27	46	27	11.2	2.72	8.3	17.4

Artificial rain water (ARW) with composition 0.085mM NaCl and 0.015mM $CaCl_2$ was used as the feed solution in all column experiments. Water dispersible colloidal solution (WDC) was prepared by mixing ARW and red-yellow soil in 1:100 (w/w) ratio, shaking for 24 hours and then letting it settle for another 20 hours. The RYS-WDC having Stoke's diameter less than 2 µm was siphoned from the supernatant and filtered by 1 µm filter paper to be used in the experiments.

Column experiments

The sampled red-yellow soil was wet packed in a column (4.8cm in diameter and 10cm in height) to a bulk density of 1.05g/cm^3. A 105 µm nylon filter was used at the bottom of the column to prevent any loss of fine soil particles.

Table 2. Experimental conditions in column experiments.

Column No.	Flow	Water flux cm $hour^{-1}$	pH of influent		Initial concentration of influent		Solution schedule
			ARW	WDC	WDC mg L^{-1}	Br^- mg L^{-1}	PVs: pore volumes
No.1	low	5.59	6.1	none	none		ARW 60 PVs →
No.2		5.99	6.1	none	none		
No.3		5.66	6.1	7.5	141	91	ARW 20 PVs → WDC 20 PVs → ARW 20 PVs →
No.4		6.01	6.1	7.5	141	91	
No.5	high	30.09	6.1	none	none		ARW 60 PVs →
No.6		30.52	6.1	none	none		
No.7		31.09	6.1	7.7	199	85	ARW 20 PVs → WDC 20 PVs → ARW 20 PVs →
No.8		32.42	6.1	7.7	199	85	
No.9		30.82	3.8	none	none		ARW 60 PVs →
No.10		30.64	3.8	none	none		
No.11		31.61	3.8	4.0	230	77	ARW 20 PVs → WDC 20 PVs → ARW 20 PVs →
No.12		31.27	3.8	4.0	230	77	

Natural: No.1–No.4, No.5–No.8; low: No.9–No.12

Two sets of experiments with duplicates were conducted for each condition. The first two column experiments (No. 1 and No.2) were irrigated with ARW at an intensity of about 6cm/hr with peristaltic pump for a period of 60 pore volume. In the other two column experiments (No. 3 and No. 4), two types of solution were fed to the column consecutively. ARW was first applied for a period of 20 pore volumes and water dispersible colloids extracted from red-yellow soil (RYS-WDC) was applied for next 20 pore volumes and finally ARW was again applied for the last 20 pore volumes. Similar procedure was applied for high flux and low pH conditions. The experimental conditions and application sequences are given in table 2. The effluents were collected and monitored for turbidity, pH, EC, particle size distribution and tracer bromide concentration.

Results

Mobilization and leaching of natural soil colloids

The results of mobilized natural colloid leaching from saturated repacked red-yellow soil at low flow rate-natural pH, high flow rate-natural pH, and high flow rate-low pH conditions are illustrated in Figure 1-No.1, No.5, and No. 9, respectively. The leached natural colloids showed a similar trend but different magnitude with highest colloid leaching observed in low flow rate-natural pH conditions, which is twice as much as in high flow rate-natural pH condition. This is likely due to the more contact time. The least colloid leaching was observed at high flow rate-low pH condition. The colloid concentration increased immediately after the application of feed solution, reached maximum peak at around 4 pore volumes and gradually decreased with time. The results indicated that highly mobile colloid particles, weakly attached to the soil aggregate are released in the initial flush giving rise to the breakthrough curve (BTC). The colloids, which are strongly attached to the aggregate move slowly and become mobile colloids resulting in the tailing in the BTC.

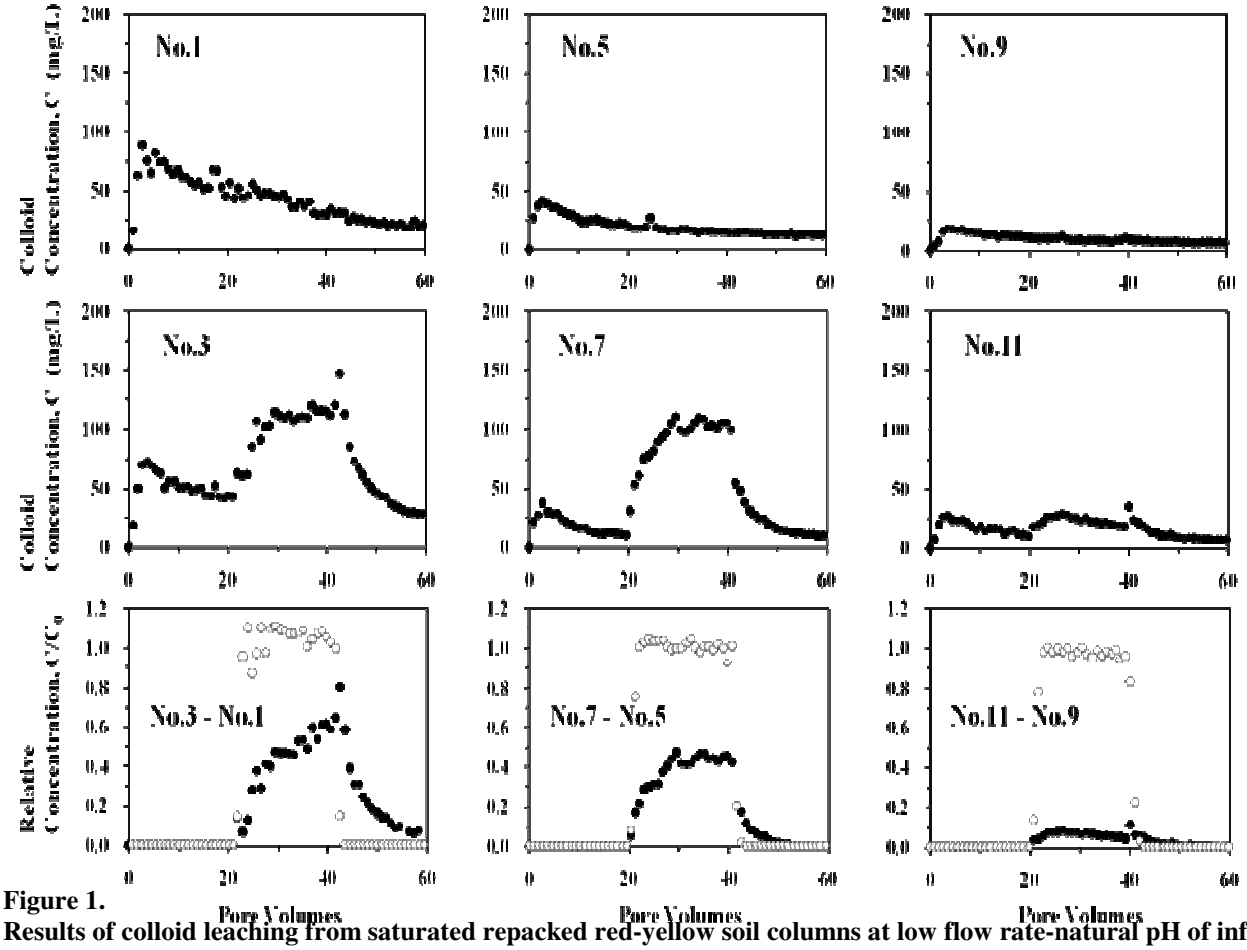

Figure 1.
Results of colloid leaching from saturated repacked red-yellow soil columns at low flow rate-natural pH of influent, high flow rate-natural pH, and high flow rate-low pH conditions. No. 1, 5, and 9 represents mobilized natural colloid leaching breakthrough curves (BTC); No. 3, 7, and 11 represent natural and applied colloids BTC. The lowest figures show the breakthrough curves for the applied colloids obtained by the deduction of No. 1, 5, and 9 from No. 3, 7, and 11, respectively. Open circles represents BTC for tracer bromide ion.

Transport of applied water dispersible colloids
Breakthrough and breakdown curves of applied water dispersible colloids with natural colloid leaching curves are shown in Figure 1 No. 3, No. 7 and No. 11 for the three different conditions. Assuming that the leaching of natural colloids and transport of applied water dispersible colloids occur independently, the breakthrough and breakdown curves for applied water dispersible colloids (total colloids minus natural colloids) were obtained in Figure 1 (bottom three Figures).

The applied colloid breakthrough seemed to have reached plateau before breakdown, especially for high flow rate-natural pH. The curves also illustrate that both irreversible and reversible attachments of colloids are dominant in low flow rate condition but the irreversible attachment of colloids is more dominant in high flow rate conditions. Less tailing effect was observed for the transport of applied water dispersible colloids than for natural colloid leaching and thus, indicates that natural colloid leaching and transport of WDC follow a different kinetics. About 90% of the total applied colloids deposited at high flow rate and low pH conditions, while about 50% were leached for natural pH conditions indicating the significant effect of pH in colloid mobilization and transport. The particles size distribution (PSD) of influent applied colloid is similar to the PSD of natural colloids (Figure 2).

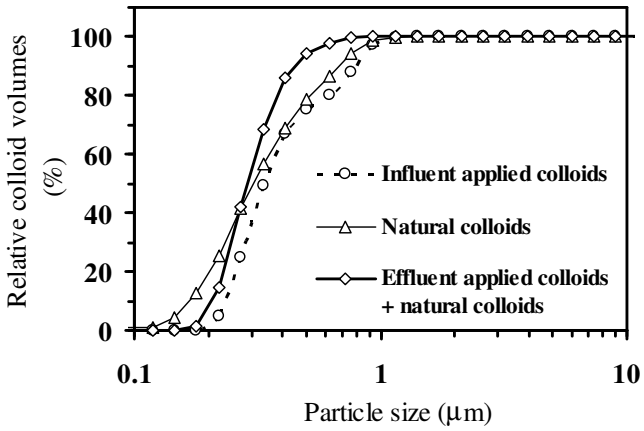

Figure 2. Particle size distribution for influent applied water dispersible colloids, effluent natural colloids, and total of effluent applied colloids and natural colloids.

Conclusion

A series of column experiment were conducted to investigate the leaching and transport of soil colloids from red-yellow soil. Continuous natural colloid leaching was observed when artificial rain water was applied at the top of the column. When water dispersible colloid solution was applied, about 50% of the colloids were recovered from the effluent without tailing for high and low flux at natural pH condition. However, almost all of applied colloids were retained (only 10% recovered) at high flux and low pH condition. Natural colloid leaching and applied colloid transport follow different transport mechanisms, although the parent material for the both condition is from the same red-yellow soil. The knowledge regarding the colloid fate and transport in natural soils, obtained from laboratory experiments and numerical analysis is required for better prediction of colloid facilitated transport of contaminants.

Acknowledgement

This work was partially supported by a grant from the Research Management Bureau, Saitama University and grant-in-aid for Young Scientists (A) (No. 18686039) from the Japanese Ministry of Education, Science, Sports, and Culture (Monbukagakusho) and grant from Japan Interaction in Science and Technology Foundation (JIST Foundation).

References

Bradford SA, Yates SR, Bettahar M, Simunek J (2002). Physical factors affecting the transport and fate of colloids in saturated porous media. *Water Resour. Res*. **38 (12)**, Art No. 1327, doi.

Grolimund D, Borkovec M (2001) Release and transport of colloidal particles in natural porous media: 1. Modeling. *Water Resour. Res*. **37(3)**, 559-570.

Grolimund D, Borkovec M, Barmettler K, Sticher H (1996). Colloid facilitated transport of strongly sorbing contaminants in natural porous media: a laboratory column study. *Environ. Sci. Technol*. **30(10)**, 3118-3123.

Kersting AB, Efurd DW, Finnegant DL, Rokop DJ, Smith DK, Thompson JL (1999). Migration of Plutonium in groundwater at the Nevada Test Site. *Nature* **397**, 56-59.

Ryan JN, Elimelech M (1996) Colloid Mobilization and transport in groundwater. *Colloid Surf.,* A **107**, 1-56.

Multifractal characterization of pore size distributions measured by mercury intrusion porosimetry

E. Vidal Vázquez[A], R. García Moreno[A], A.M. Tarquis[B], A. Saa Requejo[B], J.M. Mirás-Avalos[A] and **J. Paz-Ferreiro**[C]

[A] Facultad de Ciencias. Universidad de La Coruña- UDC, Spain
[B]CEIGRAM (Centre for Studies and Research on Agricultural and Environmental Risk Management), Universidad Politécnica de Madrid, Spain.
[C]Department of Biological Sciences, Lancaster University, Lancaster, United Kingdom, Email jpaz@udc.es

Abstract
The aim of this work was to assess the multifractal characteristics of pore size distributions measured by mercury injection porosimetry (MIP). Two pairs of soil samples were collected in plots with different topographic position and soil use, with each pair differentiated by distinct proportion of fine particles and organic matter contents. Macropore volume was higher on samples with higher clay and organic matter content. Mass exponent function, singularity spectra and generalized dimension spectra showed that multifractal distribution was a suitable model for mercury injection curves. Multifractal parameters extracted from singularity spectra and generalized dimension spectra reflected the main characteristics of the pore size distributions (PSDs). Therefore, it was concluded that multifractal analysis is useful for distinguishing between different patterns of pore size distributions obtained by Hg injection.

Key Words
Pore-size-distribution, indirect methods, multifractality, texture, organic matter content

Introduction

The pore size distribution (PSD) of a soil depends on the combined effects of texture and structure. The frequency distribution of soil pore sizes controls water and air storage and their transport into the profile. Greenland (1981) distinguished three pore size categories: i) transmission pores (>50 μm) responsible for water flow during drainage, ii) storage pores (50–0.5 μm) retaining most available water and iii) residual pores (<0.5 μm) where chemical reactions occur. These criteria show a rough correspondence with soil hydraulic properties. Frequently, PSDs are obtained by indirect methods, even if they provide little information on pore geometry. The water retention curve is the most widely used method to estimate PSDs. Mercury injection porosimetry (MIP) also has been recognized as an useful tool for characterizing the intra-aggregate porosity, from about 100 to 0.005 μm, which includes the so-called textural pore domain and the smaller classes of the structural compartment (e.g. Fiès, 1992).

Fractal models have been widely applied in soil science. Pore size distributions measured by MIP have been proven to be fractal in a limited range of scales (Bartoli *et al*., 1991). Interest has recently turned to multifractal analysis of porous media. The use of multifractal tools to understand soil porosity means that the PSD can be viewed as a singular statistical distribution and it is reasonable to explain it as a multifractal measure. Several authors carried out multifractal studies of PSDs obtained from image analysis (e.g. Posadas *et al.*, 2003; Grau *et al.*, 2006). Multifractal analysis of MIP data sets (Vidal Vázquez *et al.*, 2008) is more recent. The aim of this study was to evaluate the performance of multifractal analysis for distinguishing between PSDs of soils with differences ~~i~~n both textural composition and organic matter content.

Methods

Two loam-silty soils were selected from Mabegondo (Coruña province) and Raigoso (Orense province), both located in Northwestern Spain, on the basis of differences in clay, silt and organic matter content. These soils will be next referred to as soil 1 and soil 2, respectively. Parent material was basic schist in Mabegondo and quaternary sediments in Raigoso. The soils were classified as Umbrepts according to the US Soil Taxonomy. Two different soil uses, grassland and cultivated were sampled on each site. Grassland plots were located at the footslope and exhibited hydromorphic features, whereas cropland plots were at the backslope.

Pore size distributions were estimated by MIP, which enables the measurement of both the pressure required to force mercury into the voids of a dry soil sample and the intruded Hg volume at each pressure. The pressure required to force Hg into soil pores is a function of the contact angle, size, and geometry of pores and surface

tension. If the pores are cylindrical, then the relation between pressure, P (expressed in Pa), and equivalent pore diameter, d (expressed in mm), is given by the Young-Laplace equation:

$P = -4\gamma\cos\theta/d$ (1)

where θ is the mercury-solid contact angle and γ is the surface tension of mercury. The values of θ and γ were taken as 140º and 0.480 Nm^{-1}, respectively (Fiès, 1992). The PSDs were determined using a "Thermaquest Pascal 440" porosimeter. The equipment operates from 10 kPa to 300 MPa, equivalent to pores with diameter, d, ranging from 150 μm to 0.005 μm, respectively.

Multifractal analysis of PSDs supported on an interval I = [a,b] with a diameter L requires a set of different boxes or subintervals of I with equal length. A common choice is to consider dyadic scaling down (e.g. Vidal Vázquez *et al.*, 2008), which means successive partitions of the support in k stages (k=1,2,3…) that generate a number of cells $N(\delta) = 2^k$ of characteristic size length, $\delta = L \times 2^{-k}$, covering the initial interval I. The size interval of the experimental MIP curves ranged from 0.005 to 100 μm. Following this approach, the probability mass distribution, $p_i(\delta)$, for each box was estimated as a proportion according to:

$$p_i(\delta) = \frac{N_i(\delta)}{N_t} \quad (2)$$

where $N_i(\delta)$ is the pore volume of the i^{th} box and N_t is the total volume of the system. To analyze the multifractal spectrum of the probability mass function the moment method was used which involves three functions: mass exponent, τ_q, singularity spectrum, $f(\alpha)$, and generalized dimension, D_q. First, the partition function $\chi(q,\delta)$ was estimated from the $p_i(\delta)$ values. The partition function scales with the box size, δ, as:

$$\chi(q,\delta) \propto \delta^{-\tau(q)} \quad (3)$$

where τ(q) is the mass exponent or scaling function of order *q*. For multifractal measures, the probability mass function, $p_i(\delta)$, also scales with the box size, δ, as:

$$p_i(\delta) = \delta^{\alpha_i} \quad (4)$$

where α_i is the *Hölder* or singularity exponent, characterizing the scaling property peculiar to each i^{th} box. On the other hand, the number $N_\delta(\alpha)$ of boxes of size δ, where the probability has singularity exponent values between α and $\alpha_i + d\alpha$, obeys a power law as:

$$N(\alpha) \propto \delta^{-f(\alpha)} \quad (5)$$

where $f(\alpha)$ is a scaling exponent of the boxes with a common α, called the singularity exponent. A plot of $f(\alpha)$ versus α is called the singularity spectrum. Following Chhabra *et al.* (1989), the functions α and $f(\alpha)$ can be determined by Legendre transformation as:

$$\alpha(q) = \frac{d\tau(q)}{dq} \text{ and } \quad f(\alpha) = \alpha(q)q - \tau(q) \quad (6)$$

Multifractal sets can also be characterized by their spectrum of generalized dimension, D_q, which can be introduced (for all $D_q \neq 1$) by the following scaling relationship:

$$D_q = \lim_{\delta \to 0} \frac{1}{q-1} \frac{\log[\chi(q,\delta)]}{\log \delta} \quad (7)$$

For the particular case where *q*=1 equation (7) becomes indeterminate, so D_q is estimated by l´Hôpital's rule. The generalized dimension, D_q, is related to the other sets of multifractal exponents. Hence, D_q, is obtained from the relationship with mass exponent, τ_q, which can be defined as:

$$\tau(q) = (1-q)D_q \quad (8)$$

The generalized dimensions, D_q for $q = 0$, $q = 1$ and $q = 2$, are known as the capacity, the information (Shannon entropy) and correlation dimensions, respectively.

Results

Table 1 lists general properties of the studied soil samples. Soil reaction was very strongly acidic in Mabegondo and extremely acidic in Raigoso. Organic matter content of the soil samples under cropland was lower than under grassland in the two soils. Also differences in finer particles between soil uses were large with greater silt and clay values under grassland than under cultivated land.

Table 2 shows the partial porosity values measured by MIP, for the equivalent diameter range from 100 to 0.005 μm (i.e. the total cumulative intrusion size range) and also for the 100 to 50 μm, 50 to 0.5 μm and 0.5 to 0.005 μm subintervals. On average the Hg volume injected over pore diameters between 100 and 0.005 μm was higher

under grassland than under cultivated land and for soil 2 compared to soil 1. The smaller porosity of aggregates sampled in cultivated plots is an expected result owing to differences in silt + clay and organic matter content. Each pair of samples showed great volume differences in the pores size class 100-0.5 μm, whereas residual pore volume (< 0.5 μm) was little affected by soil use and fine particle content.
The three multifractal functions mass exponent, τ_q, (Figure 1) singularity spectrum, $f(\alpha)$, and generalized dimension, D_q (Figure 2) will be shown to be useful for describing multifractality. Mathematically, the multifractal property can be completely determined only by the entire fractal spectrum functions. Some characteristic values of these functions, however, portray the main characteristics of multifractality.

Table 1. Composition of samples of the two studied soils under grassland and cropland.

Soil	Soil use	pH	O.M. ($g\ kg^{-1}$)	Sand ($g\ kg^{-1}$)	Silt ($g\ kg^{-1}$)	Clay ($g\ kg^{-1}$)
1 Mabegondo	Grassland	5.0	75.5	111	680	208
1 Mabegondo	Cultivated	5.1	34.7	235	601	164
2 Raigoso	Grassland	4.0	79.6	125	665	210
2 Raigoso	Cultivated	4.3	20.4	204	625	171

A comparison between the moment scaling function, τ_q, of all the studied PSDs and the scaling function of the simulated monofractal type is shown in Figure 1. The slope of the τ_q functions for $q < 0$ were different from that of $q > 0$, which means a multiple scaling nature, so that low and high density regions of the studied variable, the soil porosity, scale differently.

Table 2. Pore volume in different diameter size classes of the two studied soils. Total pore size is 100-0.005 μm.

Soil	Soil use	100-0.005 μm (cm^3kg^{-1})	100-50 μm (cm^3kg^{-1})	50-0.5 μm (cm^3kg^{-1})	<0.5 μm (cm^3kg^{-1})
1 Mabegondo	Grassland	326	5	219	102
1 Mabegondo	Cultivated	272	5	155	112
2 Raigoso	Grassland	502	22	339	141
2 Raigoso	Cultivated	365	7	222	136

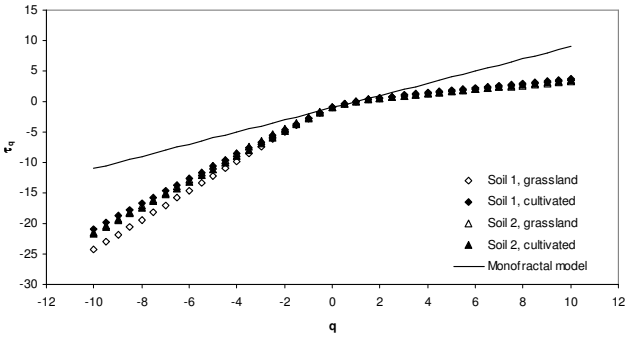

Figure 1. Mass exponent function τ_q, versus *q* for the studied pore size distributions.

Singularity spectra, $f(\alpha)$ versus α, shown on Figure 2 have a strongly marked asymmetric concave down parabolic shape, also indicative of multifractal behavior. These are a powerful tool for charcaterize the simililarity and/or differences between the scaling properties of the measure and also enable us to examine the local property of the studied variable. The wider the spectrum (i.e. the greater the α_{max}-α_{min} value) the higher is the heterogeneity in the local scaling indices of the variable and vice versa. Moreover, dominance of extremely high or extremely low data values is related to the left- (q>>1) and right-hand (q<<-1) sides of the $f(\alpha)$ spectrum, respectively.
The generalized dimension, D_q, would be a constant in the case of scale-invariant distributions but changes with *q* for multifractal measures, so that $D_0 > D_1 > D_2$. The capacity or box-counting dimension, D_0, was not significantly different from 1.00, which correspond to an Euclidean support. Results for D_1 and D_2 (Table 3) clearly support the hypothesis of singular behavior of relative pore volume distributions. The entropy or information dimension, D_1, of the individual PSDs varied between 0.757 and 0.866 for the initial surface and between 0.656 and 0.727, whereas D_2 ranged from 0.508 to 0.580. The R^2 fits leading to a Dq spectrum were higher than 0.925 in the range of q moments $-10 < q < 10$. Results of the generalized dimension analysis are in agreement with observations from the mass exponent function τ_q presented above.

1 – 6 August 2010, Brisbane, Australia. Published on DVD.

Table 3. Mean values and standard deviation of selected multifractal parameters from D_q spectra.

Soil	Soil use	D_1	D_2	D_{-10}	D_{10}
1 Mabegondo	Grassland	0.656 ± 0.024	0.508 ± 0.012	2.197 ± 0.625	0.386 ± 0.001
1 Mabegondo	Cultivated	0.700 ± 0.036	0.580 ± 0.059	1.896 ± 0.452	0.401 ± 0.056
2 Raigoso	Grassland	0.727 ± 0.043	0.569 ± 0.056	1.948 ± 0.235	0.367 ±0.072
2 Raigoso	Cultivated	0.663 ± 0.075	0.525 ± 0.102	1.961 ± 0.483	0.385 ± 0.101

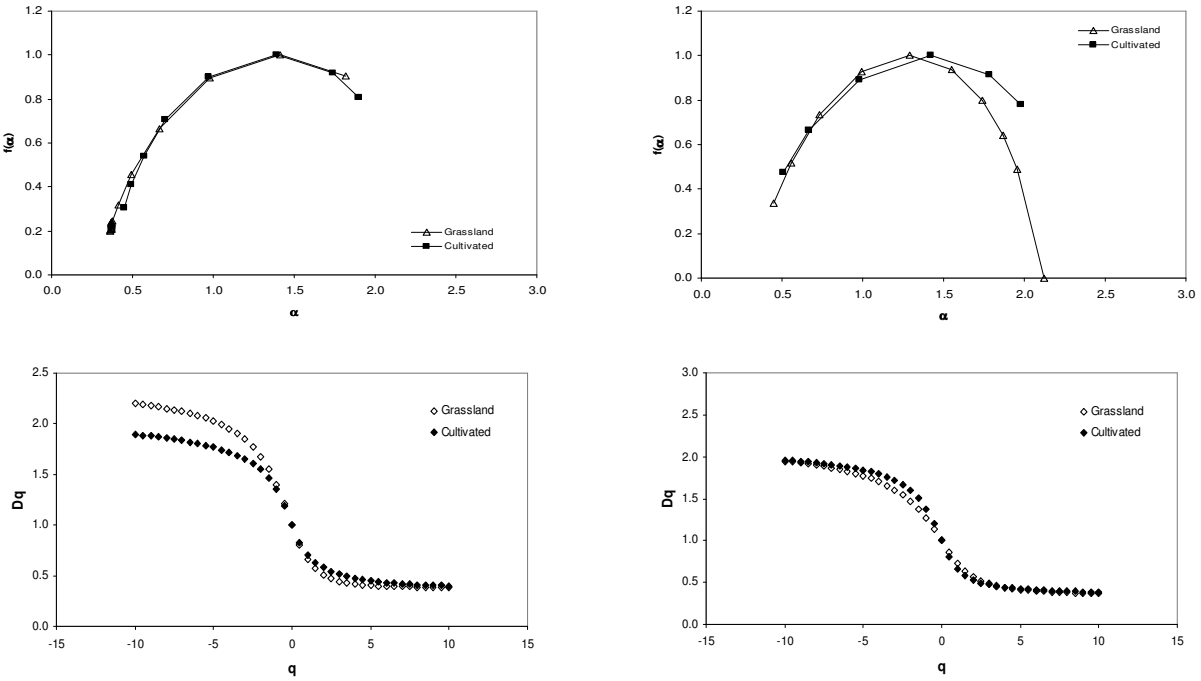

Soil nº 1 (Mabegondo) **Soil nº 2 (Raigoso)**

Figure 2. Singularity spectra f(a) and generalized dimensions, D_q, versus q for the studied PSDs.

Conclusion

Mercury intrusion analysis showed an increase of storage and transmission pore categories with increasing clay + silt and organic matter contents, whereas no changes were detected in residual porosity. The scaling properties of PSDs measured by MIP could be fitted reasonably well with multifractal models. Multifractal analysis allowed discrimination between different patterns of pore size distributions.

Acknowledgements

This work was supported by Spanish Ministry of Education and Science (project AGL2005-08219-C02-01/HID) and by Xunta de Galicia (project INCITE08PXIB 162169PR).

References

Bartoli F, Philippy R, Doiresse M, Niquet S, Dubuit M (1991). Structure and self-similarity in silty and sandy soils: the fractal approach. *Journal of Soil Science* **42,** 167-185.

Grau J, Méndez V, Tarquis AM, Díaz MC, Saa A (2006) Comparison of gliding box and box-counting methods in soil image analysis. *Geoderma* **134,** 349-359.

Fiès JC (1992). Analysis of soil textural porosity relative to skeleton particle size, using mercury porosimetry. *Soil Science Society of America Journal* **56,**1062-1067.

Greenland DJ (1977). Soil damage by intensive arable cultivation. Temporary or permanent? *Philosophical Transactions of the Royal Society Series B* **281,** 193-208.

Posadas AN, Giménez DD, Quiroz R., Protz R. (2003) Multifractal characterization of soil pore systems. *Soil Science Society of America Journal* **67,** 1361-1369.

Vidal Vázquez E, Paz Ferreiro J, Miranda JGV, Paz González A (2008) Multifractal analysis of pore size distributions as affected by simulated rainfall. *Vadose Zone Journal* **7,** 500-511**.**

Pore rigidity in structured soils – only a theoretical boundary condition for hydraulic properties?

R. Horn[A], S. Peth[A], T. Baumgartl[B], S. Gebhardt[A], H. Fleige[A], J. Doerner[C] and XH. Peng[D]

[A]Institute for Plant Nutrition and Soil Science, Christian Albrechts University zu Kiel, Olshausenstr. 40, Kiel, Germany, Email rhorn@soils.uni-kiel.de
[B]CMLR, University of Queensland, Brisbane, Australia
[C]Universidad Austral de Chile, Valdivia, Chile
[D]Institute of Soil Science, CAS Nanjing, China

Abstract
The quantification of fluxes in structured unsaturated soils requires rigid pore systems as the key background parameter. Swelling and shrinkage, chemical, mechanical, and biological processes alter the internal soil strength and consequently also the pore diameter, continuity and pore functions as soon as the structural shrinkage, or precompression stress is exceeded by a more intense drying, or the corresponding stresses applied. The absolute error in quantifying the water retention functions for sandy, silty, clayey, as well as peat soils will range in between 3–10 vol. % water which also results in a variation of the hydraulic conductivity/matric potential relation of up to 2–4 orders of magnitude up to pF 3.

Key Words
Rigidity of pores, water retention curve, hydraulic conductivity, shrinkage, soil aggregation

Introduction
Darcy's Law describes the 1-dimensional water flux under given boundary conditions which have to be fulfilled. Apart from this 1-dimensionality, also the laminar flow, inert properties, and complete pore rigidity are required in order to obtain validated results. Thus, these restrictions limit the applicability of the Darcy's Law mostly to coarse textured or coarse sandy soils (if no turbulent flow occurs), while silty, loamy, and clayey textured substrates mostly would not fulfill these boundary conditions. Most current approaches for calculating water flow are based on a mass balance equation and Darcy's Law. The use of material coordinates, instead of fixed spatial coordinates such as normally used for nonswelling soils, leads to a flow equation analogous to the Richards equation (Smiles, 2000). Thus, Darcy's Law relates the volume flux of water, q, to the gradient in the hydraulic potential and the soil hydraulic conductivity. If arable, forest, or anthropogenic soils are considered it is obvious that aggregate formation due to wetting and drying as well as due to biological activity occur as soon as soils contain some clay, but even if soils are coarser but more saline or have more expansive clay minerals also remarkable cracks are to be detected and proof that volume changes and reformation of pores generally occur.

Generally, when matric potential decreases, menisci forces pull adjacent soil particles closer to each other and consequently decrease soil volume. Based on the findings of Baumgartl (2003), who described the parallelism of mechanical stress–strain curves and hydraulic stress (matric potential) and volume change behavior, Peng *et al*. (2007) showed that the link between the mechanical and the hydraulic prestresses result in nearly identical shrinkage curves. Additionally, Baumgartl (2003) explained the differences between the mechanically induced collapse and the matric potential dependent shrinkage pattern by the dimensionless X factor. Stange and Horn (2005) showed the effect of nonrigidity on hydraulic functions as well as they developed corrected model equations for homogenized substrates. In the present paper we therefore discuss the following hypotheses: 1) soil hydraulic properties are only reliable in the preshrinkage i.e. structural shrinkage range and depend on the in situ hydraulic history; and 2) exceeding the structural shrinkage range results in a new 3-dimensional volume decline and altered retention curve and conductivity pressure head relations.

Material and Methods
Several disturbed and undisturbed soil samples were taken from various soil profiles with different geological origin in Northern Germany under arable and pasture conditions: Stagnic Luvisol (*SS-LL*), Gleysol (*GGn*), Stagnosol (*SSn*), Tschernosem (*TTn*), Lowland peat (*HNn*), Histic Gleysol (*HN-GH*). Table 1 informs some physical properties of the investigated sites. Both the water retention and the shrinkage characteristics of these undisturbed soil core samples (v = 470 cm³) were determined after complete saturation by capillary rise and drainage to fixed soil moisture tensions.

1 – 6 August 2010, Brisbane, Australia. Published on DVD.

Table 1. Soil types, texture (according to the German classification system), structure, and bulk density of the investigated sites.

abbreviation	texture	Structure	ρt	clay	fine	middle silt	coarse	fine	middle sand	coarse
				< 2	< 6,3	< 20	< 63	< 200	< 630	< 2000
			[g cm^{-3}]				[µm]			
SS-LL (15, 25)	**Su3**	**coh - subangular blocky**	1,59	7,4	4,3	6,6	16,5	29,7	29,0	6,5
SS-LL (35)	**Su2/Su3**	**platy**	1,73	4,3	2,6	7,6	14,3	31,1	32,8	7,3
SS-LL (50)	**Ls3**	**Subang. blocky**	1,68	20,4	8,6	11,9	18,1	22,1	15,1	3,8
SS-LL (75)	**Sl3**	**blocky–prism**	1,77	8,1	2,1	6,3	14	29,5	34,5	5,5
GGn (40)	**Tu3**	**coh– blocky**	1,46	34,9	17,1	20,5	20,1	5,8	1,4	0,2
SSn (50)	**Ts2/Tl**	**coh – blocky)**	1,72	64,9	9,1	3,7	2,2	8,7	10,4	1,0
TTn (40)	**Ut4**	**Subang. blocky**	1,45	19,24	23,54	44,19	97,93	98,64	99,49	100
HN (30)	**Torf**		0,81							
HN-GH (40)	**Lt3**	**Coh**	1,08	39,9	11,5	15,9	6,7	17,8	7,8	0,4

Key: SS-LL: Stagnic Luvisol, GGn: Gleysol, SSn: Stagnosol, TTn: Tschernosem, HNn: Lowland peat, HN-GH: Histic Gleysol.

The used drainage steps were -3, -6, -15, -30 und -50 kPa with ceramic suction plates, 300, 600 und 1500 kPa with pressure chambers and 105°C in the oven. After each drainage step, the weight of every sample as well as the volume decrease due to shrinkage was measured assuming an isotropic i.e. identical vertical and horizontal deformation. The vertical height change was determined by a digital measuring caliper with an accuracy of 0.05 mm at eight fixed point at the sample surface. The total height change was then calculated from the arithmetic mean of these eight values. The change of sample height multiplied by the actual surface area gives the vertical volume change. The saturated hydraulic conductivity was determined under instationary conditions (Hartge 1966). The hydraulic conductivity/ matric potential ratio was determined and calculated for undisturbed samples via 2 microtensiometers and 2 TDR probes inserted in a vertical distance of 2 cm.

Results

In order to test the assumption that the 3-d shrinkage can be taken as isotropic, we chose the weakest soil samples from the Histic Gleysol with coherent structure (Figure 1). It is obvious that the pattern of the retention curves without consideration of the volume loss due to soil shrinkage results in a complete misinterpretation of corresponding ecological data for the soil volume like the air capacity (from saturation to pF 1.8) or plant available water capacity (from pF 1.8–4.2). If the vertical shrinkage is considered the air capacity values decrease while the amount of plant available water increases. If finally the 3-d shrinkage is determined and included in the calculations we can find a further decline in the air capacity and even in the plant available water capacity values, while the amount of fine pores in the soil sample increases.

The shrinkage curves for all analyzed soil samples are shown in Figure 2. The Stagnic Luvisol SS-LL (15–75) had the smallest shrinkage behavior at all depths (not shown) but the 4 shrinkage ranges can still be differentiated. Thereby the samples taken from the ploughed layer SS-LL (15, 25) are more sensitive to volume changes while with increasing bulk density and/or stronger aggregation the volume reduction decreases. With increasing clay content (> 30%) very pronounced shrinkage curve ranges can be detected (Figure 2). It becomes obvious, that the moisture ratio ranges for the structural shrinkage differ with soil aggregation and therefore also with the previous drying history derived from the general description of the sites. The Axh horizon from the Tschernosem with subangular blocky structure is characterized by a large structural shrinkage range, i.e. it shows a very rigid pore system, followed by a small proportional shrinkage and a well defined residual and zero shrinkage range, while both the Gleysol samples and especially those of the Stagnosol show a very pronounced proportional shrinkage range but only a small structural shrinkage behavior. Both curves show similar residual and zero shrinkage patterns.

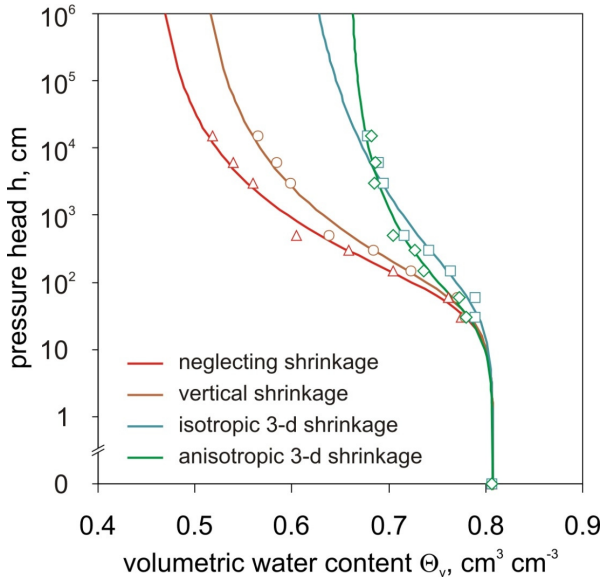

Figure 1. Effect of soil shrinkage on the pattern of the water retention curve of the peat clay (HN-GH). The differences in the water contents at given matric potential hPa (i.e. pressure head cm) is obvious and also proves the assumption of nearly identical curves for the 3-d shrinkage behavior.

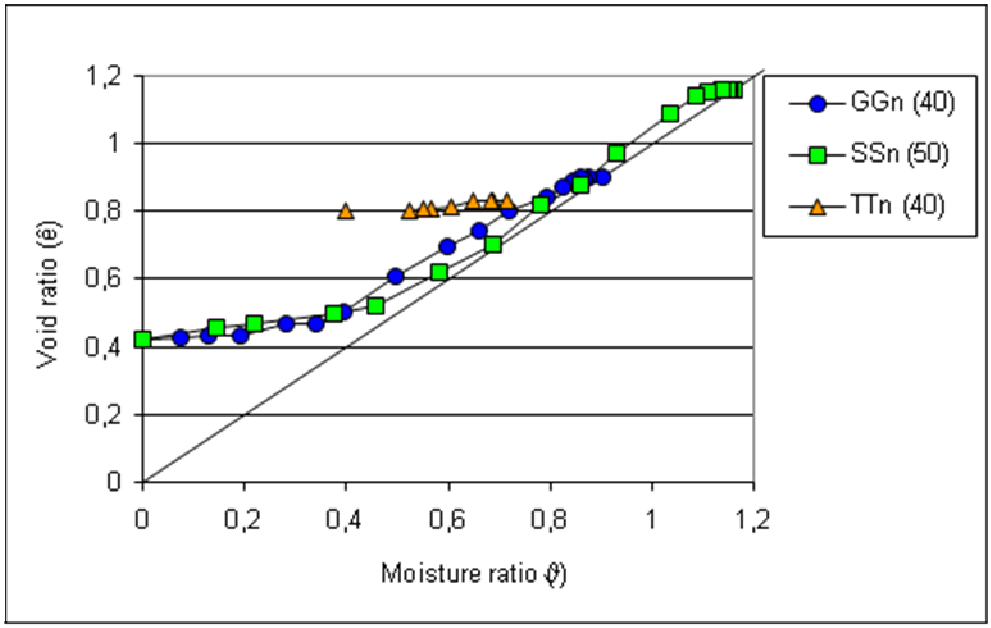

Figure 2. Shrinkage curves of selected soil horizons of the Gleysol (GGn), Stagnosol (SSn) and the Tschernosem (TTn). The number behind the abbreviation defines the soil depths.

The calculated theoretical water content loss due to shrinkage reveals severe differences between the analyzed soils. We can find for the soils with higher clay content and/or less pronounced soil aggregation an increased "misinterpretation of the retention data as soon as the soil samples dried out more than to -200 hPa.(Fig.3) The Axh horizon of the Tschernosem with a subangular blocky structure showed a strong rigidity with negligible small shrinkage induced "water loss", while the actual shrinkage induced changes in the available pore space approached even 12% at pF 4.2 for samples with smaller aggregate strength (e.g. coh) and increasing organic carbon content. The high values for the lowland peat samples with more than 10% at pF 4.2 demonstrated also the influence of the low bulk density on shrinkage induced misinterpretation. If the HNn and the SSn curves are compared it becomes obvious that even a very high bulk density does not always coincide with high internal soil strength (cf. bulk density 0.81 and 1.72 g/cm³ in Table 1).

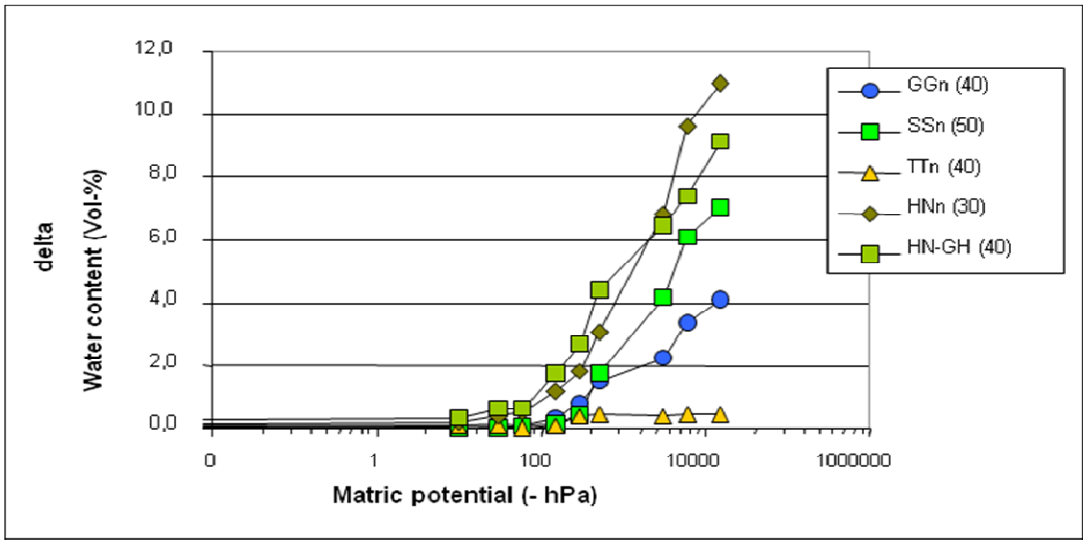

Figure 4. Calculated water loss due to shrinkage as a function of matric potential.

At a given bulk density of approx. 1.45 g/cm³ is the shrinkage induced volume loss (calculated as water loss) more pronounced in the GGn with up to 4% due to a weaker soil structure as compared with the TTn samples.

These nonrigidity effects also alter the pattern of the hydraulic conductivity matric potential curves revealing that if curves are derived from alpha, n and m values together with the measured ks value (van Genuchten/Mualem approach) a strong discrepancy to measured curves occurs.

Three general effects can be defined for these curves:

- If soils are mostly rigid (demonstrated e.g. by the SS-LL and TTn samples) we cannot detect any effect of shrinkage on the calculated curves as they are identical. The introduction of reduction factors for ks only results in a parallel shift of the curves.
- If shrinkage induced changes in the soil/or pore volume and pore size distribution occur, differences between the measured curves with and without actual shrinkage consideration result in a pronounced curve pattern variation. Thus, some remarkable differences can be derived. If shrinkage is neglected in the measured curves, the pattern is mostly parallel to the calculated ones, while if the actual shrinkage process is included when calculating the actual curves, they bend only intensely after exceeding the structural shrinkage range. This matric potential can be therefore also considered as a rigidity index.
- At the transition to the proportional shrinkage range we can also find a corresponding increase in the number of grain contact points.

References

Baumgartl T (2003) 'Kopplung von mechanischen und hydraulischen Bodenzustandsfunktionen zur Bestimmung und Modellierung von Zugspannungen und Volumenänderungen in porösen Medien'. Bd.62. (Schriftenreihe des Instituts für Pflanzenernährung und Bodenkunde: Kiel).

Groenevelt P, Grant C (2001) Re-evaluation of the structural properties of some British swelling soils. *European Journal of Soil Science* **52**, 469-477.

Peng X, Horn R, Smucker A (2007) Pore shrinkage dependency of inorganic and organic soils on wetting and drying cycles. *Soil Science Society of America Journal* **71**, 1095-1104.

Smiles ? (2000)

Stange and Horn (2005)

Tuller M, Or, D (2003) Hydraulic functions for swelling soils: pore scale considerations. *Journal of Hydrology* **272**, 50-71.

van Genuchten MT (1980) A closed form equation for predicting the hydraulic conductivity of unsaturated soils. *Soil Science Society of America Journal* **44**, 892-898.

Rheological investigations of Rothamsted soils: Long-term effects of fertilizing systems on soil microstructure

Wibke Markgraf[A], Chris Watts[B], Richard Whalley[B] and Rainer Horn[A]

[A]Christian-Albrechts-University zu Kiel, Institute for Plant Nutrition and Soil Science, Hermann-Rodewald-Str. 2, D-24118 Kiel, Germany, Email w.markgraf@soils.uni-kiel.de
[B]Soil Science Department, Rothamsted Research, Harpenden, Hertfordshire, AL5 2JQ, United Kingdom

Abstract
A rotational rheometer with a parallel-plate measuring device is used to achieve stress-strain parameters, which define soil as viscoelastic material according to rheological theory. Hence, data deriving from conducted amplitude sweep tests with controlled shear deformation on Rothamsted Soils (Broadbalk long-term experiment) will be presented. The application of farm yard manure over more than 120 years led to an accumulation of organic carbon, resulting into a more rigid microstructural stability – with respect to the three-phase system soil – primarily due to a network of micro roots, and an increased water holding capacity and cation exchange capacity. Water content, texture, organic matter compounds, fungi and hyphae, contents and kinds of clay minerals, carbonates, (hydr)oxides, and cations have an effect on the microstructural stability (rigidity, stiffness), and shear behaviour. Storage modulus G' (elasticity) and loss modulus G" (viscosity), the linear viscoelastic range (LVE), pre-yielding and yield point (intersection of G' and G") characterise the three stages of microstructural degradation of soil on the particle-to-particle scale. A semi-quantitative classification of rigid-nonrigid or elastic-viscous material is applied considering the loss factor tan δ and integral z, delivering fundamental information about microstructural strength of investigated soil samples and their 'internal network'.

Key Words
Rheology, Rothamsted, micromechanics, stiffness degradation, long-term fertilization

Introduction
Rheometry is a useful tool to investigate microstructural changes in soil, which is defined as viscoelastic material. By conducting oscillatory tests, in detail amplitude sweep tests (AST) with controlled shear deformation (CSD), the degree of stiffness or elasticity-viscosity ratio, which is represented by the loss factor tan δ, can be calculated. As the loss factor defines elastic *and* viscous components, this ratio may function as link to microstructural processes, depending on texture, clay mineralogy, water content and organic matter.

Material and Methods
A silty loam from Rothamsted, UK (long term experiment since 1885) (Powlson 1994; Watts *et al.* 2006), was taken and analysed, considering different properties such as texture, clay mineralogy, soil organic carbon (SOC) content, and manure application. In **Table 1** physicochemical properties are summarised.

Table 1. Physicochemical characteristics of investigated substrates, Rothamsted (Broadbalk).

	Sand	Silt	Clay	SOC
		(%)		
FYM*+ N_2	21	58	21	2.7
FYM				2.8
N_1PK(Na)Mg	19	58	23	1.0
N_2PK(Na)Mg				1.0
N_4PK(Na)Mg‡				1.1
N_6PK(Na)Mg†				1.2
Wilderness (grass)	21	57	22	4.0
Bare fallow§ (Highfield)	7	68	25	1.1

*FYM farm yard manure (since 1885; N_2 added since 1968) ‡since 1968
†since 1985 §Bare fallow – plough/autumn (since 1959) N_1, N_2, N_4, N_6 = 48, 96, 192, 284 kg N as ammonium nitrate

1 – 6 August 2010, Brisbane, Australia. Published on DVD.

Amplitude Sweep

According to the method introduced by Markgraf *et al.* (2006), amplitude sweep tests were conducted with a modular compact rheometer MCR 300 to achieve data of stress-strain correlations on the micro scale (particle-particle contact). Recent collected data show significant differences of resulting micromechanical parameters i.e. storage and loss moduli G' and G" (Pa), and loss factor tan δ (-) as function of deformation γ (%), which are correlated to the water content, and other factors that may affect the matric potential: texture, single particle properties, pore size distribution, influence of (cat)ions (osmotic potential), and other physicochemical properties. A representative recorded plot of an amplitude sweep test is shown in **Figure 1.** The plots of storage and loss modulus (G' and G") are generated automatically during a test (Markgraf and Horn 2009).

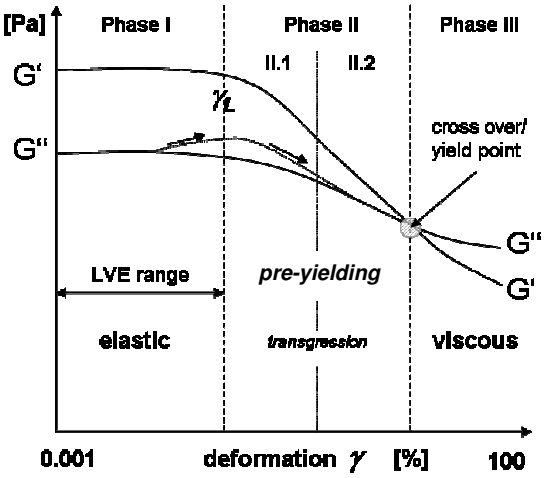

Figure 1. Idealised generated plots of storage modulus G' (Pa) and loss modulus G" (Pa) vs. deformation γ (%). In general, three stages of elasticity loss can be defined, showing a gradual transition of an elastic (G'>G") to a viscous (G'<G") character. In phase 1 an elastic behaviour predominates, and a parallel run of G' and G'' is given. By reaching deformation limit γ_L (%) a yielding character is already given in phase 2 (pre-yielding); an intersection of G' and G" marks an absolute yield point. In phase 3 a microstructural collapse occurs and a viscous character is obtained.

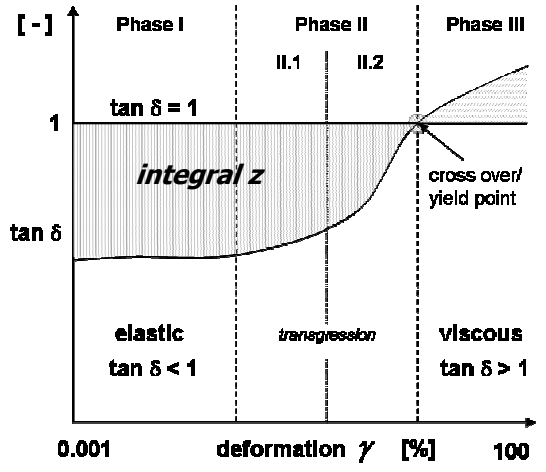

Figure 2. Deriving from one data set, results can be plotted in a loss factor vs. deformation coordinate system. Loss factor tan□ δ (-) equals the ratio of loss modulus to storage modulus (=G''/G'), and may function as analogue expression of elastic (tan δ <1), viscoelastic (tan δ ≤1) or viscous (tan δ >1) behaviour. For further comparison, the integral *z* of tan δ□(γ) lim γ=0.00%1 to lim γ="cross over point", with tan δ=1 as defined limit on the y-axis can be calculated.

Natural viscoelastic substances react with a temporal delay. This is represented by the phase shift angle δ, where tan δ equals the relation of the loss modulus G" (Pa) to the storage modulus G' (Pa), defining the relation of imaginary ("lost") to stored elasticity. If tan δ<1, G' prevails G", a gel character is given. Viscous behaviour is defined in case of tan δ>1, G" predominates G'. Furthermore, a correlation between in **Figure 1** presented stages (Phases I-III) and phases of stiffness degradation in **Figure 2** become obvious. Due to a decrease of G',

the ratio of G''/G' (= tan δ) increases; if tan δ=1 is reached, elastic and viscous parts are equivalent, and an absolute yield point (=cross-over) is given at a defined deformation (%). If tan δ>1, a viscous character predominates, and a structural collapse occurs; at this stage deformation is irreversible. For further comparison, the integral *z* of tan δ□(γ) lim γ=0.00%1 to lim γ="cross over point", with tan δ=1 as defined limit on the y-axis can be calculated. This method may allow an even more precise definition of elasticity, rigidity, or stiffness of a soil at the particle-particle scale.

Results

Collected rheological data from conducted AST was used to achieve information about the influence of different manure applications on microstructural stability, in dependence on soil organic carbon (SOC) as well as inorganic nitrogen applications in combination with farmyard manure (FYM). In **Figures 3 a** and **b** results from conducted AST with samples deriving from the Rothamsted Broadbalk long term experiment are shown. In general, curve characteristics are influenced by (i) water content: saturated (**Figure 3a**); unsaturated (**Figure 3b**), (ii) by treatments: N_xPK(Na)Mg, farm yard manure (FYM), bare fallow or wilderness (grass), (iii) SOC content, and (iv) texture. In comparison, different curve shapes are characteristic: in **Figure 3a** tan(δ) increases slightly within the section of γ=0.01…1%; an intersection with the tan(δ)=1-line does occur in few cases only: N_2PK(Na)Mg, N_4PK(Na)Mg, and bare fallow (unsaturated) variations. Furthermore, a slight increase in structural stability can be found as given in **Figure 3a**: FYM+N_2 > FYM >> N_6PK(Na)Mg ≥ N_4PK(Na)Mg > N_2PK(Na)Mg ≥ N_1PK(Na)Mg; samples which have been treated with farm yard manure since 1885 show a higher degree of stiffness compared to those which have been treated with N_xPK(Na)Mg within the last 40 years (e.g. N_4PK(Na)Mg).

Secondly, differences in soil organic carbon content may have an effect on the microstructural stability as organic matter leads to a higher water retention, which results into a more stable system. This instant is well defined in **Figure 3b**. Pre-drained samples of wilderness (grass) show a higher microstructural stability than bare fallow, and N_2PK(Na)Mg. If, in addition, FYM (pre-drained) plots in **Figure 3a** are considered, the influence of SOC becomes even more obvious: wilderness plots have the highest SOC contents (4.0%), followed by FYM (2.7%), bare fallow, and N_2PK(Na)Mg (**Table 1**). Although bare fallow and N_2PK(Na)Mg have similar SOC contents (1.1%), textural differences affect shear behaviour, and, deriving from this, stiffness degradation: a more silty texture in case of bare fallow (68% silt) occurs to be less rigid than a loamy clay (N_2PK(Na)Mg, 56% silt). By calculating integral *z*, these structural differences can be expressed in absolute numbers; according to **Figure 3a**, this results into:

$z_{N_xPK(Na)Mg\ saturated} < z_{FYM;\ FYM+N2\ -150hPa}$,

in case of **Figure 3b** into:

$z_{bare\ fallow\ -60hPa} < z_{N_2PK(Na)Mg\ -60hPa} < z_{wilderness\ -60\ hPa}$.

Conclusions

Investigated Rothamsted samples, which have been treated with farmyard manure since 1885, showed a high degree in microstructural stability, as well as wilderness plots. This is congruent to findings of Tisdall and Oades (1982), Haynes and Naidu (1998), and Watts *et al.* (2006). Furthermore, Haynes and Naidu (1998) pointed out, that 'there is a strong correlation between the amount of fertilizer N applied annually and the quantity of organic C accumulated in the soil'. This instant is also true, if N_xPK(Na)Mg-treated plots are considered, higher N-contents are correlated to a slight increase in C; due to this, microstructural stability is increased stepwise from N_1, N_2, to N_4, and N_6PK(Na)Mg treatments. In general, soil organic carbon improves soil structure and its functionality (Lemmermann and Behrens 1935, Haynes and Naidu 1998). Occurring menisci forces, which are formed due to drainage, maintain pore continuity, and as mentioned above, soil structure. It can be concluded, that rheological techniques and resulting parameters such as G', G", tan (δ) and *z* are a useful tool not only to describe and quantify microstructural stability, but also to link structuring processes, which are relevant for up-scaling considerations e.g. improving soil aggregation.

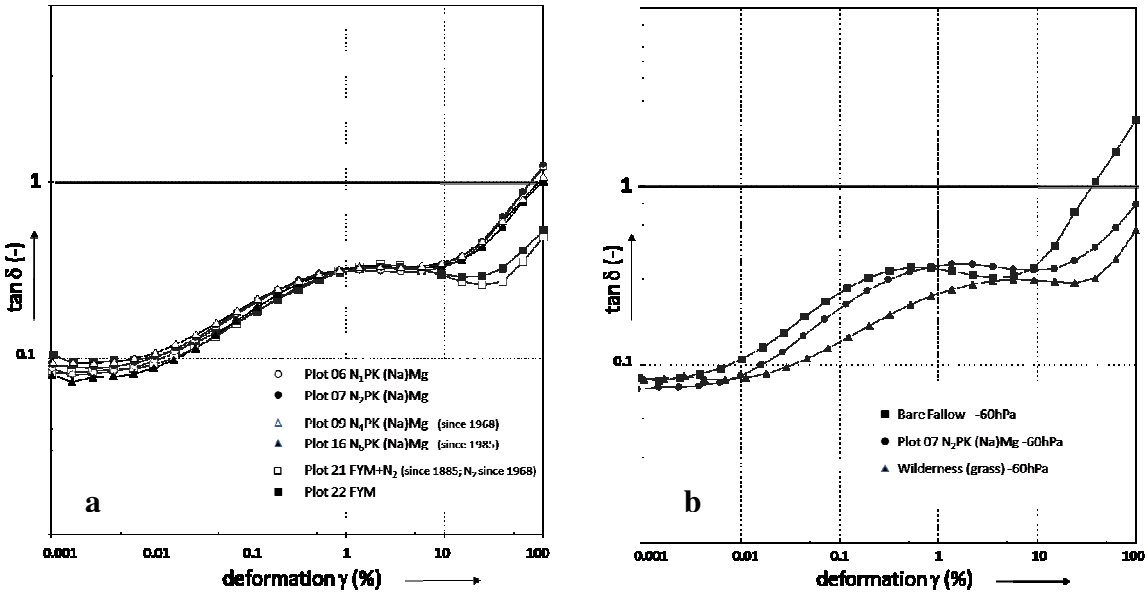

Figure 3a. Resulting graphs with tan δ (γ) of conducted amplitude sweep tests (AST) with Rothamsted Broadbalk samples: N_xPK(Na)Mg (saturated), and farm yard manure (FYM; pre-drained) treatments.

Figure 3b. Resulting graphs with tan δ (γ) of conducted amplitude sweep tests (AST) with Rothamsted Broadbalk samples under unsaturated conditions (pre-drained at -60hPa): bare fallow, N_2PK(Na)Mg, and wilderness (grass).

References

Haynes RJ, Naidu R (1998) Influence of lime, fertilizer and manure applications on soil organic matter content and soil physical conditions: a review. *Nutrient Cycling in Agroecosystems* **51**, 123-137.

Lemmermann O, Behrens WU (1935) On the influence of manuring on the permeability of soils. *Zeitschrift für Pflanzenernährung, Düngung und Bodenkunde* **37**, 174-192.

Markgraf W, Horn R, Peth S (2006). An Approach to Rheometry in Soil Mechanics: Structural Changes in Bentonite, Clayey and Silty Soils. *Soil and Tillage Research* **91**, 1-14.

Markgraf W, Horn R (2009) Rheological Investigations in Soil Micro Mechanics: Measuring Stiffness Degradation and Structural Stability on a Particle Scale. In: 'Progress in Management Engineering'. (Eds LP Gragg, JM Cassell), chapter 9 (Nova Science Publishers: Hauppauge).

Powlson DS (1994) Quantification of nutrient cycles using long-term experiments. In: 'Long-term experiments in agricultural and ecological sciences'. (Eds RA Leigh, AE Johnston). Chapter 6, pp. 97-115 (CAB International:Wallingford).

Tisdall JM, Oades JM (1982) Organic matter and water-stable aggregates in soils. *Journal of Soil Science* **33**, 141-163.

Watts CW, Clark LJ, Poulton PR, Powlson DS, Whitmore AP (2006) The role of clay, organic carbon and long-term management on mouldboard plough draught measured on the Broadbalk wheat experiment at Rothamsted. *Soil Use and Management* **22**, 334-341.

Simulation of Br movement in disturbed columns of soil by HYDRUS-ID model

Mojtaba Kord[A], Leila Derakhshan[B] , Arash Akhavan [C] and Hamidreza memarian[D]

[A]Water resources management company, Ministry of Energy, Tehran, IRAN, Email kord2086@yahoo.com
[B]Babol, Iran, Email l.derakhshesh@gmail.com
[C]Water resources management company, Ministry of Energy, Tehran, IRAN.
[D]Babol, Iran, Email memarianhamid@yahoo.com

Abstract
Water and contaminants moving through the vadose zone are often subject to a large number of simultaneous physical and chemical nonequilibrium processes. Modification the transport of one component is difficult, time consuming and expensive, therefore its important to simulate this movement. In the present article our purpose was study Br movement and its simulations by HYDRUS-ID model for soil columns. For this, we used 2 soil textures (Sandy loam and Loamy sand), 3 Br doses (10, 20 and 30 mg/kg soil) were added to columns then we made saturated columns by a leaching process. After that we measured Br concentration in output leachates and after leaching for different depths in columns, then compared observations with data estimated by the model. Results show that the model could efficiently predict the time of reaching maximum concentration and the extent of maximum concentration.

Key Words
Nonequilibrium, Br, simulation, leachate

Introduction
Amount of leaching is related to the velocity of water movement in soil and the conservation potential of solutes by soil. The most important things that affect solute movement include: texture, structure and capillary conductivity that are influenced by management and tillage (Agus *et al.* 1992). Usual anions in soil also have a particular importance and this is because of their importance for salinity, productivity and groundwater pollution. Most anions are inactive and do not adsorb at adsorption sites, and that is why they are important to study because they can be leached easily from profiles and add to groundwaters. Many researches use Br as a tracer and this is because of its low concentration in most soils, it is a conservative tracer that is not subject to microbial transformation and gaseous losses. By defining types of tracer movement in soil, modeling it, and obtaining some coefficients and changes we can predict movements of other solutes and use such models in other situations (Bowmas 1984).

Methods
Soil columns were constructed from sandy loam and loamy sand soils with 10.17 cm diameter and 25 cm height. Bulk density was similar to the field situation. At the end of columns closed 5 cm sand washed with acid was placed to inhibit soil loss, and end parts of columns closed using aluminum net, experiments were done in 18 columns with 3 replications. Three different doses of Br (10, 20 and 30 mg Br/kg dry soil) were dissolved in 250 ml distilled water, after applied solute pulse treatments to columns, leaching them in saturated situation with 5 cm constant head. With the end of leaching, we sectioned columns and took samples at every 2 cm for 0-12 centimeters depth, at every 4 cm for 12-20 centimeters depth and every 5cm for 20-25 centimeters depth so that there was one sample for this depth. Then Br concentration was measured with a Br selective electrode. Bulk densities were determined by a core method (Klute 1986), saturated hydraulic conductivity determination was made by constant head method (Klute 1986), texture with pipette method (Klute 1986). Electric conductivity of soil extracts and cation exchange capacity was determined by an ammonium acetate method.

Results
After measurement of Br concentration, all necessary data for modeling were collected from columns and were compared with leachate concentrations predicted by the model. As we can see in Figure 1, most of output leachate concentration of Loamy sand soils was within 100 to 120 minutes after starting leaching whereas this time for Sandy loam texture was 150 minutes after starting leaching. Due to the finer texture of loamy sand compared with sandy loam, water and solute movement were slower and the time of reaching maximum output leachate concentration was longer. In the case of prediction of leachate concentration, model could efficiently determine time of reaching maximum concentration and measure the extent of maximum concentration for the two studied textures. End of leaching is after the exit of four pore volume of leachate from columns and because

pore volume of loamy sand texture is less than of Sandy loam textures the speed of water movement in pores is more than in sandy loam. Thus loamy sand reach the end of leaching sooner, as is clear in the diagram.

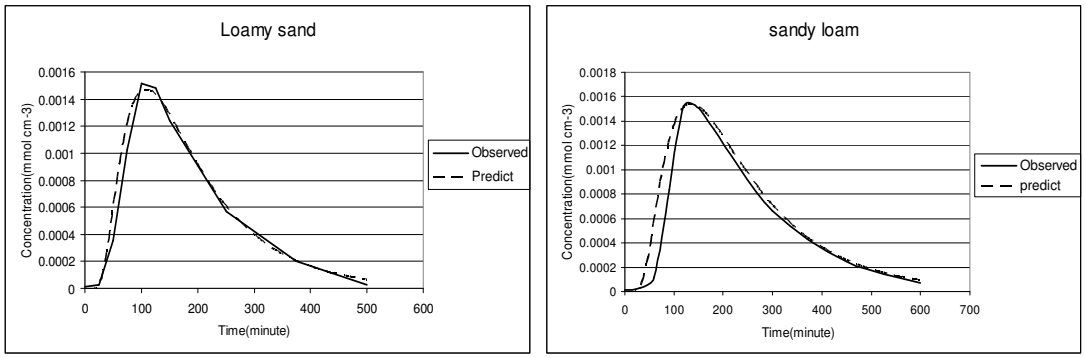

Figure 1. Simulation of output leachate concentration for the third level of Br treatment on sandy loam and loamy sand textures.

Acknowledgment

This work has been financial supported by Iran Water Resource Management Company.

References

Abdalla NA, Lear BN (1975) Determination of inorganic bromide in soil and plant tissues with bromide selective-ion electrode. *Commun in Soil Sci. and plant Analysis* **6,** 489-494.

Agus F, Cassel DK (1992) Field scale bromide transport as affected by tillage. *Soil Sci. Soc. Am. J.* **56,** 254-260.

Bowmas RS (1984) Evaluation of some new tracers for soil water studies. *Soil Sci. Soc. Am. J.* **48,** 987-993.

Brooks SC, Taylor DL, Jardin PM (1988) Termodynamics of bromide exchange on ferrihydrite: implication for bromide transport. *Soil Sci. Soc. Am. J*. **62,** 1275-1279.

Klute A (1986) 'Method of soil Analysis. Part 1- physical and mineralogical methods. 2nd edition'. (Ed A Klute) (American Society of Agronomy Inc.: Madison, WI).

Klute A (1986) 'Method of soil Analysis. Part 2- Chemical and Biochemical methods. 2nd edition'. (Ed A Klute) (American Society of Agronomy Inc.: Madison, WI).

Ryan MC, Graham GR, Rudelph DL (2001) Contrasting nitrate adsorption in andisoil of two coffe plantation in Casta Rica. *J. Environ. Qual*. **30,** 1848-1852.

Soil erosion characteristics under rainfall simulator conditions of the Jeju soil in Korea

Ho-Jun Kang[A], Shin-chan Lee[A], Sang-Ho Yang[A], Sang-Soon Lee[A], Seong-Jun Koh[A], Sang-Keon Ha[A] and Seung-Oh Hur[B]

[A]Jeju Special Self-governing Province Agricultural Research and Extension Services, Jeju, Republic of Korea, Email khj4066@jeju.go.kr
[B]National Academy of Agricultural Science, RDA, Suwon, Republic of Korea.

Abstract
In order to investigate the effect of soil physical properties, runoff and infiltration water on soil erosion, soil samples were collected from 5 sites of dark brown soil(DBS), 6 sites of very dark brown volcanic ash soil(VDBAS), and 8 sites of black volcanic ash soil(BVAS) in Jeju. The relations between soil erosion and some physical characteristics of the soil were tested. The relationship between soil erosion and runoff was positively correlated, but infiltration water and saturated hydraulic conductivity were negatively correlated with soil erosion in all soils. In DBS, the soil erosion was negatively correlated with clay, clay/silt, clay+very fine sand, clay/(silt+very fine sand) and clay+fine sand(0.02-0.2 mm), but positively correlated with silt/clay. In BVAS, the soil erosion was negatively correlated with silt/clay and positively correlated with clay+fine sand (0.02-0.2 mm). The relationship between soil erosion and water stable aggregate was observed only in the DBS and VDBAS. Soil erosion in DBS was positively correlated with water stable aggregate (0.25-0.5 mm, 0.1-0.25 mm + 0.25-0.5 mm, 0.1-0.25 mm + 0.25-0.5 mm + 0.5-1.0 mm), but the water stable aggregates (0.5-1.0 mm + 1.0-2.0 mm + >2.0 mm and 1.0-2.0 mm + >2.0 mm) were prone to decrease soil erosion without statistical significancy. Soil erosion in VDBAS was positively correlated with water stable aggregate (0.1-0.25 mm, 0.25-0.5 mm and 0.1-0.25 mm + 0.25-0.5 mm), but negatively correlated with water stable aggregate (0.5-1.0 mm + 1.0-2.0 mm + >2.0 mm and 1.0-2.0 mm + >2.0 mm). In DBS and VDBAS, soil erosion decreased with increasing of soil organic matter content, but in BVAS, there was no relationship between soil erosion and organic matter content.

Key Words
Soil erosion, volcanic ash soil, rainfall simulator, soil physical properties

Introduction
Soil of the Jeju in Korea is affected by severe soil erosion. Most areas are under conventional tillage, by which the upper soil layer is turned after harvest before sowing, this results in an uncovered soil surface during July, August and September. These months are characterized by the highest rainfall amounts. Soil erosion caused by water is primarily due to particle detachment and transport by rainfall and runoff. The physical soil properties and interactions that affect K values are many and varied. The objective of this study was to relate erodibility factors and physical properties of volcanic ash soil from the Jeju Island in Korea under simulated rainfall. Another goal was to determine the erodibility factors for volcanic ash soil from Jeju Island.

Methods
Soil samples were collected at field moisture condition. After air-drying, the soil was passed through a 2mm sieve and then packed in soil pan (width : 26×30cm, depth : 10cm). The soil then was saturation with distilled water. After saturation, the pan was set at 10% slope and allowed to drain for about 24 hour. Rain was applied for 30 minute at 150mm/h using a simulated rainfall (Diameter of drops 5.9mm, Mass of drops 0.1g, Number of capillary tubes 49) at a height of 0.4m. Infiltrating water was collected from the bottom, while runoff plus sediments were sampled at the upper of the pan using a tall beaker. The organic matter of soil was estimated using 0.4N $K_2Cr_2O_7$ as oxidant and 0.2N $Fe(NH_4)_2(SO_4)_2$as titrant. Particle size analysis was determined on the < 2 mm fraction by the pipette method. Water stable aggregate analysis was determined on the 2-4mm fraction by a Yoder-type aggregate distribution analyzer.
Soil properties used in the study are summarized in Table 1 and 2. Table 1 shows the particle size for the different soils. The average contents of sand, silt and clay were 13.6%, 67.1% and 19.4% in DBS, 12.3%, 66.8% and 20.9% in DBVAS, and 10.2%, 71.0% and 18.8% in BVAS, respectively.

1 – 6 August 2010, Brisbane, Australia. Published on DVD.

Table 1. Particle size of soils used in the experiment.

Soil colors	Soil series	U. S. Department of Agriculture								International Soc. of Soil Sci.			
		Sand						Silt	Clay	Coarse sand	Fine sand	Silt	Clay
		(----------%----------											----------)
		2.0-1.0	1.0-0.5	0.5-0.25	0.25-0.1	0.1-0.05	Total	0.05-0.002	<0.002	(2.0-0.2)	(0.2-0.02)	(0.02-0.002)	<0.002
		(----------mm----------											----------)
Dark brown soil	Gyorye	3.9	6.0	6.4	6.4	3.4	26	52.0	22.1	17.2	30.9	29.9	22.1
	Gueom	0.4	0.9	1.6	2.6	1.4	6.9	78.9	14.3	3.4	17.7	64.6	14.3
	Donggwi	1.8	4.0	4.1	4.9	2.4	17.3	70.6	12.2	10.8	18.6	58.4	12.2
	Donghong	0.5	1.4	1.9	2.7	3.0	9.4	55.0	35.6	4.1	40.9	19.4	35.6
	Jocheon	0.2	1.1	2.0	3.8	1.2	8.3	79.2	12.6	3.9	16.9	66.6	12.6
	Mean	1.4	2.7	3.2	4.1	2.3	13.6	67.1	19.4	7.9	25.0	47.8	19.4
Very dark brown volcanic ash soil	Gujwa	0.5	1.8	2.9	4.0	2.8	12.0	62.6	25.4	5.8	31.6	37.2	25.4
	Ora	0.4	1.2	2.2	3.2	1.9	8.8	73.1	18.0	4.4	22.5	55.1	18.0
	Jeju	0.6	1.8	2.5	3.2	2.0	9.9	73.6	16.5	5.3	21.1	57.0	16.5
	Jungmun	0.2	1.0	1.8	3.3	4.5	10.8	68.8	20.4	3.5	27.7	48.5	20.4
	Jungeom	0.1	0.3	0.4	0.7	1.4	2.9	72.4	24.7	1.0	26.7	47.6	24.7
	Hallim	2.4	4.9	7.7	11	3.2	29.2	50.3	20.5	16.4	33.3	29.8	20.5
	Mean	0.7	1.8	2.9	4.2	2.6	12.3	66.8	20.9	6.1	27.1	45.9	20.9
Black volcanic ash soil	Gimnyeong	3.5	3.8	2.5	2.6	3.0	15.4	61.2	23.4	10.2	28.7	37.7	23.4
	Namwon	0.4	0.6	0.9	1.5	2.2	5.5	74.9	19.6	2.0	23.1	55.3	19.6
	Songdang	1.0	2.2	2.9	5.8	3.3	15.3	64.7	20.1	6.8	28.5	44.6	20.1
	Sineom	0.2	0.4	0.4	0.6	1.7	3.4	76.6	20.0	1.1	22.3	56.6	20.0
	Wimi	0.2	0.5	0.5	2.0	2.6	5.8	78.6	15.6	1.4	20.0	63.0	15.6
	Pyeongdae	0.3	1.0	1.1	1.0	3.2	6.7	76.7	16.6	2.6	20.7	60.1	16.6
	Hangyeong	0.2	0.7	1.1	2	2.2	6.2	73.3	20.6	2.3	24.5	52.8	20.6
	Haengwon	4.1	4.9	4.8	6.5	3.2	23.5	62.2	14.3	14.6	23.2	47.9	14.3
	Mean	1.2	1.8	1.8	2.8	2.7	10.2	71.0	18.8	5.1	23.9	52.3	18.8

Organic matter content and saturated hydraulic conductivity were remarkably high in BVAS, and very low in DBS. DBS had higher bulk densities, VDBVS medium ones, and BVAS lower ones. The average abundance of water stable aggregates was 68.6% in DBS, 81.8% in VDBVS, and 81.4% in BVAS, respectively(Table 2).

Table 2. Physical characteristics of soil used in the experiment.

Soil colors	Soil series	Water stable aggregate (%)						Organic matter (g/kg)	Bulk density (g/cm^3)	Saturated hydraulic conductivity (cm /h)
		0.1-0.25 mm	0.25- 0.5 mm	0.5 -1.0 mm	1.0 -2.0 mm	>2.0 mm	Total			
Dark brown soil	Gyorye	8.8	9.9	12.0	16.3	6.8	53.9	23.3	1.20	0.85
	Gueom	14.7	21.7	20.9	19.5	3.1	79.9	21.9	1.45	0.08
	Donggwi	17.3	23.1	14.6	7.7	2.1	64.9	21.6	1.41	0.20
	Donghong	4.4	9.7	19.2	29.3	28.3	90.9	51.3	1.12	1.06
	Jocheon	23.4	16.6	6.1	6.7	0.5	53.3	20.8	1.50	0.11
	Mean	13.7	16.2	14.6	15.9	8.2	68.6	27.8	1.34	0.46
Very dark brown volcanic ash soil	Gujwa	0.3	0.3	0.4	4.9	70.7	76.5	200.0	0.70	2.30
	Ora	3.6	8.2	15.3	27.1	28.8	83.0	44.3	1.12	0.37
	Jeju	4.5	9.6	16.7	29.9	28.2	88.9	61.3	1.09	0.46
	Jungmun	8.3	10.2	10.3	14.3	23.0	66.1	72.5	0.92	0.15
	Jungeom	1.5	2.9	6.6	23.9	53.6	88.5	59.9	1.09	0.85
	Hallim	1.2	2.4	3.8	13.6	66.8	87.8	90.8	0.76	0.56
	Mean	3.2	5.6	8.9	19.0	45.2	81.8	88.1	0.95	0.78
Black volcanic ash soil	Gimnyeong	0.4	0.8	1.0	12.9	68.0	83.2	221.0	0.65	1.13
	Namwon	3.1	7.0	14.9	31.3	37.5	93.9	152.0	0.71	0.11
	Songdang	1.5	2.3	4.3	17.7	68.1	93.9	193.0	0.68	0.85
	Sineom	4.8	9.5	13.4	18.4	33.5	79.6	147.0	0.63	1.17
	Wimi	3.8	7.2	13.2	27.7	40.6	92.5	180.0	0.68	1.53
	Pyeongdae	0.1	0.1	0.2	5.8	57.0	63.3	135.0	0.59	2.27
	Hangyeong	1.9	2.9	5.3	20.5	59.8	90.4	182.0	0.56	0.22
	Haengwon	0.6	0.5	0.7	8.4	43.9	54.2	172.0	0.72	0.96
	Mean	2.0	3.8	6.6	17.8	51.1	81.4	172.8	0.65	1.03

Results

Figure 1 shows the relationship of soil erosion with runoff and infiltration water. The relationship between soil erosion and runoff was positively correlated, but infiltration water was negatively correlated with soil erosion.

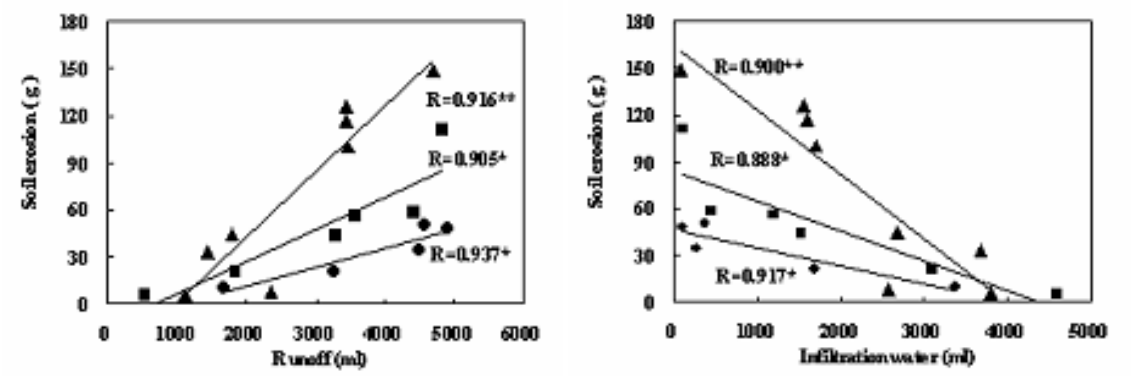

Figure 1. Relationship between soil erosion, runoff and infiltration in dark brown soil (●), very dark brown volcanic ash soil(■) and black volcanic ash soil (▲).

Table 3 shows the relationship between soil erosion and soil particle size. In DBS, the soil erosion was negatively correlated with clay, clay/silt, clay + very fine sand, clay/(silt + very fine sand) and clay + fine sand(0.02-0.2 mm), but positively correlated with silt/clay. In VDBAS, the relationship between the soil particle size and soil erosion was not significant, while in BVAS, the soil erosion was negatively correlated with silt/clay and positively correlated with clay + fine sand (0.02-0.2 mm).

Table 3. Relationship between soil erosion and particle size.

Particle size	Correlation coefficient		
	Dark brown soil (n=5)	Very dark brown volcanic ash soil (n=6)	Black volcanic ash soil (n=8)
Clay(<0.002 mm)	-0.901*	-0.599	0.642
Silt(0.002-0.05 mm)	0.801	0.202	-0.378
Very fine sand(0.05-0.1 mm)	-0.637	0.633	-0.063
Clay/Silt	-0.921*	-0.526	0.635
Clay+Very fine sand	-0.901*	-0.379	0.649
Clay/(Silt+Very fine sand)	-0.920*	-0.579	0.643
Silt/Clay	0.890*	0.460	-0.727*
Silt£+Very fine sand+Fine sand	0.848	0.452	-0.435
Clay+Fine sand(0.02-0.2 mm)	-0.913*	-0.462	0.723*

*Significant at P<0.05.

Table 4 shows the relationship between soil erosion and water stable aggregate. Soil erosion in DBS was positively correlated with water stable aggregate (0.25-0.5 mm, 0.1-0.25 mm + 0.25-0.5 mm, 0.1-0.25 mm + 0.25-0.5 mm + 0.5-1.0 mm), but the water stable aggregates (0.5-1.0 mm + 1.0-2.0 mm + >2.0 mm and 1.0-2.0 mm + >2.0 mm) were prone to decrease soil erosion without statistical significancy. Soil erosion in VDBAS was positively correlated with water stable aggregate (0.1-0.25 mm, 0.25-0.5 mm and 0.1-0.25 mm + 0.25-0.5 mm), but negatively correlated with water stable aggregate (0.5-1.0 mm + 1.0-2.0 mm + >2.0 mm and 1.0-2.0 mm + >2.0 mm). However, in BVAS soil erosion was not correlated with water stable aggregate.

Table 4. Relationship between soil erosion and water stable aggregate.

Water stable aggregate	Correlation coefficient		
	Dark brown soil (n=5)	Very dark brown Volcanic ash soil (n=6)	Black volcanic ash soil (n=8)
0.1-0.25 mm	0.719	0.954**	0.084
0.25-0.5 mm	0.976**	0.849*	0.063
(0.1-0.25 mm)+(0.25-0.5 mm)	0.917*	0.914*	0.071
(0.1-0.25 mm)+(0.25-0.5 mm)+(0.5-1.0 mm)	0.949*	0.782	0.005
(0.5-1.0 mm)+(1.0-2.0 mm)+(>2.0 mm)	-0.631	-0.843*	0.666
(1.0-2.0 mm)+(>2.0 mm)	-0.762	-0.893*	0.650
(0.1-0.25 mm)+(0.25-0.5 mm)+(0.5-1.0mm) + (1.0-2.0 mm)+(>2.0 mm)	-0.227	-0.550	0.560

**Significant at P<0.01, *Significant at P<0.05.

Table 5 shows the relationship between soil erosion and bulk density, soil organic matter and saturated hydraulic conductivity. The bulk density did not significantly affect soil erosion, but the relationship between soil erosion and bulk density in DBS was considerably higher in comparison to VDBAS and BVAS. In DBS and VDBAS, soil erosion decreased with increasing soil organic matter content, but in BVAS, there was no relationship between soil erosion and organic matter content. Soil erosion was negatively correlated with saturated hydraulic conductivity for all soils.

Table 5. Relationship between soil erosion and physical characteristics.

Physical characteristics	Correlation coefficient		
	Dark brown soil (n=5)	Very dark brown volcanic ash soil (n=6)	Black volcanic ash soil (n=8)
Bulk density	0.860	0.253	-0.374
Organic matter	-0.762	-0.664	0.390
Saturated hydraulic conductivity	-0.919*	-0.787	-0.841**

**Significant at P<0.01, *Significant at P<0.05.

Conclusion

The soil erodibility factor (K) represents the effect of soil properties and soil profile characteristics on soil loss. The physical, chemical, and mineralogical soil properties and their interactions that affect K values are many and varied. Therefore, this study emphasizes some factors affecting soil erodibility of the Jeju soil in Korea. For Dark brown soil and Very dark brown soil, soil erodibility factor(K-factor) were runoff water, infiltration water, soil particle size, water stable aggregate, soil organic matter and saturated hydraulic conductivity, and for Black volcanic ash soil were runoff water, infiltration water, soil particle size and saturated hydraulic conductivity.

References

Fontes JC, Pereira LS, Smith RE (2004) Runoff and erosion in volcanic soila of Azores : simulation with OPUS. *Catena* **56**, 199-212.

Miller WP (1987) Infiltration and soil loss of three gypsum-amended ultisols under simulated rainfall. *Soil Sci. Soc. Am. J.* **51**, 1314-1320.

Poulenard J, Podwojewski P, Janeau JL, Collinet J (2001) Runoff and soil erosion under rainfall simulation of andisols from the Ecuadorian Paramo : effect of tillage and burning. *Catena* **45**, 185-207.

Reichert JM, Norton LD, Huang CH (1994) Sealing, amendment, and rain intensity effects on erosion of high-clay soils. *Soil Sci. Soc. Am. J.* **58**, 1199-1205.

Truman CC, Bradford JM, Ferris JE (1990) Antecendent water content and rainfall energy influence on soil aggregate breakdown. *Soil Sci. Soc. Am. J.* **54**, 1385-1392.

Soil permeability as affected by repulsive potential energy

Munehide Ishiguro

Graduate School of Environmental Science, Okayama University, Okayama, Japan, Email ishi@cc.okayama-u.ac.jp

Abstract
The repulsive potential of soil affects its pore structure and consequently water permeability. This is evident in Allophanic Andisols, which have a significant pH-dependent charge. Therefore, at low and high pH, soil dispersion and swelling occur easily due to electric repulsive force. The permeability of the soil then decreases because of structural changes that occur when dilute monovalent acid or alkaline solution is percolated in the soil. However, soil permeability does not decrease, rather increases, when dilute H_2SO_4 is percolated in the soil. This is because SO_4^{2-} strongly adsorbs on the soil surface at low pH and the soil remains flocculated. The difference of permeability is explained by the calculated repulsive potential energy based on zeta potential. Permeability of a high humic soil with only negative charge decreases when an anionic surfactant solution is percolated. The surfactant is adsorbed in the soil by hydrophobic interaction. The repulsive potential energy increases and the permeability decreases due to the increase of negative charge.

Key Words
Electric charge, permeability, repulsive potential energy, soil structure, soil dispersion

Introduction
Charge characteristics of soils strongly influence pore structure and permeability. Although permeability is supposed to decrease in response to an increase in electric repulsive force among soil particles, the relationship between permeability and repulsive potential energy has not been evaluated (Ishiguro *et al*., 2003). A numerical solution of the equation for swelling pressure in mixed systems with nonsymmetrical electrolytes was proposed (Bresler, 1970). However, research into repulsive potential energy in multivalent counterion systems has been rare (Ishiguro *et al*., 2003). In this research, soil structure and permeability changes of the allophanic Andisol, which is characterized by a number of variable charges, were investigated. Especially, the repulsive potential energies were evaluated in an NO_3–SO_4 systems in relation to permeability. The permeability change of high humic Andisol whose negative charge was increased by adding anionic surfactant was also investigated.

Materials and Methods
Soils
An allophanic Andisol (Hapludand) was obtained from a field at the National Institute of Agro-Environmental Sciences in Tsukuba, Japan, from a depth of approximately 90 cm (4Bw1 horizon). The predominant clay minerals were allophane and imogolite. The sand content was 130 g/kg, silt content was 375 g/kg, and clay content was 495 g/kg. The organic C content was 11.6 g/kg. The <2-mm sieved field moist soil was used in all experiments. As pH decreased, the cation exchange capacity (CEC), the negative charge of the soil, decreased, and the anion exchange capacity (AEC), the positive charge of the soil, increased. Both the CEC and the AEC increased with an increase in ion strength. A non-allophanic high humic Andisol at a pasture in Daisen Mountain in Tottori prefecture, Japan, from the A horizon was also used. The total carbon content was 138 g/kg, the sand content was 436 g/kg, the silt content was 318 g/kg, and the clay content was 246 g/kg. The CEC was 12.3 $mmol_c$/kg in 1 mmol/L potassium solution, and the AEC was 0 $mmol_c$/kg at pH 6.

Hydraulic conductivity study under different pH conditions
Saturated hydraulic conductivity (*K*) for the allophanic Andisol was determined at a constant hydraulic gradient of 3 m/m using a column 3-cm long and 3-cm ID. The initial soil solution pH was under natural condition at about pH 6. The electrolyte concentration of the influent solutions (Na-H-Cl-OH system) was 1 $mmol_c$/L under different pH conditions (pH 3 to 11).

Hydraulic conductivity study at pH 3 and 4
Values of *K* for the allophanic Andisol were determined at a constant hydraulic gradient of 5 m/m using a column 3-cm long and 3.2-cm ID. The initial soil solution pH was under natural condition at about pH 6. The influent solutions were mixtures of HNO_3 and H_2SO_4 at pH 3 and pH 4 with different mixed proportions.

1 – 6 August 2010, Brisbane, Australia. Published on DVD.

Hydraulic conductivity study during the percolation of anionic surfactant solutions
Values of *K* for the non-allophanic high humic Andisol were determined at a constant hydraulic gradient of 3 m/m using a column 13-cm long and 5-cm ID during the percolation of anionic surfactant (sodium dodecyl sulfate, SDS) solutions.

Results and Discussion

Hydraulic conductivity study under different pH conditions
The results of the hydraulic conductivity study with different pH solution percolation are shown in Figure 1(a). The values of *K* decreased drastically when HCl at pH 3 was percolated as shown in Figure 1(a). *K* also decreased when NaOH at pH 11 was percolated (Nakagawa and Ishiguro, 1994). Photo 1(a) shows the surface structure of the soil before HCl percolation when soil aggregates were observed. Photo1 (b) shows the surface structure with collapsed aggregates after HCl at pH 3 percolation. The collapse of the structure was caused by swelling of the soil aggregates and the clogging of larger pores resulted from soil dispersion. This structural change in the upper layer caused a decrease in permeability (Ishiguro, 2005). The influence of the solution pH on soil dispersion is shown in Figure 1(b) in which the vertical line indicates the dispersion ratio of the absorbance of the soil suspension after 12 hours of settling to that just after shaking. The soil was well dispersed in solutions with lower pH levels due to the predominant positive charge and in those with higher pH levels due to the predominant negative charge (Nakagawa and Ishiguro, 1994). This phenomenon corresponds to the decrease in the saturated hydraulic conductivity.

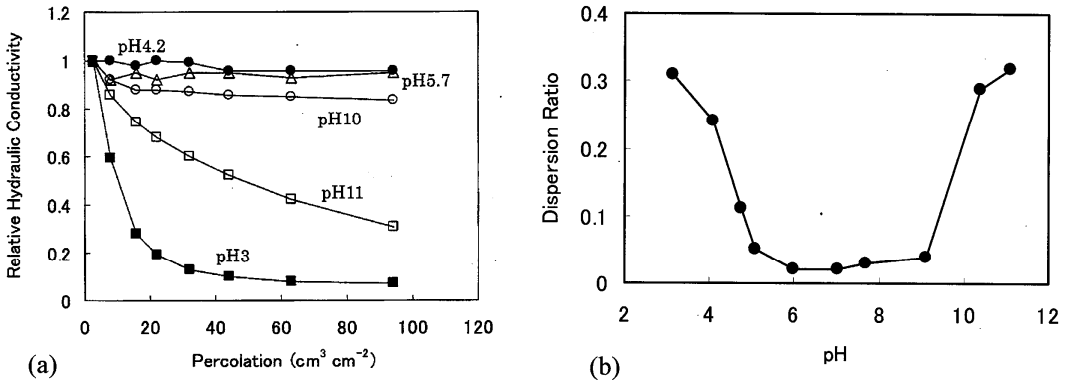

Figure 1. (a) Influence of influent pH on saturated hydraulic conductivity with Na-H-Cl-OH system. The pH values in the figure denote those for influent solutions. (b) Influence of pH on soil dispersion with the same system (Nakagawa and Ishiguro, 1994).

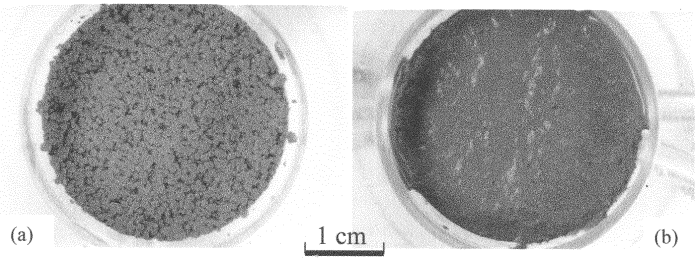

Photo 1. Surface soil structure (a) before and (b) after the percolation of a HCl solution. (Ishiguro, 2005).

Hydraulic conductivity study at pH 3 and 4
Values of *K* were found to decrease when dilute HNO_3 was percolated in the soil as shown in Figure 2. However, this decrease was restricted as the proportion of SO_4^{2-} to total anions in the solution increased. We also performed a dispersion study under the same solution conditions as those in the soil column for the hydraulic conductivity study. The soil was well dispersed at higher proportions of NO_3^- to the total anions in the solution, and well flocculated at higher proportions of SO_4^{2-}, corresponding to the change in *K* values (Ishiguro and Nakajima, 2000; Ishiguro *et al*., 2003). The electric repulsive potential energies, V_ς, between soil clay particles in mixtures of HNO_3 and H_2SO_4 at pH 3 and 4 were calculated with the following equation using the Gouy-Chapman theory (Ishiguro *et al*., 2003) and electrophoretic mobility data as shown in Figure 3.

$$V_\varsigma = -2\int_b^0 \Pi \, \mathrm{d}D,$$

$\Pi = RT\Sigma(C_i - C_{0,i})$

where Π is the osmotic pressure difference between the midpoint of two soil clay particles and the bulk solution, D is the distance from the plane of the zeta potential to the midpoint, b is the distance from the zeta potential plane to the boundary of the bulk solution, R is the gas constant, T is the absolute temperature, C_i is the concentration of ion i at the midpoint, and $C_{0,i}$ is the concentration of ion i in the bulk solution. The horizontal axis in Figure 3 indicates the concentrations of NO_3^- and SO_4^{2-} ($mmol_c/L$) in the acid solution at pH 3 and 4. The repulsive potential energy increased with an increase in NO_3^- proportion, and the increase near 100% NO_3^- proportion was particularly steep. Repulsive potential energy caused dispersion and swelling of the soil at higher NO_3^- proportions under low pH conditions, and permeability decreased as a result of this dispersion and swelling. On the other hand, the repulsive potential energy decreased and the soil flocculated more with an increase in SO_4^{2-} proportion, because SO_4^{2-} forms complexes on the clay surface at low pH (Ishiguro *et al.*, 2006).

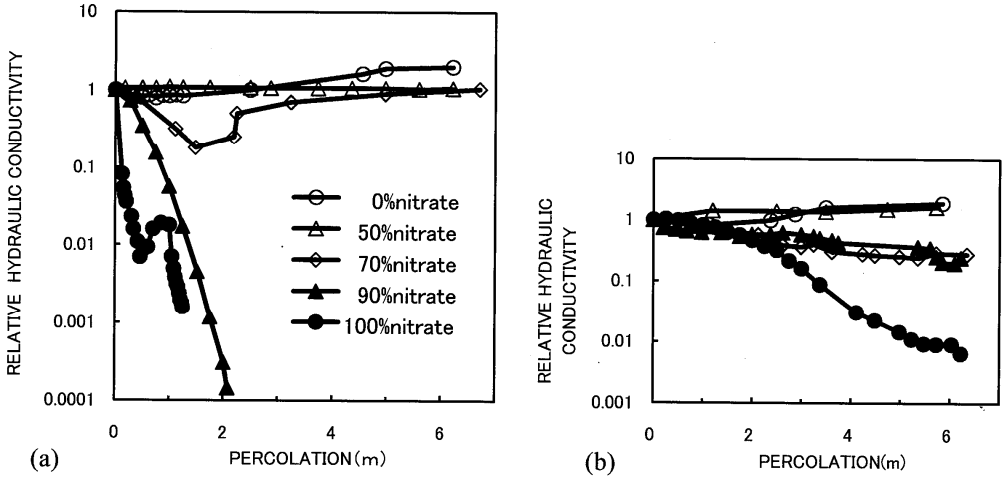

Figure 2. Relative hydraulic conductivity change during the leaching of dilute acid at (a) pH 3 and 1 $mmol_c/L$ and (b) pH 4 and 0.1 $mmol_c/L$. The percentages denote the ratio of NO_3^- to NO_3^-+ SO_4^{2-} concentrations in the leaching acids (Ishiguro *et al.*, 2003).

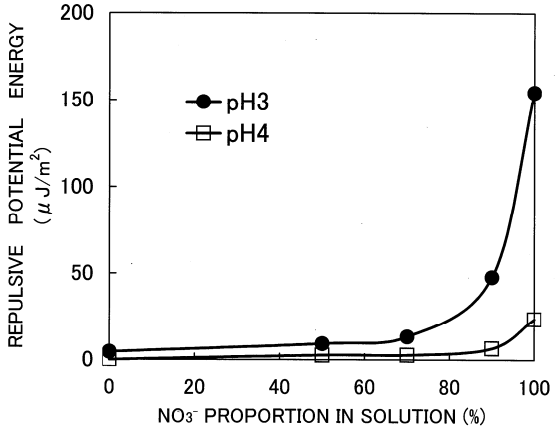

Figure 3. Calculated repulsive potential energies in dilute acids (Ishiguro *et al.*, 2003).

Hydraulic conductivity study during the percolation of anionic surfactant solutions

Values of K decreased with the increase of SDS percolation amount and the decrease of SDS concentration in the discharged solution except for that of 10 mmol/L SDS solution as shown in Figure 4 (Ishiguro *et al.*, 2008). The surface negative charge of the soil increased during the SDS percolation due to SDS adsorption. Then, the repulsive potential energy between soil particles increased and the soil swelled and dispersed. This caused the decrease of K. The K of the 10 mmol/L solution, which was higher than cmc, did not decrease well, because of highest electrolyte concentration.

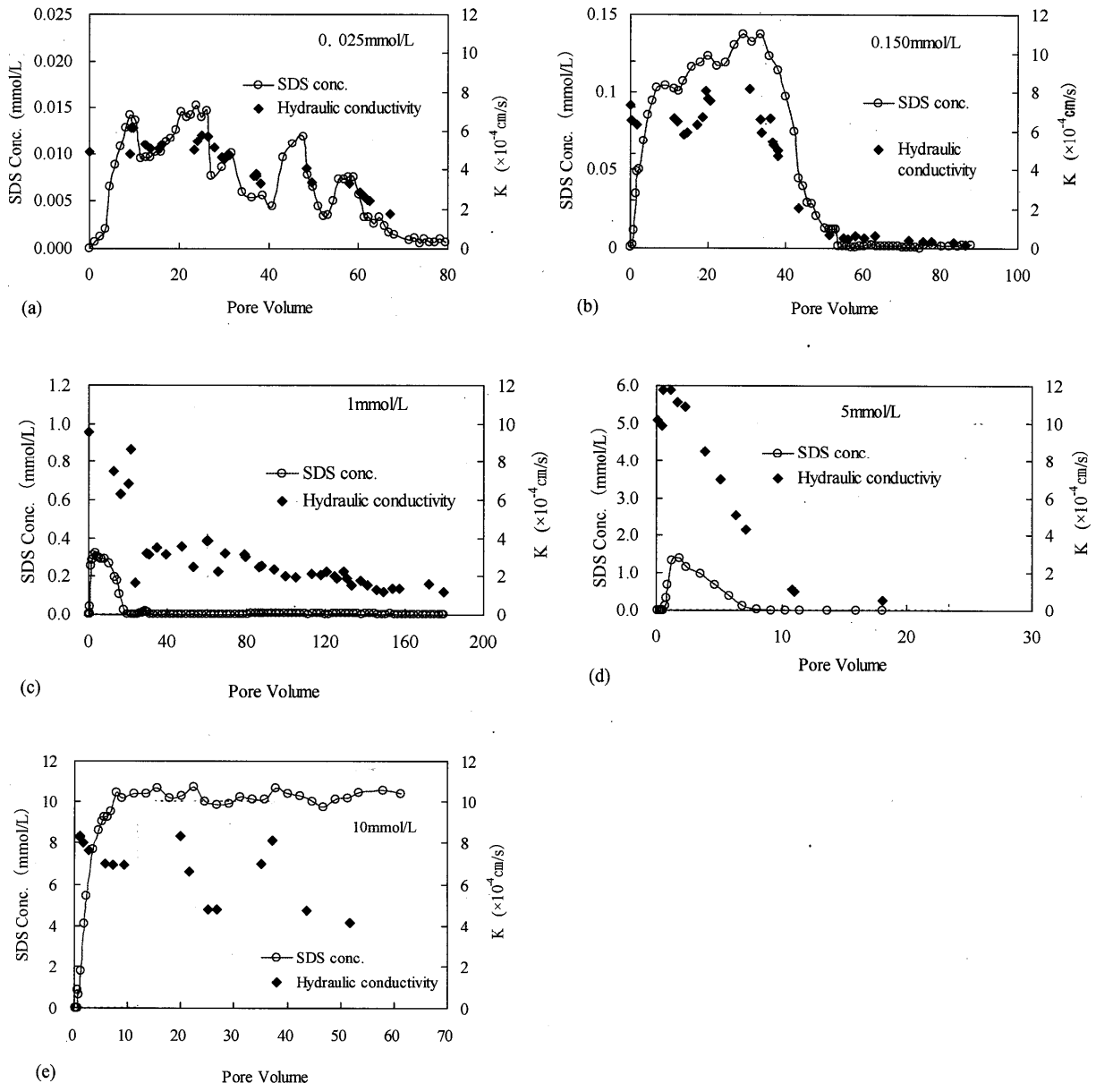

Figure 4. Anionic surfactant (SDS) breakthrough curves and hydraulic conductivities. Pore Volume is the effluent volume divided by water volume in the soil column (Ishiguro *et al.*, 2008).

References

Bresler E (1970) Numerical solution of the equation for interacting diffuse layers in mixed ionic systems with nonsymmetrical electrolytes. *Journal of Colloid and Interface Science* **33,** 278-283.

Ishiguro M, Nakajima T (2000) Hydraulic conductivity of an allophanic Andisol leached with dilute acid solutions. *Soil Science Society of America Journal* **64,** 813-818.

Ishiguro M, Nakaishi K, Nakajima T (2003) Saturated hydraulic conductivity of a volcanic ash soil affected by repulsive potential energy in a multivalent anionic system. *Colloids and Surfaces A* **230,** 81-88.

Ishiguro M (2005) Ion transport and permeability in an allophanic Andisol at low pH. *Soil Science and Plant Nutrition* **51,** 637-640.

Ishiguro M, Makino T, Hattori Y (2006) Sulfate adsorption and surface precipitation on a volcanic ash soil (Allophanic Andisol). *Jourrnal of Colloid and Interface Science* **300,** 504-510.

Ishiguro M, Torigoe T, Kameoka Y, Akae T (2008) Linear Anionic Surfactant (SDS) Transport in High Humic Volcanic Ash Soil and its Permeability. *Transactions of Japanese Society of Irrigation Drainage and Reclamation Engineering* **258,** 7-13 (in Japanese with English abstract).

Nakagawa T, Ishiguro M (1994) Hydraulic conductivity of an allophanic Andisol as affected by solution pH. *Journal of Environmental Quality* **23,** 208-210.

Soil water retention under drying process in a soil amended with composted and thermally dried sewage sludges

Gerardo Ojeda[A] and Josep M. Alcañiz[B]

[A] IMAR Instituto do Mar - Coimbra Interdisciplinary Centre, Department of Zoology, University of Coimbra, Portugal.
Email: g_ojeda@student.zoo.uc.pt
[B] CREAF (Centre for Ecological Research and Forestry Applications), Department of Animal and Plant Biology and Ecology, Autonomous University of Barcelona, 08193 Bellaterra (Spain), Email JosepMaria.Alcaniz@uab.es

Abstract
We report soil water desorption modifications during air drying in a soil amended with six different sewage sludges (composted or thermally dried). The time required to change water retention from wilting point (-1.5MPa) to dryness (ψ = -25 MPa) was increased by composted sludges but not by thermally dried sludges, although both sludges were able to increase soil water retention under drying. Changes in the water desorption rates are hypothesised to be due to low wettability of the soil treated with composted sludges.

Introduction
Soil drying after wetting is a process that occurs continuously in the field, due to evaporation or infiltration. The soil water content (θ) and its corresponding energy state or suction (ψ) differs under wetting or drying processes. This arises from differences in the processes of filling or emptying soil pores (Braddock *et al.* 2001). However, while soil wetting can occur within minutes in some cases, soil drying requires hours (Ojeda *et al.* 2009a). This gives importance to the soil drying process in terms of water plant uptake or water availability to microbial activity. In soil reclamation processes, sewage sludge is currently used as organic amendment in order to improve many soil properties such as fertility, soil water retention and aggregate stability. Water is retained in soil by capillary forces at high saturations (low suction regime) (Nitao and Bear 1996) and by forces of molecular attraction at low saturations (high suction regime) (Pozdnyakov *et al.* 2006). However, due to the potential hydrophobicity of organic matter (Bachmann *et al.* 2008), the temporal dependency of soil water retention can be modified by sludge amendments. The main objective of this study is to assess the effects of two kinds of sewage sludge (composted or thermally dried) on the time involved in the drying process of a soil obtained from quarrying activities. We apply a segmented model to quantify temporal changes in soil water content. The relationship between water holding time and soil organic carbon was analyzed.

Proposed model
The critical gravimetric water content (w_c) was obtained using the relationship between gravimetric water content (w) and time (t), in both low and high suction regimes (Ojeda *et al.* 2009a):

$$w = -a_1 t + b_1 \qquad t_e \le t \le t_c \qquad (1) \qquad\qquad w = -a_2 t + b_2 \qquad t_c \le t \le t_\infty \qquad (2)$$

where a_1 and a_2 are constants, t_e is the time when air entry suction occurred and t_c is the time when low suction regime changes to high suction regime. The negative sign of a_1 corresponds to water losses during drying process. The interception of both straight lines (Eqs. 1 and 2), corresponding to the transition point where low suction regime changes to high suction regime, is determined by a change of slope (Figure 1a). The t_c and w_c values were calculated and the ψ_c value was determined from the water retention curve (WRC) using the w_c value (Figure 1b). The composite fractal model of Ojeda *et al.* (2006) was used to fit WRC, as this model covers both the low and high suctions regimes, where A_1 and A_2 (Figure 1b) are constants, while D_1 and D_2 are pore-solid and surface fractal dimensions, respectively.

Materials and methods
The soil samples were obtained from a limestone quarry (Begues municipality, Barcelona, Spain) that produces a soil resulting from excavation processes. It has characteristics of a red Mediterranean soil (*Spolic Technosol calcaric*), with a loamy texture, being low in organic matter (organic C = 0.47 %), but rich in lime ($CaCO_3$ = 39.3 %) and coarse fragments (62.0 %). The soil was amended with six types of treated sludge produced in various municipal waste-water treatment plants from medium-sized towns of Catalonia (NE Spain). All sludges were digested and partially dewatered (20% dry matter) before being subjected to either a composting or a thermal drying process (Table 1). Dewatered sludge from Manresa was composted with crushed pinewood bark, while dewatered sludge from Blanes and Vilaseca was composted with pinewood splinters. All sludges were applied to soil as granules, except the thermally dried sludge from Sabadell which was added as a pellet (1 cm in diameter). A

nominal dose of about 35 Mg ha^{-1} (dry weight) of each sludge was mixed with the soil and distributed in 28 lysimeters of 150 L with a surface area of 0.3 m^2. There were 4 replicates per treatment. The experiment was maintained in the quarry for 13 months. Samples were taken after one month (T1) and twelve months (T2) after the start of the experiment. Soil samples (0 – 20 cm depth) of each lysimeter were air-dried at room temperature, passed through a 2 mm sieve, and stored at 4ºC in the dark before analysis. Table 2 gives information about treatments and the main physicochemical properties of the amended soils at T1.

The main drying branches of the water retention curve were measured in the laboratory at 25ºC, using a WP4 Dew Point PotentiaMeter (Decagon Devices, Inc. Pullman, WA). Samples of approximately 1.2 g of air-dry soil (< 2 mm) from each plot were placed in sample cups (40 mm dia.×10 mm) resulting in a monolayer of aggregates that completely covered the bottom of the sample cups. Both the sample and sample cup were previously weighed and saturated by capillarity for 10 minutes using one band of filter paper in contact with a free water table approximately 10 mm above the soil surface. After this, excess water was removed. A balance and the WP4 Dew Point PotentiaMeter were then used to record *w* and ψ periodically over time, as the sample dried by evaporation. Approximately 8-12 paired measurements of *w* and ψ were obtained. The time required for the soil drying processes was measured using a chronometer and the relationships between gravimetric water content and time were analyzed. The drying time that elapsed between suction at -1.5 MPa (wilting point: $\psi_{-1.5}$) and suction at 25 MPa (dryness: ψ_{-25}), called Δt_{total} and its corresponding gravimetric water content (Δw_{total}) were considered as parameters. Total organic carbon was determined by the wet oxidation method.

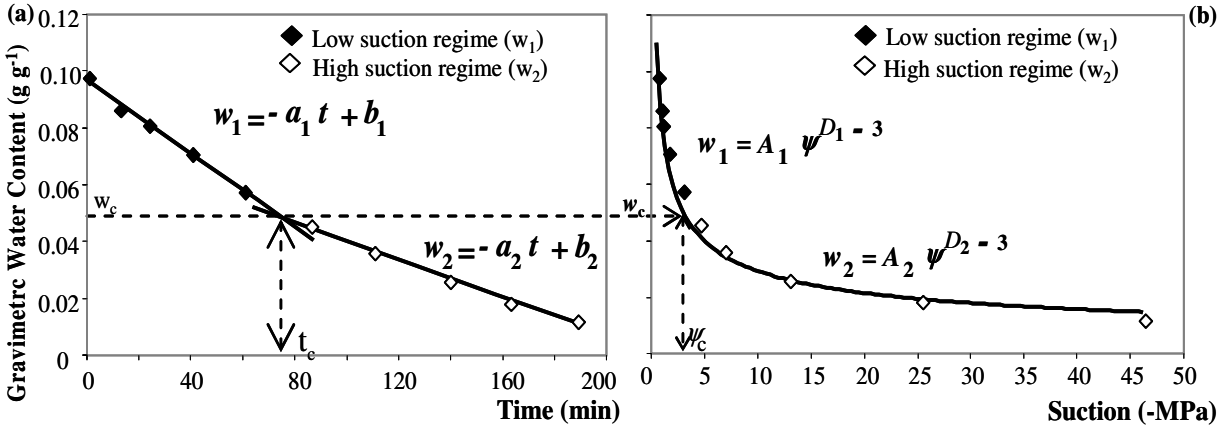

Figure 1. Determination of: (a) critical gravimetric water content (w_c) and the corresponding vapour wetting time (t_c), as the critical point that separates high and low suction regimes in the interception of w_1 and w_2 straight lines, (b) determination of the corresponding critical suction (ψ_c) from the soil water retention curve. Modified from Ojeda *et al.* 2009a.

Table 1. Treatments, composition and identification code of the sewage sludge types used as organic amendment (Ojeda *et al.* 2009a).

Origin† (WWTP)	Type of digestion	Code*	Organic matter (%)	Stability degree‡ (%)	N (%)	P (%)	pH	EC (dS/m) ¶
Blanes	Anaerobic	C_{BL}	56.6	29.0	3.2	7.0	6.5	7.6
Manresa	Anaerobic	C_{MR}	55.5	40.6	2.3	4.3	7.1	3.9
Vilaseca	Aerobic	C_{VL}	58.3	35.8	3.0	5.8	6.9	8.5
Besós	Physico-chemical	T_{BS}	72.3	8.6	2.2	4.0	6.1	1.4
Mataró	Anaerobic	T_{MT}	74.0	40.4	3.5	3.3	6.2	5.8
Sabadell	Anaerobic	T_{SB}	62.2	39.5	3.9	5.8	7.3	0.9

† WWTP: identification of municipal waste water treatment plant. * Composted sludge from Blanes (C_{BL}), Manresa (C_{MR}) or Vilaseca (C_{VL}), and thermally-dried sludge from Besós (T_{BS}), Mataró (T_{MT}) and Sabadell (T_{SB}). ‡ Stability degree: percentage of organic matter resistant to acid hydrolysis. ¶ EC: Electrical conductivity (1:5 water extract).

Table 2. Mean values of the physicochemical properties of <2 mm fraction of the soil amended with different types of sewage sludge (Ojeda *et al.* 2009a).

Type of sludge	Treatment†	Sand %	Silt %	Clay %	pH (H_2O)	E.C. (dS/m) 1:5	SOM* %	N %	P-Olsen mg/kg
Composted	C_{BL}	44,2	35,2	20,6	8,0	1,1	1,8	0,15	51
	C_{MR}	45,7	34,3	20,0	8,1	0,9	1,6	0,10	46
	C_{VL}	38,3	36,2	25,5	8,0	1,0	2,4	0,22	101
Thermally dried	T_{BS}	46,2	34,0	19,8	8,2	0,5	1,9	0,12	35
	T_{MT}	38,6	41,3	17,4	8,1	0,5	2,9	0,16	49
	T_{SB}	51,0	31,6	20,1	8,3	0,7	1,2	0,08	10
Control	O_{MS}	42,5	35,0	22,5	8,5	0,5	0,8	0,06	6

† See Table 1 to identify sewage sludge treatment. *SOM: organic matter. O_{MS}: soil without sludge.

Results

The measured values of *w* and ψ for amended soil under drying processes ranged from 0.01 to 0.15 g g^{-1} and from -0.5 to -50 MPa, respectively, where increases in ψ always resulted in decreases in *w*. The time required to air dry the non-amended soil from wilting point (-1.5 MPa) to dryness (-25 MPa) reached a maximum value of 82.5 min. Analyzing the Δt_{total} parameter, one month after sludge addition (T1) the soil treated with composted sludges required more air drying time (55 %) in a soil layer < 2 mm, whilst one year after sludge addition (T2) one of the studied thermally dried sludges was able to reduce the time required for water evaporation (27%). Comparing with the corresponding soil gravimetric water content retained between -1.5 and 25 MPa (Δw_{total}, Figure 2b), at T1 all sludges (except the thermally dried sludge from Sabadell) increased the soil water retention, whilst at T2 only the composted sludge from Vilaseca and the thermally dried sludge from Mataró showed a significative increase. This means that composted sludges were possibly more useful to increase the soil water content at short term, because the water desorption was slower during soil evaporation compared to the soil amended with thermally dried sludges.

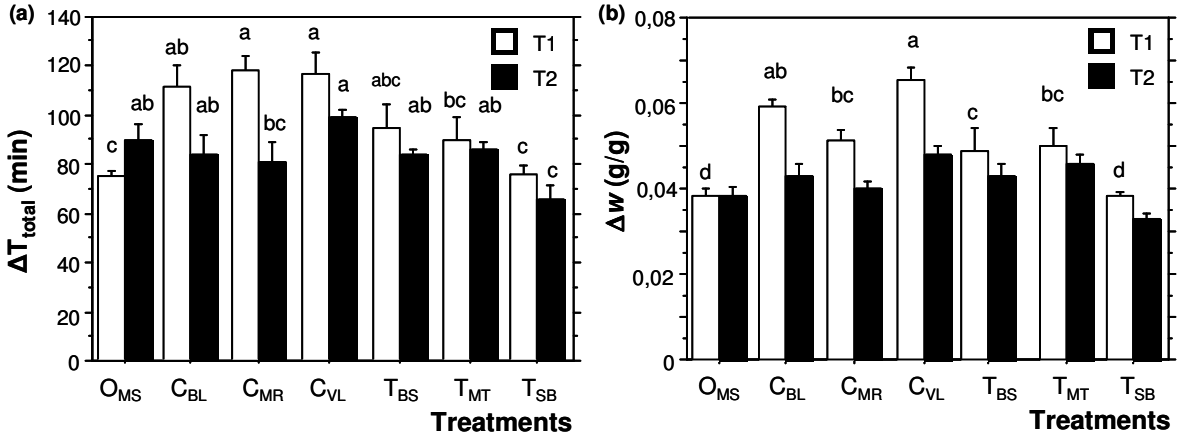

Figure 2. Mean values of (a) time elapsed between wilting point (ψ = -1.5 MPa) and dryness (ψ = -25 MPa) called Δt_{total} (from Ojeda *et al.* 2009a) and (b) its corresponding gravimetric water (Δw_{total}) for the different sludge treatments (see Table 1) at sampling time one (T1) and two (T2). Bars with the same letter are not significantly different at p<0.05.

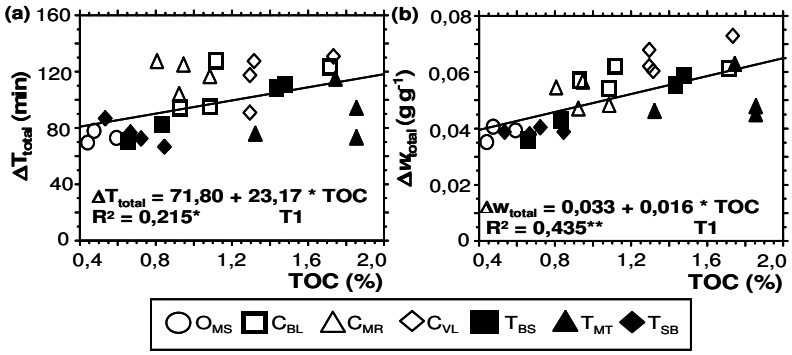

Figure 3. Relationships between total organic carbon (TOC) with (a) water holding time (Δt_{total}) (from Ojeda *et al.* 2009a) and (b) the corresponding gravimetric water (Δw_{total}) for the different sludge treatments (see Table 1) at sampling time T1.

With respect to the relationship between the total organic carbon (TOC) with the water holding time (Δt_{total}) and its corresponding gravimetric water content (Δw_{total}) (Figure 3), it was observed that increases in TOC corresponded with increases in Δt_{total} only at T1 and with Δw_{total} at both samplings. However, the r^2 values suggest that TOC could better explain the increases in Δw_{total} than the increases in Δt_{total}, because not all increments in TOC corresponded with increments in the water holding time. This is possibly due to the fact that sludge organic matter could be hydrophobic.

On the other hand, during wetting and drying processes, water is present in soil at different places e.g. totally filling pore soil, at the asperities of pore walls, in pendular rings between grains, in bridges between grains separated by small gaps, in pore throats between larger pores, or in structures formed by a combination of these water morphologies (Ojeda *et al.* 2009a). Ojeda *et al.* (2009b) observed that during wetting process composted sludges incremented the time required to the same soil to change its water content from dryness (-25 MPa) to wilting point (-1.5 MPa), possibly by low wettability induced by sludge amendments. Thus, it is possible that during drying process, when the water film that links the different water morphologies start to disappear, the isolated soil wet areas could be surrounded by soil dry areas with low wettability in the soil treated with composted sludge, which could reduce the movement of water on soil pores during air drying.

Conclusions

Composted and thermally dried sludges modified the water holding time and the soil water retention. Because of low wettability, composted sludges can increase soil water retention due to restrictions of water movement. Possibly, this is due to the fast drying of surface pores which were initially wetted recovering water repellency during the drying process, thus limiting the water desorption. Thermally dried sludges also increase soil water retention but without increasing the water holding time and in some case, reducing it. In terms of microbial water availability, composted sludge could be more useful as a soil amendment.

Acknowledgements

This research was carried out under the RESMINLOD project (CTM2006-14163-C02-01/TECNO projects of Spanish Ministry of Environment, respectively). We thank the Fundação para a Ciência e a Tecnologia (FCT) for postdoctoral fellowship of Gerardo Ojeda and the collaborators of RESMINLOD project.

References

Bachmann J, Guggenberger G, Baumgartl T, Ellerbrock R, Urbanek E, Goebel M, Kaiser K, Horn R, Fisher WR (2008) Physical carbon-sequestration mechanisms under special consideration of soil wettability. *Journal of Plant Nutrition and Soil Science* **171**, 14-26.

Braddock RD, Parlange JY, Lee H (2001) Application of a soil water hysteresis model to simple water retention curves," *Transport in Porous Media* **44**, 407-420.

Nitao JJ, Bear J (1996) Potentials and their role in transport in porous media. *Water Resourses Research* **32**, 225-250.

Ojeda G, Perfect E, Alcañiz JM, Ortiz O (2006) Fractal analysis of soil water hysteresis as influenced by sewage sludge application. *Geoderma* **134**: 386-401.

Ojeda G, Marando G, Bonmati M, Alcañiz JM (2009a) Time dependence of soil water hysteresis in a soil reclaimed by sewage sludge amendments. In 'Poromechanics IV'. (DEStech Publications, Inc, PA) pp. 537 – 542. (New York, USA) ISBN 978-1-60595-006-8.

Ojeda G, Alcañiz JM, Bonmatí M, Woche SK, Bachmann J (2010) Wetting process and soil water retention of a soil amended with composted and thermally dried sludges. Sent to *Geoderma* and moderate revision.

Pozdnyakov AI, Pozdnyakova LA, Karpachevskii LO (2006) Relationship between water tension and electrical resistivity in soils. *Eurasian Soil Science* **39** (Suppl.), S78-S83.

Spatial and temporal changes of soil physical properties of an Andisol in southern Chile as a consequence of grazing and wetting and drying cycles

Dorota Dec[A], José Dörner[A] and Oscar Balocchi[A]

[A]Faculty of Agricultural Sciences, Austral University of Chile, Valdivia, Chile, Email dorkadd@gmail.com, josedorner@uach.cl, obalocch@uach.cl

Abstract
Weather, human activity and different soil management are factors that lead to spatial and temporal variations in soil physical properties. The aim of this study was to study the effects of grazing and wetting and drying (WD) cycles on some time-space dependent physical properties of an Andisol (Duric Hapludand) in southern Chile. Temporal changes in soil water content (WC) influenced the penetration resistance (PR), and were also related to the aggregate strength (AS) and precompression stress (Pv). Soil compaction caused by livestock not only affected PR spatially, but also disturbed the pore continuity, thus reducing the air conductivity of the soil.

Key Words
Grazing, soil water content, mechanical strength, pore functions, spatial and temporal variability

Introduction
The water regime in soils is very important to aggregate formation, morphology of soil structure, processes occurring in the soil, plant-growth and the functioning of microorganisms. This, in turn, depends on the ability of soil to provide nutrients, gases, heat, water and a rootable pore system. These properties are exposed to continuous changes, whether due to natural phenomenon (WD cycles) or human activities (tillage-induced disturbance and grazing events). The latter often causes severe changes in soil structure which have a detrimental impact on soil functions, e.g. soil disturbance due to tillage or grazing that represents the most dynamic and influential modification (in time and space) of soil physical properties such as bulk density, water and air conductivity (Schäfer-Landefeld *et al.* 2004). Until now, temporal and spatial changes of soil physical properties are not well known in southern Chile. Therefore, the purpose of this study was to illustrate the spatial and temporal changes of soil's physical properties (WC, PR) measured in the field relating them to the grazing events, changes in WC and soil strength and pore functions measured in the laboratory.

Methods
Soil and management
The investigation was conducted in an experimental field located in Valdivia (Santa Rosa). Before starting the experiment, the soil (Duric Hapludand, Serie Valdivia) was cultivated and *Lolium perenne* and *Trifolium repens* were seeded in April, 2008. The grazing (2 animals/400 m^2) began in September, 2008 and was the same in all plots.

Soil sampling and measurements
The soil samplings and measurements were conducted from November, 2008 until April, 2009 (SR1- 03.11.08; SR2- 10.11.08; SR3- 09.01.09; SR4- 10.03.09; SR5- 15.04.09; SR6- 20.04.09; Figure 1) depending on the soil water content (WD cycles) and grazing. The experimental field consisted of 6 plots (20x20m). The water content (TDRs) and penetration resistance (Penetrometer) were measured on each plot, arranged along transects 3m apart with each transect divided into 13 points (separation: 1.5 m). When field measurements were done, undisturbed soil samples in metallic cylinders and soil aggregates were collected from 2 to 10 cm depths.

Laboratory determinations
Saturated hydraulic conductivity (Ks, cylinders of 250 cm^3, n: 10) was measured with a water permeameter using the constant head method. Ks was measured after 1 and 72 hours of continuous water flow. In order to define the pore size distribution, the water retention curve (cylinders of 220 cm^3, n: 7) was measured using sand tanks and pressure chambers. The precompression stress (Pv, cylinders of 110 cm^3, n: 6), determined in an odometer after equilibration of the soil samples at a matric potential of 60hPa, was calculated according to the Casagrande method (Rico and del Castillo 1978). In order to define the structural and functional resilience of pores, the air conductivity (Ka) was measured before (bC) and after (aC) compaction. The crushing test (n: 20) was conducted in order to describe the aggregate strength (Dexter and Kroesbergen, 1985). For this purpose

1 – 6 August 2010, Brisbane, Australia. Published on DVD.

aggregates were saturated, equilibrated at -60, -330hPa and 30°C and then crushed between two parallel splints by adding water.

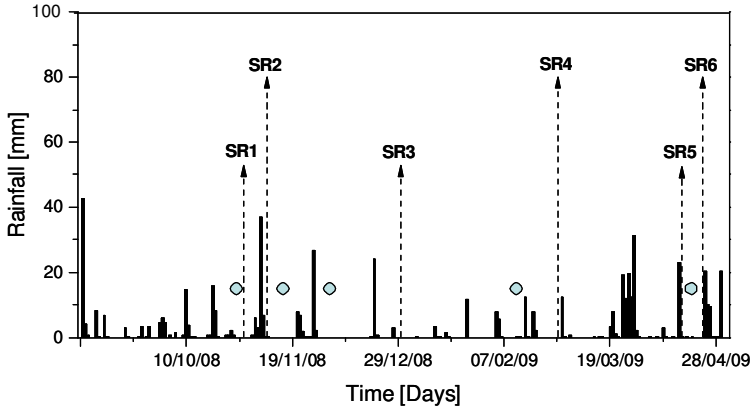

Figure 1. Development of rainfall during the experiment. SR indicates the soil samplings and circles the grazing events.

Results

Temporal and spatial changes in soil strength as a consequence of grazing events and WD cycles

The decrease in water content in the soil induced an increase in PR. The latter, however, is spatially dependent as a consequence of the grazing events. Animal trampling leads to the degradation of the soil's physical quality and the deterioration of soil structure through hoof action of the grazing animals. Compacted soil causes soil deformation and changes soil's physical properties such as e.g. PR (Reszkowska *et al.* 2009).

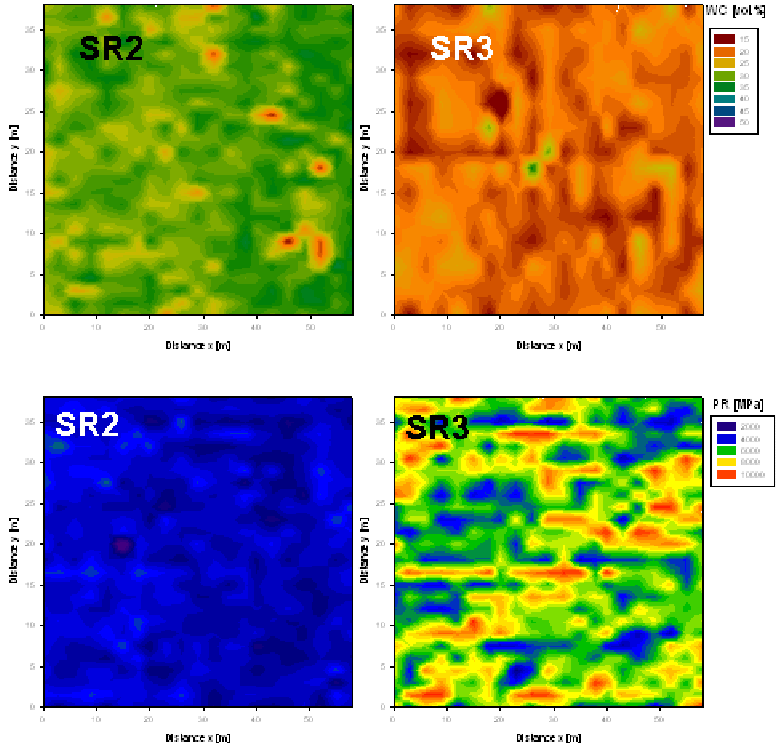

Figure 2. Spatial distribution of volumetric water content (WC) and penetration resistance (PR) in SR2 (10.11.08) and SR3 (09.01.09).

The observed values of PR in the present investigation are similar to those presented by Bachmann *et al.* (2006) in a Typic Hapludand under pasture. Soil penetration resistance is a mechanical property that has been used by many authors as an indicator of soil compaction (Draghi *et al.* 2005). In wet soils, where pore space is filled with water, the menisci forces cause the soil particles to loose contact between them. This, in turn, increases the soil's susceptibility to compaction. The water menisci forces build up during drying induced and increase in PR, which exceeds critical values to root growth (2000 kPa, Bengamin *et al.* 2003). We believed, however, that this great PR do not affect the root growth because of the low bulk density (< 0.9 g/cm^3) caused by the great amount

of organic soil carbon and the presence of allophane which are typical characteristics of Andisols (Dörner *et al.* 2009). The latter, however, need further investigation.
Temporal changes were also observed for other soil properties (Figure 3) which are related to the grazing events and WC cycles. The changes in mechanical strength registered by PR were also observed at the soil aggregate and core scales, i.e. an increase in penetration resistance also meant greater values of aggregate strength and precompression stress. After the grazing event occurred between SR5 and SR6 (17 April, 2009) both PR and AS increased.

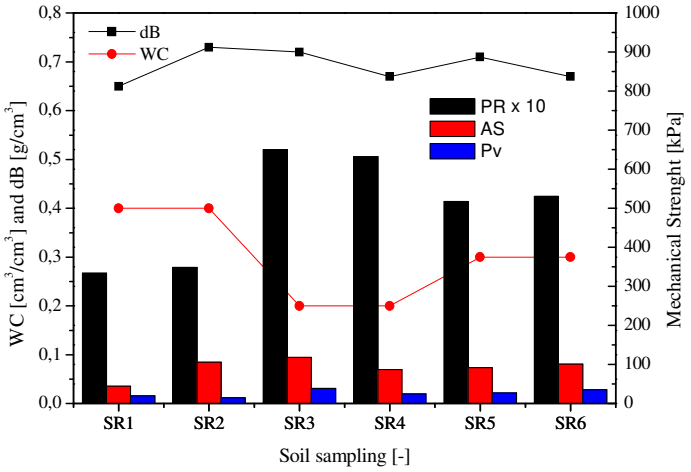

Figure 3. Temporal (soil sampling SR1-SR6) changes in penetration resistance (PR), water content (WC), bulk density (dB, SR1-SR4), precompression stress (Pv, SR1-SR5) and aggregate strength (AS).

Temporal changes in soil structure and pore functions as a consequence of grazing events and WD cycles
Temporal changes were also observed in air conductivity (Figure 4). Ka showed a slight decrease between the first and third soil samplings. The third sampling event (SR3) occurred 1 month after the last grazing event which did not allow enough time for the soil to recover its functional integrity. The changes in water content during summer and autumn induced crack formation due to the great shrinkage but low swelling capacity of these soils (Dörner *et al.* 2009). The latter explains the increase in Ka. After the consolidation experiment, Ka decreased; i.e. soil deformation and partial recuperation of the volume affect the continuity and efficiency of the porous system.

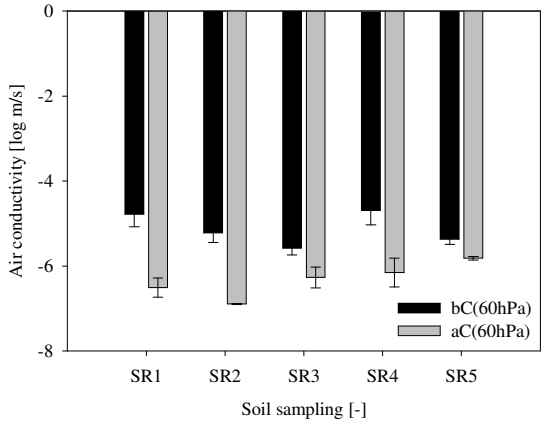

Figure 4. Air conductivity before (bC) and after (aC) compaction as a function of time (soil samplings SR1-SR5).

A redistribution of soil pores was observed during the experiment (Figure 5a). While the larger pores (wCP) remained constant, the narrow (nCP) and mesopores (MP) decreased 5.9% and 2.5%, respectively, and micropores (FP) increased 2.67% between SR1 and SR4. On the other hand, variations in water permeability (Figure 5b) reflect changes presented in PR (Figure 2, 3), bulk density (Figure 3) and pore size distribution (Figure 5a). These dynamic changes in the soil's hydraulic properties are caused not only by WD cycles but also by grazing events where simultaneous compaction, shearing, kneading and homogenization (Warren *et al.* 1986) lead to intensive disruption of soil structure (especially topsoil) which, in turn, changes soil porosity and the connectivity of the porous system (Figure 5).

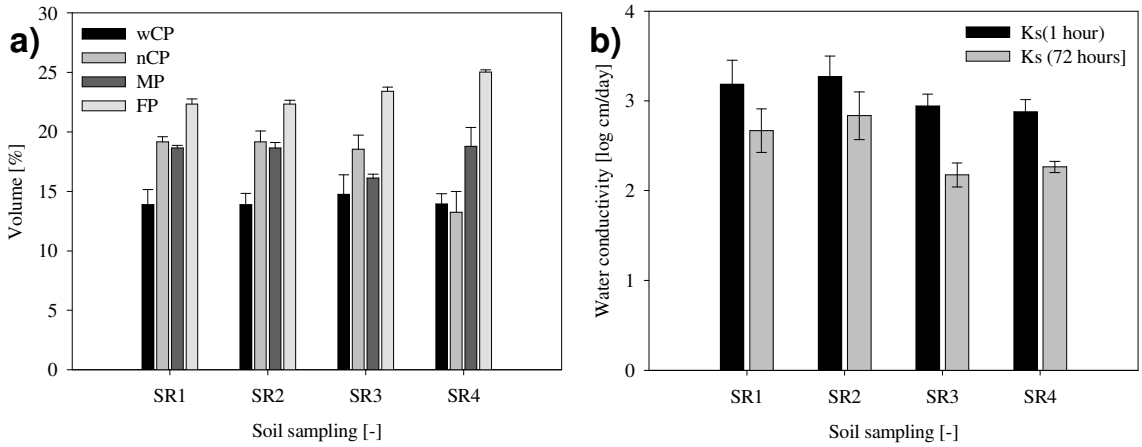

Figure 5. a) Pore size distribution (wCP:>50µm, nCP:50-10µm, MP:10- 0.2µm, FP:< 0.2µm and b) saturated water conductivity as a function of time (soil samplings SR1-SR4).

Conclusion

The penetration resistance changed in time and space in relation to soil water content and the grazing events. Changes in penetration resistance reflected the aggregate strength and the precompression stress. The pore system and its distribution were dynamic, changing temporarily as a consequence of internal and external forces. The latter also induced changes in mechanical strength and pore functions as observed in water and air conductivity, e.g. soil compaction caused by livestock disturbs continuity of pores and, consequently, reduced the air conductivity in the soil.

Acknowledgment

This study was sponsored by FONDECYT 3090038. The authors also thank the "Consorcio Lechero" Project M2P12 (4101.39.14).

References

Bachmann J, Contreras K, Hartge KH, MacDonald R (2006) Comparison of soil strength data obtained in situ with penetrometer and with vane shear test. *Soil and Tillage Research* **87**, 112-118.

Bengamin JG, Nielsen DC, Vigil MF (2003) Quantifying effects of soil conditions on plant growth and crop production. *Geoderma* **116**, 137-148.

Dexter A, Kroesbergen, B (1985) Methodology for Determination of Tensile Strength of Soil Aggregates. *Journal Agricultural Engineering Research* **31**, 139-147.

Dörner J, Dec D, Peng X, Horn R (2009) Change of shrinkage behavior of an Andisol in southern Chile: Effects of land use and wetting/drying cycles. *Soil and Tillage Research* **106**,45-53.

Draghi LM, Botta GF, Balbuena RH, Claverie JA, Rosatto H (2005) Diferencias de las condiciones mecánicas de un suelo arcilloso sometido a diferentes sistemas de labranza. *Revista Brasileira de Engenharia Agricola e Ambiental* **1**, 1415-4366.

Reszkowska A, Peth S, Horn R (2009) Cyclic compressibility of grassland soils as affected by grazing in inner Mongolia, China. In 'ISTRO 18th Triennial Conference Proceedings' (Izmir: Turkey).

Rico R, del Castillo H (1978) 'La Ingeniería de Suelos en Vías Terrestres, Carreteras, Ferrocarriles y Aeropistas'. (Limusa: México).

Schäfer-Landefeld L, Brandhuber R, Fenner S, Koch HJ, Stockfisch N (2004) Effect of agricultural machinery with high axle load on soil properties of normally managed fields. *Soil and Tillage Research* **75**, 75-86.

Warren SD, Nevil MB, Blackburn WH, Garza NE (1986) Soil response to trampling under intensive rotation grazing. *Soil Science Society of America Journal* **50**, 1336-1340.

Study of the effects of structure on soil aggregate stability using a 3D network model

Nicola Dal Ferro[A], Antonio Berti[A], Peter Matthews[B], Luigi Giardini[A] and Francesco Morari[A]

[A]Department of Environmental Agronomy and Crop Productions, University of Padua, Italy, Email nicola.dalferro@unipd.it
[B]Environmental and Fluid Modelling Group, University of Plymouth, Devon, PL4 8AA, U.K. Email P.Matthews@plymouth.ac.uk

Abstract
Aggregate stability strongly influences soil structure and has relevant implications to soil organic carbon protection. We studied the physico-chemical and physical mechanisms of soil structural stability in a long-term experiment in north-eastern Italy. A 3D void network model was used to investigate subtle structural changes in aggregates and their hydraulic properties (intrinsic permeability). The study demonstrated the central role of organic carbon on aggregate stabilization, partly by reducing the intrinsic aggregate permeability and soil wettability.

Key Words
Soil structure, aggregate stability, SOC, Pore-Cor, long-term experiment, organic fertilizers

Introduction
Aggregate stability is an important factor influencing soil fertility. Aggregate breakdown is strongly affected by physico-chemical and physical mechanisms. Recent studies showed the importance of soil organic carbon (SOC) and its humic compounds in aggregate stabilization by at least two different mechanisms: first by increasing soil hydrophobicity and then reducing its breakdown by slaking (Chenu, 2000). Secondly, organic carbon increases the aggregates' inter-particle cohesion. Effects of SOC on porosity and indirectly aggregate stability have recently been suggested (e.g. Lugato *et al*., 2009; Papadopoulos, 2009). Fertilizers with a high organic carbon content, such as manure, would therefore be expected to increase aggregate stabilization. However, little is known about the relative importance of chemical and physical soil stability mechanisms. Organic carbon can maximize the effect of stability indices with different pre-treatments. In addition, a 3D void network model can be used to investigate subtle structural changes in soils based on intrusion curves (e.g. Holtham *et al*., 2007). In this work we used a 3D void network model combined with physico-chemical and physical measurements to investigate the factors affecting soil aggregate stability in a long-term experiment.

Methods
The long-term experiment is located in north-eastern Italy at the Experimental Farm of the University of Padua. It has been underway since 1962, comparing organic (farmyard manure and slurry), mineral and mixed (organic and mineral) fertilizers. The experimental layout is a split-plot with three replications. This work considers 8 treatments with maize as main crop. Half of the treatments also include crop residue incorporation. Wet sieve analyses were carried out on 1-2 mm aggregates after pre-treatments with ethanol (ETOH), benzene (BENZ), fast and slow wetting with water (FW and SW). The aggregate stability index was calculated according to Diaz-Zorita *et al.* (2002). Soil organic carbon characterization included humic fractions (nominal molecular weight: >100 kDa, 100-10 kDa and <10 kDa) and functional group analysis. Wettability was measured by the capillary rise method (Siebold 1997). Aggregate pore distribution in the range 0.0037-58 μm was analyzed by mercury porosimetry with Thermo Finnigan Pascal 140 and Thermo Finnigan Pascal 240. To evaluate the effect of soil structure on aggregate stability, pore distribution curves were analyzed with Pore-Cor (Price *et al.* 2009), a network void model that can generate a simple 3D stochastic representation of soil structure and then quantify its features. The model approximates the geometry of a void unit cell containing 1000 cubic pores connected by up to 3000 cylindrical throats.

Pore-Cor's uniqueness over other modeling approaches is that it creates a physically realizable geometry and generates five parameters that are real properties resulting from the closeness between simulated and experimental curves. Intrinsic hydraulic conductivity (Perm) was estimated from primary parameters. At least ten fits were conducted per replication, corresponding to different stochastic generation numbers. To emphasize the effect of soil structure on wetting and consequently on aggregate stability, fast dynamic wetting with water was modeled on the basis of previously generated unit cells.

1 – 6 August 2010, Brisbane, Australia. Published on DVD.

Results

The aggregate stability index varied according to treatments and soil characteristics. Aggregates pre-treated with benzene maximized the effect of organic matter, increasing hydrophobicity. Indeed, contact angle measurements were correlated to SOC, high-weight humic fraction (HF1) and stability structure index (pre-treated with benzene). On the contrary, the stability index with fast and slow wetting pre-treatments was influenced by porosity, especially in the 5-0.1 μm range (ultramicropores). Pore-Cor parameters showed high variability among replicates and no significant differences were observed among treatments. However, connectivity (Conn, i.e. the average number of connected throats per pore) and correlation level (CorLevel, i.e. the local degree of clustering within the unit cell) had higher variability in mineral treatments than organic ones. All modeled samples showed a bimodal throat size distribution (throat spread greater than 0.55), with higher values in mineral treatments (0.83) than in organic ones (e.g. 0.60 in farmyard manure). Even if the differences were not significant, the trend distinctly underlined a smaller throat spread at increasing levels of organic input. According to Lugato *et al.* (2009), organic carbon positively affects soil microporosity, reducing the widening effect towards small pores. This is also confirmed by the positive relationship ($p<0.05$) between SOC and ultramicropores (5-0.1μm). The effect of the different pore sizes on fast wetting is shown in Figure 1.

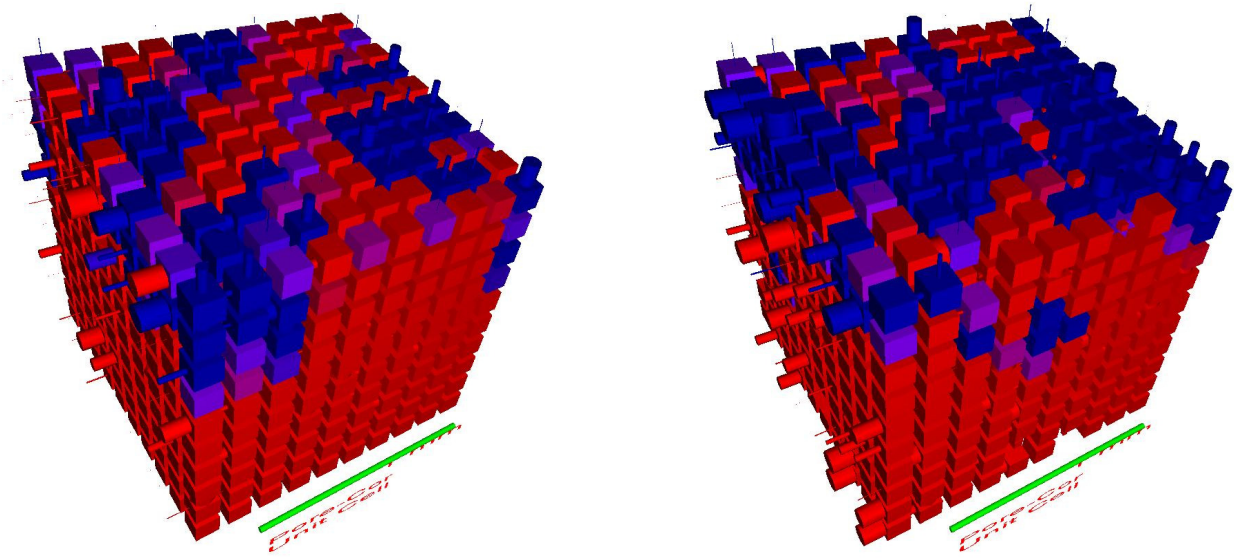

Figure 1. 3D modeled structures (unit cell) after 10 minutes of simulated fast wetting at unit pressure. Wetting rate is visibly lower with farmyard manure which has high microporosity (left) than in mineral fertilization + residues, with low microporosity (right). Colors of throats and pores vary from blue (completely full, 100%), to purple, to red (completely empty, 0%).

Principal Component Analysis (PCA) performed on 18 variables (aggregate stability indexes, SOC and humic fractions, porosity classes, Pore-Cor parameters) emphasized the essential role of water repellency on aggregate stabilization, clustering organic carbon content (OC), contact angle (WET) and high weight humic fraction with wet sieve analysis pre-treated with benzene (Figure 2). PCA also highlighted the positive effect of intrinsic permeability on breakdown mechanisms (higher slaking) due to the faster water infiltration in the aggregates (Figure 2). Correlation level seems to be the only Pore-Cor parameter affecting permeability (see cluster in Figure 2), most likely because it reduces the shielding effect of small throats around large pores.

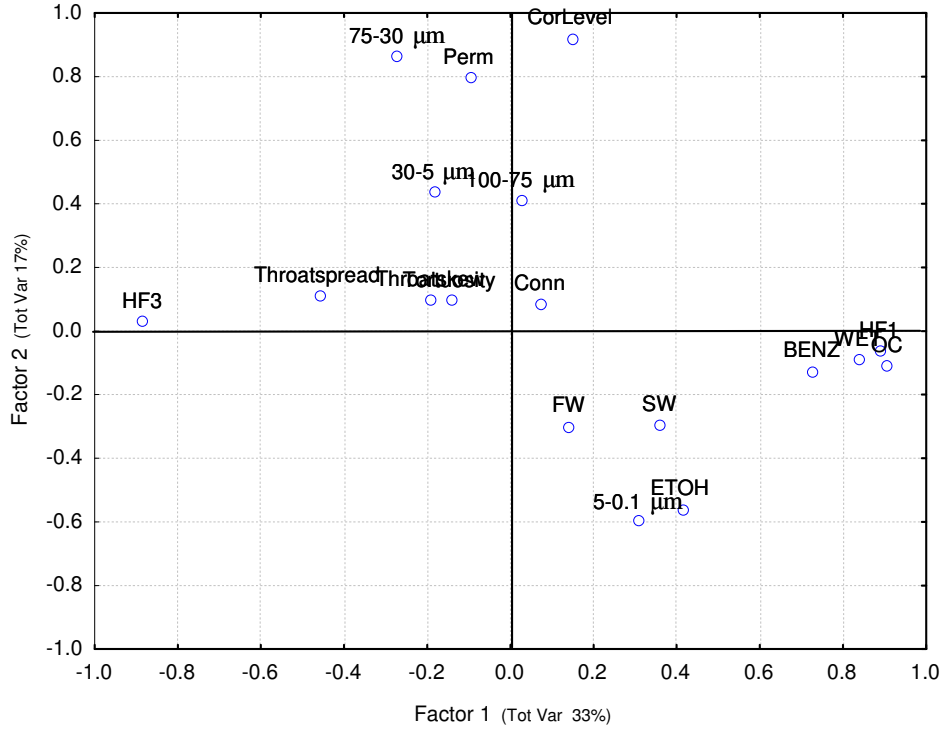

Figure 2. Factor loadings for 18 parameters selected for principal component analysis.

Conclusion

Physico-chemical and physical mechanisms affected aggregated stability in the experiments. The former were mainly due to the influence of organic carbon on soil wettability. Organic carbon also had a partial effect on the physical protection mechanisms influencing void size distribution. In this case ultramicropores were decisive in reducing fast wetting and therefore aggregate stability.

References

Chenu C (2000) Organic matter influence on clay wettability and soil aggregate stability. *Soil Science Society of America Journal* **64**, 1479-1486.

Diaz-Zorita M, Perfect E, Grove JH (2002) Disruptive methods for assessing soil structure. (Special Issue: Soil fragmentation and seedbed characterization). *Soil & Tillage Research* **64**, 3-22.

Holtham DAL, Matthews GP, Scholefield DS (2007) Measurement and simulation of void structure and hydraulic changes caused by root-induced soil structuring under white clover compared to ryegrass. *Geoderma* **142**, 142-151.

Lugato E, Morari F, Nardi S, Berti A, Giardini L (2009) Relationship between aggregate pore size distribution and organic-humic carbon in contrasting soils. *Soil & Tillage Research* **103**, 153-157.

Papadopoulos A (2009) Investigating the effects of organic and conventional management on soil aggregate stability using X-ray computed tomography. *European Journal of Soil Science* **60**, 360-368.

Price C, Matthews GP, Quinlan K, Sexton J, Matthews AGG (2009) A depth filtration model of straining within the void networks of stainless steel filters, *AIChE Journal*, DOI 10.1002/aic.11925.

Siebold A (1997) Capillary rise for thermodynamic characterization of solid particle surface. *Journal of Colloid and Interface Science* **186**, 60-70.

Suitability of electro-remediation for clean-up of PAH-contaminated clays

Ana T. Lima[A], J.P. Gustav Loch[A] and Katja Heister[B]

[A]Department of Earth Sciences, Geochemistry, Faculty of Geosciences, Utrecht University, PO Box 80.021, 3508 TA Utrecht, The Netherlands
[B]Department für Ökologie und Ökosystemmanagement, Technical University of Munich, D-85350 Freising-Weihenstephan, Germany

Abstract
The removal of PAH from soils, especially clayey soils, is a difficult task. Electro-osmosis is a technique which has been applied for the mobilization and cleanup of contaminants in clayey soils. The present focus is on the laboratory study of electroosmosis in two clayey materials: Wyoming bentonite and a contaminated peaty clay soil from Olst, the Netherlands. The results were quite disparate, but Olst soil experiment achieved a quite promising coefficient of electro-osmotic conductivity and a good base for field applications.

Key words
Electro-osmosis, clay, polycyclic aromatic hydrocarbons (PAH), clay weathering, remediation

Introduction

Clay layers act as semi permeable membranes, where water transport can be induced by a gradient in electrical potential. This flow type, termed electro-osmosis, is significant in materials of very low permeability, i.e. of hydraulic conductivity $\leq 1 \bullet 10^{-9}$ m /s(Mitchell 1993). Fluid flow by hydraulic force is impeded, whereas electro-osmosis is far more effective for creating fluid flow. The electro-osmotic volume flux of a solution (J_v in m/s) is expressed by the following phenomenological equation:

$$J_v = k_e \nabla(-E)$$

where E is the electrical potential (V), and k_e is the coefficient of electro-osmotic conductivity (m^2/V/s). The practical range for k_e of fine-grained soils is between $1 \bullet 10^{-9}$ and $1 \bullet 10^{-8}$ m^2/V/s.

Electro-osmosis has been applied for the mobilization and cleanup of contaminants in clayey soils (Pamucku and Wittle 1992; McNab and Ruiz 1999; Saichek and Reddy 2005) and may be a promising and cost-effective technology, in particular for the removal of hydrophobic organic contaminants (HOC) from clays. A common group of HOC in soils are the polycyclic aromatic hydrocarbons (PAH). Recent studies (Saichek and Reddy 2005) have focused on electro-remediation of PAH-contaminated clayey soils and emphasize the large enhancement of PAH-mobility by surfactants. Until now successful application of electro-osmosis for cleanup of contaminated sites has been scarce. In part this is due to insufficient knowledge of geochemical processes involved. Electro-osmosis in clay has resulted in unexpected side effects, e.g. acidification and subsequent clay mineral degradation and precipitate formation in the soil. At large voltages electrolysis of water occurs, causing production of H^+ and O_2(g) at the anode and of OH^- and H_2(g) at the cathode (Grundl and Michalski 1996; Chen and Murdoch 1999). In lime-deficient soils the resulting low pH front moves through the clay, meeting the hydroxyl-ions near the cathode. Since at low pH soil-Fe and -Al and contaminant heavy metals become mobile, they may precipitate as salts near the cathode and/or cause changing surface charge of the minerals, leading to declining electro-osmotic and hydraulic conductivities (Cherepy and Wildenschild 2003). We studied these effects of electro-osmosis in contaminated clay soil and clean Wyoming bentonite The soil is contaminated by PAH, which are hard to remove by hydraulic flow. The major objectives of this presentation are to quantify the magnitude of electro-osmosis in the selected clayey materials, to identify geochemical processes and effects of electro-osmosis in the solid and liquid fractions of the clay and to quantify the transport of polycyclic aromatic hydrocarbons from clays by means of electro-osmosis.

Methods

Two soils were studied in the laboratory: a pure Wyoming bentonite clay and a contaminated peaty clay soil, from a former asphalt factory terrain in Olst, the Netherlands. The pH of the bentonite clay and contaminated soil was determined in a standard 1:2.5 KCl suspension, using a glass electrode; cation exchange capacity (CEC) was quantified by the silver–thiourea method, and the exchangeable ions were determined by inductively coupled plasma mass spectrometry (ICP-MS); zeta-potential measurements were performed by Malvern Zetasizer Nano equipment; PAH were extracted according to Hartmann (1996) and quantified by gas chromatography–mass spectrometry (GC-MS); organic carbon and carbonate content were determined by TGA, using a Metler AT200.

1 – 6 August 2010, Brisbane, Australia. Published on DVD.

An experimental cell was designed for the study of electro-osmotic flow and geochemical side effects in clayey soils (Figure 1). The current density used to study the electroosmotic flow in bentonite was 0.005 A m^{-2}. For the contaminated soil, current density was increased to 0.1 A m^{-2}. The cylindrical cell, made of PVC, consists of a top and bottom part in between which a layer of dry bentonite or soil is fitted in a circular space of about 6 mm thick and 50 mm diameter. The resulting bulk density of the clay is 0.85 g cm^{-3}. On each side of this clay slab a porous stone is present of about 5 mm thick. On the interface of each porous stone with the clay, a gold wire is placed to function as electrode. By means of tygon tubing through the top and bottom of the cell the clay is in contact with equilibrium reservoirs containing influent and effluent aqueous solutions. Initial equilibrium composition of both reservoirs is 10 mmol/L NaCl in demineralized water. Water saturated clay is placed in the cell and subsequently brought in equilibrium with the reservoir solutions during 5 days. Each reservoir is connected to a capillary standpipe with an internal diameter of 2.93 mm. Thus inflow and outflow rates are monitored. The volumes of anolyte and catholyte reservoirs are approximately 10 ml each. The volume of the water-saturated bentonite is kept constant by means of clamp screws, inserted on the cell, to prevent it from swelling. Throughout the experiments both reservoirs are continuously recirculated.

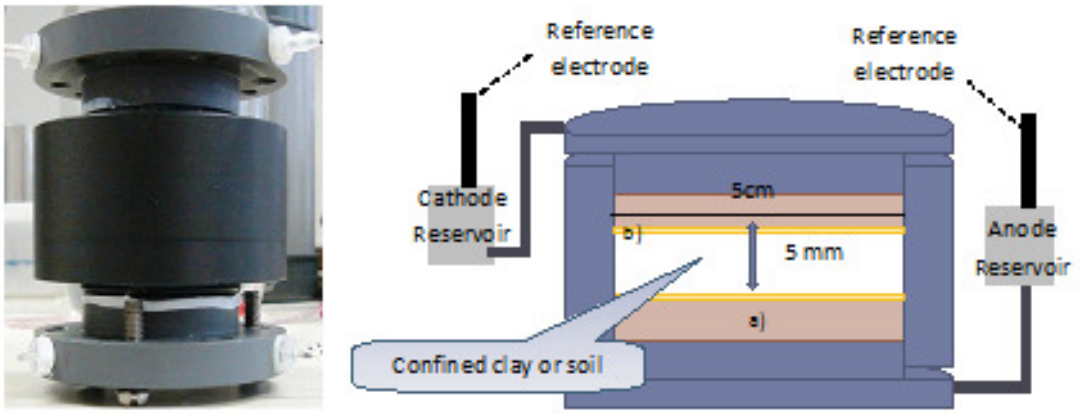

Figure 1. Experimental cell and schematic representation. a) porous stone; b) gold electrodes

During the electro-osmotic experiment the pH is monitored in both the anolyte and catholyte reservoirs. Furthermore the voltage difference between the electrodes is monitored as well as the reservoir voltages. Both electro-osmotic flow and pH are recorded for 34 days. After termination of electro-osmosis both reservoirs are sampled for analysis of PAH by GC-MS and the clay layer is cut in four slices perpendicular to the flow direction. .

Results and discussion

The two clayey materials are strongly different, in terms of contaminant content and composition. Table 1 shows some of the characteristic features of the materials. There is a noticeable difference in pH. Bentonite's higher pH and lime content strongly buffer the acidic front generated by the electric field. Figure 2 exemplifies the pH differences occurring during electroosmosis in Olst soil.

Table 1. Summary of the material characteristics; *CEC occupied by Ca,K, Mg, Na; ** in 0.01M NaCl solution

Parameter	Olst soil	Bentonite
pH	4.84	7.51
*CEC (cmol·kg)**	10.78 ± 0.263	18.69 ± 0.645
$CaCO_3$ (%)	n.d.	10.63
*Zeta potential (mV)***	-42.10	-52.8 ± 4,55
Organic carbon (%)	1.6	0.0064
PAH (mg/kg)	2751.5±113	n.d.

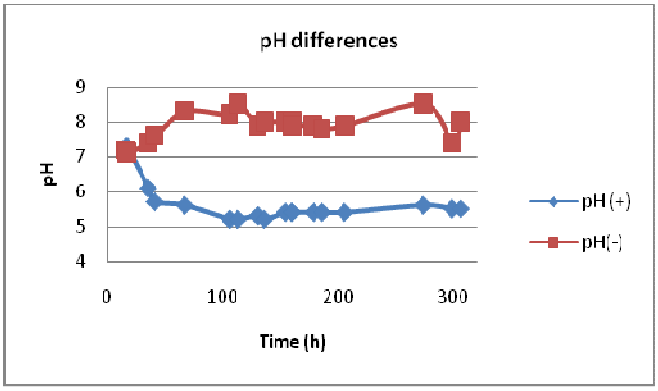

Figure 2. Development of the acidic front (pH +) from the anode, and alkaline front (pH -) from the cathode during electroosmosis in Olst soil.

The achieved electroosmotic flow significantly differed between the bentonite and the contaminated soil. After determining the total quantity of water transported to the cathode (or anode, depending on environmental conditions), the coefficient of electro-osmotic conductivity was determined. The bentonite experiment resulted in a $k_e = 4.2 \cdot 10^{-8}$ m^2 /V/s. Figure 3 shows the water flows during the electroosmotic experiment in the Olst soil. This experiment has a $k_e = 2.2 \cdot 10^{-8}$ cm^2 /V/s. This increase of electroosmosis is in the optimistic range of literature, which says that k_e for soil should be between $1 \cdot 10^{-8}$ and $1 \cdot 10^{-9}$ m^2 /V/s (Mitchell 1993). This value is quite promising for electroosmotic remediation in the field. Almost 300 ml have passed though a 5 mm soil plug during 12 days at a voltage gradient range of 0.58 to 8.0 V/cm.

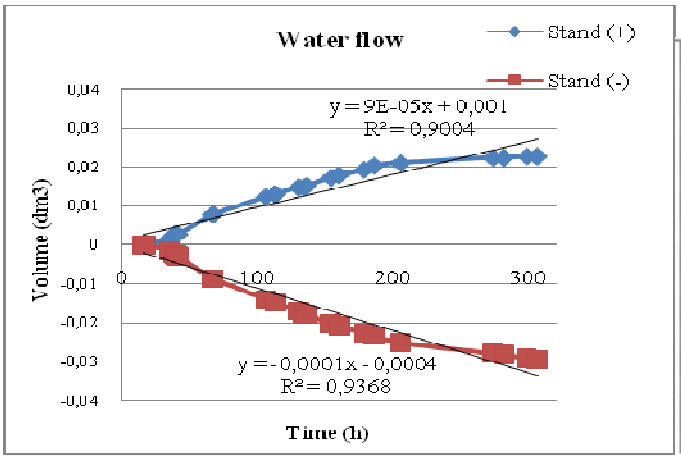

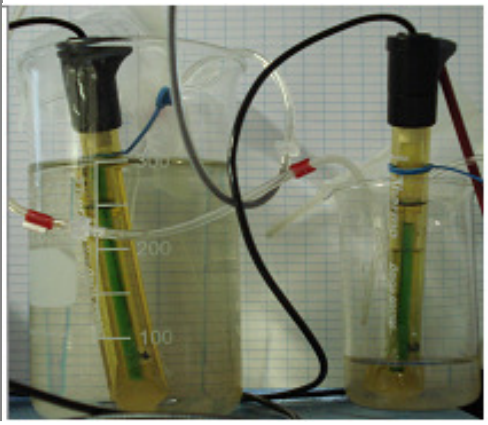

Figure 3. Graph presents the water flow during the experiment from cathode to anode, while the picture on the right shows the difference in water level after 12 days of experimental time

However, the water flow in the Olst soil was the opposite to the expected direction. Migration of water towards the anode is expected in specific cases, e.g. where the pH of the soil is below its zero point of charge. Minerals such as Fe_2O_3, $Fe(OH)_3$ and $Al(OH)_3$ have a positive surface charge in the pH-range below about 7 (e.g. Sposito 2008). FeS_2 was identified by Scanning Electron Microscopy (SEM) as a possible species existing in the Olst soil (Figure 4).

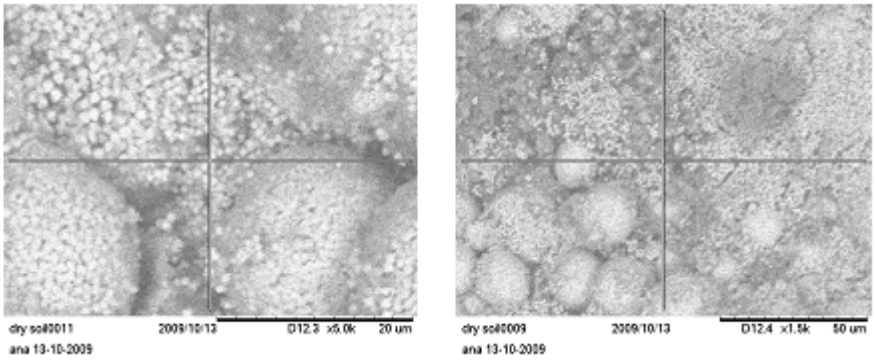

Figure 4. Scanning Electron Microscope images of Olst soil showing possible presence of FeS_2 species.

References

Chen J-L, Murdoch L (1999) Effects of electroosmosis on natural soil: field test. *Journal of Geotechical and Geoenvironmental Engineering* **125**, 1090-1098.

Cherepy NJ, Wildenschild D (2003) Electrolyte management for effective long-term electro-osmotic transport in low-permeability soils. *Environmental Science and Technology* **37**, 3024-3030.

Grundl T, Michalski P (1996) Electroosmotically driven water flow in sediments. *Water Research* **30**, 811-818.

Hartmann R (1996) Polycyclic aromatic hydrocarbons (PAHs) in forest soils: critical evaluation of a new analytical procedure. *International Journal of Environmental Analytical Chemistry* **62**, 161-173.

McNab WW, Ruiz R (1999) Evaluating the application of electro-osmosis to cleanup of fine-grained sediments in contaminant plume source areas at Lawrence Livermore National Laboratory. Lawrence Livermore National Laboratory. US Department of Energy, Environmental Protection Department. Oakland Operations Office, Cal. 94612

Mitchell JK (1993) 'Fundamentals of Soil Behavior', 2nd edn. (Wiley Interscience, New York).

Pamucku S, Wittle JK (1992) Electrokinetic removal of selected heavy metals from soil. *Environmental Progress* **11**, 241-250.

Saichek RE, Reddy KR (2005) Electrokinetically enhanced remediation of hydrophobic organic compounds in soils: A review. *Critical Reviews in Environmental Science and Technology* **35**, 115-192.

Sposito G (2008) 'The chemistry of soils', 2nd ed. (Oxford University Press, New York).

The dynamics of aggregate breakdown as a function of dispersive energy

ZhaoLong Zhu[A], Damien J. Field[B], Budiman Minasny[B]

[A] College of Mechanical and Electronic Engineering, Northwest A&F University, Yangling, Shaanxi, 712100, China. Email longmega@gmail.com
[B] Faculty of Agriculture, Food and Natural Resources, The University of Sydney, NSW, 2006 Australia. Email d.field@usyd.edu.au, b.minasny@usyd.edu.au

Abstract
This paper reports on the distribution of soil aggregates for Vertosols and Ferrosols as a function of the energy involved in dispersion, known as the dispersive energy. For Vertosols showing an aggregate hierarchy, the breakdown of aggregates is modelled using the aggregate liberation and dispersion characteristic curve indicating a stepwise breakdown of soil aggregates. Meanwhile, for Ferrosols, during dispersion the 2-50 μm aggregates increases monotonically with increasing dispersive energy, which is indicative of the direct release of silt and clay from the disruption of aggregates. The exponential decrease in ultrasonic power over time for the Ferrosols, as opposed to the prominent drop or steps in the curves for the Vertosols, confirms the lack of a prominent aggregate hierarchy.

Key Words
Aggregate hierarchy, dispersive energy, ultrasonics, comminution dynamics, soil structure, aggregate stability

Introduction
The interaction between soil particles has a significant effect on a range of soil physical properties such as stability, pore size distribution and erodibility. Its description has resulted in the development of concepts and models, which describes a system of aggregation as hierarchy or non-hierarchy. Determining the hierarchical order of soil aggregation has attracted considerable investigations.

But not all soils display the hierarchical system (Oades and Water 1991). In the work by Oades and Water (1991), the Oxisols were not found to have the hierarchical order. Golchin *et al.* (1998) states, the aggregate hierarchy may have universal application for soil where organic matter is the main stabilizing agent. Although this hierarchical model may hold for organically stabilized soil, the presence of individual hierarchical levels of the micro-aggregates and resulting macro-aggregates may vary in non-organic soil or those with greater clay contents.

Several methods have been developed to judge if aggregate hierarchy exists or not. Oades and Water (1991) pointed out that if aggregates are disrupted in a stepwise fashion then a hierarchy exists, but if aggregate breakdown results in direct release of silt and clay size materials there is not a hierarchical order. In the work of Field and Minasny (1999), aggregate liberation and dispersive curve (ALDC) is developed to describe the stepwise breakdown of an aggregate hierarchy for Vertosols subjected to ultrasonic agitation, which implies the hierarchy for Vertosols. Furthermore, the ratio between the rate constants in the ALDC model can be used to establish if there is a stepwise breakdown of larger aggregates, a criterion required to establish the presence of an aggregate hierarchy (Field *et al.,* 2006). The energy reported in the above work using ultrasonic instruments is not the energy required to disrupt soil aggregates but in terms of total energy applied as determined calorimetrically, and thus the aggregate breakdown dynamics under a certain dispersive energy is still not clear.

Recently, a technology for measuring soil aggregate dispersive energy using ultrasonic dispersion was proposed by Zhu *et al.* (2009a) , and its method was developed to characterize the aggregate dispersion characteristic curve (Zhu *et al.,* 2009b) . This paper furthers the method to take insight into aggregate breakdown dynamics by simultaneously modelling the dynamics of aggregates in a range of soil particle-sizes (<2 μm, 2–50 μm, 50–2000 μm) as the increasing dispersive energy of aggregates by ultrasonics.

Materials and Methods
Surface samples from the top 300 mm of soil from five sites throughout New South Wales, Australia, were collected for this study. The Vertosols were collected from Narrabri (149°32'E, 30°11'S) and the Namoi valley (149°28'E, 30°15'S). The Ferrosols were obtained from Wongarbon (148°40'E, 32°15'S) and Mt. Wilson (150°23'E, 33°30'S).

All the samples were air-dried and then gently ground and sieved to obtain a 0.25 to 1 mm fraction. The air-dry equivalent of 3g of oven-dry (105°C) soil was immersed in 30 ml de-ionized water in a 50 ml beaker. Samples were sonified in the beaker which was insulated with polystyrene materials. Ultrasound was applied via a conical probe, and each suspension was treated with ultrasound for various time periods up to dispersion. The effect of sonification on aggregate breakdown was determined by measuring the size distribution of aggregates and particles (<2 μm, 2–50 μm, 50–2000 μm) as described in Field *et al*. (2006). The dispersive energy is derived by measuring the total input power of the ultrasonic device (active power with a resolution of 0.05 W) and the energy used to heat the system (calorimetrically using platinum resistors with a resolution of 0.01°C). The procedure for deriving the dispersive energy is described in Zhu *et al.* (2009a).

Results and discussion

The dynamics of aggregate breakdown as a function of dispersive energy is summarized in the aggregate disruption characteristic curves (ADCC, particles 50–2000 μm), soil dispersion characteristic curves (SDCC, particles <2 μm) and aggregate liberation and subsequent dispersion curves (ALDC, aggregates 50–2000 μm) as presented in Figure 1.

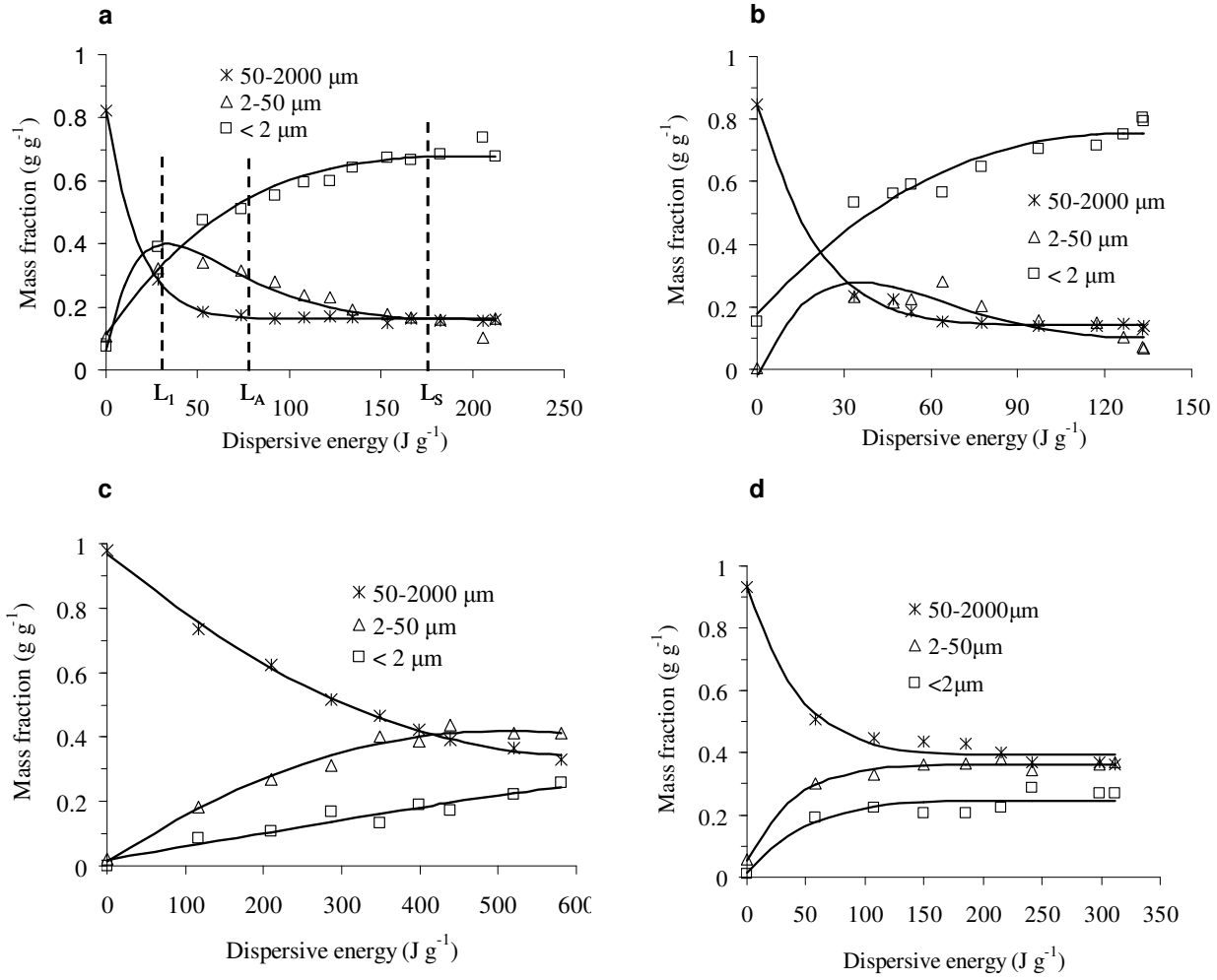

Figure 1. Particle-size distribution of soil related to dispersive energy for (a) Narrabri Vertosol, (b) Namoi Vertosol, (c) Mt. Wilson Ferrosol, and (d) Wongarbon Ferrosol

For the Vertosols (Figure 1a and b), the observed trends in the aggregate liberation and dispersion is consistent with Field *et al*. (2006), indicating that the rate of aggregate liberation is greater than dispersion until the energy input exceeds L_1, where the rate of dispersion exceeds aggregate liberation. By comparison the ALDC's for the two Ferrosol samples do not exhibit an observable inflection in the curve (L_1) characteristic of a non-hierarchical aggregated soil (Figure 1c, d). This implies that the breakdown of macro-aggregates in the Ferrosols results predominately in either the direct release of discrete particles or the redistribution of aggregates in and out of the particle size range at a similar rate. The notation of L_A and L_S on Figure 1a highlights when the all

macro-aggregates (50-2000 µm) are disrupted and all micro-aggregates (2-50 µm) are all dispersed, respectively.

The evolution of dispersive power as a function of input energy is illustrated in Figure 2 for all samples with the corresponding ALDC curve superimposed. The power used for successive sonifications to disperse the aggregates generally could be described as decreasing exponentially. An important point to notice is that the Vertosols (Figure 2a, b) exhibit prominent steps in the dispersive power resulting in discontinuities. These steps coincide with the condition when the 2-50 µm aggregates were completely dispersed. Meanwhile for the Ferrosols (Figure 2c, d) the dispersive power curve decreases exponentially, without any observable steps.

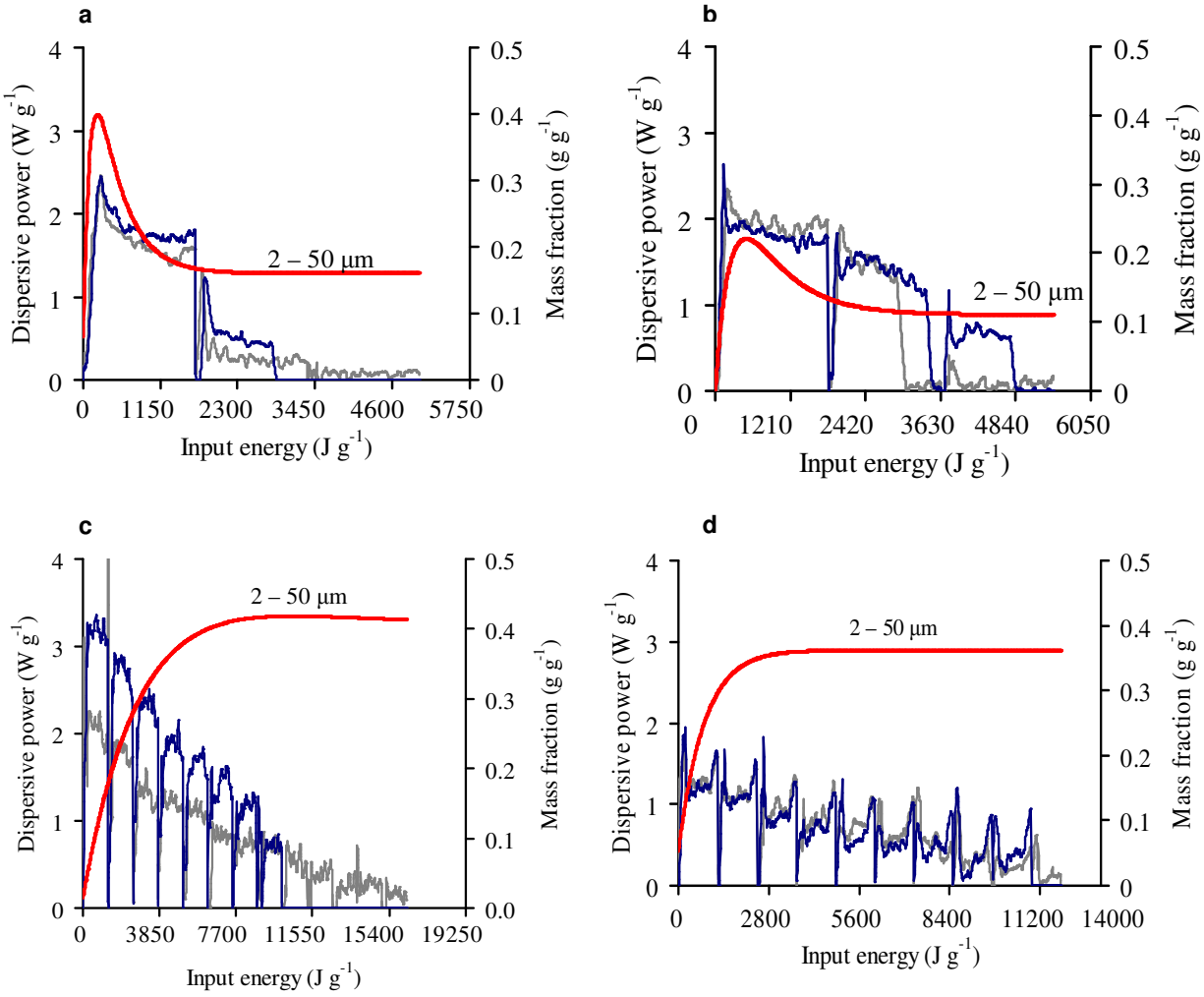

Figure 2. The relationship between dispersive power and input energy with the corresponding aggregate liberation and dispersion curve superimposed for (a) Narrabri Vertosol, (b) Namoi Vertosol, (c) Mt. Wilson Ferrosol, and (d) Wongarbon Ferrosol.

Conclusion

This work investigates the hierarchy of soil aggregates by modelling their breakdown under a certain dispersive energy. For the Vertosols and Ferrosols used in this study, the relationship between dispersive energy and input energy is not linear. The Vertosols show hierarchy for that the aggregate liberation and subsequently dispersion under dispersive energy exists indicating the aggregates break down in a stepwise fashion under ultrasonic agitation. As for the Ferrosols, they don't have the character above because their aggregates directly release out silt and clay when broke down under dispersive energy.

Acknowledgements

We wish to thank the financial support of the International Program Development Fund, the University of Sydney, and also acknowledge the Northwest A&F University and China Agricultral University for promoting our cooperation research.

References

Field DJ, Minasny B (1999) A description of aggregate liberation and dispersion in A horizons of Australian Vertisols by ultrasonic agitation. *Geoderma* **91**(1-2)**,** 11-26.

Field DJ, Minasny B, Gaggin M (2006) Modelling aggregate liberation and dispersion of three soil types exposed to ultrasonic agitation. *Australian Journal of Soil Research* **44**(5)**,** 497-502.

Field DJ, Sullivan LA, Cattle SR, Koppi AJ (2004) Comparison of four methods for liberating various aggregate fractions in Vertosols to study their morphology. *Australian Journal of Soil Research* **42**(1)**,** 29-37.

Golchin A, Baldock JA, Oades JM (1998) A model linking organic matter decomposition, chemistry, and aggregate dynamics. In ' Soil Processes and Carbon Cycling, Advances in Soil Science Series'. (Eds R Lal, JM Kimble, RF Follet, BA Stewart) pp. 245-266. (CRC Press: Boca Raton, Florida).

Oades JM, Waters AG (1991) Aggregate hierarchy in soils. *Australian Journal of Soil Research* **29**(6)**,** 815-828.

Zhu ZL, Minasny B, Field DJ (2009a) Adapting technology for measuring soil aggregate dispersive energy using ultrasonic dispersion. *Biosystems Engineering* **104**(2), 258-265.

Zhu ZL, Minasny B, Field DJ (2009b) Measurement of aggregate bond energy using ultrasonic dispersion. *European Journal of Soil Science* **60**(4), 695-705.

The effect of time-variable soil hydraulic properties in soil water simulations

Andreas Schwen[A], Gernot Bodner[B] and Willibald Loiskandl[A]

[A]Institute of Hydraulics and Rural Water Management, University of Natural Resources and Applied Life Sciences (BOKU), Vienna, Austria, Email andreas.schwen@boku.ac.at
[B]Institute of Agronomy and Plant Breeding, University of Natural Resources and Applied Life Sciences (BOKU), Vienna, Austria.

Abstract
Modeling soil water dynamics requires an accurate description of soil hydraulic properties, i.e. the retention and hydraulic conductivity functions. Generally, these functions are assumed to be unchanged over time in most simulation studies. However, there is extensive empirical evidence that soil hydraulic properties are subject to temporal changes. In this paper, we implemented temporal changes in the soil hydraulic properties in a Richards' equation simulation of soil water dynamics. Based on repeated measurement data of the top soil water retention curve, we compared the impact of using constant vs. temporally changing hydraulic functions on water flow simulation for different tillage methods. We observed distinct differences in the soil water content between the simulations for all tillage methods. The results show the remarkable effect of time-variable retention parameters on the soil water dynamics for tilled and non-tilled top soils.

Key Words
Soil hydraulic properties, temporal variability, soil tillage, pore-size distribution

Introduction

For many applied questions in the fields of crop production and agronomy, soil water dynamics are of fundamental importance. Modeling can be a valuable tool to optimize its management (Roger-Estrade *et al.* 2009). However, such soil water modeling requires an accurate description of soil hydraulic properties, i.e. the soil water retention characteristics (WRC) and hydraulic conductivity functions. Generally, these constitutive functions are assumed to be unchanged over time in most simulation studies (Mubarak *et al.* 2009). However, there is extensive empirical evidence that soil hydraulic properties are subject to temporal changes particularly in the near-saturated range where soil structure essentially influences water flow characteristics (Alletto and Coquet 2009; Daraghmeh *et al.* 2008; Or *et al.* 2000). The structure of soil top layers is subject to changes during time, caused by wetting and drying, solution composition, agricultural operations, and biological activity. Soil tillage is used to improve soil structural properties by changing the soil pore-size distribution (PSD). Since these modifications are quite unstable over time, the PSD decreases after tillage (Leij *et al.* 2002; Or *et al.* 2000). This effect should be largest for conventional tillage (CT), where the soil is ploughed after harvest every year.

Many functions for expressing the WRC have been published (e.g. Brooks and Corey 1964; Van Genuchten 1978). They are compatible with models that describe the relative hydraulic conductivity of soils (e.g. Burdine 1953; Mualem 1976). However, most of these models are empirical curve-fitting equations and do not base on physical fundamentals (Kosugi 1994). In contrast, the soil retention model of Kosugi (1994) bases directly on the lognormal distribution of the soil pore-size distribution (PSD) as described by the Laplace-Young equation (Leij *et al.* 2002). Recent publications point out that the demand for a new model approach accounts for the temporal variability of the WRC (Alletto and Coquet 2009; Mubarak *et al.* 2009). In this study, we set up a water flow model that accounts for time variable retention characteristics in the uppermost soil layer. The effect of temporal variability of the WRC on soil water dynamics, as expressed by the volumetric water content, was tested and evaluated for different tillage systems.

Governing equations

Water flow in unsaturated or partly saturated soils can be described with the Richards' equation (Richards 1931):

$$C\frac{\partial h}{\partial t} = \frac{\partial}{\partial z}\left(K\frac{\partial h}{\partial z} - K\right) \quad (1)$$

where h is the soil water pressure head or water potential (dimension L), t the time (T), z the soil depth (L), K is the hydraulic conductivity (L/T) and C is the soil water capacity (/L). C is defined by the slope of the WRC ($d\theta/dh$), where θ is the volumetric water content of the soil (L^3/L^3). In the present study, the WRC in the upper soil is described by Kosugi's lognormal retention model (Kosugi 1994):

$$\theta(h)=\begin{cases}\left(\frac{1}{2}\operatorname{erfc}\left[\frac{\ln(h/\psi)}{\sqrt{2}\sigma}\right]+\theta_r\right)\left(\theta_s-\theta_r\right) & (h<0)\\ \theta_s & (h\geq 0)\end{cases} \quad (2)$$

where ψ (L) and σ are parameters that change the shape of the retention curve, θ_r is the residual volumetric water content and θ_s is the water content at saturation. Applying Mualem's model, the unsaturated or relative hydraulic conductivity K_r is defined as follows (Kosugi 1994):

$$K_r(\theta)=\begin{cases}K_s\sqrt{S_e}\cdot\left(\frac{1}{2}\right)^2\left[\operatorname{erfc}\left(\frac{\ln(h/\psi)}{\sqrt{2}\sigma}+\frac{\sigma}{\sqrt{2}}\right)\right]^2 & (h<0)\\ K_s & (h\geq 0)\end{cases} \quad (3)$$

According to Leij *et al.* (2002), the PSD can be obtained with a similar equation:

$$f(r)=\frac{\left(\theta_s-\theta_r\right)}{\sqrt{2\pi}\sigma r}\exp-\left(\frac{\ln\left(r/r_m\right)}{\sqrt{2}\sigma}\right)^2 \quad (4)$$

where f (/L) is the frequency of a certain pore radius r (L). r_m (L: µm) is the median pore radius that can be calculated from ψ (hPa) by $r_m = 1490/\psi \exp(\sigma^2)$ (Leij *et al.* 2002).

Methods

Field measurements were obtained on an arable field near the village of Raasdorf, Lower Austria, 20 km east of the city of Vienna. At this agricultural investigation site, the effects of different tillage methods, in specific conventional tillage (CT), reduced tillage (RT), and no-tillage (NT), were observed by our working group. For the different tillage systems the near-saturated hydraulic properties of the uppermost soil layer (0–15 cm) have been determined by infiltration measurements with tension-disc infiltrometers (Soil Measurement Systems, USA; diameter of the disc: 20 cm). Three replicate measurements were conducted for every type of tillage several times between August 2008 and July 2009 (Table 1). The adjusted hydraulic pressure heads were −10 cm, −4 cm, −1 cm, and 0 cm. Additional data points of the retention curve (0.2 – 3.0 bar) were determined by steel core samples. The software HYDRUS 2D/3D (Šimůnek *et al.* 2006) was used to fit the retention model of Kosugi (1994) inversely to the infiltration measurements. The resulting parameters were used to calculate the PSD for every time of measurement. The lower soil horizons were sampled with steel cores (volume: 200 cm^3) in depths of 40 cm and 70 cm in July 2009. The WRCs of the subsoil layers were determined in the laboratory with a low pressure plate extractor (Soil Moisture Inc., USA) at pressure heads of 0.2, 0.5, 1.0, 2.0 and 3.0 bar. The program RETC was used to fit the parameter of the Van Genuchten retention model (1978) to the observed data. For calibration of the model, data of the soil volumetric water content measured directly in the field were available over the modelled time.

Numerical model

Model geometry

The Richards' equation was solved numerically using COMSOL Multiphysics (COMSOL AB) with MATLAB (The MathWorks Inc., USA). The 2D model geometry was defined by a rectangle soil column with a width of 1.00 m and a depth of 1.20 m. According to the observed soil horizons in the field, the geometry was divided into three layers: the upper soil from 0 to 0.15 m (A-horizon, WRC determined by infiltration measurements), the lower part of the A-horizon between 0.15 m and 0.50 m, and the subsoil from 0.50 m to 1.20 m (C-horizon). The soil hydraulic properties of the lower layers were defined by the Van Genuchten retention model. Since the time-dependent effect of tillage was expected to be negligible, we set the hydraulic properties to be constant in the lower soil horizons.

Initial and boundary conditions

The model geometry was laterally confined by no-flux boundaries. The lower boundary was defined by a free drainage condition. On the basis of measured precipitation data, we used the empirical method of Allen *et al.* (1998) to calculate the potential evaporation and transpiration. The precipitation and the evaporation, the latter reduced by a pressure-head dependent reduction function, were applied to the model as upper boundary condition. Transpiration was implemented in a sink term using a growth function and a reduction function according to Feddes *et al.* (2001).

Initially, the hydraulic pressure head h_0 was set to −0.5 m for the whole model geometry. To account for the WRC changing with time in the upper soil layer, adequate functions were fitted to the measured values for the Kosugi retention model parameters ψ and σ, the saturated hydraulic conductivity K_s, and the soil water content at saturation θ_s (Table 1). For the simulations with constant hydraulic properties, median values for these parameters were used.

The accuracy of the implementation of the evapotranspiration was evaluated by a comparative simulation using HYDRUS 2D/3D. The model was calibrated with measured soil water contents. Calculations were made with constant and time variable retention parameters of the upper soil layer for all observed tillage systems.

Table 1. Retention data of the upper soil layer as observed by infiltration measurements for the different tillage methods (CT: conventional tillage, RT: reduced tillage, NT: no-tillage). The date of the infiltration measurement, the day in the simulation, the volumetric water content at saturation θ_s, the residual water content θ_s, the saturated hydraulic conductivity K_s, the parameters of the Kosugi retention model, ψ and σ, and the median pore radius r_m are listed.

tillage	date	day	θ_s (m^3 m^{-3})	θ_r (m^3 m^{-3})	K_s (m d^{-1})	ψ (kPa)	σ (-)	r_m (µm)
CT	2008-08-01	1	0.51	0.11	2.29	5.64	1.79	1.07
	2008-10-23	84	0.51	0.11	2.78	2.12	1.34	11.76
	2008-12-03	125	0.50	0.11	1.56	3.12	1.55	4.38
	2009-04-01	244	0.43	0.11	1.00	4.13	1.68	2.13
	2009-07-21	355	0.48	0.11	2.18	3.64	1.77	1.79
RT	2008-08-01	1	0.53	0.11	1.14	0.93	1.19	39.11
	2008-10-23	84	0.45	0.11	1.56	4.97	1.75	1.40
	2008-12-03	125	0.50	0.11	0.33	2.93	1.61	3.83
	2009-04-01	244	0.41	0.11	0.23	2.80	1.37	8.23
	2009-07-21	355	0.49	0.11	0.68	2.80	1.59	4.27
NT	2008-08-01	1	0.47	0.11	0.61	3.63	1.73	2.09
	2008-10-23	84	0.43	0.11	0.12	3.44	1.54	4.04
	2008-12-03	125	0.46	0.11	0.05	3.76	1.29	7.56
	2009-04-01	244	0.43	0.11	0.10	3.95	1.44	4.77
	2009-07-21	355	0.43	0.11	0.11	3.43	1.04	14.61

Results and discussion

Evolution of the pore-size distribution

The evolution of the PSD determined by the infiltration measurements showed distinct differences between the applied tillage methods. As proposed by Leij *et al.* (2002), the PSD at the CT site shifted towards smaller pore sizes after mouldboard tillage. Here, the change of the PSD is mostly dominated by the agricultural operation. Compared to the other tillage methods, a large total porosity exists, as it is also expressed by the integral of the PSD, θ_s (Table 1). On the other side, the determined PSDs for RT and NT show a smaller shift during time and a smaller total porosity. Moreover, the shift of the PSD is slightly towards larger pores. This effect might be caused by biological activities, such as earthworm burrows and plant root development (D'Haene *et al.* 2008).

Water dynamics with constant vs. time-variable hydraulic properties

The results show distinct differences between the simulations for all methods of tillage. In autumn and winter 2009, we observed the most obvious differences in the soil water content, whereas in the later part of the simulation, these differences decreased. We trace this back to high volumetric water contents in late autumn and winter in the upper soil, provided by a low evapotranspiration. This result is in agreement with the findings of Daraghmeh *et al.* (2008). The results of the CT simulations show the effect of ploughing in mid-October impressively, as the retention potential decreases shortly after it. Noticeable differences for the other tillage methods occur mainly at high precipitation events and may be traced back to an underestimation of biological induced macropore-flow in the simulations with constant soil retention properties.

Conclusion and perspective

As classical simulations of the soil water dynamics do not account for time-variable soil retention properties, we implemented a model approach that enables the flexible definition of these important control quantities. The implementation of the Kosugi retention model allowed the definition of the soil retention properties strongly connected to the PSD of the soil. However, until now we used only empirical fitted functions for the time-variable retention parameters. Recently, we began work on the adaptation of a suitable PSD-evolution model, as proposed by Or *et al.* (2000).

References

Allen RG, Pereira LS, Raes D, Smith M (1998) 'Crop evapotranspiration – Guidelines for computing crop water requirements'. FAO Irrigation and drainage paper 56, (Food and Agriculture Organization of the United Nations: Rome).

Alletto L, Coquet Y (2009) Temporal and spatial variability of soil bulk density and near-saturated hydraulic conductivity under two contrasted tillage management systems. *Geoderma* **152**, 85-94.

Brooks RH, Corey AT (1964) 'Hydraulic Properties of Porous Media'. *Hydrological Paper* **3**. (Colorado State Univ: Fort Collins, CO).

Burdine NT (1953) Relative permeability calculation from size distribution data. *Transactions of the American Institute of Mining and Metallurgical Engineering* **198**, 71-78.

Daraghmeh OA, Jensen JR, Petersen CT (2008) Near-Saturated Hydraulic Properties in the Surface Layer of a Sandy Loam Soil under Conventional and Reduced Tillage. *Soil Science Society of America Journal* **72**, 1728-1737.

D'Haene K, Vermang J, Cornelis WM, Leroy BLM, Schiettecatte W, De Neve S, Gabriels D, Hofman G (2008) Reduced tillage effects on physical properties of silt loam soils growing root crops. *Soil and Tillage Research* **99**, 279-290.

Feddes RA, Hoff H, Bruen M, Dawson T, de Rosnay P, Dirmeyer O, Jackson RB, Kabat P, Kleidon A, Lilly A, Pitman AJ (2001) Modeling root water uptake in hydrological and climate models. *Bulletin of the American Meteorological Society* **82**, 2797-2809.

Kosugi K (1994) Three-parameter lognormal distribution model for soil water retention. *Water Resources Research* **30**, 891-901.

Leij FJ, Ghezzehei TA, Or D (2002) Modeling the dynamics of the soil pore-size distribution. *Soil and Tillage Research* **64**, 61-78.

Mualem Y (1976) A new model for predicting the hydraulic conductivity of unsaturated porous media. *Water Resources Research* **12**, 513-522.

Mubarak I, Mailhol JC, Angulo-Jaramillo R, Ruelle P, Boivin P, Khaledian M (2009) Temporal variability in soil hydraulic properties under drip irrigation. *Geoderma* **150**, 158-165.

Or D, Leij FJ, Snyder V, Ghezzehei TA (2000) Stochastic model for posttillage soil space evolution. *Water Resources Research* **36**, 1641-1652.

Richards LA (1931) Capillary conduction of liquids through porous mediums. *Physics* **1**, 18-33.

Roger-Estrade J, Richard G, Dexter AR, Boizard H, de Tourdonnet S, Bertrand M, Caneill J (2009) Integration of soil structure variations with time and space into models for crop management. A review. *Agronomy for Sustainable Development* **29**, 135-142.

Šimůnek J, van Genuchten MT, Šejna M (2006) 'The HYDRUS Software Package for Simulating the Two- and Three-Dimensional Movement of Water, Heat, and Multiple Solutes in Variably-Saturated Media. Version 1.10'. (PC-Progress: Prague).

Van Genuchten MT (1978) 'Mass transport in saturated-unsaturated media: one-dimensional solutions'. Research Report No. 78-WR-11. (Water Resources Program, Princeton University: Princeton, NJ).

The impact of orchard management on macro-pore topology and function

Markus Deurer[A], Dimitri Grinev[B], Iain Young[C], Brent Clothier[A] and Karin Müller[D]

[A]Production Footprints, The NZ Plant & Food Research, Palmerston North, New Zealand, Email Markus.Deurer@plantandfood.co.nz
[B]SIMBIOS Centre, University of Abertay, Dundee, Scotland.
[C]School of Environmental and Rural Science, University of New England, Australia.
[D]Production Footprints, The NZ Plant & Food Research, Ruakura, Hamilton, New Zealand.

Abstract
We analysed the long-term effect of three common orchard management practices on the soil macropore structure and function: (1) Grass sward and a regular application of compost in the tree row; (2) Soil compaction by tractor wheels in the grassed alleys; (3) Regular application of herbicides in the tree row. We focused on the top 50 mm topsoil of the tree row and under the wheel track in the alley of an organic orchard (Practice 1, 2) and of the tree row in an adjacent conventional apple orchard (Practice 3). Both orchards had the same age, soil type, texture and previous land use. After 12 years the topsoils of the organic orchard had about 30% more soil organic carbon (SOC) sequestered than the topsoils in the tree row of the conventional orchard. We quantified the macro-pore structure (macro-pores = pores > 0.3 mm) of nine undisturbed soil columns (43 mm long, 20 x 17 mm in the plane) for each practice using 3D X-ray computed tomography. The macro-porosity under Practice 1 was significantly greater, with 7.5 ± 2.1%, than that under Practice 2, with 3.6 ± 1.1% and under Practice 3, with 2.4 ± 0.5%. The connectivity of macro-pores tended to be greatest under Practice 1, but this was not statistically significant. The macro-pores under Practice 2 had a significantly greater connectivity than under Practice 3. We simulated the diffusion through the macro-pores of aggregate-scale segments of the columns. The relative diffusion coefficients were similar under Practice 1 and 2, with 0.024 ± 0.008, and 0.015 ± 0.008, respectively, and were significantly greater than under Practice 3, with 0.0056 ± 0.0009. We hypothesize that a higher relative diffusion coefficient at the aggregate scale (e.g. Practice 1 and 2 versus 3) would lead to a lower N_2O production and emission in a wet soil. We conclude that soil carbon management in the tree row of apple orchards like using grass swards and compost, leads to more macro-pores and a better gas exchange and probably less N_2O production and emission under wet conditions compared to a tree row that regularly receives herbicides. Although the compacted soil under the wheel track had less macropores than in the grassed tree row, the gas exchange under wet conditions was still similar.

Key Words
3D X-ray CT, macro-porosity, connectivity, diffusion, soil carbon management.

Introduction
Different definitions exist for the size of macro-pores, to distinguish them from other pores. Following others we defined macro-pores as pores with a diameter larger than 0.3 mm. Macro-pores are important for several soil processes and functions. For example, macro-pores can trigger preferential flow, the fast direct transfer of contaminants such as herbicides from the soil surface to the groundwater. The macro-pore structure of the top 50 mm governs the gas exchange between the soil and the atmosphere under wet conditions. In the case of nitrous oxide (N_2O), the top 50 mm of the soil additionally were shown to be the most active zone for N_2O production (Clayton *et al.* 1994). In most soils N_2O is mainly produced as an intermediate product of denitrification which is promoted by low O_2 concentrations that occur typically in wet soils. Nitrous oxide emissions from soils account for 70% of total N_2O emissions, which are estimated to be responsible for approximately 5% of anticipated global warming. In structured soils under wet conditions, N_2O is produced in the micro-pores of soil. The O_2 concentration around the aggregates is the most important boundary condition influencing N_2O production within aggregates (Sexstone *et al.* 1985; Tiedje 1988). Near saturation, only the soil's macro-pores are filled with air, promoting rapid exchange of O_2. Atmospheric O_2 is exchanged over their interfacial areas with adjacent structures. Therefore, while the N_2O production happens at the scale of micro-pores within aggregates, it is regulated by the O_2 exchange processes at the scale of the soil's macro-pore network. Consequently, a difference in macro-porosities will modify the gas exchange between the soil and the atmosphere. For example, increasing the macro-porosity of wet soils results in greater rates of O_2 exchange with the atmosphere, and as a consequence the production and, therefore, the emission of N_2O may be reduced. Several field experiments have reported reduced N_2O emissions from soils containing comparably larger macro-porosities. We hypothesize that the emission of N_2O from soils is an environmental risk that, *inter alia,* depends on the soil's macro-pore structure.

1 – 6 August 2010, Brisbane, Australia. Published on DVD.

We compared the soil's macro-pore structures and function of the top five centimetres of soil subject to three different orchard management practices. We addressed two questions: 1) Are the soil's macro-pore structures under three different orchard management practices significantly different? 2) Is the gas exchange around aggregates under wet conditions significantly different under the three different management practices?

Methods

Study sites

We selected a pair of soils under apple orchards in Hawke's Bay (North Island of New Zealand). The topsoils are of alluvial origin, and have a silt loam texture. One of the sites contained the grassed tree rows and alleys of an organic orchard (Practice 1 and 2) and the other site had the herbicided tree rows of a neighbouring integrated apple production system (Practice 3). Both orchard systems are 12 years old. Green-waste compost has been applied to the topsoil of the tree rows of the organic system once a year at a rate of 5 to 10 t ha^{-1}. A 0.5-m wide strip under the trees has been kept vegetation-free by regular herbicide applications in the integrated system.

Analysis of the soil's 3D macropore structure

1. Sample selection and preparation: We took three undisturbed columns (70 mm diameter, 100 mm length) from each of the tree orchard management practices. The top of the columns were level with the soil surface and the main axis of the columns was perpendicular to the soil surface. Prior to the X-ray imaging we carefully cut each soil column into four sub-columns of equal dimensions. Three out of the four sub-columns of each column were randomly selected for X-ray imaging.

2. Three-dimensional X-ray Computed Tomography: For X-ray tomography imaging we used a Metris X-tek Benchtop CT system (Metris X-tek Systems Ltd., Hertfordshire, United Kingdom) at SIMBIOS Centre of the University of Abertay (Dundee, Scotland) with the 160 kV X-ray source and a 12-bit CCD camera. The three-dimensional images of attenuation coefficients with the isotropic voxel size of 86 µm were translated into a continuous stack of two-dimensional 8-bit TIFF images using the software VGStudio MAX 1.2.1 (Volume Graphics GmbH, Heidelberg, Germany). Each image slice of the stack had the thickness of 86 µm and an in-plane resolution of 86 x 86 µm.

3. Digital image processing and analysis: We conducted the digital image processing and analysis using the public domain software ImageJ (developed by W. Rasband at the National Institute of Health, USA; http://rsb.info.nih.gov/ij/), the soil-specific package of plugins for ImageJ, SCAMP, that was developed by SIMBIOS (University of Abertay, Dundee, Scotland), and a package of C-functions for image analysis QuantIM, Version 4 (Vogel 2008). We visualized the three-dimensional macro-pore structures with the software OpenDX (open source software version of IBM's Visualization Data Explorer; http://www.opendx.org/index2.php).

The image processing and analysis consisted of four steps. Firstly, we cropped the three-dimensional image data set of each sub-column to a length of 43 mm and a dimension of 20 x 17 mm in the plane. Secondly, we transformed the stack of 8-bit TIFF slices to a stack of binary images (black = pore space; white = solid phase) using a bi-level segmentation algorithm. Next, we removed all pores smaller than 344 µm in diameter from the binary images, limiting our analysis to macro-pores larger than 0.34 mm. Finally, we quantified the macro-pore volume density (i.e. macro-porosity) and the three-dimensional connectivity of macro-pores. The latter was quantified with the volumetric Euler-Poincaré characteristic for pores with a minimum pore diameter of 0.3 mm. The higher the value of the volumetric Euler-Poincaré characteristic the smaller is the connectivity of the respective pore system. For convenience we use the term 'Euler number' to denote the value of the volumetric Euler-Poincaré characteristic.

Simulation of gas diffusion through a soil's macro-pore network

We simulated the gas diffusion through segments of the three-dimensional macro-pore network and derived gas diffusion coefficients for the measured macro-pore structures. The segments were 4.3 mm long and had the dimension of 20 x 17 mm in the plane. Our objective was to analyze the gas diffusion in the macro-pores around soil aggregates. The mean weighted diameter (MWD) of water-stable aggregates in the 0-0.1 m depth of the tree rows of the organic and integrated orchard system was 1.8 mm and 1.3 mm, respectively (Deurer *et al.* 2008). Therefore, the 4.3 mm length of each segment was at least twice the MWD of the aggregates of the orchard soils, and we assume represented the relevant dimensions of gas exchange around aggregates. The

package QuantIM (Vogel 2008) contains an algorithm for simulating gas diffusion through a continuous stack of two-dimensional binary images. For the simulation we assumed the following set of initial and boundary conditions. At the top of the segment the concentration was fixed to a constant value while the concentration at the bottom of the segment was set to zero throughout the simulation. The initial concentration within the pore space of the segment was set to zero. The vertical boundaries of the segment were assumed to be impermeable to gas. Once the gas flow at the bottom of the sample reached an asymptotic state, the relative apparent diffusion coefficient D_r [-] was calculated by relating the simulated asymptotic diffusive flow through the macro-pore space at the bottom of the segment to the diffusive flow through the same segment that now consisted only of free air (= 100% porosity).

Results

We analysed how different orchard management practices impact on the macro-pore structure of topsoils. The Practice 1 of using a grass sward and the regular application of compost represents a typical soil carbon management that is known to increase both soil carbon sequestration and soil health and is used in organic orchard systems (Deurer *et al.* 2008). The Practice 2 represents the typical impact of soil compaction by long-term tractor traffic in a grassed alley that occurs both in organic and integrated orchard systems. The Practice 3 represents the lack of any soil carbon management as is typical for the tree rows of most integrated apple orchard systems. We reconstructed the detailed macro-pore networks in three dimensions with X-ray CT (Figure 1). Under Practice 1, with 7.5 ± 2.1 Vol.%, the macro-porosity was significantly ($P < 0.05$) higher than under Practice 2 with 3.6 ± 1.1 Vol.%, and under Practice 3 with 2.4 ± 0.5 Vol.% (Table 1). Other studies with a similar definition of macro-pores reported similar macro-porosities ranging from 1.3 to 14 Vol.% for fine-textured top-soils under arable or pastoral land use. The connectivity tended to be highest under Practice 1 (Table 1). However, this was not statistically significant as the variability of the Euler number under Practice 1 was extremely high (Table 1). Practice 2 limited macro-porosity less than did Practice 3 (Table 1). Our range of Euler numbers for pores with a diameter larger 0.3 mm agreed well with other comparable studies.

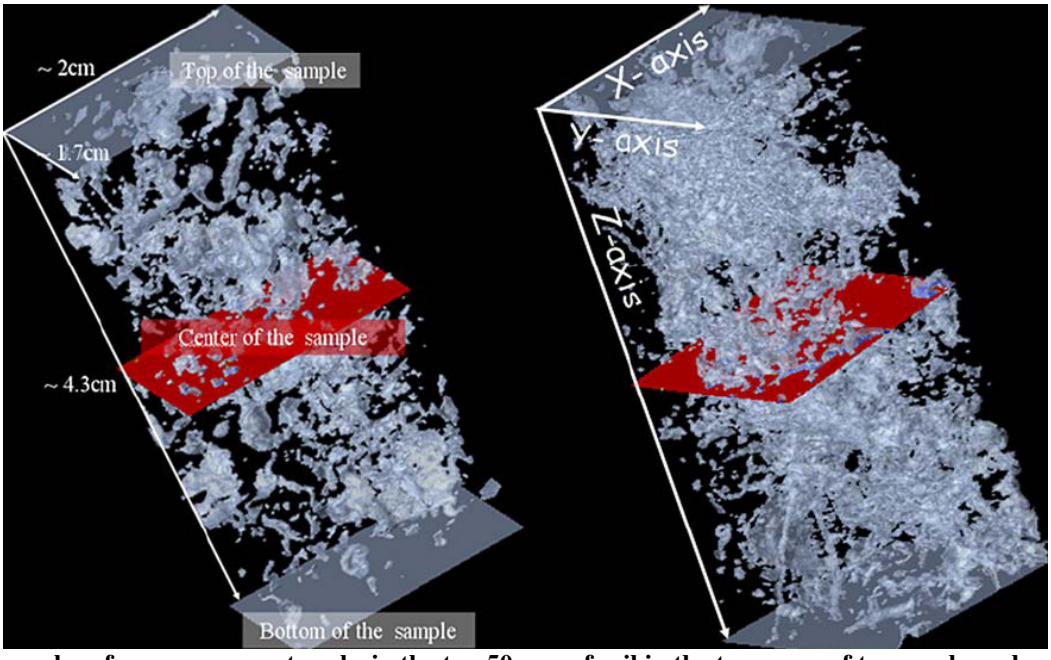

Figure 1. Examples of macro-pore networks in the top 50 mm of soil in the tree rows of two apple orchard systems in Hawke's Bay, New Zealand. The gray coloured areas are macro-pores. The three x-y planes are shown to mark the top, centre and bottom of the sample. Left: **Macro-pore network of the herbicided tree row of the integrated orchard system (Practice 3). The macro-porosity is 2.9 Vol.%.** Right**: Macro-pore network of the grassed tree row of the organic orchard system (Practice 1). The macro-porosity is 8.3 Vol.%.**

From our gas exchange simulations around the aggregates for wet conditions we found that the relative diffusion coefficients were similar under Practice 1 and 2, with 0.024 ± 0.008, and 0.015 ± 0.008, respectively, and were significantly higher than under Practice 3, with 0.0056 ± 0.0009 (Table 1). We suggest that the larger relative diffusion coefficients in the soils of the organic orchard (Practices 1 and 2) indicate less favourable physical conditions for N_2O production and emission. Therefore, this indicates that soil C management as Practice 1 possibly combats climate change in two ways. It firstly leads to C sequestration, and secondly might also contribute indirectly to a reduction in N_2O emissions.

Table 1. Macropore structure and function as consequence of three different apple orchard management practices. Practice 1: Using a grass sward and the regular application of compost in the tree row. Practice 2: Soil compaction by the tractor wheels in the grassed alley. Practice 3: Regular application of herbicides in the tree row. The values represent the means of three soil columns with the standard deviation of the mean in brackets.

Property	Practice 1	Practice 2	Practice 3
Macro-porosity [Vol.%]	7.5 (2.1)	3.6 (1.1)	2.4 (0.5)
Euler number [/mm^3]	6.6×10^{-3} (2.9×10^{-2})	6.3×10^{-3} (3.3×10^{-3})	2.0×10^{-2} (4.8×10^{-3})
Relative diffusion coefficient [-]	2.4×10^{-2} (7.9×10^{-3})	1.5×10^{-2} (7.9×10^{-3})	5.6×10^{-3} (9×10^{-4})

Several studies have stressed that diffusive gas exchange in soils depends on both the porosity and the connectivity of the gas-filled pore space, especially at the wetter end of the soil water content range (Tuli and Hopmans 2004; Weerts *et al.* 2001). In a multiple regression, 76% of the variability of the aggregate scale relative diffusion coefficient in the soil under Practice 3 was explained with macro-porosity and the Euler number as the significant variables. However, in the regression for the soil under Practice 1 and 2 only the macro-porosity was a significant variable and explained 71% and 83% of the variability respectively.

Conclusions

We studied how three different orchard management practices affected the soil macro-pore structure and the near-surface gas exchange under wet conditions. We found that all three orchard management practices had an impact on soil macro-pore structure and function of the top 50 mm of soil. We conclude that soil carbon management in the tree row like using grass swards and compost (Practice 1) leads to more macro-pores and a better gas exchange under wet conditions and probably less N_2O production and emission compared to a tree row that regularly receives herbicides (Practice 3). Although the compacted soil under the wheel track (Practice 2) had less macropores than in the grassed tree row, the gas exchange under wet conditions was still similar.

References

Clayton H, Arah JRM, Smith KA (1994) Measurement of nitrous oxide emissions from fertilized grassland using closed chambers. *Journal of Geophysical Research* **99**, 599-607.

Deurer M, Sivakumaran S, Ralle S, Vogeler I, McIvor I, Clothier BE, Green S, Bachmann J (2008) A new method to quantify the impact of soil carbon management on biophysical soil properties: The example of two apple orchard systems in New Zealand. *Journal of Environmental Quality* **37**, 915-924.

Sexstone AJ, Revsbech NP, Parkin TB, Tiedje JM (1985) Direct measurement of oxygen profiles and denitrification rates in soil clods. *Soil Science Society of America Journal* **60**, 1428-1438.

Tiedje JM (1988) Ecology of denitrification and dissimilatory nitrate reduction to ammonium. In 'Biology of anaerobic microorganisms'. (Ed. AJB Zehnder) pp. 179-244. (Wiley: New York).

Tuli A, Hopmans JW (2004) Effect of degree of fluid saturation on transport coefficients in disturbed soils. *European Journal of Soil Science* **55**, 147-164.

Vogel H-J (2008) 'QuantIm - Some useful C/C++ functions for scientific image processing'. (Helmholtz Center for Environmental Research: Halle).

Weerts AH, Kandhai D, Bouten W, Sloot PMA (2001) Tortuosity of an unsaturated sandy soil estimated using gas diffusion and bulk soil electrical conductivity: Comparing analogy-based models and Lattice-Boltzmann simulations. *Soil Science Society of America Journal* **65**, 1577-1584.

The impact of soil water content and water temperature on wet aggregate stability. What answer do you want?

Nelly Blair[A]

[A]Ourfing Partnership, "Nioka", 640 Boorolong Rd., Armidale, NSW , 2350, Australia.

Abstract
Wet aggregate stability determined by immersion wet sieving is commonly used as a measure of the stability of soil aggregates. Over the years different researchers have used a variety of methods with a wide range of sieve sizes, amplitudes, cycles, sieving times and pre-drying methods. The most common drying measurement prior to sieving is air drying but the soil water content after drying is generally not stated and often not determined. This water content can vary depending on soil texture, clay mineralogy and the air temperature at drying. This experiment studied the impact of soil water content following drying at different temperatures prior to wet sieving, and on the temperature of the sieving water, on the mean weight diameter (MWD) results obtained for three different soil types. The drying temperature affected the resulting soil water content particularly for the high clay soils and this also influenced the MWD results, with the lower drying temperature and higher soil water content resulting in a greater MWD in the soils with higher clay contents. The soil with the highest clay content and predominantly montmorillinite clay mineralogy had a MWD following drying at 15^{o}C more than five times greater than its MWD after drying at 25^{o}C. The results for the sandy loam soil were not significantly different as there was little difference in the soil water content across the range of drying temperatures. The temperature of the sieving water also significantly affected the MWD results for all soils with different soil types being affected differently. This is likely to be because of the different solubilities of binding agents within the soils. MWD results can vary significantly unless drying temperatures and the temperature of the water during sieving are standardized. The choice of conditions can significantly bias results.

Key Words
Wet sieving, Soil drying temperature, water sieving temperature

Introduction

Maintenance of a high aggregate stability in soils is desirable for sustainable land use as it is essential for the preservation of agricultural production, minimizing soil erosion and degradation and reducing environmental pollution (Amezketa 1999). Aggregation of soil particles will result in conditions that are favorable for plant growth and soil microbial and faunal activity (Whitbread 1995), while good soil structure is the most important soil characteristic for sustaining agricultural productivity and retaining environmental quality (Amezketa 1999). Wet aggregate stability determined by immersion wet sieving has been used by numerous researchers over many years as a measure of the stability of soil aggregates (Yoder 1936; Zotarelli *et al.* 2005; Blair *et al.* 2006a, b; N'Dayegamiye 2006; Goverts *et al.* 2007; Wagner *et al.* 2007; Dimoyiannis 2009). The mean weight diameter (MWD) is commonly used to express aggregate stability as it determines the size distribution of aggregates and is essentially a measure of macro-aggregate stability as the aggregates that remained on each sieve must be stable to the wetting and sieving processes (Amezketa 1999).

The measurement of wet aggregate stability by immersion wet sieving has been characterized by the variability in methods used with a wide range of sieve sizes, amplitudes, cycles, sieving time and pre drying methods. The soil is commonly air dried prior to measurement but the moisture content of the soils prior to sieving is generally not stated and often not determined, but it is likely that it can have a large influence on the results obtained. This can be of particular relevance when determining the seasonal aggregate stability of soils or when comparing aggregate stability over time, where the temperature in the drying area may vary widely. The temperature of the water used for the sieving process may also vary and it is possible for this to also effect results obtained. This experiment was carried out to determine the effect of soil water content over a range of soil drying temperatures and water temperature used for sieving on the aggregate stability of three different soil types.

Methods

Soils

Three contrasting soils that had been collected for other experiments were used for this trial. They were a Red Clay (RC) (Chromic Vertisol; FAO 1990) soil (Blair *et al.* 2006b), a Black Earth (BE) (Pellic Vertisol; FAO 1990) soil (Blair *et al.* 2006b) and a Sandy Loam (SL) (Chromic Luvisol; FAO 1990) soil (Blair 2000). The Red Clay soil contained 320 g/kg sand, 220 g/kg silt and 460 g/kg clay, while the Black Earth soil had 290 g/kg sand, 170 g/kg silt and 540 g/kg clay and the Sandy Loam contained 570 g/kg sand, 240 g/kg silt and 180 g/kg clay (International system). The clay minerals in the Red Clay consisted of predominantly quartz and kaolinite, with some illite and a small amount of montmorillonite. By contrast the Black Earth contained predominantly montmorillonite with small amounts of quartz, kaolinite and illite. The clay mineralogy of the Sandy Loam was predominantly kaolinite, quartz and illite with a small amount of halloysite.

Soil water content wet sieving experiment

The three different soils were wet by misting to 75% of their field capacity and then incubated in the laboratory in sealed plastic bags for seven days to ensure moisture equilibrium was reached. Each soil was then divided into six sub-samples and gently broken down using fingers before each sub-sample was dried in fan forced incubators at six different temperatures, 15°C, 20°C, 25°C, 30°C, 35°C and 40°C to simulate air-drying at different temperatures. Following drying, the soil samples were broken down to pass through a 4 mm sieve. To achieve this, the soil was gently rolled on a board that had 4 mm high ridges on the sides to maintain a gap between the board and the roller. This prevented total disruption of the sample and ensured that each soil sample received a similar energy input. Soil water content was determined for each sub-sample at each drying temperature. Three replicates of each soil from each drying temperature were then wet sieved as per the method below.

Water sieving temperature experiment

Soil that had been prepared as for the soil water content experiment and dried at 25°C was used for this experiment. The soil was wet sieved, as per the method below, in water at five different temperatures 15°C, 20°C, 25°C, 29°C and 36°C. The water was equilibrated for each temperature in an incubator for 48 hours prior to sieving and three replicates of each soil were sieved at each water temperature. Water temperature was measured immediately prior to commencing sieving.

Wet sieving

A modification of the Yoder wet sieving procedure (Whitbread 1996) was used to determine wet aggregate stability. A set of five 100 mm diameter sieves of 2000, 1000, 500, 250, 125 µm size screens was used. A further 125 µm sieve was used for a lid. The 30 g sample of the soil (<4 mm) was placed onto the top sieve and immersed in distilled water at approximately 25°C (or as stated for the water temperature experiment) for 30 sec before being sieved for 10 min through an amplitude of 17 mm at 34 cycles/min. Following sieving, the sieves were drained and the soil dried at 40°C for 24 h prior to weighing. Soil weights for soil dried at less than 40°C were corrected for water content before calculations were made. Mean weight diameter (MWD) was calculated for each soil by the formula:

$$\text{MWD} = \sum_{i=1}^{n} x_i w_i$$

where x_i is the mean diameter of any particular size range of aggregates separated by sieving, and w_i is the weight of aggregates in that size range as a fraction of the total dry weight of soil used.

Results

Soil water content wet sieving experiment

The Black Earth soil had the widest range in soil water content for the different drying temperatures while the Sandy Loam soil showed the lowest range (Table 1). The water contents of the three different soils at each drying temperature are shown in Table 1. The relative MWD was calculated by dividing the MWD at any given drying temperature by the MWD result for the 25°C drying temperature for each individual soil. This was then converted to a percentage. There was no significant difference between any of the MWD's for the Sandy Loam soil, while for the Red Clay soil, the MWD at the water content when dried at 15°C was significantly different from all other water contents (Table 1). However the Black Earth soil showed a wide range in MWD over the different water contents, with significant differences between drying at 15°C, 20°C and 25°C but no difference between the MWD results for the three lowest water contents following drying at the three higher temperatures

(Table 1). When calculating the MWD following wet sieving it is necessary to correct the soil weights to the moisture content of the drying temperature used to dry the samples following wet sieving, particularly for soils with high clay contents. For the Black Earth soil dried at 15°C the MWD for the corrected (for drying at 40°C) and uncorrected value ranged from 1.437 mm to 1.327 mm, respectively, while after drying at 20°C it ranged from 0.536 mm to 0.512 mm, respectively.

Table 1. The soil water content (WC) (%) and the relative mean weight diameter (Rel. MWD) expressed as a percentage of that at 25°C for each soil at each drying temperature.

	Sandy Loam		Red Clay		Black Earth	
Drying Temp. (°C)	WC (%)	Rel. MWD	WC (%)	Rel. MWD	WC (%)	Rel. MWD
15	1.8	106a[1]	6.1	111a	14.6	566a
20	1.7	98a	5.5	102b	9.4	206b
25	1.3	100a	3.5	100b	5.7	100c
30	1.3	101a	2.3	99b	5.0	79d
35	1.1	101a	2.0	98b	4.7	78d
40	1.0	100a	2.0	94b	4.2	66d

[1] Numbers in the same column followed by the same letter are not significantly different according to Duncan's MRT.

Water sieving temperature experiment

The relative MWD was calculated by dividing the MWD at any given water temperature by the MWD result for the 25°C water temperature for each individual soil. This was then converted to a percentage. The only significant difference for the Sandy Loam soil was for the water temperature at 36°C which was significantly lower than all other temperatures (Table 2). The Red Clay soil showed a significant difference in relative MWD between 15°C, 20°C and 25°C but there was no difference between the results for the three highest water temperatures (Table 2). For the Black Earth soil, a significant difference was shown between the relative MWD for the two lower water temperatures and the three higher water temperatures while the relative MWD at 25°C water temperature was significantly higher than that at a water temperature of 36°C (Table 2).

Table 2. Relative mean weight diameter (MWD) expressed as a percentage of that at 25°C for the different water temperatures used for wet sieving for the three different soil types.

Soil	15°C	20°C	25°C	29°C	36°C
Sandy Loam	103a[1]	101a	100a	101a	89b
Red Clay	124a	112b	100c	99c	98c
Black Earth	110a	111a	100b	98bc	91c

[1] Numbers in the same row followed by the same letter are not significantly different according to Duncan's MRT.

Conclusion

When comparing different soil samples for aggregate stability using the immersion wet sieving method it is essential that soils are dried at the same temperature. This is particularly necessary when collecting soil samples at different times of the year when temperatures in drying areas may vary significantly. It should also be ensured that corrections for soil water content are made when the drying temperature of the soil sample differs from the drying temperature of the sieved samples. The high clay content soils exhibited the greatest differences under these conditions. The clay types are also likely to be influencing the results with the soil containing predominantly montmorillonite clay showing the greatest differences.

When determining aggregate stability using the immersion wet sieving method, water temperature should be monitored as differences in water temperature can significantly influence the results obtained. Different soil types are affected in different ways and this is likely to be influenced by the solubility of the various binding agents found in the different soil types. The MWD results can vary significantly unless soil drying temperatures and the temperature of the sieving water are standardized. The choice of conditions used can significantly bias the results.

References

Amezkeka E (1999) Soil aggregate stability: a review. *Journal of Sustainable Agriculture* **14**, 83-151.

Blair N (2000) The impact of cultivation and sugarcane trash management on soil carbon fractions and aggregate stability. *Soil and Tillage Research* **55**, 183-191.

Blair N, Faulkner RD, Till AR, Poulton PR (2006a) Long-term management impacts on soil C, N and physical fertility. I: Broadbalk experiment. *Soil and Tillage Research* **91**, 30-38.

Blair N, Faulkner RD, Till AR, Crocker GJ (2006b) Long-term management impacts on soil C, N and physical fertility. Part III: Tamworth crop rotation experiment. *Soil and Tillage Research* **91**, 48-56.
Dimoyiannis D (2009) Seasonal soil aggregate stability variation in relation to rainfall and temperature under Mediterranean conditions. *Earth Surfaces, Processes and Landforms* **34**, 860-866.
Goverts B, Sayre KD, Lichter K, Dendooven L, Deckers J, (2007) Influence of permanent raised bed planting and residue management on physical and chemical soil quality in rain-fed maize/wheat systems. *Plant and Soil* **291**, 39-54.
N'Dayegamiye A (2006) Mixed paper mill sludge effects on corn yield, nitrogen efficiency and soil properties. *Agronomy Journal* **98**, 1471-1478.
Whitbread AM (1995) Soil organic matter: its fractionation and role in soil structure. In 'Soil Organic Matter Management for Sustainable Agriculture'. (Eds RDB Lefroy, GJ Blair, ET Craswell) ACIAR Proceedings No 56 Ubon Thailand, 24-26 August 1994 pp. 124-130. (ACIAR: Canberra, ACT).
Whitbread AM (1996) The effects of cropping system and management on soil organic matter and nutrient dynamics, soil structure and the productivity of wheat. PhD thesis. University of New England, Armidale.
Wager S, Cuttle SR, Schollar T (2007) Soil aggregate formation as influenced by clay content and organic matter amendments. *Journal of Plant Nutrition and Soil Science* **170**, 173-180.
Yoder RE (1936) A direct method of aggregate analysis of soils and a study of the physical nature of erosion losses. *Journal of American Society of Agronomy*. **28**, 337-351.
Zotarelli L, Alves BJR, Urquiaga S, Torres E, dos Santos HP, Paustian K, Boddey RM, Six J (2005) Impact of tillage and crop rotation on aggregate-associated carbon in two Oxisols. *Soil Science Society of America Journal* **69**, 482-491

The rheology of rhizosphere formation by root exudates and soil microbes

Paul D. Hallett[A], Sandra Caul[A], Tim J. Daniell[A], Pierre Barré[A,B] and Eric Paterson[C]

[A]Scottish Crop Research Institute, Invergowrie, Dundee, United Kingdom, Email paul.hallett@scri.ac.uk
[B]Geology Laboratory (CNRS-ENS), Ecole normale supérieure, 24 rue Lhomond, 75005 Paris, France, Email pierre.barre@normalesup.org
[C]Macaulay Land Use Research Institute, Aberdeen, United Kingdom, Email eric.paterson@macaulay.ac.uk

Abstract
One of the major inputs driving the formation of soil structure is exudation from plant roots. We used approaches from rheology to test the hypothesis that root exudates initially disperse soil, thus easing root penetration and releasing nutrients, followed by gelling (i.e. aggregation) if the compounds are transformed by soil microbes. Soils were amended with 0, 1.5 and 15 mg/g soil of root-exudate compounds consisting of a mix of sugars, amino acids and organic acids and incubated for 13 days at either 2ºC, to reduce microbial action, or 16ºC. Incubation at 2ºC significantly suppressed respiration rates compared to 16ºC, suggesting microbial processes were impaired. A parallel plate rheometer was used to quantify the rheological behaviour of the incubated soils amended with root-exudate compounds. The drop in flow point (stress where breakdown occurs) at 2ºC incubation and rise in flow point at 16ºC incubation suggests dispersion by the root exudates followed by gelling if root exudates are transformed by microbes.

Key Words
Rhizosphere, rheology, root-exudates, microbiology, aggregation

Introduction
Plant root exudates and their mineralization by soil microbes drive the formation of the distinct structural zone around roots termed the rhizosphere (McCully 1999). The rhizosphere has enhanced particle aggregation, microbial biomass and water retention compared to bulk soil, which is critical to the functioning of plants as these processes impact fluxes of nutrients, water and oxygen (Hinsinger *et al.* 2009). Our research is examining how root exudates and their transformation by soil microbes influence the rheological behaviour of wet soil. Rheology is the study of the flow of matter and it should help quantify the underlying processes driving soil structure formation and stabilisation. We hypothesise that root exudates initially disperse soil, thus easing root penetration and releasing nutrients. Soil microbes then transform exudates into biological glues that gel soil. To test this hypothesis we measured the rheological behaviour of soils equilibrated to a range of water contents and amended with root-exudate compounds. Incubations of the soil at 2ºC and 16ºC were used to control microbial activity.

Methods
In this preliminary paper we report data from one soil, but data on more soils will be collected before the World Congress of Soil Science 2010. A Eutric Cambisol derived from undifferentiated sandstone, with 71% sand, 19% silt and 10% clay, pH (H_2O) 6.2, 1.9% C and 0.07% N was sampled from 0-100 mm depth. It was from Bullion Field, situated at the Scottish Crop Research Institute, Dundee. The soil was air-dried and then passed through a 400 μm sieve.

Soil was first pluviated dry into 3 rings and then water retention at 0, -5, -10, -20 and -50 kPa potentials was measured on a tension table. From these data we selected a water content of 0.43 g/g because it occurred at a water potential (-10kPa) and water filled pore space (75%) that would minimise water and aeration stresses to microbes.

Larger air-dry soil samples of 600 g were then wet to 0.23 g/g^1 using a fine mist and incubated at 16ºC for 2 weeks to allow the microbial community to re-establish and to mineralise carbon released from drying. The sample was then divided into three and amended with 0, 1.5 or 15 mg C/g soil of root-exudate compounds. The compounds were a mix of sugars, amino acids and organic acids that are found in natural root exudates (Paterson *et al.* 2007). Soil subsamples were further subdivided and then sealed in 1 litre Kilner jars fitted with a Suba-seal in the lid to allow gas sampling. Three replicates of each amendment rate were incubated at 16ºC, which is the typical local soil temperature in summer, and another three replicates at 2ºC to suppress microbial activity. The jars were vented regularly and carbon dioxide measured in the headspace on days 1, 3, 7, 10 and

1 – 6 August 2010, Brisbane, Australia. Published on DVD.

13 with a syringe sample injected into a gas chromatograph. After 13 days incubation, the soil from each jar was divided into subsamples to measure rheology and microbial properties. Only respiration and rheological data will be presented here.

The rheology subsamples were subdivided and wet to water contents ranging from no added water (stiff, aggregated soil) to a flowing liquid. The samples were mixed thoroughly and placed in a sealed bag for 24 h at 2°C to improve equilibration and minimize biological activity. A Haake MARS Parallel Plate Rotational Rheometer (Thermo Scientific, Waltham, MA, USA) using 35 mm diameter serrated stainless steel plates and a 2 mm gap setting provided measurements of rheological behaviour. Samples less than 10 g were needed. A stress controlled amplitude sweep test with an oscillation frequency of 50Hz and stress ramp from 0.1 to 10^4 Pa was used. Data on zero-shear viscosity and flow-point were used to describe rheological behaviour. Zero-shear viscosity is the resistance to flow of an unstressed material. With increasing stress, shear-thinning decreases the viscosity of materials like soil until structural collapse occurs at the flow-point. Soil water content was measured for each sample tested in the rheometer.

The viscosity and flow point were plotted against water content for all experimental treatments. Linear regression with groups was used to assess differences between treatments following a log-log transformation. Analysis of variance was used to assess differences in respiration rates between treatments.

Results and Discussion

The amount of added root-exudate compounds and incubation temperature had significant effects on soil respiration ($P<0.001$; Figure 1). Incubation at 2ºC resulted in about 3% of the respiration at 16ºC for the largest amendment rate. From these results, the microbial transformation of root-exudate compounds at 2ºC was only a small fraction of the total, leaving most of the root-exudate compounds in their original form. The impact of the root-exudate compounds alone can thus be taken as the 2ºC results and microbially transformed root-exudate compounds as the 16ºC results. For the 15 mg/g amendment rate, root-exudate compounds caused a large reduction in Flow Point at 2ºC and a large increase at 16ºC ($P<0.001$). This suggests that root-exudates cause dispersion followed by gelling once the compounds are transformed by soil microbes. These data are different from Barré and Hallett (2009), who found the model root exudate polygalacturonic acid gelled soils, but this is likely due to the different chemical properties of the exudates. They also found that a fungal exudate gelled soil, which corresponds with our results.

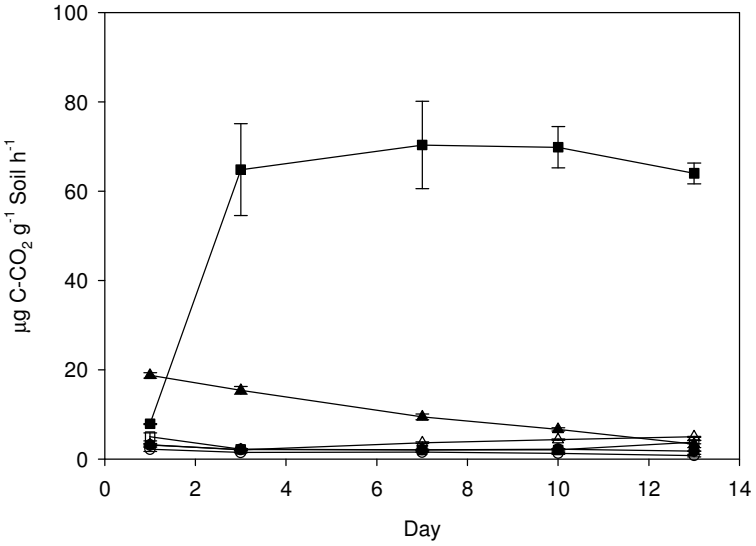

Figure 3. Respiration rate for soils amended with 0 (circle), 1.5 (triangle) and 15 (square) mg/g soil of root-exudate compounds incubated at 2ºC (hollow) and 16ºC (solid).

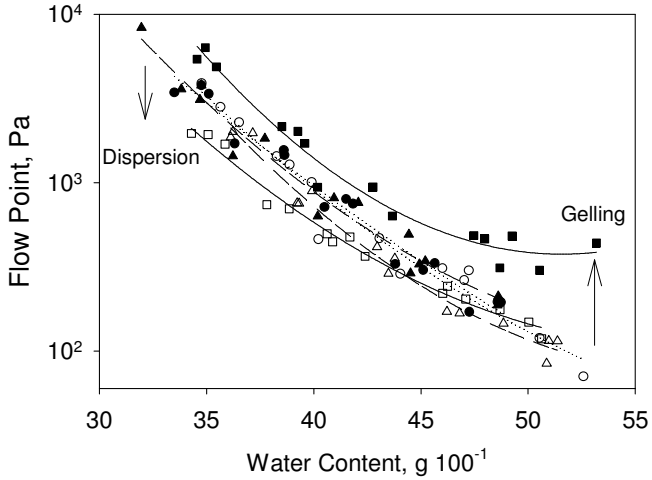

Figure 4. Flow Point for soils amended with 0 (circle), 1.5 (triangle) and 15 (square) mg/g soil of root-exudate compounds incubated at 2ºC (hollow) and 16ºC (solid).

The added root-exudate corresponds to daily (1.5 mg/g soil) and total (15 mg/g soil) amounts that would be expected from a growing root (Paterson *et al.* 2007). Moreover, the complexity of the compounds provides a realistic surrogate for real root-exudates that are very difficult to collect in the volumes required for mechanical testing. However, future research will collect rhizosphere soil and attempt to harvest real root exudates to test whether similar effects are found. Barré and Hallett (2009) found the impact of exudates on rheology was dependent on clay mineralogy and soil texture, and Tarchitzky and Chen (2002) showed the rheology of dilute soil suspensions was pH dependent, so both will be tested using exudates and soil water contents more typical of natural conditions.

Conclusion

We have demonstrated that root exudates initially disperse soil followed by gelling once transformed by soil microbes. Quantification of the underlying mechanical process using rheology provides data that will be useful in understanding and modeling the development of rhizosphere soil structure. The initial dispersion by root-exudate compounds may lead to particle reorientation that eases root penetration, releases previously inaccessible nutrients and the formation of new aggregates. Microbial transfromation of root-exudate compounds gels soils, which along with accentuated cycles of wetting drying at the root-soil interface, forms the very stable and structurally distinct zone of soil termed the rhizosphere.

References

Barre P, Hallett PD (2009) Rheological stabilization of wet soils by model root and fungal exudates depends on clay mineralogy. *European Journal of Soil Science* **60,** 525-538.

Hinsinger P, Bengough AG, Vetterlein D, Young IM (2009) Rhizosphere: biophysics, biogeochemistry and ecological relevance. *Plant and Soil* **321,** 117-152.

McCully ME (1999) Roots in soil: Unearthing the complexities of roots and their rhizospheres. *Annual Review of Plant Physiology And Plant Molecular Biology* **50,** 695-718.

Paterson E, Gebbing T, Abel C, Sim A, Telfer G (2007) Rhizodeposition shapes rhizosphere microbial community structure in organic soil. *New Phytologist* **173,** 600-610.

Tarchitzky J, Chen Y (2002) Rheology of Sodium-montmorillonite suspensions: Effects of humic substances and pH. *Soil Science Society of America Journal* **66,** 406-412.

Tillage effects on bulk density and hydraulic properties of a sandy loam soil in the Mon-Dak Region, USA

J.D. Jabro, W.B. Stevens, W.M. Iversen and R.G. Evans

Northern Plains Agricultural Research Laboratory, USDA-ARS, 1500 N. Central Avenue Sidney MT, 59270, USA. Email jay.jabro@ars.usda.gov.

Abstract
We evaluated the effects of conventional (CT) and strip (ST) tillage practices on bulk density (ρ_b), water content (θ_w), infiltration rate (I_r) and hydraulic conductivity (K_s) in a Lihen sandy loam soil. Soil cores were collected during growing season from each plot at 0 to 10 and 10 to 30 cm depths under each tillage practice to measure ρ_b and θ_w. *In-situ* I_r and K_s measurements were determined using a pressure ring infiltrometer (PI) and a constant head well permeameter (CHWP) at the soil surface and 10–30 cm depths, respectively. Soil ρ_b and θ_w did not differ significantly between CT and ST in both years with the exception of ρ_b in 2007. The log-transformed I_r was significantly affected by tillage at $P \leq 0.1$ in 2007 while I_r did not differ significantly between CT and ST practices in 2008. The effects of tillage on soil K_s were significant in 2007 and 2008 at $P \leq 0.05$ and at $P \leq 0.1$, respectively. The K_s values were 68% and 56% greater for ST than for CT in 2007 and 2008, respectively. It was concluded that the CT operations increased soil compaction, which consequently altered ρ_b, thereby reducing K_s in the soil.

Key Words
Tillage, bulk density, infiltration, hydraulic conductivity, soil compaction

Introduction

Tillage is one of the most influential management practices affecting soil physical and hydraulic characteristics (Lal and Shulka 2004). Strip tillage (ST) was performed using a single operation with special equipment that provided alternating 30-cm wide strips of tilled and untilled soil while conventional tillage (CT) consisted of six to seven separate operations using different tillage implements following the harvest of one crop in preparation for the next crop.

Two of the most commonly measured soil physical properties affecting hydraulic conductivity are the soil bulk density and effective porosity as these two properties are also fundamental to soil compaction and related agricultural management issues (Strudley et al. 2008).

Saturated hydraulic conductivity is considered one of the most important parameters for water flow and chemical transport phenomena in soils (Reynolds and Elrick 2002). As little research has been reported regarding the effect of strip tillage on soil physical and hydraulic properties the objective of this study was to evaluate the effects of conventional (CT) and strip (ST) tillage practices on bulk density (ρ_b), gravimetric water content (θ_w), final infiltration rate (I_r), and saturated hydraulic conductivity (K_s) in a sandy loam soil of the Mon-Dak region (north eastern Montana and north western north Dakota), USA.

Materials and methods

The research site was located at the Nesson Valley Mon-Dak Irrigation Research and Development Project approximately 37 km east of Williston, ND (48.1640 N, 103.0986 W). The soil is mapped as Lihen sandy loam (sandy, mixed, frigid Entic Haplustoll) consisting of very deep, somewhat excessively or well drained, nearly level soil that formed in sandy alluvium, glacio-fluvial, and eolian deposits in places over till or sedimentary bedrock. Particle size distribution analysis indicated the textural class of the surface horizon (0 to 30 cm) to be consistently within the sandy loam classification. The amount of sand, silt, and clay in the soil at 0 to 30 cm depth ranged from 640 to 674, 176 to 184, and 150 to 166 g kg^{-1}, respectively.

The experimental design at the Nesson site was a randomized complete block design with six replications. Treatments consisted of two crop rotations (sugarbeet/potato [*Solanum tuberosum* L.]/malting barley [*Hordeum vulgare* L.] and sugarbeet/malting barley/potato), two tillage practices (conventional and strip) under sugarbeet using a linear-move overhead sprinkler irrigation system. The CT plots were tilled just prior to planting in the spring of 2007 and 2008, while the ST operation was completed 9/07/2006 and 9/20/2007 for the 2007 and 2008, respectively.

1 – 6 August 2010, Brisbane, Australia. Published on DVD.

Soil I_r and K_s measurements were made approximately 1 m apart in the center of crop rows within CT and ST sugarbeet plots in July 17–20, 2007 and July 9–12, 2008.

Using a soil core sampler, we collected undisturbed soil cylindrical core samples (5 cm long × 5 cm in diameter) from each plot at 0–10 and 10–30 cm depths under each tillage system. Soil cores were used to measure bulk density (ρ_b) as mass of oven dried soil per volume of core (Mg m^{-3}) and gravimetric water content (θ_w) as mass of water in the soil sample per mass of the oven dried soil (kg kg^{-1}). Each measurement was replicated four and eight times at 0 to 10 and 10 to 30 cm depths, respectively.

Soil I_r measurements were determined using the single head pressure ring infiltrometer method, PI (Reynolds and Elrick 2002). The PI consists of a Mariotte-type reservoir, similar to that of the constant head well permeameter (CHWP), sealed to a stainless steel ring with a radius of 10 cm, driven to a depth of 5 cm into the soil surface (Reynolds and Elrick 2002).

In-situ K_s ($L\ T^{-1}$) using a steady state flow rate of water from a cylindrical borehole augured to a given depth below the soil surface was measured using a CHWP (Reynolds and Elrick 2002).

Soil I_r and K_s measurements were replicated four and eight times, respectively, in each year.

Results and discussion

Soil ρ_b and θ_w did not significantly differ between CT and ST in both years with the exception of ρ_b in 2007, which was significantly affected by tillage treatment at $P \leq 0.05$ (Table 1). Soil ρ_b was numerically greater in CT plots than in ST plots in both years, suggesting that the CT operations increased soil compaction due to frequent traffic passes induced by this tillage system. Nevertheless, ST is perceived as having greater porosity and wetter soil conditions compared with CT (Licht and Al-Kaisi 2005). Elimination of secondary tillage and more limited vehicular traffic in ST plots probably contributed to decreased ρ_b compared to CT plots as the ST system includes only a single in-row soil disturbance event that decreases soil ρ_b and conserves water to a greater degree than the CT system (Licht and Al-Kaisi 2005).

The log-transformed I_r and K_s under both CT and ST tillage systems in 2007 and 2008 are illustrated in Figures 1 and 2, respectively. Data indicated that I_r was significantly affected by tillage at $P < 0.1$ in 2007 while I_r did not differ significantly between CT and ST practices in 2008 (Figure 2). Although variations in I_r between CT and ST practices existed in both years, these variations were not significant at $P < 0.05$ (Figures 1 and 2). However, the similarity in I_r between CT and ST at the surface suggests that the CT and ST tillage systems are similar in terms of soil disturbance at this depth.

Table 1. Effect of tillage on soil bulk density (ρ_b) and gravimetric water content (θ_w) averaged across two depths (0–10 and 10 - 30 cm) for conventional (CT) and strip (ST) tillage practices.

Year	Tillage	ρ_b (Mg m^{-3})	θ_w ($m^3\ m^{-3}$)
2007	CT	1.60[a†]	0.0734[a]
	ST	1.52[b]	0.0803[a]
		Analysis of Variance, P > F	
		0.038	0.271
2008	CT	1.55[a]	0.0922[a]
	ST	1.52[a]	0.0948[a]
		Analysis of Variance, P > F	
		0.184	0.592

†Means followed by the same letter are not different at the 0.05 probability level ($P \leq 0.05$).

The effects of tillage on soil K_s were significant in 2007 and 2008 at $P < 0.05$ and at $P < 0.1$, respectively (Figures 1 and 2). The K_s values were 68% and 56% greater for ST than for CT in 2007 and 2008, respectively. Results in Table 1 and Figures 1 and 2 showed that K_s increases as the ρ_b decreases and soil total porosity increases, indicating that soil compaction influences K_s measurements at the 10–30 cm depth. Overall, these findings agree with results reported by Jabro et al. (2009) who found that greater K_s values correspond with lower soil bulk density values at the subsurface depths.

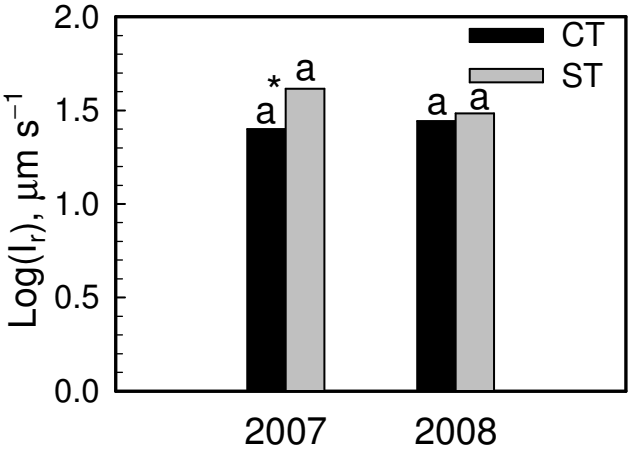

Figure 1. In-situ infiltration rate (I_r) as affected by conventional tillage (CT) and strip tillage (ST) practices in 2007 and 2008. An '*' signifies that a difference is significant at the 0.1 probability level.

The results of this study suggest that the CT operations increased soil compaction, which consequently altered soil ρ_b, thereby reducing K_s (Table 1, Figures 1 and 2). The compacted soil and higher ρ_b in CT rows was likely responsible for the lower K_s values compared with ST plots in both years. Moreover, the ST system likely produced a greater volume of macropores (Wienhold and Tanaka 2000; Lipiec et al. 2005) resulting in more pronounced vertical pore connectivity in ST plots than in CT plots.

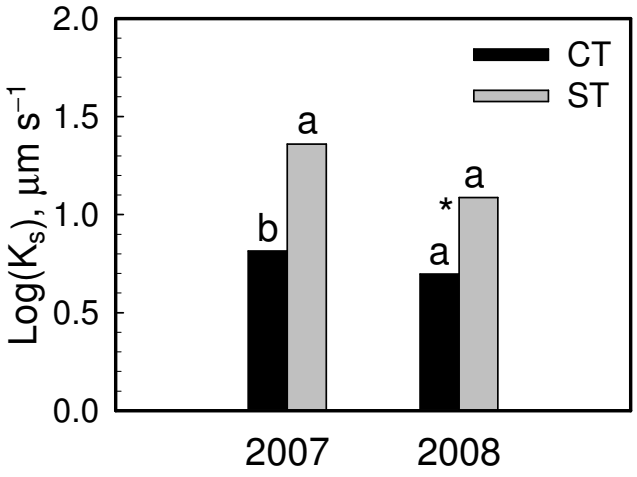

Figure 2. In situ saturated hydraulic conductivity (K_s) as affected by conventional tillage (CT) and strip tillage (ST) practices in 2007 and 2008. Different letters indicate that means are significantly different at the 0.05 probability level. An '*' signifies that a difference is significant at the 0.1 probability level.

Conclusions

It was concluded that soil ρ_b and θ_w did not significantly differ between CT and ST in both years with the exception of ρ_b in 2007. Soil ρ_b was numerically lower in ST plots than in CT plots while θ_w were greater for ST than for CT in both years. Soil I_r was significantly affected by tillage at $P < 0.1$ in 2007 while I_r did not differ significantly between CT and ST practices in 2008. The effects of tillage on soil K_s were significant in 2007 and 2008 at $P < 0.05$ and at $P < 0.1$, respectively. The I_r and K_s values were greater in ST plots than CT plots in both years. The variation in K_s values in soil was likely due to differences in soil compaction and vehicular traffic passes peculiar to the CT and ST systems. The ST plots likely had better volume of macropores than CT plots, producing greater water flow through the ST soil profile.

References

Jabro JD, Stevens WB, Evans RG, Iversen WM (2009) Tillage effects on physical properties in two soils of the Northern Great Plains. *Applied Engineering in Agriculture* **25**, 377-382.

Licht MA, Al-Kaisi M (2005) Strip-tillage effect on seedbed soil temperature and other soil physical properties. *Soil Tillage Research* **80**, 233-249.

Lal R, Shukla MK (2004) 'Principles of soil physics'. (Marcel Dekker, Inc.: New York, NY).

Lipiec L, Kus J, Slowinska-Jurkiewicz A, Nosalewicz A (2005) Soil porosity and water infiltration as influenced by tillage methods. *Soil Tillage Research* **89**, 210-220.

Strudley MW, Green TR, Ascough II JC (2008) Tillage effects on soil hydraulic properties in space and time. *Soil Tillage Research* **99**, 4-48.

Reynolds WD, Elrick DE (2002) Pressure infiltrometer. In 'Methods of Soil Analysis: Part 4. Physical methods'. (Eds JH Dane, GC Topp). pp 826-836. (Soil Science Society of America: Madison, WI).

Wienhold BJ, Tanaka DL (2000) Haying, tillage, and nitrogen fertilization influences on infiltration rates at a conservation reserve program site. *Soil Science Society America Journal* **64**, 379-381.

Using the dye tracer experiment for characterisation of parameters of the dual-permeability model

Radka Kodešová[A], Karel Němeček[A], Veronika Jirků[A], Antonín Nikodem[A], Miroslav Fér[A], Ondřej Jakšík[A], Martin Kočárek[A] and Anna Žigová[B]

[A]Dept. of Soil Science and Soil Protection, Czech University of Life Sciences Prague, Prague, Czech Republic, Email kodesova@af.czu.cz
[B]Institute of Geology, Academy of Sciences of the Czech Republic, Prague, Czech Republic

Abstract
This study is focused on the visualization of the preferential flow in different soil types and their horizons using a dye tracer experiment method. The field ponding dye infiltration experiments were performed on two soil types: Haplic Luvisol and Haplic Cambisol. The tension disc infiltrometer and the Guelph permeameter measurements were performed in the field on various horizons to study the impact of macropores on water flow. In addition, thin soil sections were made and micromorphological images were used to study soil aggregate structure and dye distribution at a microscale. The staining patterns within the vertical and horizontal sections documented very different natures of preferential flow in different soil types and also within the soil profiles. While preferential flow in Haplic Luvisol was caused by soil aggregation and biopores, preferential flow in Haplic Cambisol was caused only by biopores and large gravitational soil fractures. Micromorphological images showed that the dye was primarily distributed either in the interagregate pores and then in the pores inside the aggregates, or in the isolated large pores connected to the dye source and then into the matrix pores. Information about the dual-domain geometry and the dual-permeability models in HYDRUS 2/3D were then used to simulate preferential flow in studied soil types and to estimate parameters characterizing transport properties of bi-modal soil-porous medias.

Key Words
Soil structure, preferential flow, dye tracer experiment, micromorphological images, parameter optimisation

Introduction

It was observed that water flow and contaminant transport in structured soils is frequently influenced either by water and solute temporal immobilization or by preferential flow. To describe such non-equilibrium water flow and solute transport in soils, many numerical models have been recently developed. Overviews of non-equilibrium water flow and solute transport evidence, and various experimental and mathematical approaches to study and describe these phenomena were given by Gerke (2006), Jarvis (2007), Šimůnek and van Genuchten (2008), or Köhne *et al.* (2009a,b). Common physically based models for simulation of water flow and solute transport in structured soils assume (one) continuum and bi- or multi-continuum approaches. To apply various approaches, the properties characterizing water flow and solute transport must be specified. The numerical inversion and parameter estimation from the observed water flow and solute transport data are usually applied to obtain desired information. (See review articles mentioned above.) However, to obtain reliable results many parameters must be independently measured or determined from the literature. A summary of various approaches for independent parameter determination is given by Köhne *et al.* (2009a).

Various dye tracers are frequently used to study soil structure and preferential flow phenomena (Flury and Wai 2003). The most often applied dye is the food color Brilliant Blue FCF. There are many studies dealing with the food color Brilliant Blue FCF characteristics (Flury and Flühler 1995, Morris *et al.* 2008) and studies using this dye for visualization of non-equilibrium water flow and dye transport in soils (Flury *et al.* 1994, Kasteel *et al.* 2005, Sander and Gerke 2007).

Preferential water flow and herbicide transport was studied in the field and laboratory by Kodešová *et al.* (2008, 2009). They applied the dual-porosity and dual-permeability models in HYDRUS-1D (Šimůnek *et al.* 2008) to simulate observed data. Micromorphological images of studied soils were used to determine parameters describing dual-domains geometry. A goal of this study is to characterize dual-domain geometry of previously studied soils in macro and micro-scale using the dye tracer experiment. An additional goal is to use this information and measured transient flow data for characterization of parameters of the dual-permeability model.

Methods

The study was performed in Haplic Luvisol in Hněvčeves and Haplic Cambisol in Humpolec in the Czech Republic. Details of soil chemical, physical and transport properties are given by Kodešová *et al*. (2008, 2009). The field dye infiltration experiment was carried out in year 2009 using the similar procedure to that described by Sander and Gerke (2007). 100 (Haplic Luvisol) and 50 (Haplic Cambisol) liters of solution with food color Brilliant Blue FCF (5 kg m^{-3}) was infiltrated in a 1 x 1 m plot (applying an initial ponding depth of 10 and 5 cm, respectively) immediately after the wheat harvest. On the next day, one half of the plot was sliced horizontally and another half vertically to study the dye distribution within the soil profile to the depth of 100 cm. Micromorphology of soil structure and the dye distribution was studied on thin soil sections prepared from large soil aggregates, taken in the field. Thin sections were prepared according to the methods presented by Catt (1990). The tension disc infiltrometer (a disc radius of 10 cm) was used to measure cumulative water infiltration under unsaturated conditions created using the pressure head of -2 cm. The Guelph (well) permeameter was used to measure cumulative water flux under ponding conditions. Measurements were performed at various horizons to study possible impact of macropores. Therefore the depth of the drilled well was variable. The well radius was always 3 cm, and the well ponding depth was 5 cm.

The analytical expressions presented by Wooding (1968) and Zhang *et al.* (1998) are usually used to calculate K values from the tension disc and the Guelph permeameter, respectively. The radially symmetric single-porosity and dual-porosity models in HYDRUS 2/3D (Šimůnek *et al.* 2008) were applied here to estimate parameters of the soil hydraulic functions (van Genuchten 1980) of both models using both field experiments. First, the single-porosity flow model in HYDRUS 2D/3D was used to estimate the saturated hydraulic conductivity, K_s, via a numerical inversion of the data from the tension disc infiltrometer, and using the soil water retention curve parameters obtained in the laboratory from ponding infiltration test presented by Kodešová *et al.* (2009). Second, the dual-permeability flow model in HYDRUS 2D/3D was used to estimate the saturated hydraulic conductivity, K_{sf}, in the macropore domain using the Guelph permeameter cumulative infiltration. In this case, the parameters obtained from the tension disc infiltrometer experiment were used to describe the matrix domain, and the parameters characterizing water retention in the macropore domain and mass exchange between macropore and matrix domains were either set (at measured or average values) or optimized. Parameters characterizing the aggregate geometry were set based on the field ponding dye infiltration experiment and micromorphological study.

Haplic Luvisol in Hněvčeves **Haplic Cambisol in Humpolec**

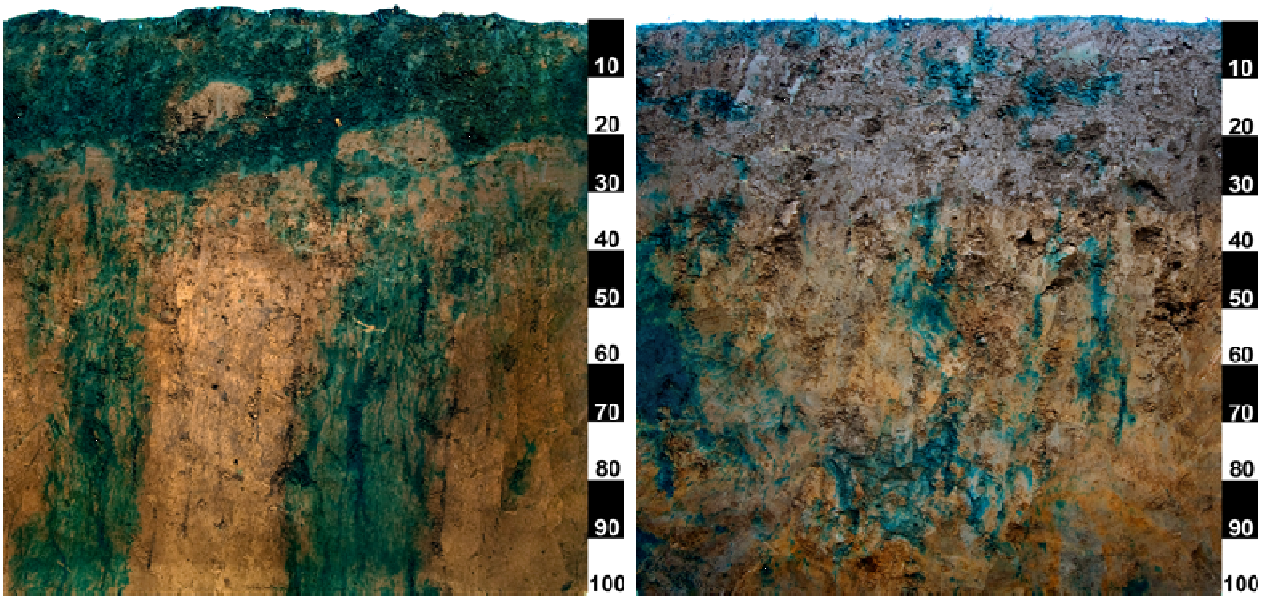

Figure 1. Examples of staining patterns within the vertical sections in Haplic Luvisol in Hněvčeves (left) and Haplic Cambisol in Humpolec (right). Diagnostic horizons of Haplic Luvisol: Ap_1 (0 – 25 cm), Ap_2 (25 - 35 cm), Bt_1 (35 - 75 cm) and Bt_2 (75 - 100 cm). Diagnostic horizons of Haplic Cambisol: Ap (0 – 33 cm), Bw (33 - 65 cm) and C (65 – 100 cm).

Results

Here we show only examples of staining patterns within the vertical sections in Haplic Luvisol in Hněvčeves (Figure 1 left) and Haplic Cambisol in Humpolec (Figure 1 right). Left figure shows that while dye tracer was

partly regularly transported and only some isolated domains were visible in the surface Ap_1 horizon, the significant preferential flow occurred in the subsurface horizons. The preferential flow in the upper subsurface Ap_2 horizon (plow pan) was caused by the gravitational biopores in the very compact matrix structure, which considerably slowed down the dye transport. In the case of deeper horizons (Bt_1 and Bt_2), the preferential flow occurred due to the gravitational biopores and extensively developed prismatic structure, which was highly affected by organo-mineral coatings. Right figure shows that the dye tracer transport in Haplic Cambisol was in all horizons (Ap, Bw, C) mainly affected by the preferential flow caused by the gravitational fractures and biopores.

Various soil structures were also documented on micromorphological images of soil structure studied on thin soil sections prepared from large soil aggregates (not shown). The micromorphological images of the Haplic Luvisol soil samples showed higher-order aggregates of the Ap_1 horizon, dense structure of the Ap_2 horizon, well-developed soil structure affected by clay coatings of the Bt_1 horizon and isolated pores with clay coatings inside the large aggregates of the Bt_2 horizons. Aggregates in all horizons (Ap, Bw, C) of the Haplic Cambisol were poorly developed. The pore system did not show intrapedal or interpedal pores, pores were developed mainly along gravel particles. Correspondingly to the different soil structure compositions, dye tracer was differently distributed in the soil. Images did not show a regular dye distribution. It was evident that the dye was primarily distributed either in the interagregate pores and then in the pores inside the aggregates, or in the isolated large pores connected to the dye source and then into the matrix pores. Accumulated organic matter, clay coating, larger soil grains and isolated larger capillary pores, which initially did not contain the dye tracer, behaved as less-permeable or impermeable barriers.

An example of measured and simulated transient flow data using the dual-permeability model in HYDRUS 2/3D is shown in Figure 2. In this case, the K_{sf} value for the macropore domain of the dual-permeability model was estimated using the Guelph permeameter cumulative infiltration data measured in the Ap_1 horizon of Haplic Luvisol.

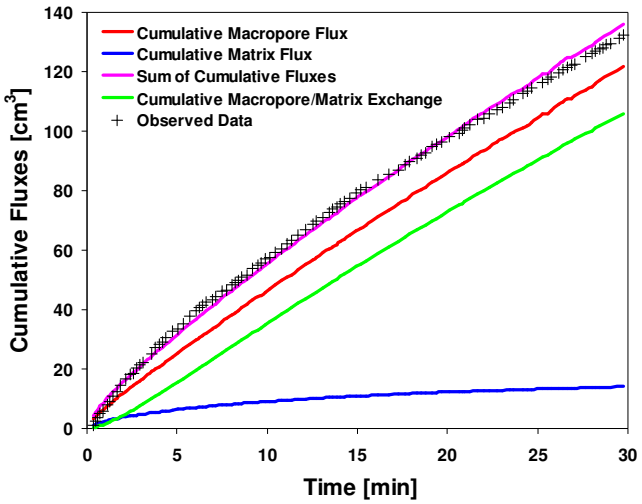

Figure 2. Measured and simulated (using the dual-permeability model) cumulative infiltrations for the Guelph permeameter test performed in the Ap1 horizon of Haplic Luvisol. Cumulative Macropore Flux = direct (from the infiltration well) cumulative infiltration into the macropore domain, Cumulative Matrix Flux = direct cumulative infiltration into the matrix domain, Sum of Cumulative Fluxes = Sum of direct cumulative fluxes, Cumulative Macropore/Matrix Exchange = cumulative infiltration from the macropore domain into the matrix domain.

Parameters characterizing the aggregate geometry (the shape factor for spherical aggregates β =15, the characteristic length of an aggregate a = 1.5 cm) and macropore domain fraction (f_w = 0.0277) were set based on the field ponding dye infiltration experiment and micromorphological study. The soil hydraulic parameters (θ_{rm} = 0 cm^3cm^{-3}, θ_{sm} = 0.428 cm^3cm^{-3}, α_m = 0.0124 cm^{-1}, n_m = 2.001, K_{sm} = 1.25 10^{-4} cm min^{-1}) obtained for the single-porosity model in HYDRUS 2/3D using the tension disc infiltrometer data were assumed to characterize the matrix domain. The parameters characterizing water retention in the macropore domain (θ_{rf} = 0 cm^3cm^{-3}, θ_{sf} = 0.428 cm^3cm^{-3}, α_f = 0.1 cm^{-1}, n_f = 3) were either equal to the parameters in the matrix domain or set to average values (characteristic macropore soil water retention curve shape parameters published in the literature). The saturated hydraulic conductivity (K_{sf} = 0.182 cm min^{-1}) was optimized together with the effective saturated hydraulic conductivity of the interface between the macropore and matrix domains (K_{sa}= 5.3 10^{-5} cm min^{-1}).

Conclusion

Information about the fraction of the macropores existing in studied soils and information about the shape and size of the aggregates, biopores and soil fractures were further used to describe the dual-domain geometry in the dual-permeability model, which was applied to simulate preferential flow in these soils.

Acknowledgement

Authors acknowledge the financial support of the Grant Agency of the Czech Republic (grant No. GA CR 526/08/0434) and the Ministry of Education, Youth and Sports of the Czech Republic (grant No. MSM 6046070901). Authors also acknowledge H.H. Gerke for his help in the field and valuable discussions.

References

Catt JA (1990) Paleopedology manual. *Quaternary International* **6**, 1-95.

Flury M, Flühler H, Jury WA, Leuenberger J (1994) Susceptibility of soils to preferential flow of water – Field-studies. *Water Resources Research* **30**, 1945-1954.

Flury M, Flühler H (1995) Tracer characteristic of Brilliant Blue FCF. *Soil Science Society of America Journal* **59,** 22-27.

Flury M, Wai NN (2003) Dyes as tracers for vadose zone hydrology. *Reviews of Geophysics* **41**, Art. No: 1002.

Gerke HH (2006) Review article. Preferential flow descriptions for structured soils. *Journal of Plant Nutrition and Soil Science* **169**, 382-400.

Jarvis N (2007) Review of non-equilibrium water and solute transport in soil macropores: principles, controlling factors and consequences for water quality. *European Journal of Soil Science* **58**, 523-546.

Kasteel R, Burkhardt M, Giesa S, Vereecken H (2005) Characterization of Field Tracer Transport Using High-Resolution Images. *Vadose Zone Journal* **4**, 101-111.

Kodešová R, Kočárek M, Kodeš V, Šimůnek J, Kozák J (2008) Impact of soil micromorphological features on water flow and herbicide transport in soils. *Vadose Zone Journal* **7**, 798-809.

Kodešová R, Vignozzi N, Rohošková M, Hájková T, Kočárek M, Pagliai M, Kozák J, Šimůnek J (2009) Impact of varying soil structure on transport processes in different diagnostic horizons of three soil types. *Journal of Contaminant Hydrology* **104**, 107-125.

Köhne JM, Köhne S, Šimůnek J (2009a) A Review of Model Applications for Structured Soils: a) Water Flow and Tracer Transport. *Journal of Contaminant Hydrology* **104**, 4-35.

Köhne JM, Köhne S, Šimůnek J (2009b) A Review of Model Applications for Structured Soils: b) Pesticide Transport. *Journal of Contaminant Hydrology* **104**, 36-60.

Morris C, Mooney SJ, Young SD (2008) Sorption and desorption characteristics of the dye tracer, Brilliant Blue FCF, in sandy and clay soils. *Geoderma* **146**, 434-438.

Sander T, Gerke HH (2007) Preferential flow patterns in paddy fields using a dye tracer. *Vadose Zone Journal* **6**,105-115.

Šimůnek J, van Genuchten MTh, Šejna M (2008) Development and applications of the HYDRUS and STANMOD software packages, and related codes. *Vadose Zone Journal* **7**, 587-600.

Šimůnek J, van Genuchten MTh (2008) Modeling nonequilibrium flow and transport with Hydrus. *Vadose Zone Journal* **7**, 782-797.

van Genuchten MTh (1980) A closed-form equation for predicting the hydraulic conductivity of unsaturated soils. *Soil Science Society of America Journal* **44**, 892-898.

Wooding RA (1968) Steady infiltration from large shallow circular pond. *Water Resources Research* **4**, 1259-1273.

Zhang ZF, Groenevelt PH, Parkin GW (1998) The well shape-factor for the measurement of soil hydraulic properties using the Guelph permeameter. *Soil and Tillage Research* **49**, 219-221.

Elution patterns and distribution of salts from multi-layer reclaimed soils with subsurface layer of porous granules in the newly reclaimed Saemangeum tidal area

J. H. Ryu[A], C. H. Yang[A], T. K. Kim[A], S. B. Lee[A], S. Kim[A], W. Y. Choi[A], N. H. Baek[A], S. J. Kim[A] and D. Y. Chung[B]

A Department of Rice and Winter Cereal Crop, NICS, RDA, Iksan 570-080, Korea, Email Jin001kr@korea.kr
B College of Agricultural and Life Sci. Chungnam National Univ. Daejeon 305-764, Korea, Email dychung@cnu.ac.kr

Abstract
This study was carried out to identify the elution patterns and distribution of salts from multi-layer reclaimed soils with a subsurface layer of porous granule in the newly reclaimed Saemangeum tidal area. To do this, paddy and upland plots were established with a layer of porous granule below the surface layer of the indigenous reclaimed soils at a depth of 30~60 cm. Soil samples were taken from the surface and subsurface (porous granule applied) layers at each plot to measure changes of EC of each soil layer at intervals of 1 month during the experiment. The results of EC measurements showed that in the paddy plot with porous granules EC of the top soil (0~30 cm) after 5 months rice cultivation was drastically decreased from 10.54 dS/m to 0.81dS/m while EC decreased from 5.74 dS/m to 0.82 dS/m in the control plot. In the upland plot, EC of top soil decreased from 18.08dS/m to 12.25 dS/m, while in the control upland plot EC value increased from 14.01dS/m to 28.41dS/m. From these results we could assume that the porous granule layer placed at 30~60cm enhanced leaching of salts from the surface layer and cut off capillary rise of salts from the subsurface soil, resulting in lowering the level of salinity to values that would not affect any plant growth.

Key Words
Reclaimed land, desalinization, EC, salinity

Introduction
On the western coast of Korea, tidal flats are extensive with wide distances between the high and low tide levels. These areas are suitable for tideland reclamation and the comprehensive tidal land reclamation projects have been implemented for satisfying the demand of land and water resources increased since the beginning of 1970s(Son *et al.* 2000). However, changes of tides and land use caused by practising tideland reclamation may influence the environment in the area. The majority of reclaimed land in Korea was made through dike construction and had very high salt concentrations in early periods, so to cultivate crops in newly reclaimed lands, soils must be desalinized. Soil salinity plays a very important role in determining plant productivity (Yang *et al.* 2008; Maas *et al.* 1984; Lee *et al.* 2003; U.S. Salinity Laboratory Staff1954). A quantitative and systematic investigation on the characteristics of soil salinity and its distribution in the newly reclaimed soil is not only important to the understanding of tidal soil systems to determine the utilization of the reclaimed land but also for potential development of reclamation methods for the newly established tidal soils in Korea(Jung *et al.* 2003). For salt-affected soil with relatively good permeability, desalinization through vertical drainage can be effective for rapid and desirable desalinization. In this research, we investigated elution patterns and distribution of salts from multi-layer reclaimed soils with subsurface layer of porous granule (coal bottom ash) which could be applied as modification of water flow in newly reclaimed saline soil.

Materials and methods
Study area
Saemangeum was an estuarine tidal flat on the coast of the West Sea in Korea. It was dammed by the government of South Korea in April 2006 and is scheduled to be converted into either agricultural or industrial land. Saemangeum is at the mouths of the Dongjin and Mangyeong Rivers, on the coast of Jeollabuk-do. It is just south of the estuary of the Geum River. Neighboring districts include Gunsan City, Buan County, and Gimje City. After the estuary has been completely filled, an area of about 400 km² (roughly two-thirds the size of Seoul) will have been added to the Korean peninsula, making it one of the biggest landfills in history.

Figure 1. Pictures of Saemangeum rclaimed tidal land area located on the mid-western coast in Korea.

An experimental field was located on Saemangeum reclaimed land, Korea. The soil series was Munpo and soil texture was sandy loam. Experimental paddy and upland plots were made. These plots were established with layer of the porous granule below the surface layer of the indigenous reclaimed soils at depth of 30~60cm. For paddy plots, irrigation water was applied and maintained 10cm above the surface soil during the experimental period, while in the upland plots rainfall was the water sources throughout the experiment. Soil samples were taken from the layers of surface and subsurface (porous granule applied) at each plot to measure changes of EC of each soil layer at intervals of 1 month during the experiment. The chemical properties of the tidal soils obtained from the Saemangeum area are shown in Table 1.

Table 1. Chemical properties of the tidal soils obtained from Saemangeum area.

Soil series	pH	EC	T-N	OM	Av. P2O5	Ex. Cations (cmolc/kg)			
	(1:5)	(dSm-1)	(g /kg)	(g /kg)	(mg /kg)	K	Ca	Mg	Na
Moonpo	7.4	22.5	0.6	8.4	75	2.25	3.9	7.2	23.8
Yumpo	6.9	12.3	0.3	3.1	38	1.61	1.4	5.6	13.3
Poseung	8.1	4.1	0.2	1.9	26	0.90	1.1	2.9	15.1

Results and discussion

Figure 2 shows the changes of EC values of top soil in the paddy plot during the experiment. For surface depth of 0~10 cm, EC decreased from 11.36 dS/m to 0.80d S/m (93.0% of salt was lost). Intermediate depth of 10~20 cm, EC value decreased from 10.78 dS/m to 0.64 dS/m (94.1 % of salt was lost). Bottom depth of 20~30 cm, EC value decreased from 9.47 dS/m to 0.99d S/m (89.5% of salt was lost), showing soil was desalinized. Figure 3 shows the changes of EC values in top soil in the upland plot during experiment. EC values decreased or increased according to amounts of rainfall. For surface depth of 0~10 cm, the EC value increased from 17.50 dS/m to 22.07 dS/m (26.1% of salt increased). Intermediate depth of 10~20cm, the EC value decreased from 19.33d S/m to 10.58 dS/m (45.3% desalinized). Bottom depth of 20~30 cm, EC value decreased from 17.40 dS/m to 4.09 dS/m (76.5% desalinized). On the other hand in the control upland plot, EC values of top soil (0~30 cm) increased from 14.01 dS/m to 28.41 dS/m(102.8% increased).

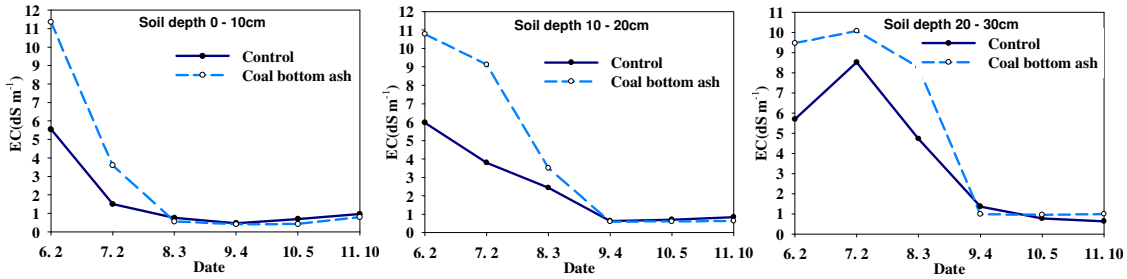

Figure 2. Changes of EC values in multi-layer paddy soil with subsurface layer of porous granules.

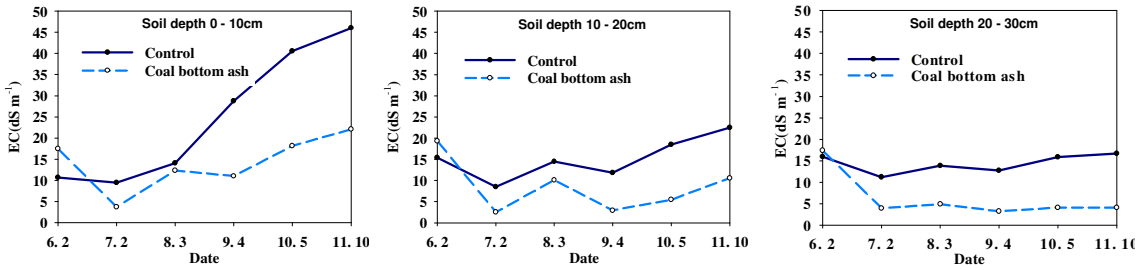

Figure 3. Changes of EC values in multi-layer upland soil with subsurface layer of porous granules.

Conclusion

Multi-layer reclaimed soil with subsurface layer of porous granules (coal bottom ash) show enhanced leaching of salts from the surface soil and diminished capillary rise of salts from the subsurface soil. Therefore, we could conclude that the porous granule layer can be useful as a soil ameliorator for upland cropping in newly reclaimed saline soil.

References

Son JG, Koo JW, Choi JK, Song JD (2000) Determination of leaching requirements in the unripened tidal reclaimed paddy fields. Journal of Korean Society of Agricultural Engineers 42, 55-62.

US Salinity Laboratory Staff (1954) 'Diagnosis and improvement of saline and alkali soils'. Handbook No. 60 (USDA: Washinton, DC).

Jung YS, Lee WH, Joo JH, Yu IH, Shin WS, Ahn Y, Yoo SH (2003) Use of electromagnetic inductance for salinity measurement in reclaimed saline land. Korean Journal of Soil Science and Fertilizer 36, 57-65.

Lee SH, Hong BD, Ahn Y, Ro HM (2003) Relation between growth condition of six upland-crops and soil salinity in reclaimed land. Korean Journal of Soil Science and Fertilizer 36, 66-71.

Yang CH, Yoo CH, Jung JH, Kim BS, Park WK, Ryu JH, Kim TK, Kim JD, Kim SJ, Baek SH (2008) The change of physico-chemical properties of paddy soil in reclaimed tidal land. Korean Journal of Soil Science and Fertilizer 41, 94-102.

Maas EV, Lesch SM, Francois LE, Grieve CM (1984) Salt tolerance of plants. In 'Handbook of plant science in agriculture'. pp. 57-75. (CRC Press Inc.: Boca raton, FL).